THERMAL PAVEMENT CRACKING IN WEST TEXAS

by

Samuel H. Carpenter
Robert L. Lytton

Reserach Report Number 18-4F

Environmental Deterioration of Pavement
Research Study 2-8-73-18

conducted for the
State Department of Highways
and Public Transportation

in cooperation with the
U.S. Department of Transportation
Federal Highway Administration

by the

TEXAS TRANSPORTATION INSTITUTE
Texas A&M University
College Station, Texas

October, 1977

TECHNICAL REPORT STANDARD TITLE PAGE

1. Report No.	2. Government Accession No.	3. Recipient's Catalog No.
FHWATX77-18-4F		

4. Title and Subtitle	5. Report Date
Thermal Pavement Cracking in West Texas	October, 1977
	6. Performing Organization Code
7. Author(s)	8. Performing Organization Report No.
Samuel H. Carpenter and Robert L. Lytton	Research Report No. 18-4F
9. Performing Organization Name and Address	10. Work Unit No.
Texas Transportation Institute Texas A&M University College Station, Texas 77843	11. Contract or Grant No. Study No. 2-8-73-18
	13. Type of Report and Period Covered Final - September, 1972 August, 1977
12. Sponsoring Agency Name and Address	14. Sponsoring Agency Code
Texas State Department of Highways and Public Transportation; Transportation Planning Division P.O. Box 5051 Austin, Texas 78763	

15. Supplementary Notes

Research performed in cooperation with DOT, FHWA.
Study Title: Environmental Deterioration of Pavement

16. Abstract

Transverse cracking is a form of environmental deterioration that accounts for the expenditure of some twenty million dollars a year in maintenance in west Texas alone. This form of deterioration has not been predictable by previous mechanisms. A study of the environment in west Texas and installations of psychrometers beneath new construction show that freeze-thaw cycling is a major factor in west Texas, and acts primarily in the base course.

The base course undergoes volumetric contraction upon freezing that is an order of magnitude larger than that of the asphaltic concrete. This contraction is related to the specific surface area of the clay mineral portion of the material with models being developed for predictive purposes.

A theory of particle structure and reorientation is proposed from the data and from a theoretical interpretation of the Lennard-Jones Model for inter-particle forces. This theory is verified in scanning electron micrographs of base course samples with and without the influence of freeze-thaw cycles.

A computer model is developed which uses material properties to predict crack spacing caused by this contraction. The model uses actual climatic data to calculate the rate of crack growth and the change in crack spacing with time. An example is shown for Amarillo and Abilene to illustrate the use of the model.

Results of a series of stabilization studies to reduce the thermal susceptibility are shown. Gypsum ($CaSO_4$) shows promise as an economical additive although the percentages were very low, typically 0.5 to 0.75 (continued on back)

17. Key Words	18. Distribution Statement
Thermal activity, base course, viscoelastic prediction of thermal cracking, clay mineralogy, soil suction, climate, freeze contraction, fracture mechanics.	No Restrictions. This document is available to the public through the National Technical Information Service, Springfield, Virginia 22161

19. Security Classif. (of this report)	20. Security Classif. (of this page)	21. No. of Pages	22. Price
Unclassified	Unclassified		

Form DOT F 1700.7 (8-69)

PREFACE

This report gives a complete description of the reason that pavements crack in west Texas. It shows how the thermal properties of base course and asphalt concrete contribute to the cracking problem and also shows how stabilizing agents may be added to the base course to cut down on its thermal activity. A computer program is presented that predicts cracking in pavements taking U. S. Weather Bureau data tapes as input and using viscoelastic thermal stress analysis and fracture mechanics. This report is the final in a series of four reports from the Study entitled "Environmental Deterioration of Pavement." The study, sponsored by The State Department of Highways and Public Transportation in cooperation with the Federal Highway Administration is a comprehensive program to verify environmental cracking mechanisms and to recommend maintenance and construction measures to alleviate this pavement cracking problem.

DISCLAIMER

ABSTRACT

Transverse cracking is a form of environmental deterioration that accounts for the expenditure of some twenty million dollars a year in maintenance in west Texas alone. This form of deterioration has not been predictable by previous mechanisms. A study of the environment in west Texas and installations of psychrometers beneath new construction show that freeze-thaw cycling is a major factor in west Texas, and acts primarily in the base course.

The base course undergoes volumetric contraction upon freezing that is an order of magnitude larger than that of the asphaltic concrete. This contraction is related to the specific surface area of the clay mineral portion of the material with models being developed for predictive purposes.

A theory of particle structure and reorientation is proposed from the data and from a theoretical interpretation of the Lennard-Jones Model for inter-particle forces. This theory is verified in scanning electron micrographs of base course samples with and without the influence of freeze-thaw cycles.

A computer model is developed which uses material properties to predict crack spacing caused by this contraction. The model uses actual climatic data to calculate the rate of crack growth and the change in crack spacing with time. An example is shown for Amarillo and Abilene to illustrate the use of the model.

Results of a series of stabilization studies to reduce the thermal susceptibility are shown. Gypsum ($CaSO_4$) shows promise as an economical additive although the percentages were very low, typically 0.5 to 0.75

percent.

The analysis proposed in this report represents a new approach to the design of pavements to withstand the effects of the environment. The concepts are valid and do not rely on assumptions of arbitrary constants as have previous attempts. The mechanism and analysis are developed from laboratory data and theoretical considerations from fracture mechanics. The analysis will provide the first step in a design process based on true material properties and on considerations toward how these materials behave in the field.

IMPLEMENTATION STATEMENT

This report gives details of the way to identify base courses that will be thermally active when they freeze. Descriptions of the laboratory methods used to characterize freeze contraction properties are given in the appendixes and could be adopted as standard methods of investigating base course materials sampled from borrow pits to determine how much damage they may do.

An investigation of potassion salt, lime, and gypsum additives is reported here to show what percentages can be expected to reduce base course thermal activity.

The computer program reported here uses weather data, viscoelastic thermal stress analysis, and fracture mechanics to investigate the way asphalt and base course properties control or contribute to the cracking problem. From this study, it becomes obvious that the severity of cracking can be reduced by the following methods in descending order of effectiveness:

1. reduce tensile strength of base course
2. increase stiffness and tensile strength of surface course
3. reduce thermal coefficient of contraction of base course.

Traffic loads are not included in the computer program but their effect is to accelerate the rate of cracking in the traffic lane where they are applied.

Recommendations are made on the level of material properties that will best reduce the thermal cracking problem in west Texas.

LIST OF REPORTS

Report No. 18-1, "Environmental Factors Relevant to Pavement Cracking in West Texas," Samuel H. Carpenter, Robert L. Lytton, Jon A. Epps, describes the environment existing in west Texas and relates it to other studies to determine its severity.

Report No. 18-2, "Thermal Activity of Base Course Material Related to Pavement Cracking," by Samuel H. Carpenter and Robert L. Lytton, describes the development of a pavement cracking mechanism emanating from thermal activity of the base course layer in the pavement.

Report No. 18-3, "Prediction of Thermal Reflection Cracking in West Texas," by Hang-Sun Chang, Robert L. Lytton, and Samuel H. Carpenter, describes a rational mechanistic approach to the description of reflection cracking and overlay life through the viscoelastic thermal stress analysis and viscoelastic fracture mechanics.

Report 18-4F, "Thermal Pavement Cracking in West Texas," by Samuel H. Carpenter and Robert L. Lytton, describes the properties of base course and asphalt which cause cracking and how they may be altered, and shows how cracking may be predicted using viscoelastic thermal stress analysis and fracture mechanics.

TABLE OF CONTENTS

LIST OF TABLES

LIST OF FIGURES

LIST OF FIGURES (CONTINUED)

LIST OF FIGURES (CONTINUED)

LIST OF FIGURES (CONTINUED)

LIST OF FIGURES (CONTINUED)

LIST OF FIGURES (CONTINUED)

Figure

INTRODUCTION

A growing concern over the environmental deterioration of pavements has been realized in the last decade. This concern has been brought about by the increasing mileage of roads experiencing transverse cracking. Ample evidence of these forms of cracking exists in the colder regions of the Northern United States and Canada. Transverse cracking of this form is also found in the arid regions of the western and southwestern United States.

Recent research activities illustrate the fact that non-traffic load associated cracking may be a major cause of pavement distress (37)*. The area of west Texas, in particular, shows extensive transverse cracking commonly associated with environmental distress. In particular Districts 4, Amarillo; 5, Lubbock; 6, Odessa; 7, San Angelo; 8, Abilene; 24, El Paso; and 25, Childress, shown in Fig. 1 demonstrate similar cracking patterns which may or may not be the result of similar mechanisms.

Low Temperature Environment

There are a variety of mechanisms that have been studied to account for this extensive cracking problem in flexible pavements. These mechanisms all show some dependence on environmental factors, and involve either low temperature cracking, or moisture shrinkage in the formation of transverse cracks. The mechanism of low temperature cracking has been used in the colder regions of Canada and the Northern United States in predicting cracking during the life of a pavement (12, 20, 22). The concept of this mechanism involves the thermal contraction of the asphaltic concrete due to low temperatures. As the temperature drops, tensile stresses are

---

The format and style for this dissertation follows the pattern of the Journal of the Geotechnical Engineering Division, American Society of Civil Engineers.

* Numerals underlined in parenthesis refer to corresponding items in the list of references.

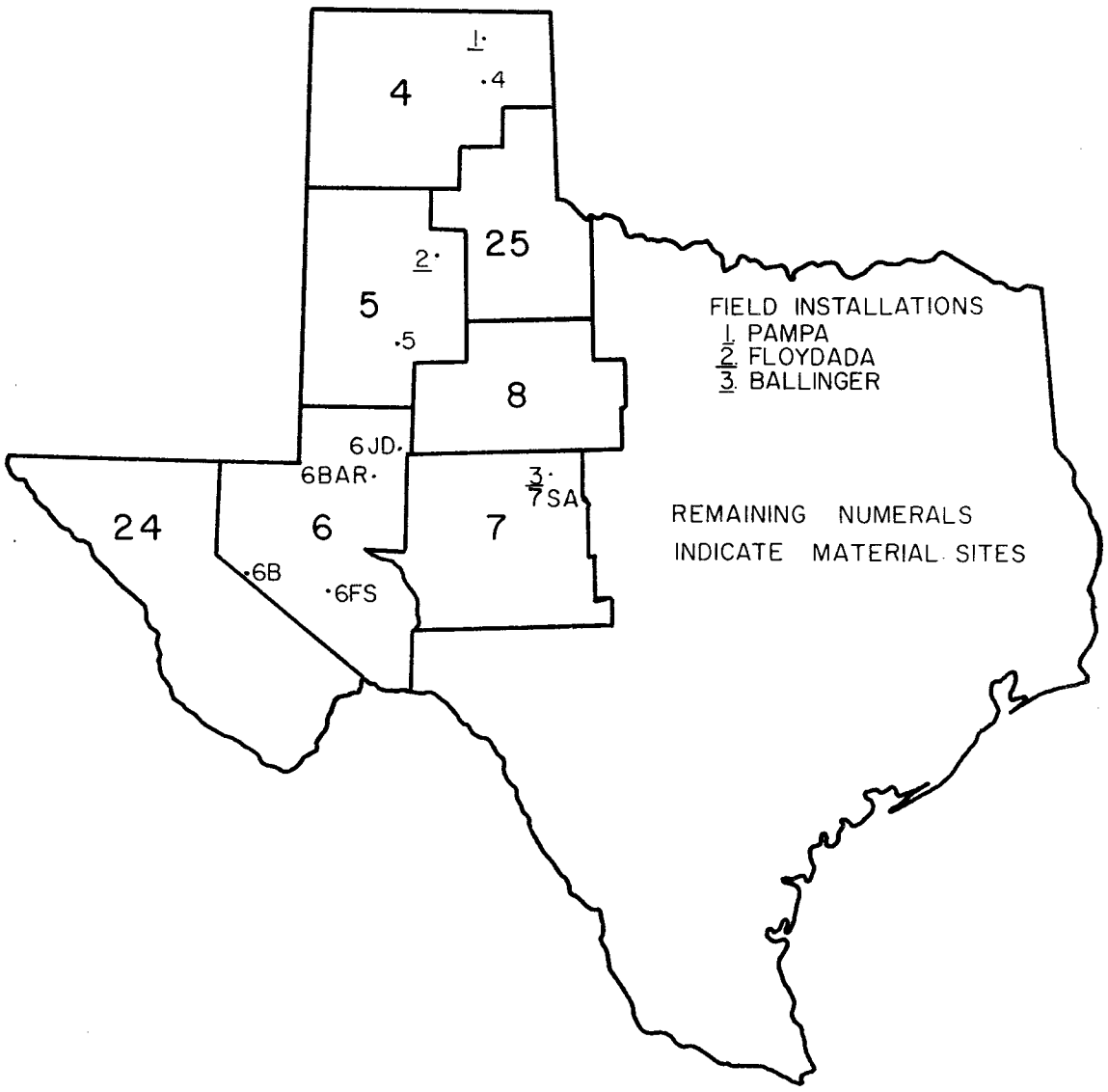

FIG. 1 - HIGHWAY DISTRICTS IN WEST TEXAS EXHIBITING EXTENSIVE TRANSVERSE CRACKING

induced due to the contraction. When these induced stresses exceed the tensile strength of the asphalt the material will crack. The extreme cold temperatures necessary to produce this form of cracking occur only rarely in Texas and thus this mechanism of cracking is not likely to occur in west Texas, as stated by McLeod (35).

This is further emphasized in a study conducted on Canadian test sections by Hajek and Haas (20). They developed a regression model from the observed behavior of these sections. Their low-temperature quantity, the winter design temperature, is defined as the "lowest temperature at or below which only one percent of the hourly ambient air temperatures in January occur for the severest winter during a ten-year period". The major point to be obtained is shown in Fig. 2. The model predicts that for a more moderate winter period, higher winter design temperature, there will be more cracking. This conclusion runs contrary to the accepted mechanisms which predict more cracking for lower temperatures. The implication is that there is another mechanism acting in addition to the low temperature phenomenon, this being the freeze-thaw mechanism.

Thermal fatigue cracking has been proposed to account for the discrepancy between observed and predicted cracking (46). This mechanism involves the fatiguing of the asphaltic concrete under the action of temperature cycling in much the same manner as repeated loading produces fatigue in metals. These studies have not applied fracture mechanics; but have assumed a fatigue law and obtained the constants necessary by forcing the result to match an actual data point. The constants thus determined were then used to predict cracking for various other pavements. The results of this procedure are not wholly satisfactory and do not provide any insight into the mechanism itself. The discrepancies imply that the freeze-thaw mechanism may be acting in another layer such as the base course.

This opens the possibility of thermal damage to the base course and/or subgrade. Initial calculations of pavement temperature profiles, which will be discussed in detail in a later section, clearly showed that the freeze-line only rarely extends into the

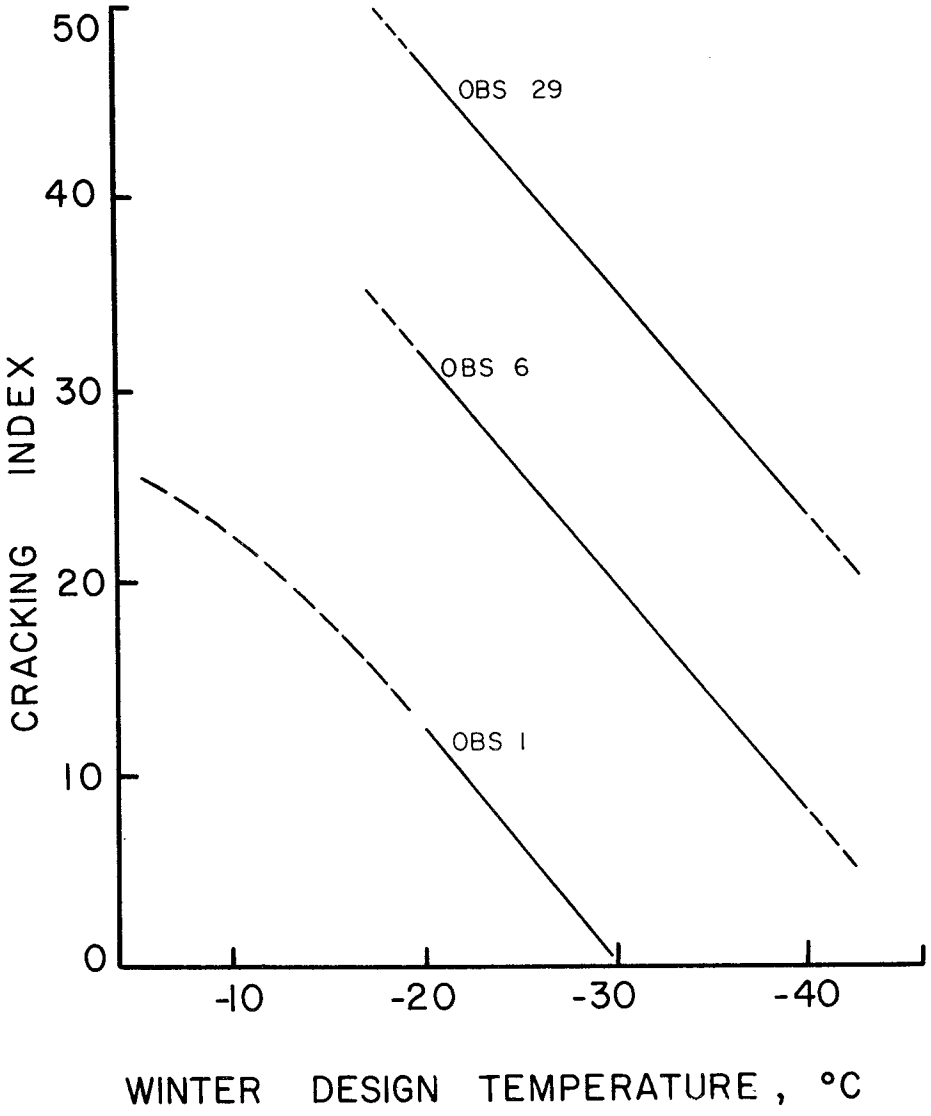

FIG. 2 - CRACKING INDEX AS A FUNCTION OF WINTER DESIGN TEMPERATURE(20)

subgrade. The majority of the freeze-thaw activity was centered in the base course for west Texas. Due to the absence of extreme low temperatures and readily available capillary moisture, it is not likely that the associated mechanism of frost heave is active. This mechanism is prevalent in Northern climates where the frost line extends several feet into the subgrade for extended periods (27).

Studies of the effect of freeze-thaw cycling on base course material without ready access to water have not been conducted as most studies have concentrated on the subgrade. Implications about the behavior of a base course undergoing freeze-thaw may be drawn from these studies. One study indicates that freezing and thawing of a soil material may produce a contraction upon freezing (21) which is contradictory to commonly accepted practice.

Hamilton has shown that the majority of the total volume change due to freezing will occur between $0^{o}C$ and $-6.7^{o}C$ with the other ten percent occurring from ambient down to $0^{o}C$ (21). Only very slight and erratic volume change was noted to occur below $-6.7^{o}C$. This is illustrated in Fig. 3 which is taken from Hamilton's study. Figure 4 shows data for two freeze-thaw cycles. The noted temperature dependence is evident, but the more important feature is the volume change noted after the first cycle. If this behavior is prevalent in base course material, with considerably less clay content than the subgrade material tested by Hamilton, the implications for pavement deterioration are apparent.

Other studies show that freeze-thaw cycles clearly change the load carrying properties of a soil material. Bergan and Monismith (5) studied the resilient modulus of a subgrade material before and after a winter's freeze-thaw activity. The resilient modulus is a measure of the dynamic elastic modulus of the material and it was found to be lower in the spring, indicating the material was deforming more under the same loading conditions. Pagen and Khosla (39) studied the viscoelastic properties of a clayey material under the effect of freeze-thaw cycling. Figure 5 illustrates the effect on the creep modulus. These data indicate a reduction in the modulus which indicates a lowering of the load carrying ability

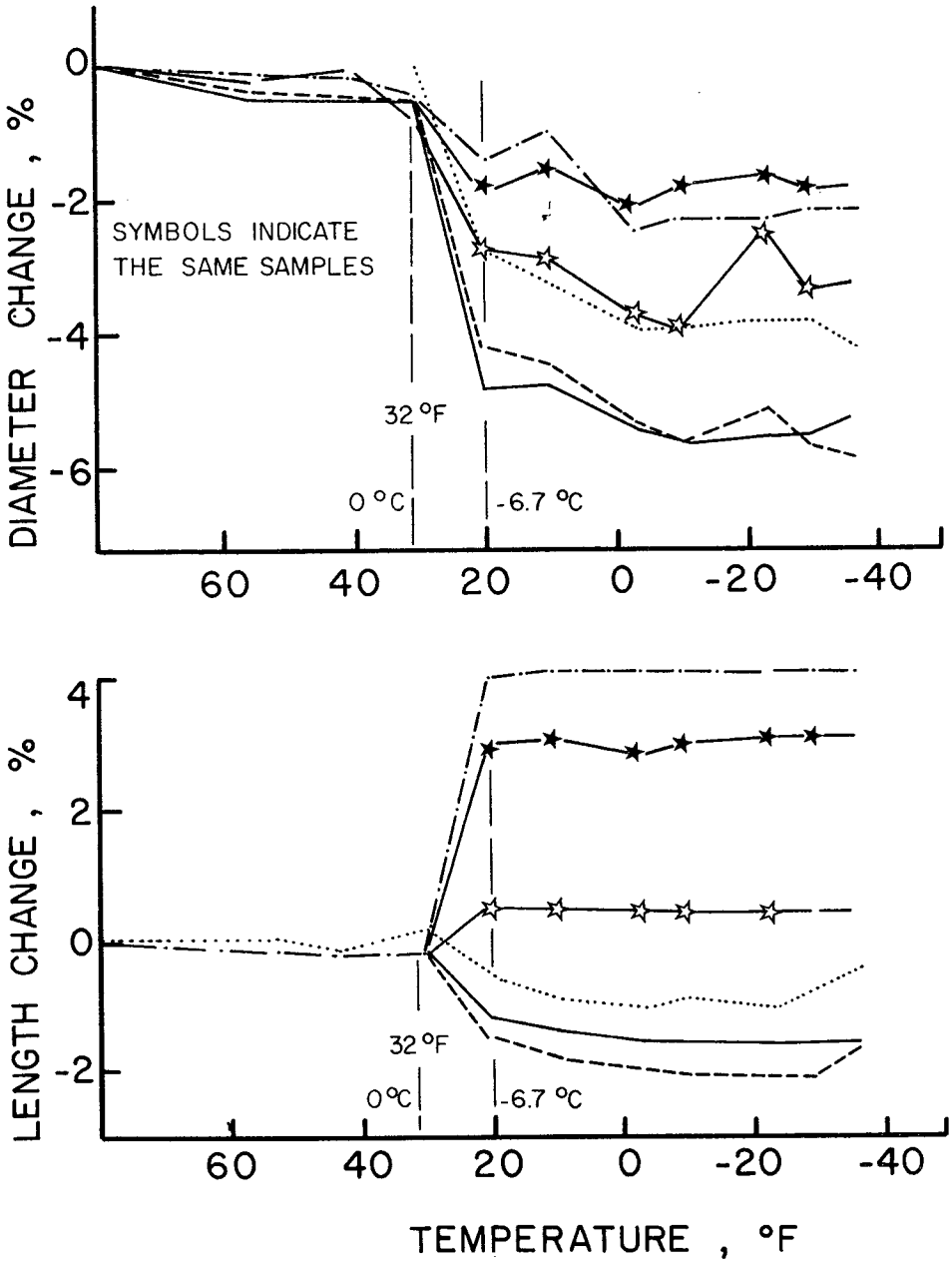

FIG. 3 - CHANGE IN LENGTH AND DIAMETER FOR SIX SAMPLES AS A FUNCTION OF TEMPERATURE (21)

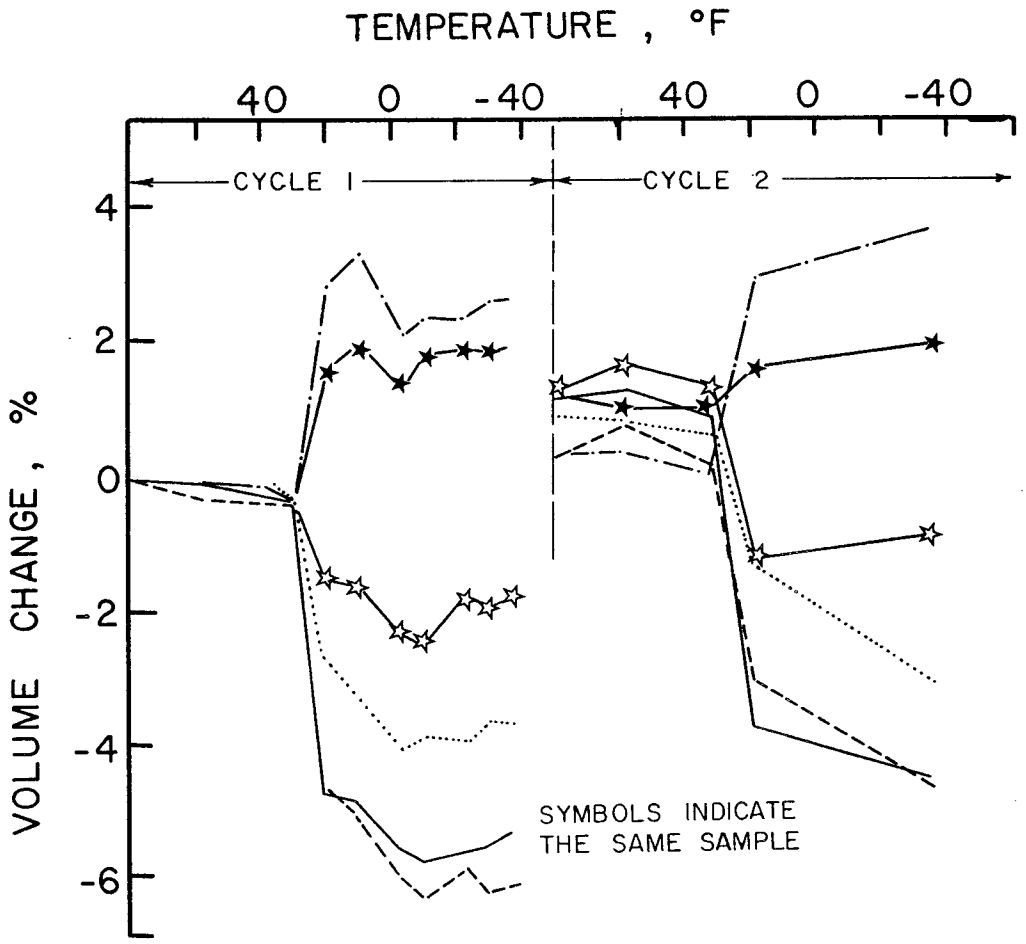

FIG. 4 - VOLUME CHANGE AS A FUNCTION OF TEMPERATURE FOR TWO FREEZE-THAW CYCLES (21)

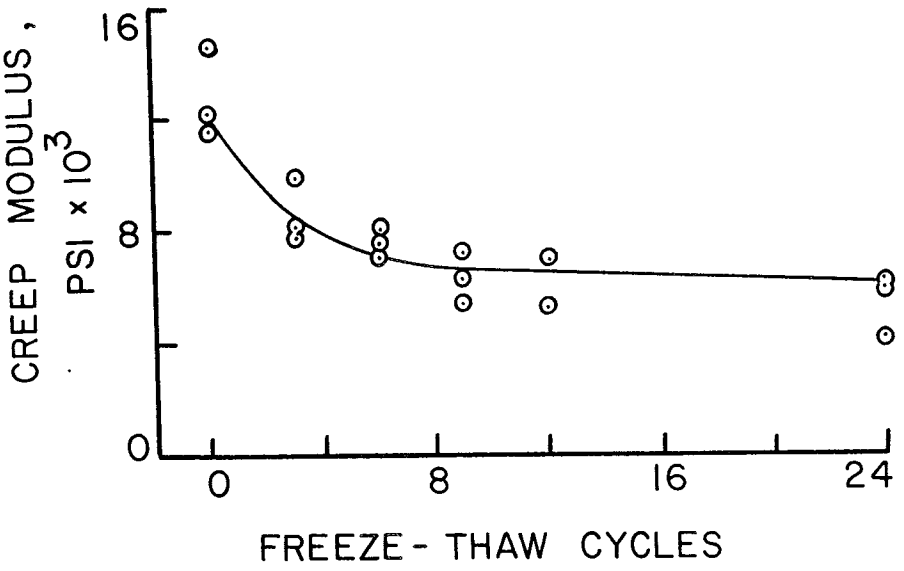

FIG. 5 - REDUCTION IN CREEP MODULUS DUE TO FREEZE-THAW CYCLES (39)

which may result in a more rapid deterioration.

High Temperature Environment

It has been shown that the low-temperature will have an effect on pavement performance through the effects of freeze-thaw. Due to the extreme temperature range in west Texas, it is therefore logical to investigate the effect of the high temperature environment on pavement performance. The importance of the high temperatures emerge in conjunction with the moisture state in the soil. The majority of the relationships formed to predict overall climatic influence have been formed through a combination of evaporation and precipitation. These quantities are relatively easy to obtain and have a major influence on the behavior of most engineering structures.

Transeau (50) developed a Precipitation-Effectiveness index which attempted to use the amount of rain and evaporation. Russell (44) developed a ratio of precipitation to evaporation. Ångström developed a humidity coefficient which is directly proportional to the amount of precipitation and inversely proportional to an exponential function of temperature. These indicators are based on measured rainfall and evaporation, which are very highly related to each other. As such, a correlation between one of these environmental indicators and the soil properties will not be truly meaningful as there can be no true independent variable.

Thornthwaite (49) introduced the concept of potential evapotranspiration. This quantity is defined as the amount of water which would be returned to the atmosphere by evaporation from the ground surface and by transpiration from plants if there were an unlimited supply of water to the plants and ground. A map of this quantity as it is distributed across Texas is shown in Fig. 6. Using this potential evapotranspiration measure as a basis, a rational classification of the climate is possible since this variable is independent of local soil and vegetation conditions. Though transpiration may not be an active mechanism in a pavement structure (43), it should be considered in order to define the total environment which will influence the performance of the pavement.

The investigators mentioned above were attempting to determine

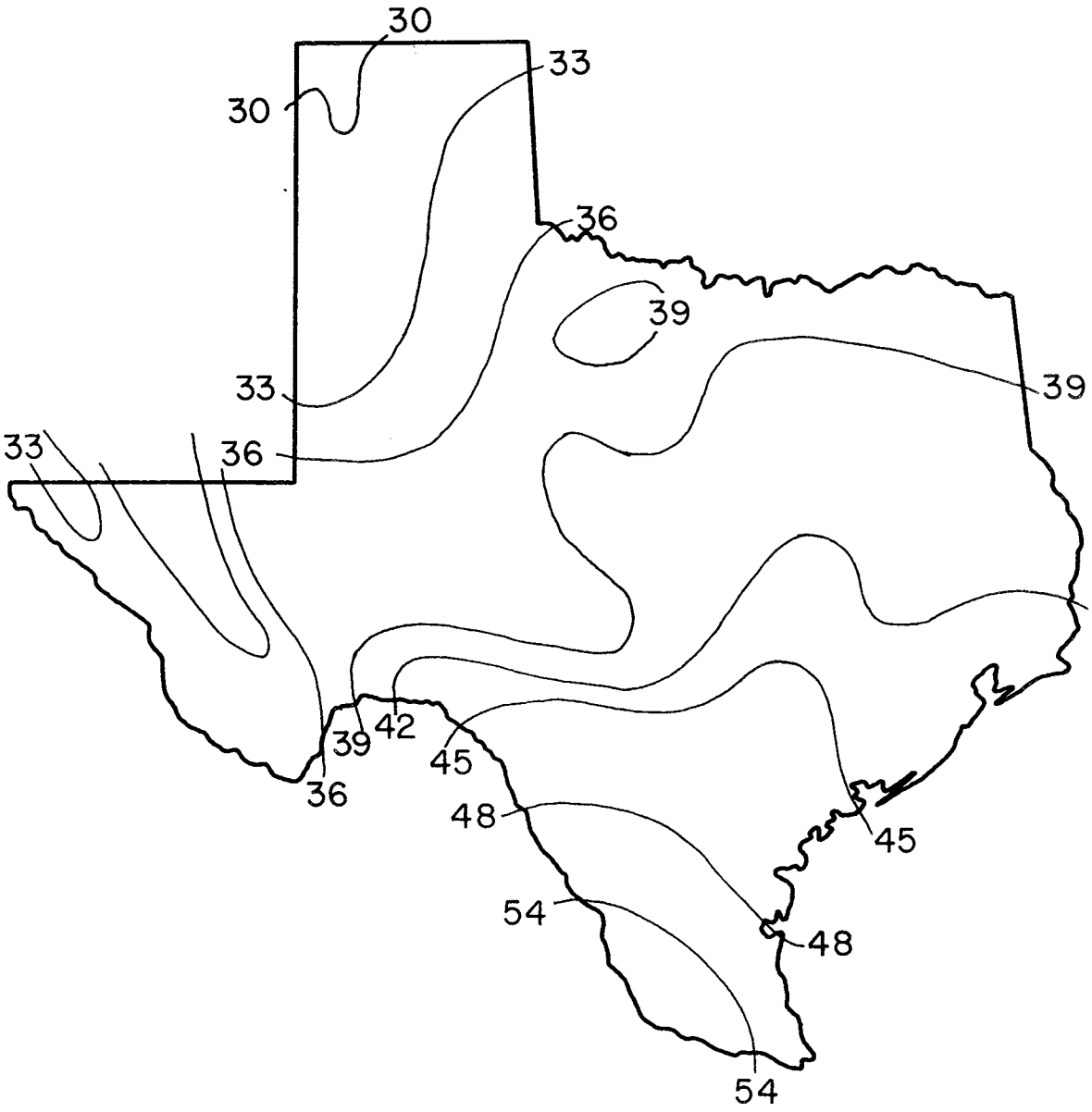

FIG. 6 - AVERAGE ANNUAL POTENTIAL EVAPOTRANSPIRATION (44)

the conditions of humidity i.e., a moisture surplus or deficit, in the soil. Using the concept of Potential Evapotranspiration, Thornthwaite proposed his moisture index.

$$Im = \frac{100S - 60d}{E_p} \qquad (1\text{-}1)$$

where

Im = moisture index,

S = surplus of water in inches,

d = deficit of water in inches, and

E_p = Potential Evapotranspiration in inches.

The surplus and deficit of moisture must be considered separately as they occur in different seasons of the year for most places. A moisture surplus will store water in the subsoil water region, thus making more water available to deep rooted plants, lessening the effect of a drought. In this manner a surplus of six inches in one season will counteract ten inches deficiency in another season. The soil may store only a finite value of rainfall, 4-6 in. (10.2-15.2 cm) before the remainder will runoff and be unavailable for the next seasonal moisture deficiency. This relationship is shown in Fig. 7 for Dalhart, Texas. By a simple bookkeeping procedure, these data may be converted to surplus and deficit moisture; and then into the moisture index. Thornthwaite's moisture index for Texas is shown in Fig. 8. The dryness of west Texas is indicated by the negative values increasing for the west Texas area.

The Thornthwaite moisture index has shown promise in relating climate to engineering performance. As applied to pavements, the moisture index has been related to the equilibrium suction level which develops in the subgrade beneath the centerline of a pavement (43). The relationship developed by Russam and Coleman is shown in Fig. 9; and has been verified for a wide variety of climatic regions (42). Using this relationship and the moisture index previously shown, a map of expected suction levels in the subgrades can be constructed. Figure 10 shows predicted equilibrium suction levels for a clay subgrade (the actual value of

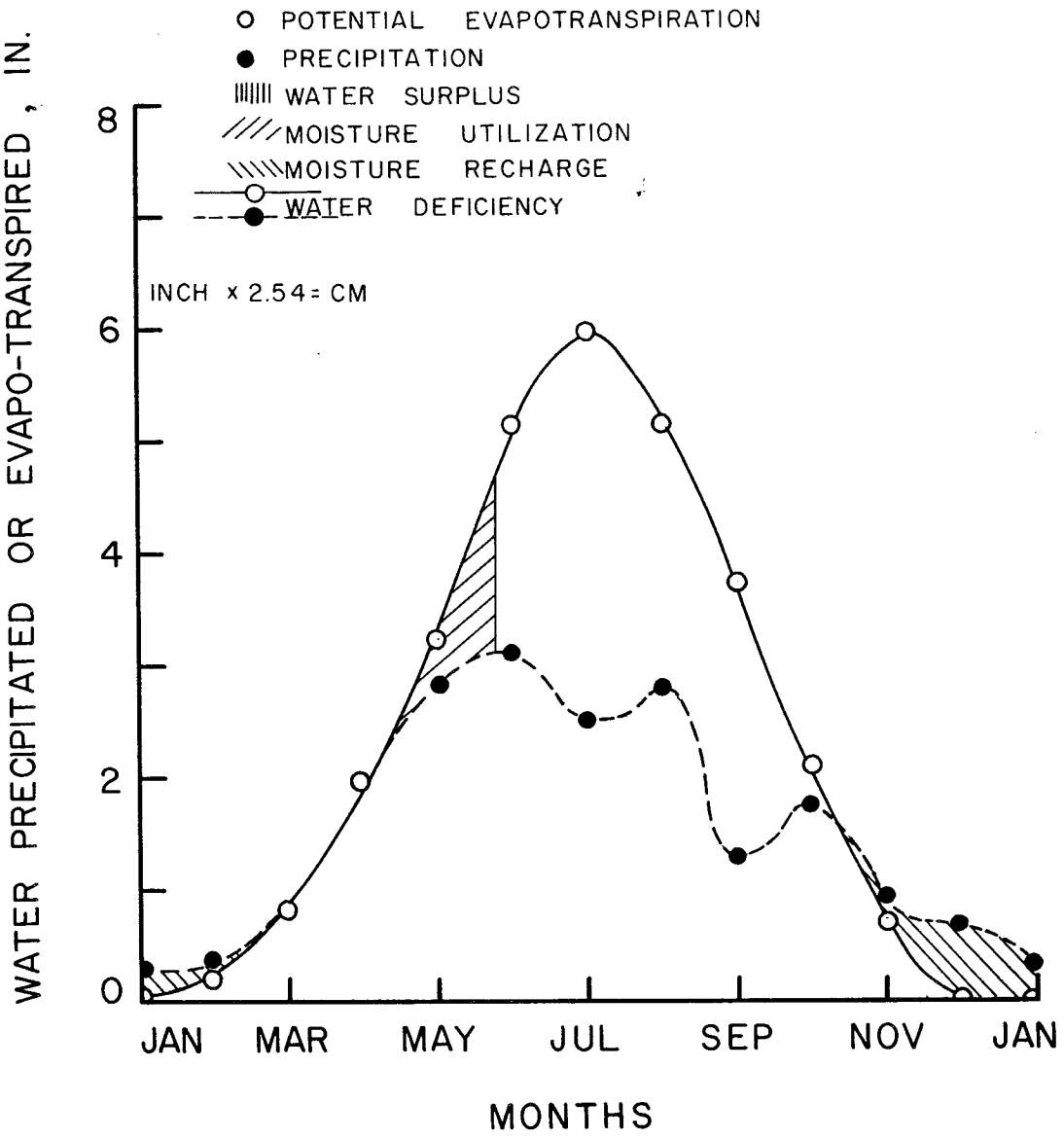

FIG. 7 - MARCH OF PRECIPITATION AND POTENTIAL EVAPOTRANSPIRATION THROUGH THE YEAR FOR DALHART, TEXAS (49)

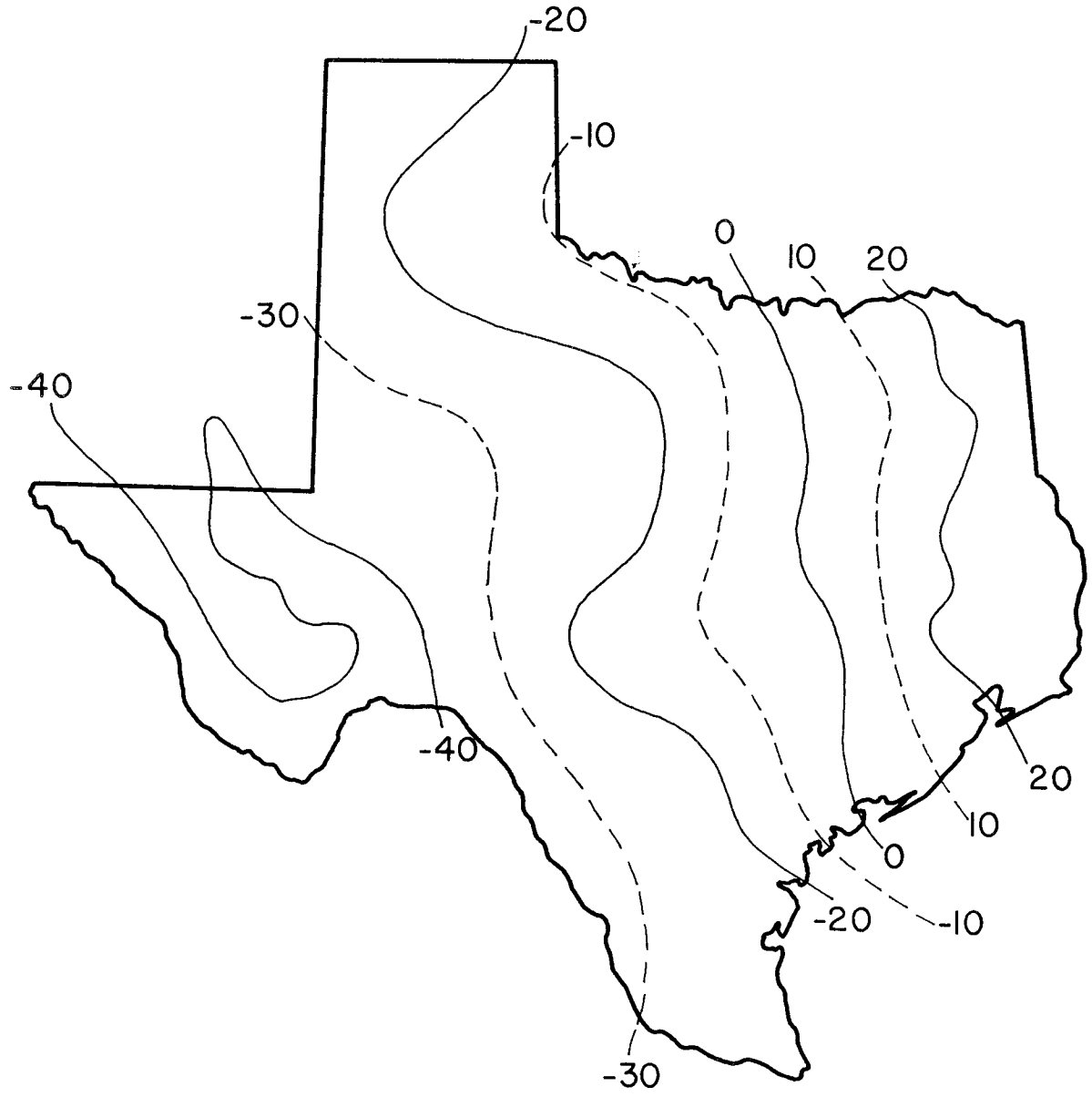

FIG. 8 - THORNTHWAITE MOISTURE INDEX (48)

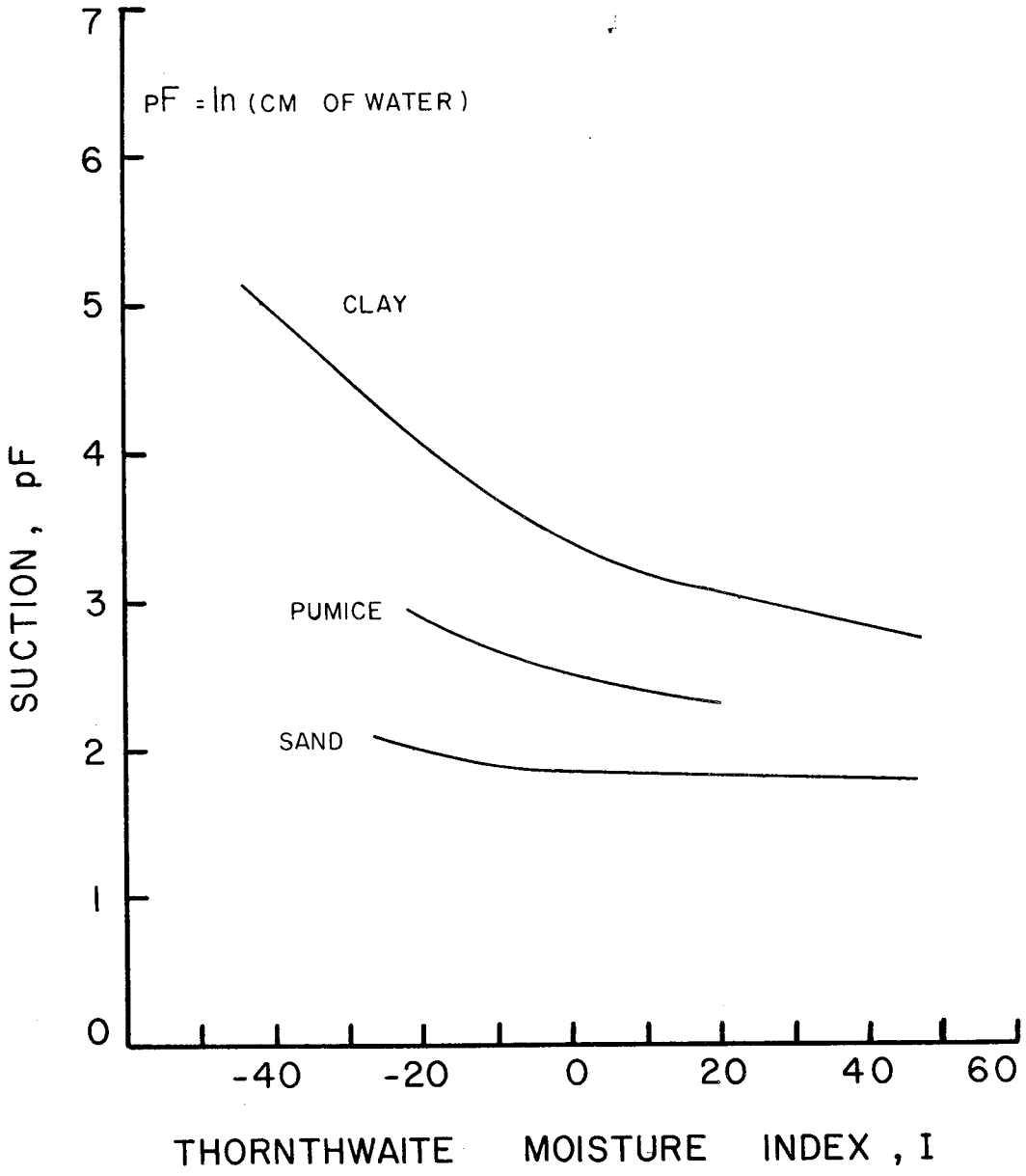

FIG. 9 - SUBGRADE SUCTION AS A FUNCTION OF THE MOISTURE INDEX (42)

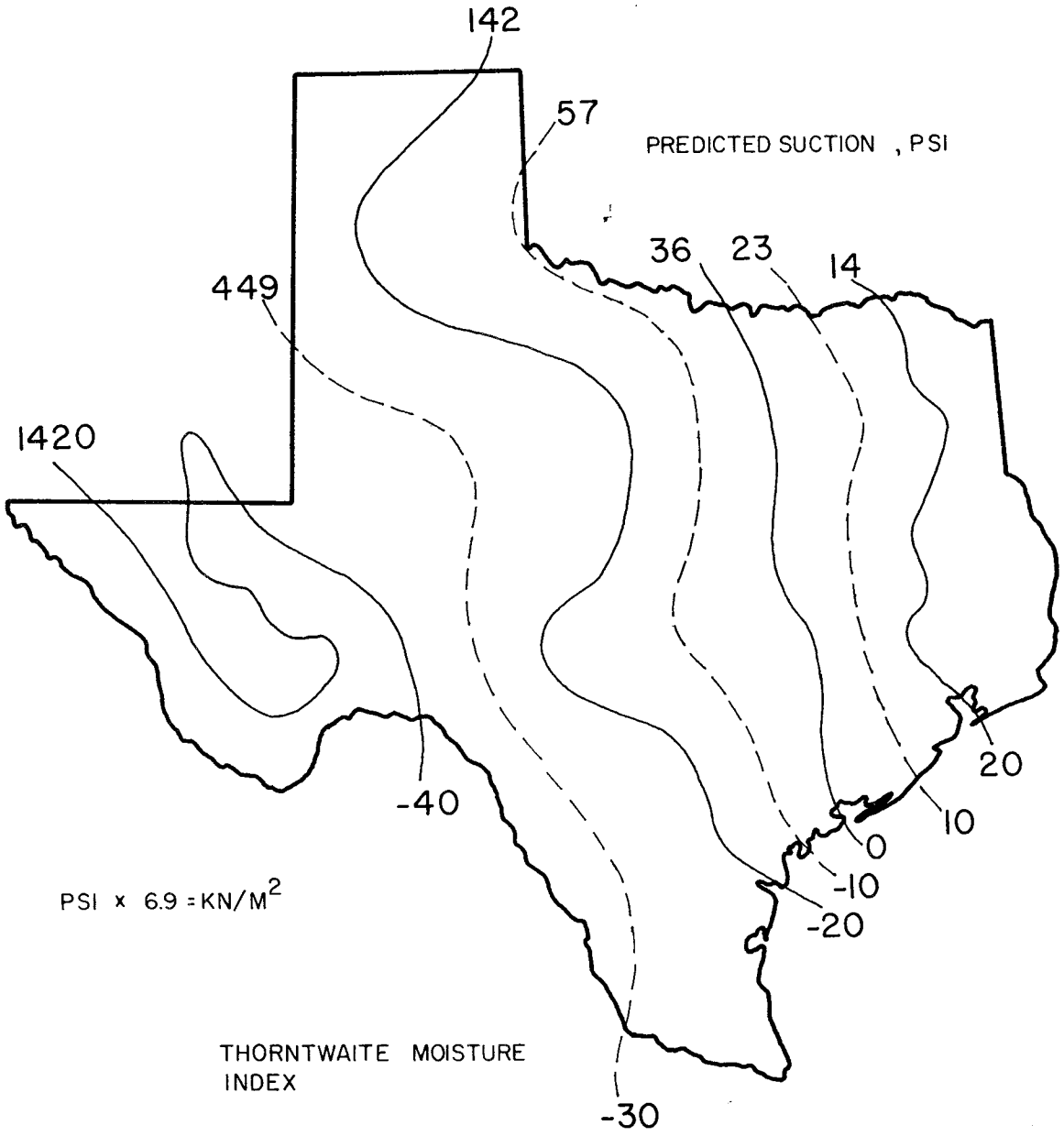

FIG. 10 - EXPECTED SUBGRADE SUCTION FROM MOISTURE INDEX , PSI

suction will vary with the existing type of subgrade soil). Suction measurements beneath newly constructed pavements have verified the relationship with the moisture index and will be discussed later in this section. The high suction values predicted for west Texas show that dry subgrades have the potential for drawing moisture out of overlying base course layers, thus causing shrinkage cracking.

Soil Moisture Suction

Soil moisture suction will be utilized extensively throughout this study to quantify the behavior of a soil material under environmental influences found in areas similar to west Texas; and as such an explanation of this relatively new engineering term and its importance in soil mechanics and highway design is in order.

Soil suction is derived from the study of moisture flow through soil media. The retention of water and the gradient which may cause flow is expressed as the free energy of the soil water relative to free pure water. The absolute free energy of a system may be expressed, as shown by Edlefsen and Anderson (16), as follows:

$$df = vdP - dw_m - sdT \qquad (1\text{-}2)$$

where

df = change in free energy,

v = specific volume,

dP = change in pressure,

dw_m = mechanical work,

dT = change in temperature, and

s = specific entropy.

With P and T constant, $df = -dw_m$, the decrease in energy is the work done. This says that if work is done to remove moisture the free energy will decrease. If the free energy of pure water is taken as a reference of zero the free energy of soil moisture in an unsaturated soil will be a negative quantity. Therefore the accepted procedure is to use the difference in free energy relative to zero for soil moisture systems, viz.

$$\Delta f = v \cdot \Delta P - s\Delta T - \Delta w_m \qquad (1\text{-}3)$$

This expression solved for suction (free energy) under isothermal conditions gives:

$$h = \frac{RT}{mg} \ln \frac{p}{p_o} \qquad (1\text{-}4)$$

where

h = suction, in cm of H_2O,

R = universal gas constant,

T = temperature in ^oK,

m = molecular weight of water,

g = gravitational force,

p = relative vapor pressure of soil moisture,

p_o = vapor pressure of free pure water.

This value represents the total suction of the soil moisture system. This total suction is composed of two major components, which are:

1. Osmotic suction which is the suction potential due to salts in the water portion of the three phase soil system.
2. Matric suction which is the suction due to the matrix, the soil particles themselves, which form capillaries.

The matric suction is of prime interest as it relates directly to the physical structure of the soil system. For most engineering problems, however, the osmotic suction is negligible and total suction may be used. This simplifies the measurement technique considerably as will be discussed in a later section.

An important point in the use of suction is that it is directly related to the moisture present and to the pore structure and size (1). The pore structure and size are in turn controlled largely by the clay minerals (particles less than 2 μm in diameter) present in the material. Thus any action effecting or affected by the clay mineralogy and particle size will affect the suction and cause a change that can be measured. Thus moisture removal due to a suction differential and freeze-thaw, which changes the phase of the water, will result in suction variations which will be directly related to the energy state in the sample.

Validation of Shrinkage Mechanism

The mechanisms proposed follow logically from the consideration of the environmental factors found in the west Texas area. The actual existence of these mechanisms must be validated by proper laboratory and field testing on base course material from west Texas. Seven samples of base course material were collected from west Texas. Table 1 gives the location of the pits and general soil information commonly available (52). These materials were selected to represent typical base courses being constructed in west Texas. Material passing the 3/8 in. (9.5 mm) sieve was used to construct samples at two compaction levels, Modified AASHTO, and Harvard Miniature calibrated to produce 95 percent of Modified AASHTO. equilibrium suction was measured in all samples and is discussed in detail in Appendix B. Figure 11 shows the resulting suction contours for one material which are similar to contours obtained by previous investigators. The suction levels near optimum moisture are considerably lower than the values expected to develop in the subgrade. Shrinkage cracking, thus, could be expected to develop if the predicted suction levels for the subgrade develop.

To validate this concept and to substantiate any laboratory data developed in this study, three field installations of psychrometers, to measure the suction, were made beneath newly constructed pavements. These installations, pictured in Fig. 12, consist of a set of six psychrometers. One psychrometer is buried in the virgin material off the shoulder. The remaining five are buried beneath the centerline of the pavement to a depth of five feet, the topmost psychrometer being embedded in the base course. Installations were made at Floydada, Ballinger, and north of Pampa, Texas, as shown in Fig. 1 (p. 2).

Psychrometers represent the most accurate and the most advanced technique available for measuring total suction both in the laboratory and the field. A psychrometer is pictured in Fig. 13. It consists of an extremely fine thermocouple bead encased in a

TABLE I. LOCATION AND SOILS DESCRIPTION OF SAMPLES

Sample No.	Location	Soil Description
4	Ochiltree County 13 miles S.E. of Perryton on US 83, District 4	mixed montmorillonitic
5	Lynn County, District 5 1 mile So. of Lubbock-Lynn Co. line, 1 mile W. of US 87	mixed, carbonitic
6B	Reeves County Weenacht Pit #2 Balhmorea, Texas	carbonitic, mixed gypsic
6JD	Martin County 2 miles East of Stanton on IH 20	mixed carbonitic
6FS	Pecos County Road cut material IH 20, Station, 840 to 0	carbonitic, mixed gypsic
7SA	Runnels County Storage pit on FM 2111	mixed, appreciable montmorillonite
6BAR	Midland Co. Barrow Pit., 1/2 mile West of Tower Road	mixed, carbonitic

See Fig. 1 (p. 2) for locations.

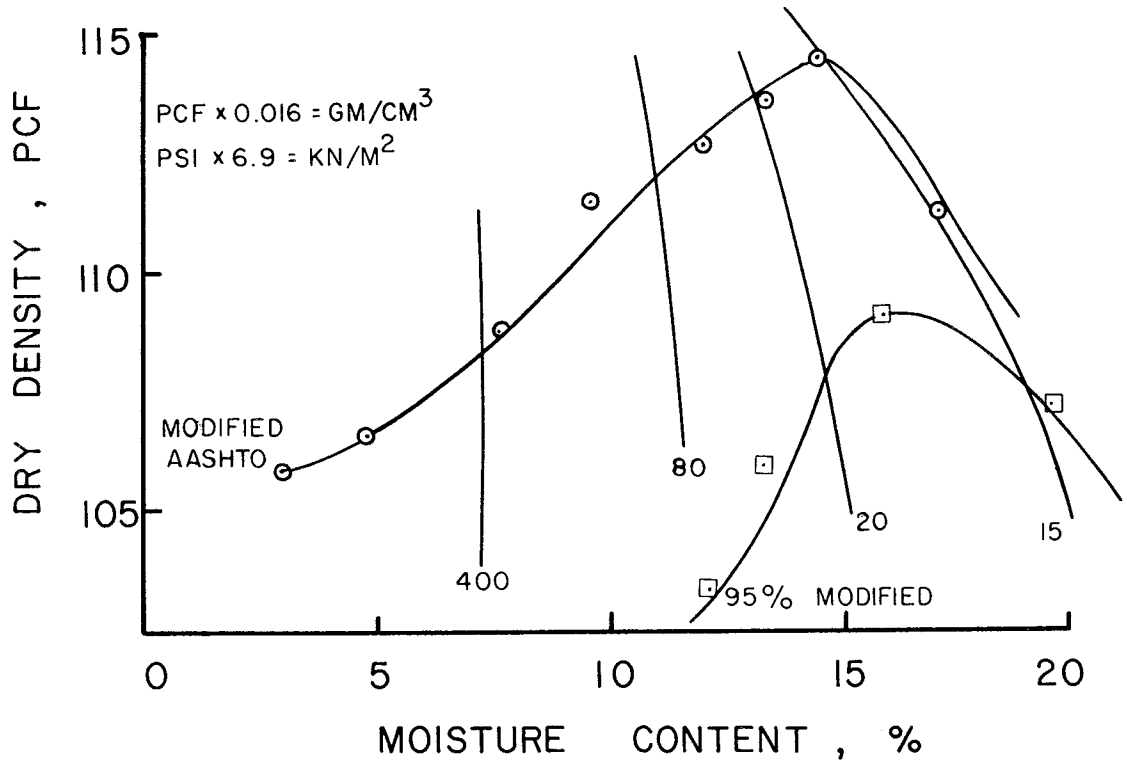

FIG. 11 - COMPACTION CURVE FOR DISTRICT 4 BASE MATERIAL WITH SOIL MOISTURE SUCTION VALUES, PSI

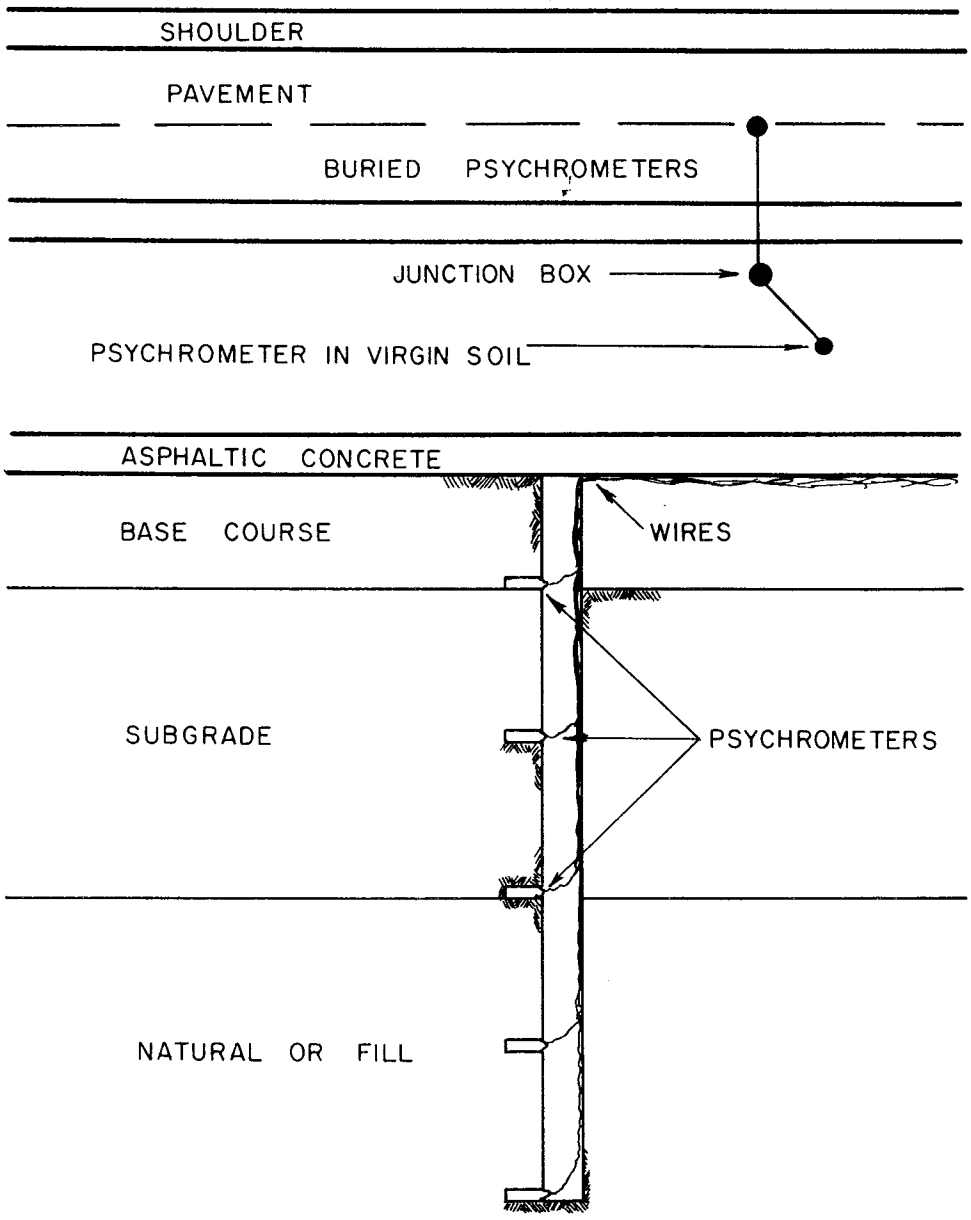

FIG. 12 - TYPICAL PSYCHROMETER INSTALLATION SHOWING PLAN AND PROFILE

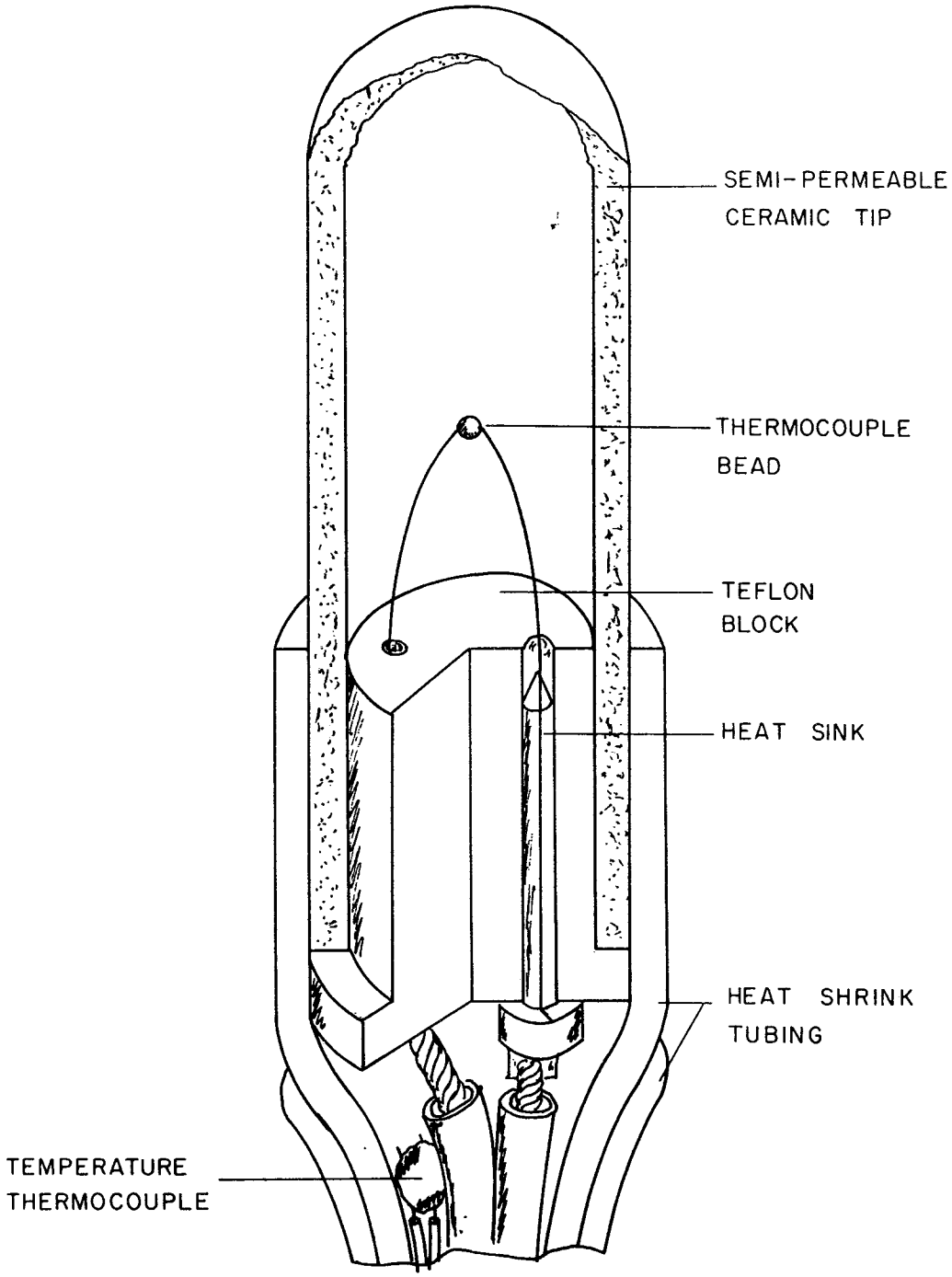

FIG. 13 - CROSS-SECTION VIEW OF A PSYCHROMETER

ceramic tip that is semi-permeable to moisture. The thermocouple bead is used to measure temperature. Soil moisture suction is determined by measuring the relative humidity of the soil moisture. This is accomplished by measuring the wet and dry bulb temperature using the thermocouple bead. The equipment and techniques used are described in detail in Appendix B. The essential point involves the dew point temperature and its change with change in the relative humidity. The thermocouple bead is electronically monitored at equilibrium to give the dry temperature. Next, by forcing a current through the thermocouple bead the temperature of the bead is lowered as a result of the Peltier cooling effect (41). This temperature drop condenses water on the thermocouple bead. When the cooling current is removed the water will be evaporated from the thermocouple bead inducing a temperature proportional to the rate of evaporation. This temperature is the wet bulb temperature. The difference in the two temperatures is proportional to the relative humidity and hence the suction.

This technique of determining soil moisture suction offers advantages over conventional devices such as the pressure plate or pressure membrane apparatus, tensiometers, gypsum blocks and resistivity gages due to its extended range and comparable accuracy in laboratory and field use. The psychrometer can measure only total suction; but as stated earlier, for an engineering analysis this will be sufficient.

The initial data collected from these psychrometers indicated the base course drying out from the subgrade was highly unlikely. Suction profiles for two of the installations are shown in Fig. 14. These clearly show the base course to possess a suction level well above that of the subgrade. This was typical of all measurements taken, regardless of soil types and pavement configuration. These data indicate that the base course, although initially placed at or slightly wet of optimum, dries out considerably before the asphaltic concrete surface is placed. This could result in the base course becoming five percent dry of optimum moisture which would produce the suction levels measured. Thus it

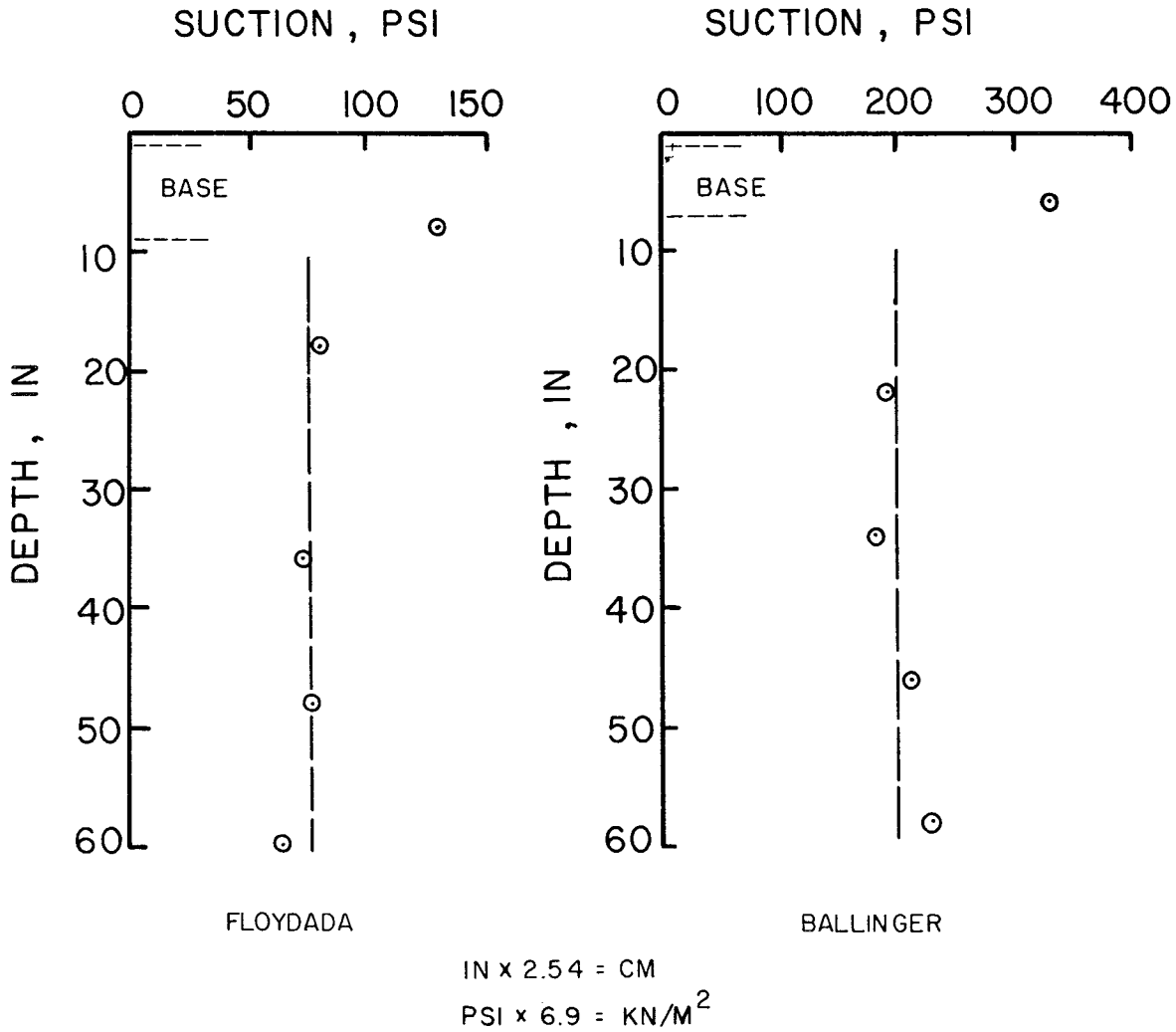

FIG. 14 - MEASURED SUCTION VALUES BENEATH TWO PAVEMENTS IN WEST TEXAS

may be inferred that due to construction practice the pavement as constructed is not at the same suction level as when it was initially compacted. The compaction curves for material 7SA, from the Ballinger installation, are given in Fig. 15 with measured suction values indicated. Allowing for a shift to the left for field compaction as is indicated in the report by Johnson and Scellberg (28), the suction near optimum would still be very much less than that measured in the base course in-situ.

The data show that although the Thornthwaite Moisture index-suction relation in Fig. 9 (p. 14) does accurately predict subgrade suction, the construction practices presently used produce a much drier base course than what is expected. Thus, the mechanism of shrinkage cracking, although a valid mechanism, is not viable in west Texas. This conclusion leaves freeze-thaw damage to the base course as the major remaining environmental deterioration mechanism.

Validation of Freeze-Thaw Mechanism

A report by H.P. Carothers (9) involved the study of freeze damage to pavements across the entire state of Texas. His conclusions were that the freeze damage in Texas was centered in the base course. The majority of the damage involved soft material which barely passed durability testing and often produced excessive fines during compaction. Although frost heave, or "boils", were not noted as causing the deterioration, the progressive damage of the pavement clearly involved excessive moisture reaching the base course. Shortly after this study the Texas State Department of Highways and Public Transportation began implementing more stringent controls on the base course materials used. The damage, however, has continued in the form of transverse cracking. The tighter controls only altered the mechanism acting. The fact that freeze damage will initiate mainly in the base course cannot be changed.

In the study reported here freeze-thaw susceptibility tests were initially set up to determine if there would be appreciable strength loss due to the freeze-thaw cycling, as was indicated in previous studies (5). It was not expected that Hamilton's

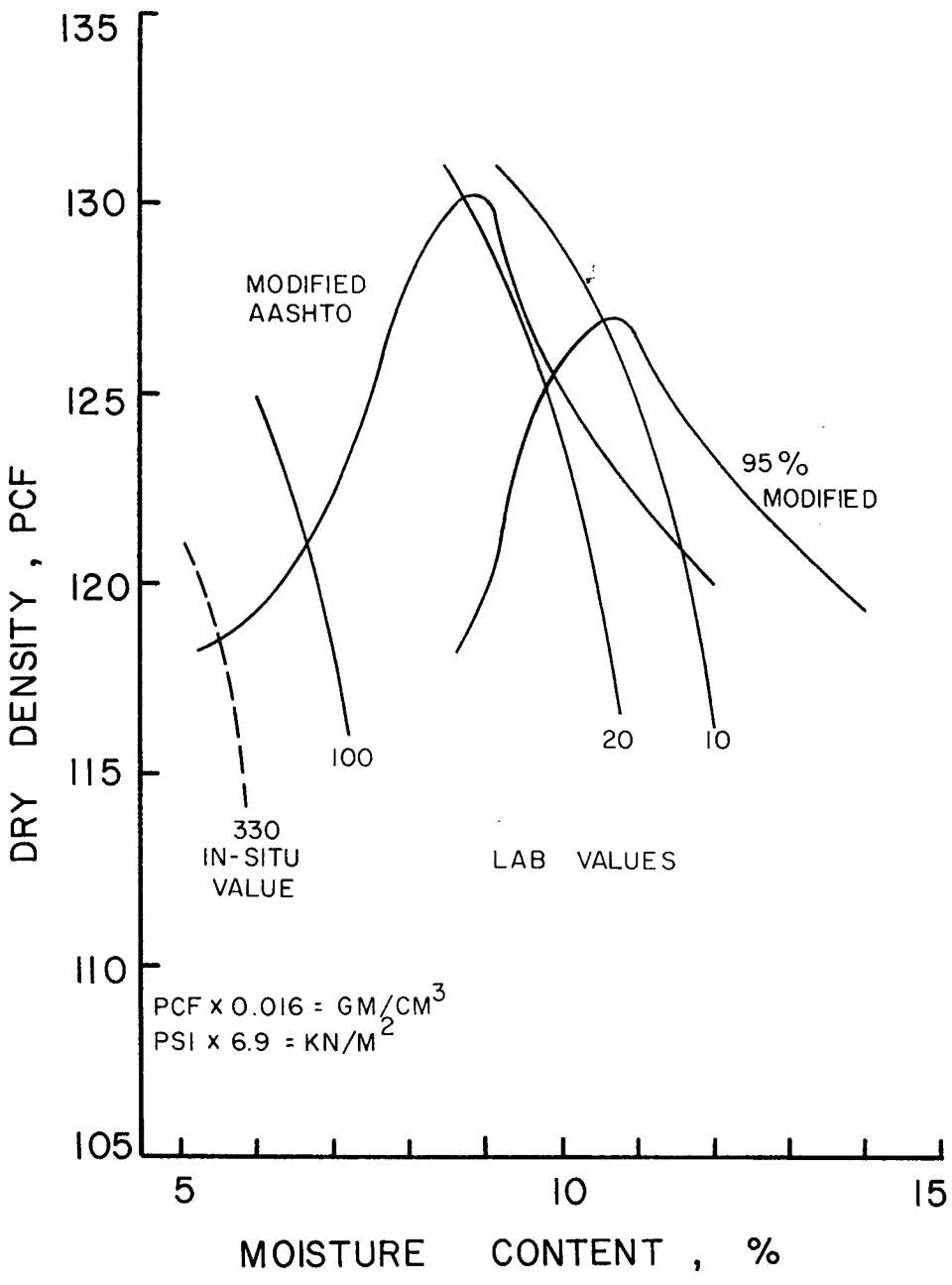

FIG. 15 - MOISTURE-DENSITY CURVE WITH LABORATORY AND FIELD SUCTION LEVELS SUPERIMPOSED, PSI

results could be duplicated in the low clay content base course materials being used here. Volume measurements on the samples, however, indicated that they were undergoing continual volume change during a series of freeze-thaw cycles in such a manner that a form of cracking similar to shrinkage cracking mignt develop. Because of this, a series of comprehensive freeze-thaw tests and property measurements was established to determine if the noted behavior could be considered typical of base course in use in west Texas, and whether the behavior could be predicted from material properties.

As will be shown later, the measured thermal activity of the base course is quite large, which raises the problem of thermal cracking in the base course due to excessive tensile stresses. The tensile stress in an initially uncracked pavement, for any layer, is given as follows:

$$\sigma = E\alpha(\Delta T) \qquad (1\text{-}5)$$

where σ=tensile stress,

E=Young's modulus,

α=coefficient of thermal activity, and

ΔT=temperature change.

The measured values for the base course were ten times larger than those for asphaltic concrete (47). The temperature change will be similar for both the base course and the asphaltic concrete. The Young's modulus for the base course will be about one-half of the value for the asphaltic concrete. The tensile stress for the base course will be nearly one-third of that for the asphaltic concrete. With these properties the base course will be expected to crack, and crack first. This is due primarily to the thermal activity of the base course and the magnitude of the freeze coefficient.

Summary

This chapter develops the concept of environmental damage to a pavement. Shrinkage due to suction diffferentials between the base course and subgrade were investigated as plausible mechanisms. For the west Texas area, however, freeze-thaw damage appears to be the only

viable deterioration mechanism; and it apparently acts in a manner completely different from previously proposed theories. The quantity termed soil moisture suction and its measurement are discussed; and the relationship with particle size, pore structure and clay mineralogy were developed. The data collection and material property relationships necessary to describe the freeze-thaw nechanism will be described in the next chapter.

DATA COLLECTION AND MATERIAL PROPERTY RELATIONSHIPS

Thermal susceptibility has been determined to be an important mechanism acting in a base course material. This chapter details the sample preparation and data collection for the seven base course materials used in this study. The relations of observed behavior with material properties is also discussed to provide insight into the cause of the mechanism.

Sample Preparation

Each material was received in sample sacks as taken from the storage pit. The material was sieved and all material was passed through a 3/8 in. (9.5 mm) sieve although the AASHTO compaction specifications for compaction call for the use of material passing the 1¼ in. (6.4 mm) size. The use of the larger aggregate was an attempt to better model the actual behavior of the material in-situ. The use of an excessive percentage of fines in the samples might tend to accentuate their behavior and give data not directly applicable to the solution of field problems.

Each material was compacted at two energy levels. The first level was Modified AASHTO, produced with the standard equipment. The second level was 95 percent of Modified using a Harvard Miniature spring loaded tamper (31). The importance of this method of compaction will be discussed later. These compactive levels produced two distinct curves for each material which allow the effects of compaction to be studied. The material was hand mixed at a given moisture content and stored overnight before compacting.

When the modified AASHTO samples were compacted, a small metallic rod was compacted in the middle layer. This rod was located, after extrusion from the mold, with a magnet and removed with a minimum of disturbance to the surrounding sample. A psychrometer, the same size as the rod, was then inserted into the void. These samples,4 in. (10.2cm) by 4.6 in. (11.7 cm) were

then wrapped in foil and sealed in wax. The psychrometers were read continuously until the moisture had become evenly distributed and an equilibrium suction value was obtained, typically three to four weeks after the sample was compacted. Once equilibrium was attained the samples were ready for freeze-thaw testing.

The psychrometers were left in the samples to monitor suction during freeze-thaw testing. This involved the removal of the wax and tin foil from small areas on the top, bottom, and sides. These openings were sealed by a thin plastic wrap with a wax seal around the edges. This is shown in Fig. 16 for both types of samples tested. This arrangement allowed measurements to be made without opening the seals, thus maintaining a constant moisture content with a minimum amount of manipulation of the sample.

The Harvard miniature samples were prepared in the same manner. However, the psychrometers were not embedded in these samples due to the small size, 2.8 in. (7.1 cm) by 1.3 in.(3.3 cm), but were sealed with the sample under the tin foil and wax to obtain equilibrium suction values. This method was not as satisfactory as the insertion procedure used in the larger samples. The volume measurements were made using a dial gage mounted on a tripod assembly and a micrometer.

The results of the compaction and equilibrium suction measurements indicate there is quite a variation between different materials which should indicate that a variety of behavior under freeze-thaw testing would be obtained. The results are comparable with results obtained by other researchers using different measurement techniques (42).

Freeze-Thaw Test Procedure

There are a variety of freeze-thaw testing procedures currently in use and each has only a narrow range of application. A base course in west Texas experiences dynamic temperature changes and not the prolonged cooling experienced in the Northern climates as will be illustrated in a subsequent chapter. Additionally, the

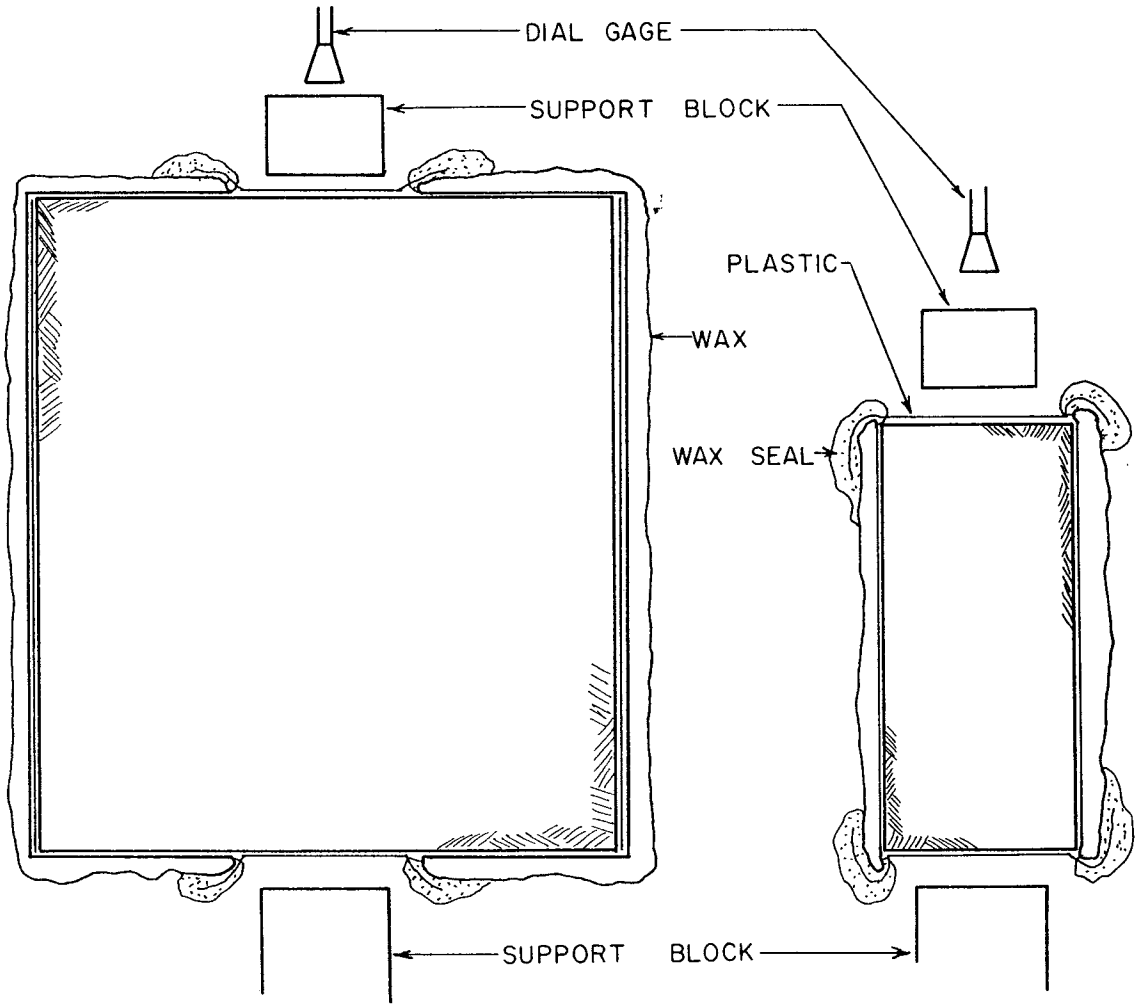

FIG. 16 - ILLUSTRATION OF SAMPLE PREPARATION TO ALLOW MEASUREMENT OF LENGTH AND DIAMETER WITHOUT OPENING SAMPLE

water table for most of west Texas is an appreciable distance below the pavement. The closed system of freezing maintains constant moisture content in the sample being frozen while the open system allows the sample free access to moisture and is of major importance primarily in the study of frost heave. Biaxial freezing was chosen since uniaxial freezing is normally important only in frost heave studies where the frost line slowly advances through the sample.

On the basis of the results obtained by Hamilton (21) in which a low temperature of $20^{o}F$ ($-6.7^{o}C$) produced essentially all the volume change, the samples were placed in a $20^{o}F$ ($-6.7^{o}C$) environmental room for freezing. Suction and deformation readings were taken after the samples were frozen and after thawing. The modified AASHTO samples were frozen for 24 hours and thawed for a similar length of time while the Harvard Miniature samples were frozen in eight hours, due to their small size, and were allowed to thaw for 16 hours.

Data Obtained From Freeze-Thaw Tests

General Description

The data collected from the freeze-thaw portion of the investigation of the base course material may be presented in three separate categories. The categories are as follows:

1. Freeze Deformation. This deformation is that caused by the freeze portion of the cycle, part of which is typically recovered during the thaw portion of the overall freeze-thaw cycle.
2. Residual Deformation. This is the deformation that is not recovered during the thaw portion of a freeze-thaw cycle. This is a permanent deformation.
3. Suction Variations. These values represent the utilization of the moisture during the freeze-thaw cycle and give an indication of the physical process occurring in the material.

These areas are discussed more fully in the following sections.

Freeze Deformation

Fig. 17 shows the thermal behavior of two samples of the same material compacted at different moisture contents. The two samples demonstrate drastically different, although predictable, behavior. The freeze deformation is shown as the change in height from a thawed condition to a frozen condition. The two samples pictured demonstrate that this deformation may be either expansion or contraction.

As this deformation represents the total change in height due to a temperature drop from ambient to below freezing it is necessary to consider the deformation in two parts, one above freezing and the other below freezing, as indicated in Hamilton's study. The first coefficient represents the ten percent change that occurs from ambient down to freezing. It may be expressed as follows:

$$TC = \left[\frac{\frac{\Delta H}{H_o}}{\Delta T_1}\right] \times 0.1 \qquad (2\text{-}1)$$

where

TC = the thermal coefficient in strain per ^{o}C,

ΔH = the change in height,

H_o = the initial height, and

ΔT_1 = the change in temperature from ambient down to freezing, in ^{o}C.

The second, and more important, coefficient is termed the freeze coefficient. It represents the change in dimensions from $0^{o}C$ to $-6.7^{o}C$ and is expressed as follows:

$$FC = \frac{(0.9)(\Delta H/H_o)}{6.7^{o}C} \qquad (2\text{-}2)$$

where the variables are as previously defined.

As was previously mentioned in reference to Fig. 17, the freeze behavior may be expansion or contraction. The relationship is illustrated in Fig. 18, which shows the freeze coefficient

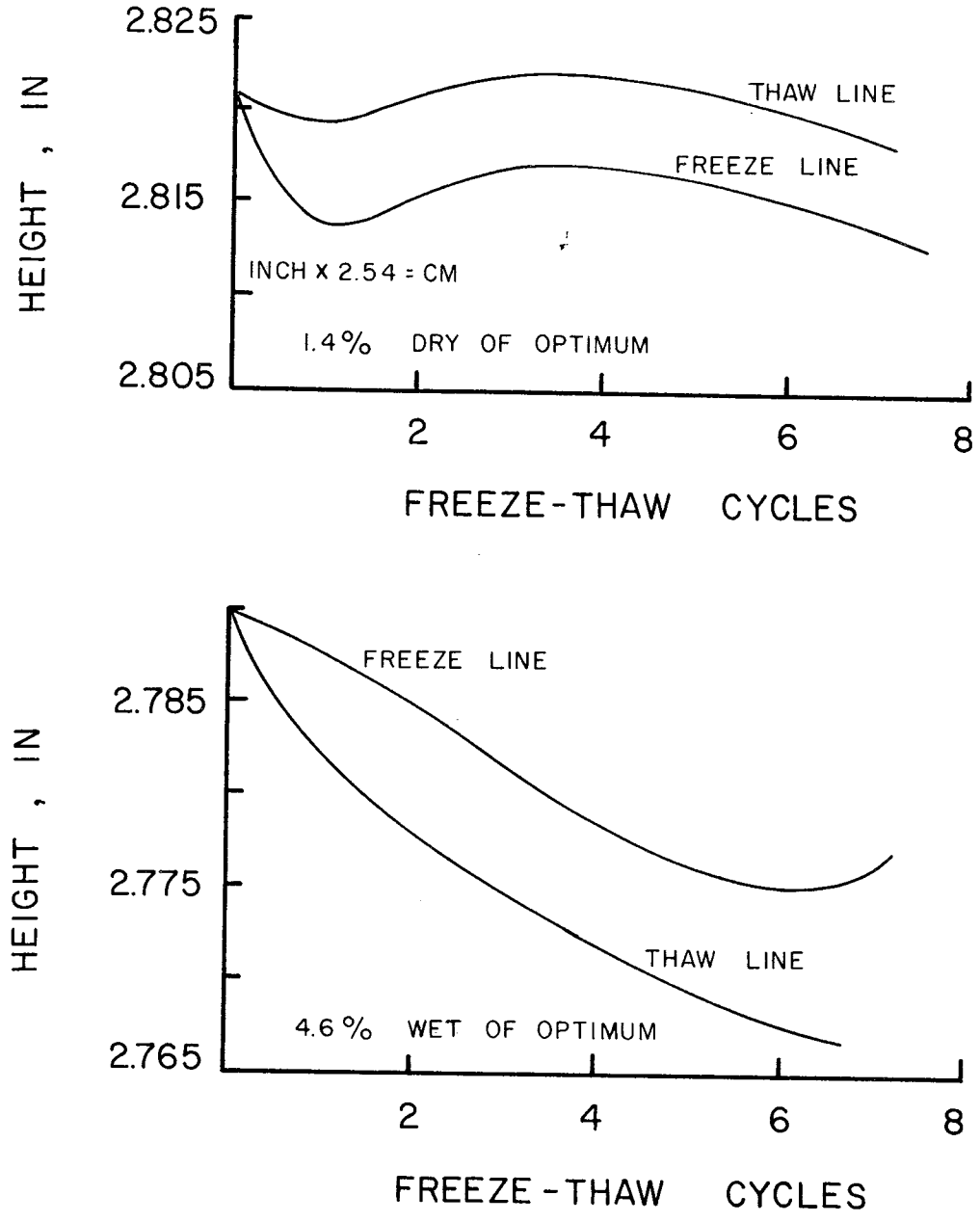

FIG. 17 - SAMPLE HEIGHT AS A FUNCTION OF FREEZE-THAW CYCLES

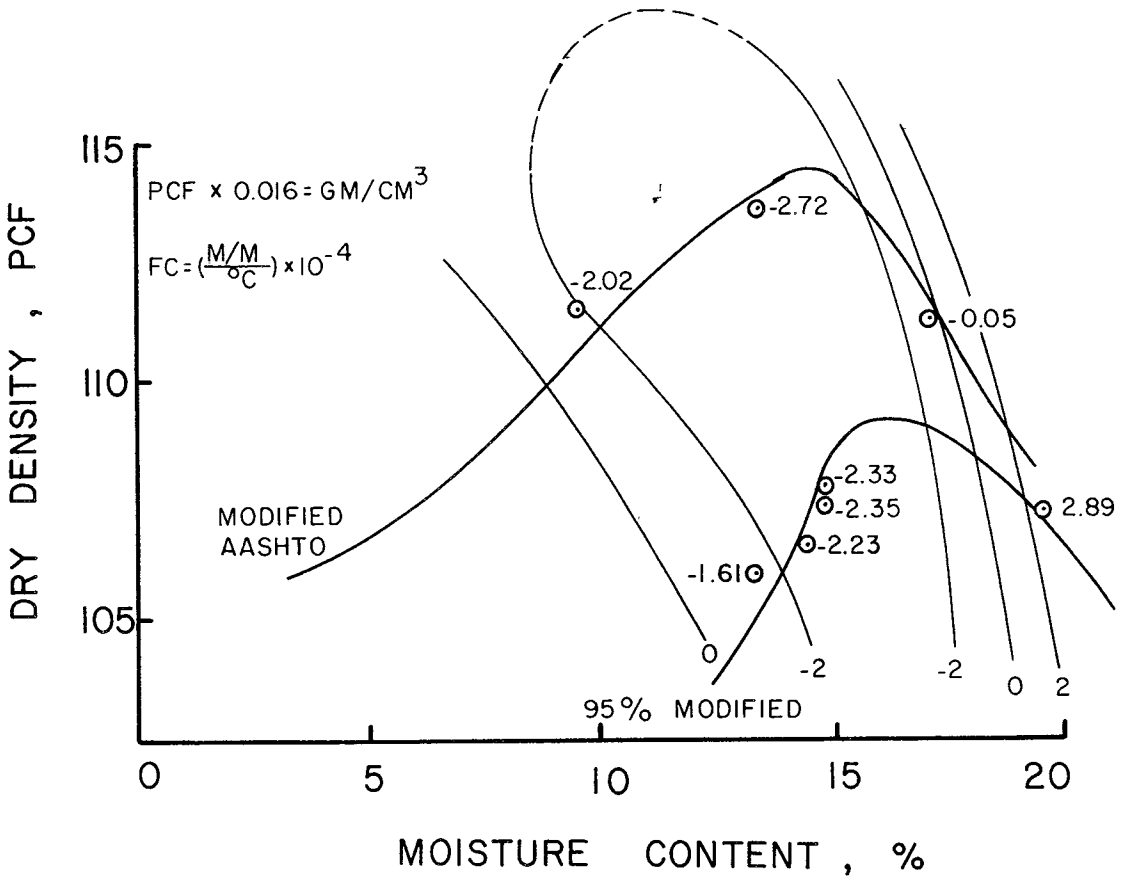

FIG. 18 - FREEZE COEFFICIENTS PLOTTED ON THE MOISTURE DENSITY CURVES FOR MATERIAL 4

superimposed over the moisture density curves. This relationship is similar to that obtained by Hamilton for a clay subgrade. There is an influence due to compaction as well as moisture which is brought out in this figure and which will be explained later in developing the mechanism.

Residual Deformation

Referring again to Fig. 17 (p.34) the two samples yield different residual deformation patterns. The residual deformation is the total deformation from the original value, that is never recovered. This deformation, similar to the freeze deformation, may be either expansion or contraction.

Unlike the freeze deformation the residual deformation cannot be used to calculate a constant coefficient of contraction or expansion since the residual deformation changes constantly with additional loadings in much the same manner as shown in repetitive triaxial loading tests. This similarity provides the initial relationship in the analysis of the data. The plot of residual strain ($\Delta H/H_0$) as a function of the logarithm of the number of freeze-thaw cycles is shown in Fig. 19. This plot produced a straight line relationship for all material tested. The applicability of this relationship is demonstrated in Table 2, which lists the regression coefficients and the statistical coefficient of determination, R^2.

From these straight line relationships the slope, B_1, could be calculated from the best fit line by standard linear regression techniques. This value, B_1, is a measure of the permanent deformation that will occur per freeze-thaw cycle after the first cycle. These values are plotted on the moisture density curves in Fig. 20. Again there is a noticeable influence due to moisture and compaction effort although not necessarily the same influence as was noted for the freeze behavior.

Suction

The equilibrium, or as-compacted, suction was determined over the entire range of the moisture density curves by the techniques

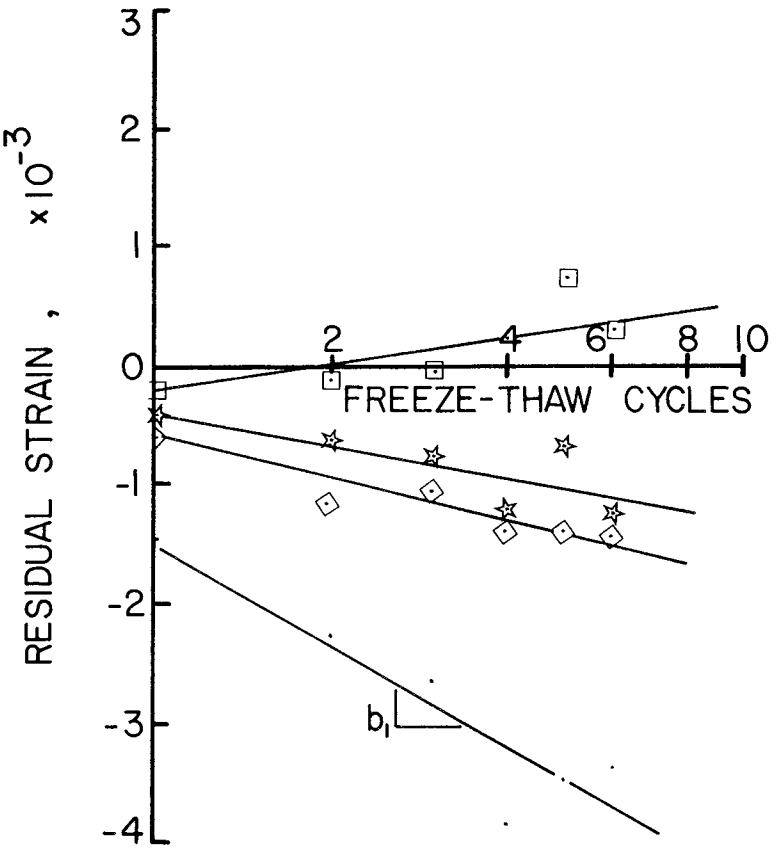

FIG. 19 - RESIDUAL STRAIN PLOTTED AGAINST LOG_{10} NUMBER OF FREEZE-THAW CYCLES, MATERIAL 4

TABLE 2. - REGRESSION RESULTS FOR RESIDUAL COEFFICIENTS

Material	Moisture Content	Residual Coefficient Equation $B_0 + B_1$ (Log #F-T)	R^2	Compactive Effort
4	17.1	-0.00150, -0.002806	0.85	Modified
	14.3	-0.00675, -0.000970	0.89	Harvard Miniature
	20.7	-0.004095, -0.004846	0.82	Harvard Miniature
	18.5	-0.002013, -0.005907	0.98	Harvard Miniature
5	10.0	+0.001523, -0.002129	0.79	Modified
	11.8	+0.003455, -0.002558	0.87	Modified
	12.9	-0.01361, -0.00155	0.64	Modified
	14.3	-0.004308, -0.00201	0.93	Modified
	13.3	-0.002756, -0.001084	0.51	Harvard Miniature
	17.0	-0.004134, -0.007537	0.43	Harvard Miniature
	18.2	+0.00889, -0.00931	0.60	Harvard Miniature
6B	9.1	+0.000309, -0.002136	0.86	Modified
	11.9	-0.0164, -0.001897	0.75	Modified
	12.5	-0.002739, -0.00381	0.81	Harvard Miniature
	13.9	-0.00241, -0.00337	0.81	Harvard Miniature
	15.7	-0.00116, -0.000899	0.48	Harvard Miniature
6JD	3.8	-0.007861, -0.001087	0.86	Modified
	8.5	-0.00414, -0.001667	0.93	Modified
	12.6	-0.001409, -0.009694	0.90	Modified
	9.7	-0.000759, -0.001194	0.64	Harvard Miniature
	12.0	-0.003289, -0.007268	0.93	Harvard Miniature
	14.6	-0.005399, +0.007212	0.91	Harvard Miniature
6FS	3.5	-0.0001688, +0.0005663	0.41	Modified
	5.1	-0.000293, -0.001102	0.69	Modified
	10.3	+0.000663, +0.005834	0.99	Modified
7SA	8.5	+0.0003349, +0.001972	0.67	Modified
	8.8	+0.00003253, -0.001006	0.95	Harvard Miniature
	11.1	-0.001906, -0.007479	0.96	Harvard Miniature
	12.2	-0.001311, -0.005464	0.83	Harvard Miniature
	14.1	-0.00582, -0.005116	0.98	Harvard Miniature

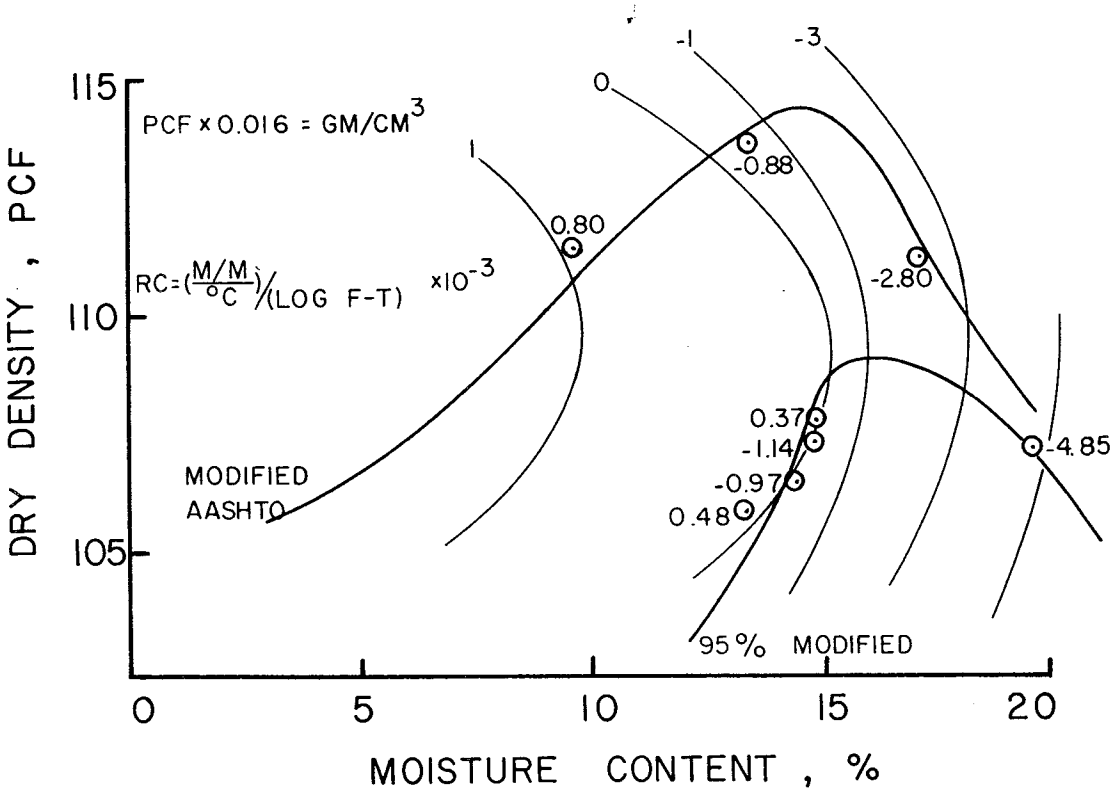

FIG. 20 - RESIDUAL STRAIN COEFFICIENTS PLOTTED ON MOISTURE-DENSITY CURVES FOR MATERIAL 4

previously discussed. Figure 11 (p. 20) showed the suction values for material 4 plotted on the moisture density curves. This relationship is typical of values determined by other investigators for a wide range of soil materials (42, 45, 1). The major feature of this information is that compaction effort has a minimal effect on the suction within the range of compaction levels normally used. The major factor in determining the suction level for any one material is the moisture content.

The fact that moisture plays such an important role in both the thermal activity and the development of the as-compacted suction indicates that a relationship with suction may be formed to predict the thermal activity of a base course. This relationship will be described further in the development of the mechanism.

The suction was monitored in the modified AASHTO samples during the freeze-thaw cycling as mentioned previously. The data collected show that the suction increased drastically when the sample was frozen. Upon thawing the suction returned to a level slightly below the original as-compacted value, indicating an internal change in the sample. Typical data in Fig. 21 show this trend for two samples compacted at different moisture contents. These data are extremely important when interpreting the proposed mechanism for freeze-thaw activity.

Basic Properties.-- For each material there were several standard tests run to determine some basic properties. These tests include:

1. Specific gravity, G_s,
2. Liquid limit, W_l,
3. Plastic limit, W_p, and
4. Grain size distribution

and are shown in Table 3.

It is evident that there is very little difference in these basic properties of the materials. There was also no difference in the grain size distribution. As suction is influenced by the grain sizes, especially the finer fractions, the type of clay mineral present could be expected to have a major

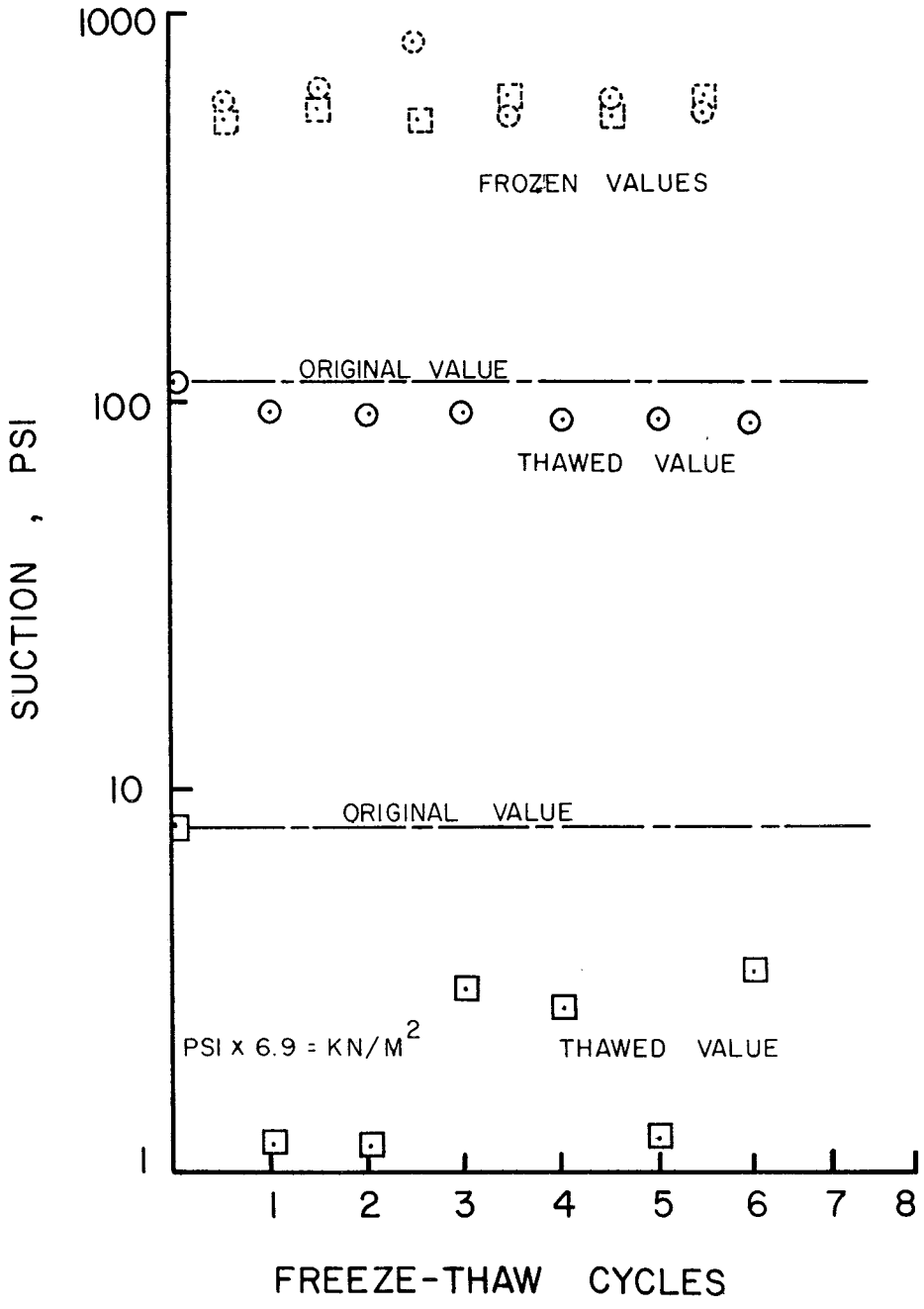

FIG. 21 - SUCTION VALUES DURING THAW CYCLE FOR TWO SAMPLES WITH FROZEN VALUES INDICATED

TABLE 3. PROPERTIES OF BASE COURSE MATERIAL TESTED

Material Number	Specific Gravity	Percent Fines (-#200 sieve)	Liquid Limit (%)	Plastic Limit (%)	Percent Clay (-2μ)	Maximum Freeze Coefficient $(\frac{M/M}{^{o}C})$
4	2.65	10	30	21	9.0	-2.7×10^{-4}
5	2.68	9	32	21	7.7	-2.5×10^{-4}
6B	2.67	10	27	17	6.2	-1.3×10^{-4}
6JD	2.69	10	22	18	4.3	-4.0×10^{-4}
6FS	2.66	9	17	16	1.6	-0.5×10^{-4}
7SA	2.68	10	22	12	6.5	-1.85×10^{-4}

influence on the behavior of the material. A clay mineralogy study was conducted to obtain this information.

Clay Mineralogy Investigation

Importance of Clay Mineralogy in Moisture Interaction

The moisture condition in a soil-aggregate system is a complex mechanism which is not yet fully understood. As such the connection and relationship with engineering phenomena have not been pursued to a great extent. The problem of freezing in a soil system is even more complex and uninvestigated. The nature of the problem of freezing soil requires an examination of the clay-water system as a basis for a mechanism of freeze-thaw damage in base course material.

A typical soil aggregate system, as commonly accepted, is shown in Fig. 22. The three basic components are the soil, water and air. The soil must be considered as being composed of aggregate, sand, silt and clay, with the clay being composed of different clay minerals. The water is composed of free water and an adsorbed water, the properties of which will depend on the type and amount of clay minerals. During freezing it is the interaction of the free and adsorbed water with the pore structure, formed mainly by the clay minerals, that is important.

The adsorbed water possesses a structure very different from that of the free water (18,36). The structure of the clay particle surface and the water molecule are such that the water molecules are pulled into a preferred orientation. Hendricks and Jefferson (23) have suggested a concept that has found widespread acceptance. In this concept the water molecules are attracted to the surface of the clay mineral by a hydrogen-oxygen bond causing rotation. This rotation of water molecule brings the remaining hydrogen atom into the plane of the oxygen atoms. This hydrogen atom is in turn attracted to the oxygen atom of the next water molecule, in the same layer, forming a hexagonal net of water molecules bonded to the clay surface. This net of water

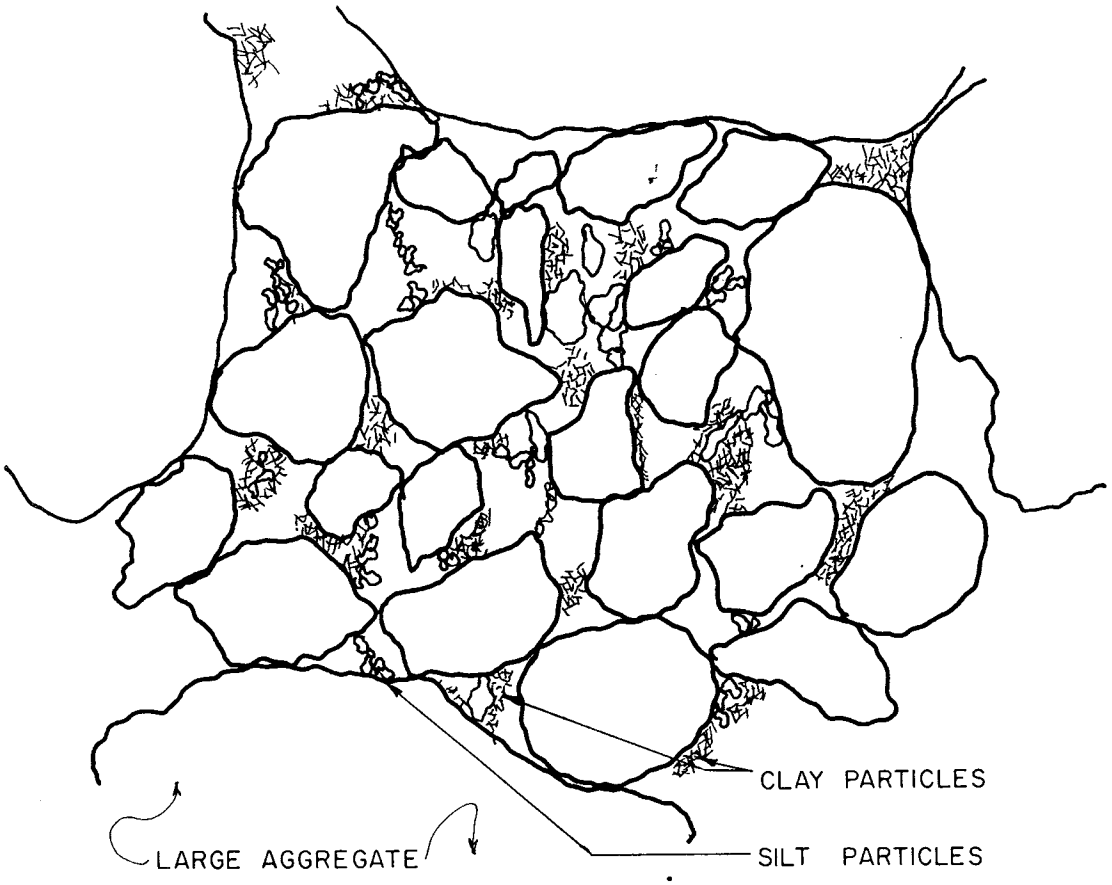

FIG. 22 - TYPICAL SOIL-AGGREGATE SYSTEM

molecules is capable of propagating itself away from the clay mineral surface with a structure that is essentially that of ice. A paper by Low and Lovell (32) discusses the nature of adsorbed water in more detail ; however, this general idea of structured water is sufficient for this study.

When a soil-water system freezes, the adsorbed water does not readily freeze and some free water held in very small pore spaces also does not freeze (32). As both the amount of adsorbed water and the pore structure are a function of the type and amount of clay minerals present, the clay mineralogy may help relate unfrozen moisture to the thermal activity.

Clay Mineralogy Determination

The universally accepted method for determining what minerals are present is x-ray diffraction analysis. The seven base course samples were prepared according to a procedure used by Dixon in his Soil Mineralogy course (14), as shown in Appendix C. This procedure involves the removal of carbonates and organics by treatment with acid and hydrogen peroxide. The remaining particles are composed of the clay minerals and the sand and silt sized particles. This material is then separated into different size fractions to concentrate the clay minerals.

The amount of material in each size fraction is shown in Table 4. The amount of carbonate for these base course materials is quite high since the major constituent is limestone, a calcium carbonate. Very little organic matter was noted in any of the material examined. The amount of carbonates lost is equivalent for all of the base course materials except for material 6FS. This difference will be discussed when the results for the material are presented subsequently.

Material 4 underwent more testing than the subsequent samples; and the data obtained for material 4 serve to show that the quantities obtained for the remaining materials are reasonably correct.

Material 4 underwent the following tests:

1. X-Ray Diffraction

TABLE 4. FRACTIONATION DATA

Material / Size fraction	4	5	6B	6JD	6FS	6BAR	7SA
>75 µm	8.7036	6.9051	7.8042	6.7461	0.3408	5.7269	9.0468
50-20 µm	0.7899	1.0462	1.8322	0.7869	0.3033	0.7515	1.5484
20-5 µm	0.5573	0.5259	1.1974	2.952	0.1643	0.7355	0.6161
5-2 µm	0.2363	0.3016	0.2413	0.2666	0.1005	0.1853	0.1766
2-0.2 µm	0.6450	0.5460	0.8440	0.3690	0.0542	1.3950	0.6710
<0.2 µm	0.5188	1.942	1.1260	1.0710	0.5340	1.0324	1.3110
Total	11.4501	11.2698	13.0451	9.5348	1.4971	9.8266	13.3699
Original Amount	19.3792	25.5445	23.9225	24.7697	25.9052	23.5997	23.7316
% Recovery	58.10	44.12	54.53	38.49	5.78	41.64	56.34
% Clay #	10.0	22.0	15.2	15.0	39.2	24.7	14.8

#based on percent recovered, not on original amount of material used which contained large sizes.

A. 50-20 μm fraction
B. 20-5 μm fraction
C. 5-2 μm fraction
D. 2-0.2 μm fraction } CLAY SIZE FRACTIONS
E. <0.2 μm fraction }

2. Differential Thermal Analysis,
3. Cation Exchange Capacity Determination, and
4. Electron Microscope Investigation.

X-Ray Diffraction.-- 50 milligram samples of the two clay fractions were saturated separately with potassium and magnesium ions as set forth in Appendix C. Each sample was then treated with a 10 percent glycerin-water solution to expand clay minerals with expansible layers such as montmorillonite. These solutions were poured onto slides and allowed to dry. This gives them a preferred orientation which enhances the x-ray diffraction technique. The potassium saturated samples were dried on special Vikor slides. These slides are heat resistant as they will be heated to 500°C to collapse the montmorillonite.

The <0.2μm fraction is shown in Fig. 23. These series of x-ray diffraction patterns clearly show the collapse of montmorillonite into a 10 Å mineral spacing. The minerals present in these patterns include montmorillonite, mica, attapulgite, kaolinite and possibly some quartz.

The 2-0.2μm fraction is shown in Fig. 24. This series of x-ray diffraction patterns shows the same mineralogy as the finer <0.2μm fraction. It is felt that the fractionation procedure did not adequately separate the particle sizes. Montmorillonite is extremely fine sized and in all probability should not have shown up in the 2-0.2μm and larger fractions.

The 5-2μm fraction shown in Fig. 25 contains montmorillonite, quartz and some kaolinite as indicated. The 20-5μm fraction shows an increase in the quartz peak and an indication of feldspar. This is to be expected as these sizes are into the sand and the silt size ranges. The 50-20μm fraction clearly indicates an extensive amount of quartz. Feldspars are indicated by the triplet of peaks

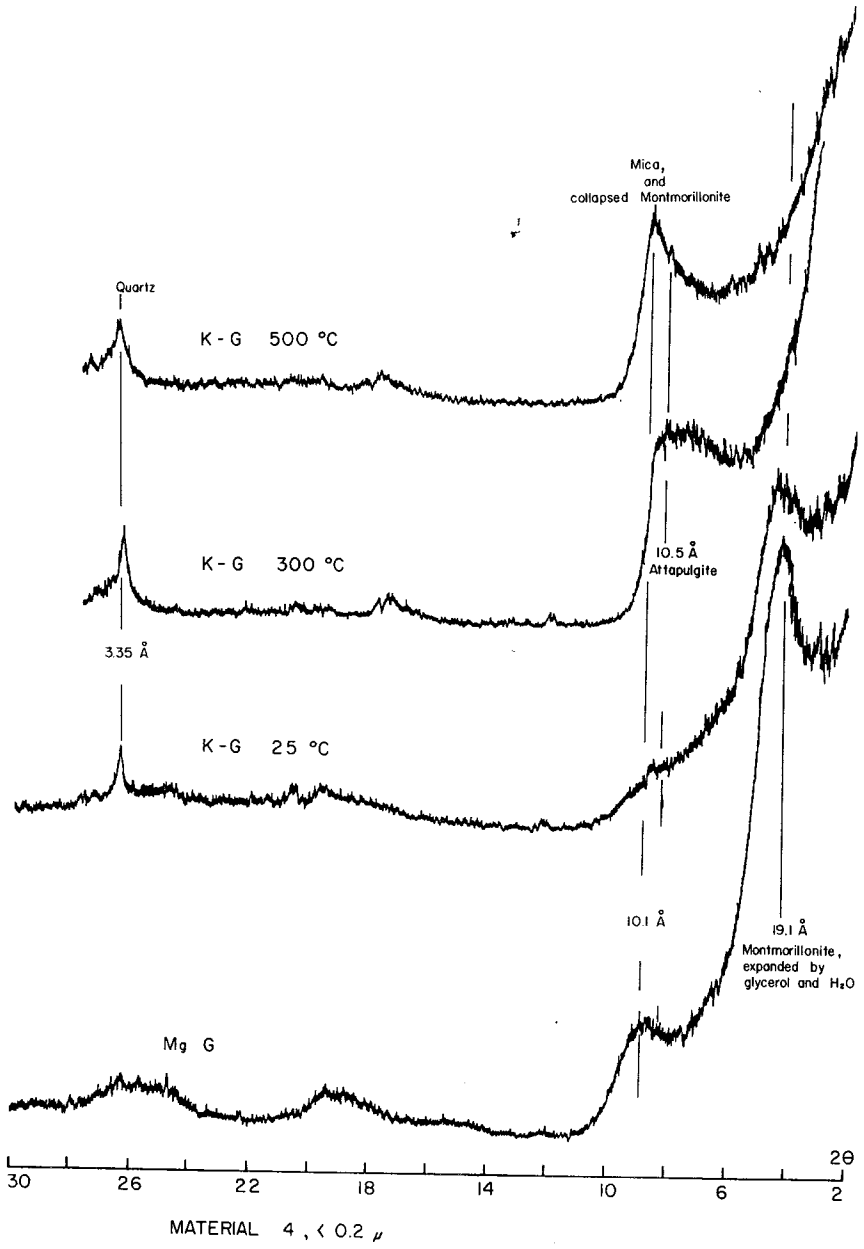

FIG. 23 - X-RAY DIFFRACTION PATTERN, <0.2μm FRACTION, MATERIAL 4

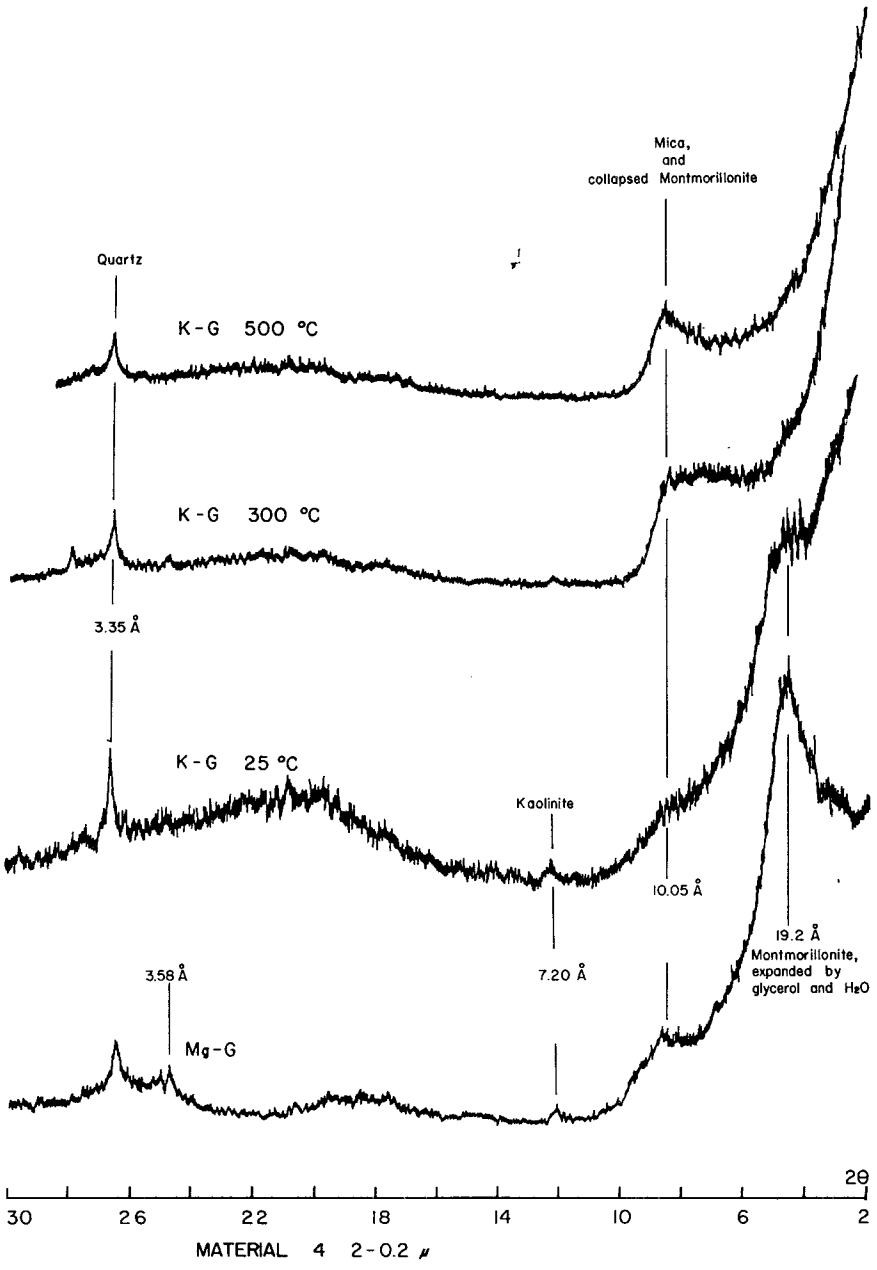

FIG. 24 - X-RAY DIFFRACTION PATTERNS, 2-0.2μm FRACTION, MATERIAL 4

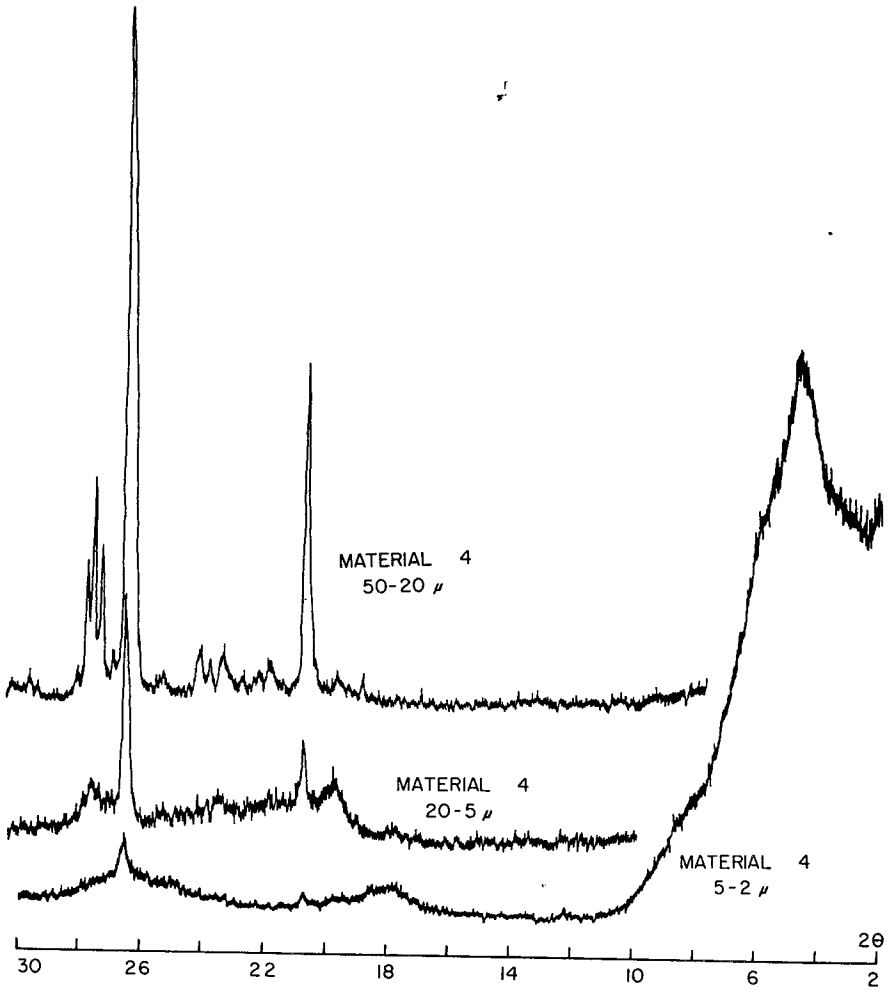

FIG. 25 - X-RAY DIFFRACTION PATTERNS FOR THE SILT AND SAND FRACTIONS, MATERIAL 4

near $28^{o}2\theta$.

Differential Thermal Analysis.-- The size fractions used in the differential thermal analysis (DTA) were prepared as indicated in Appendix C. They were magnesium saturated, dried, and ground to pass a #70 mesh sieve. DTA analysis involves heating a sample and an inert reference material in a furnace and comparing the temperature difference between the sample and the reference. The clay mineral sample will exhibit exothermic peaks, representing higher temperatures, and endothermic troughs, representing lower temperatures, which will be a characteristic of each mineral, representing phase changes and moisture losses of varying energies.

The DTA curves for material 4 are shown in Fig. 26. These curves present five major features which are:

1. Large endothermic trough below $100^{o}C$,
2. Endothermic trough around $450^{o}C$,
3. Slight endothermic trough near $840^{o}C$,
4. Exothermic peak just below $900^{o}C$, and
5. Indications of several slight sharp endothermic troughs between $200^{o}C$ and $350^{o}C$.

The large endothermic trough near $100^{o}C$ is typical of montmorillonite and represents the loss of interlayer water. The loss of hydroxyl water is indicated by the trough between $450^{o}C$ and $500^{o}C$. The difference in the temperature necessary to drive off the water is indicative of how tightly the water is being held. A standard DTA curve for montmorillonite is shown in Fig. 27.

Kaolinite exhibits only a sharp endothermic peak near $500^{o}C$. This peak will influence the montmorillonite peak at $600^{o}C$ by broadening it. This broadening can be used as a quantitative tool as will be shown presently.

Vermiculite gives a characteristic double or triple endothermic trough near $150^{o}C$ to $200^{o}C$. The slight shoulder near $200^{o}C$ could be indicative of vermiculite although no vermiculite was noted in the x-ray diffraction analysis. Mica will lose hydroxyl water from $450^{o}C$ to $650^{o}C$. This is usually all that will indicate the

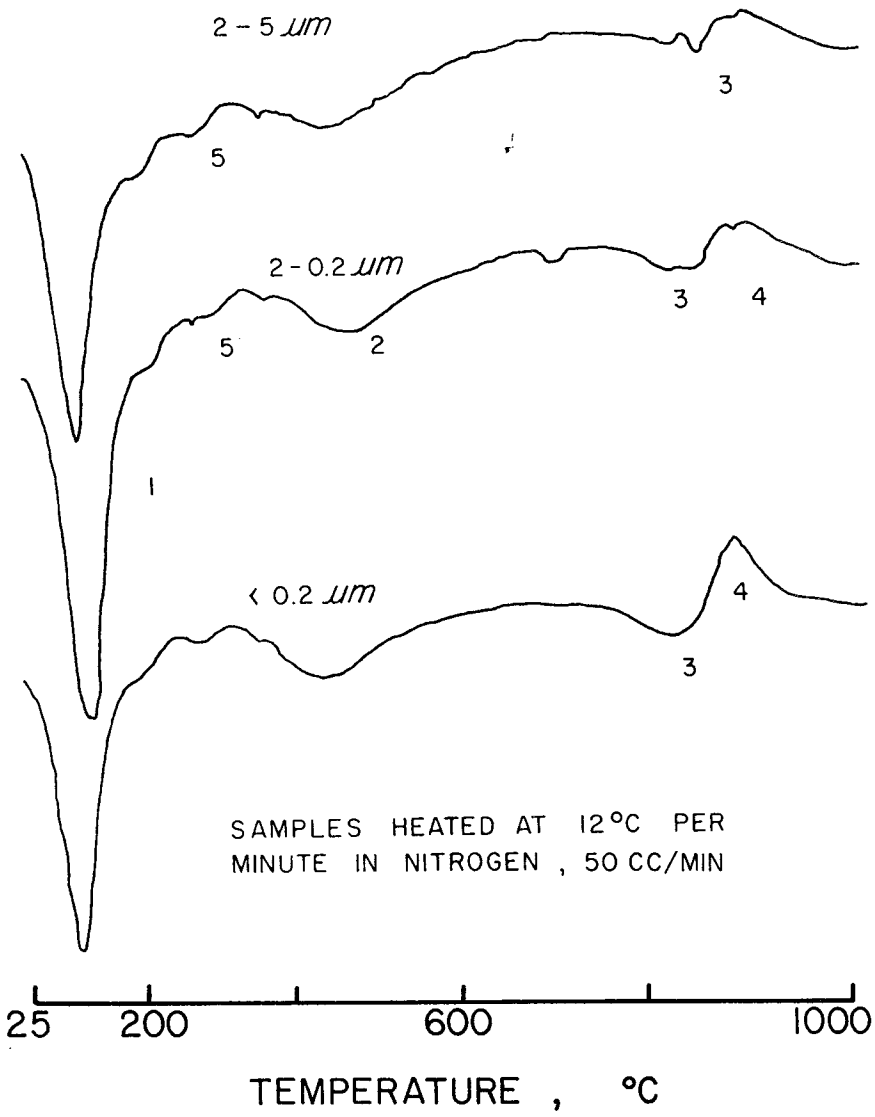

FIG. 26 - DTA CURVES FOR MATERIAL 4

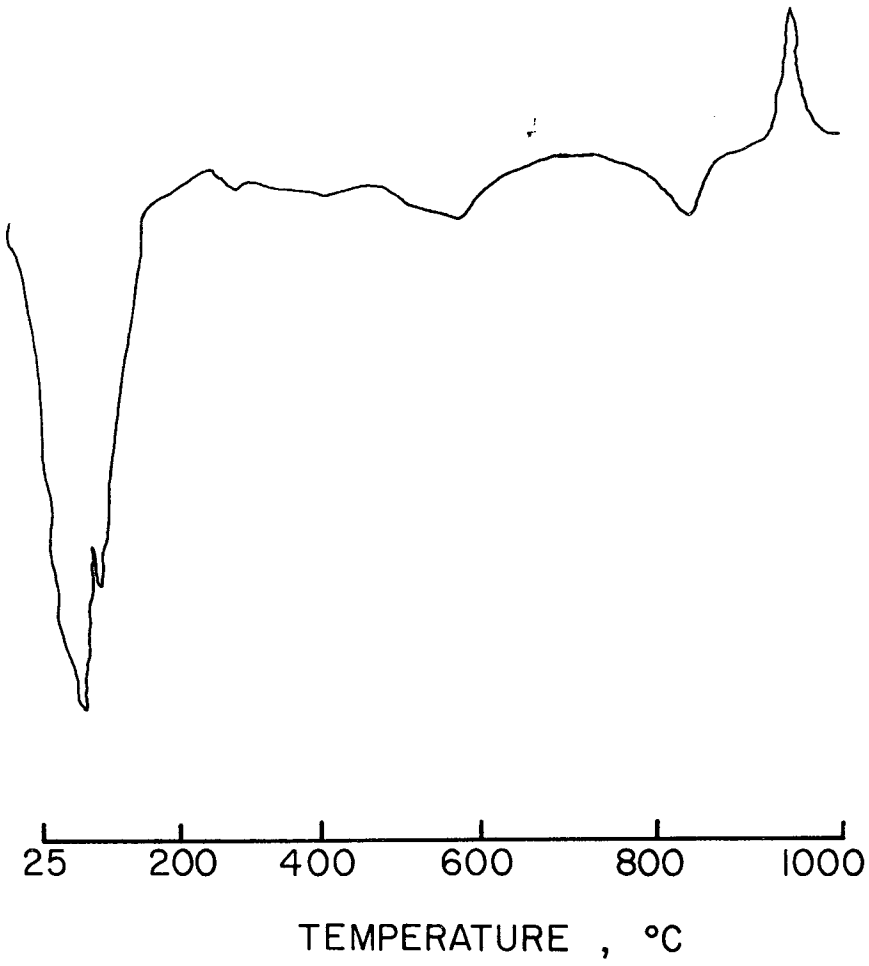

FIG. 27 - STANDARD DTA CURVE FOR MONTMORILLONITE

presence of mica in a DTA analysis.

Attapulgite will demonstrate the feature listed as number 5 above. According to Bradley (7), water molecules in the channel-like interstices of attapulgite are lost below 100°C, which indicates this water is rather loosely held, although held tighter than free water. There are additional endothermic reactions at about 225°C to 350°C and at 400°C to 525°C. Typical DTA curves for this mineral are shown in Fig. 28. They show similarities to the curves for material 4.

The percent of kaolinite and montmorillonite in a binary sample may be very roughly estimated by comparing the area of the endothermic trough of the sample with the areas obtained by analyzing binary mixtures of kaolinite and montmorillonite of known percentages. A standard curve is shown in Fig. 29. The ordinate represents the area under the endothermic curve from 350°C to 650°C. The areas for material 4 are given in Table 5. These data indicate the same information as the x-ray diffraction did, that is, montmorillonite is abundant compared to kaolinite. The actual percentages shown in Table 5 cannot be applied directly to the base course sample, however, since this material is composed of several minerals.

Cation Exchange Capacity.-- The different clay minerals each possess a rather well defined ability to absorb certain cations (or anions) and hold them in an exchangeable state. These cations will be replaced (exchanged) when the clay minerals are treated with solutions containing other cations. Typical values of the cation exchange capacity are listed in Table 6.

Knowing which minerals are present in the sample, combined with a rough estimate of the percentage of several of them, the remaining minerals may be estimated when the Cation Exchange Capacity of the sample is known. The CEC determination was conducted on the two clay size fractions according to the procedure given in Appendix C. The data for material 4 are given in Table 7.

From these data mineral estimates for montmorillonite and kaolinite may be obtained. Mica and attapulgite may be estimated

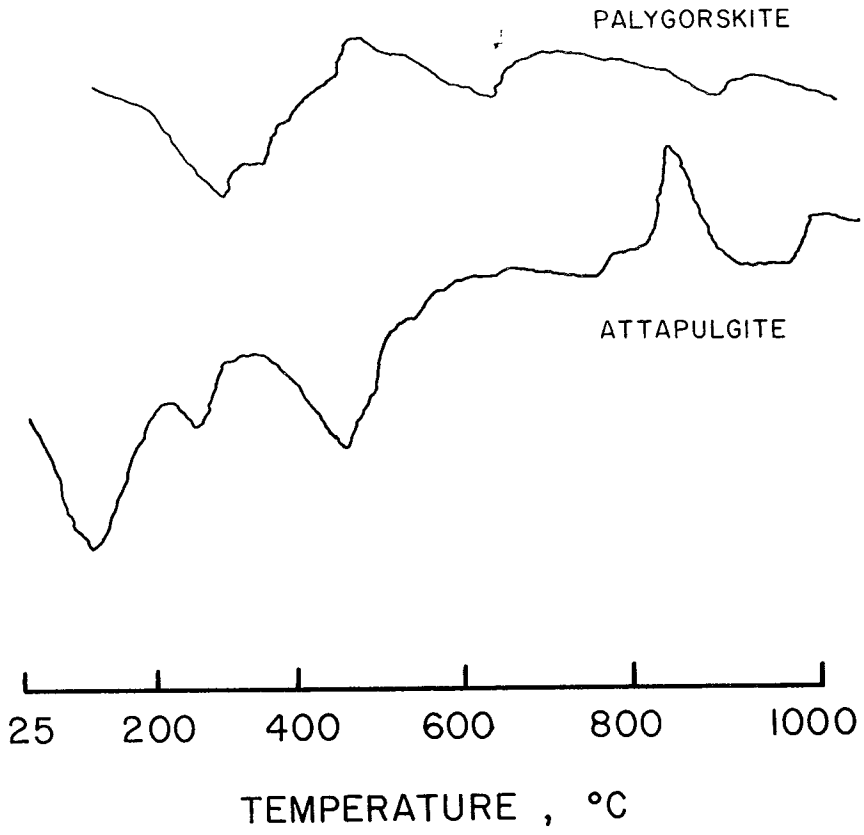

FIG. 28 - DTA CURVES FOR PALYGORSKITE, ATTAPULGITE

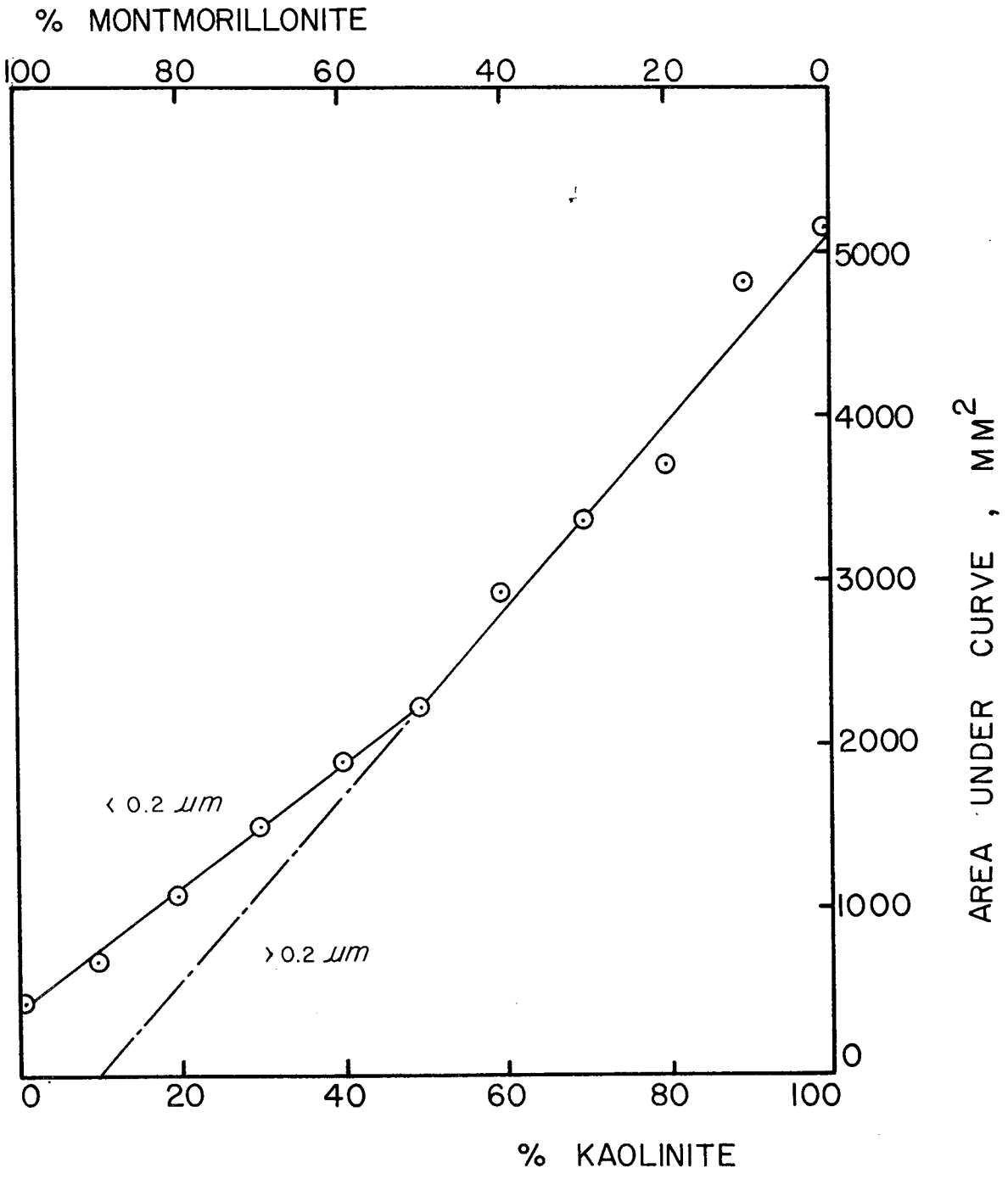

FIG. 29 - CURVES RELATING AMOUNTS OF KAOLINITE AND MONTMORILLONITE TO THE AREA IN THE DTA CURVE FOR THE ENDOTHERMIC PEAK AT 500°C

TABLE 5. VALUES CALCULATED FROM DTA ANALYSIS FOR PERCENTAGES OF MONTMORILLONITE AND KAOLINITE

Size Fraction μm	Area (mm^2)	% Kaolinite	% Montmorillonite
5-2	167	13	87
2-0.2	226	15	85
<0.2	390	0	100

TABLE 6. TYPICAL VALUES OF CATION EXCHANGE CAPACITY(18)

	Meq/100gm
Kaolinite	5-10
Montmorillonite	110
Mica (Illite)	20
Vermiculite	15
Chlorite	10-46
Sepiolite	3-15
Attapulgite	3-15
Palygorskite	3-15

together as they have essentially the same CEC. The estimates obtained from this analysis are presented in Table 8. The estimates for montmorillonite and kaolinite are in general agreement with the indications given in the DTA analysis.

Quantitive Data From X-Ray Diffraction Data.-- Jackson, et al., (24), have shown that reasonable estimates of mineral percentages may be obtained from x-ray diffraction data through comparison of the peak intensities. To do this, however, it is necessary to have several hundred diffraction patterns of laboratory prepared samples with known percentages of the minerals believed to be present. These percentages may be logically based on the weathering scheme presented by Jackson (25). This scheme is shown in Fig. 30. The assumption made is that minerals weathered in place from parent material will give a normal distribution of the percentages of the minerals in the material. As weathering proceeds, minerals that are higher in the scale (gypsum, chlorite, hornblend) will be gradually transformed by chemical weathering through biotite, albanite, quartz, mica, vermiculite (attapulgite included), montmorillonite, kaolinite, and gibbsite to the hardest and least soluble minerals hematite and anatase. The percentages of minerals obtained by the CEC analysis are plotted on Fig. 30 along with the results obtained from the x-ray diffraction. It is apparent that a normal distribution is roughly approximated and for this reason it is felt that the mineral estimates are correct and that similar materials should yield similar results.

The analysis of x-ray diffraction data was conducted on the slides prepared by magnesium saturation and glycerol solvation for all materials. The steps involved in calculating the percentages may be outlined as follows:

1. Obtain values for peak intensities of the major identification peaks.
2. Calculate percentages of total intensities.
3. Correct percentages based on the relative amount of each size fraction.

TABLE 7. CATION EXCHANGE CAPACITY DATA, MATERIAL 4

Size μm	Atomic Absorption Reading	CEC (meq/100gm)	Average
2-0.2	7.8 8.1	29.1 26.8	28.0
<0.2	11.9 12.6	76.6 78.2	77.4

TABLE 8. MINERAL ESTIMATES FROM CATION EXCHANGE CAPACITY DETERMINATION

Mineral	Size Fraction(μm)	Percentage	Total	
Quartz	2-0.2 <0.2	10 0	5.5	
Kaolinite	2-0.2 <0.2	15 10	12.8	
Montmorillonite	2-0.2 <0.2	14 69	38.5	
Mica Attapulgite	2-0.2 <0.2	61 21	43.2	11.0 32.2

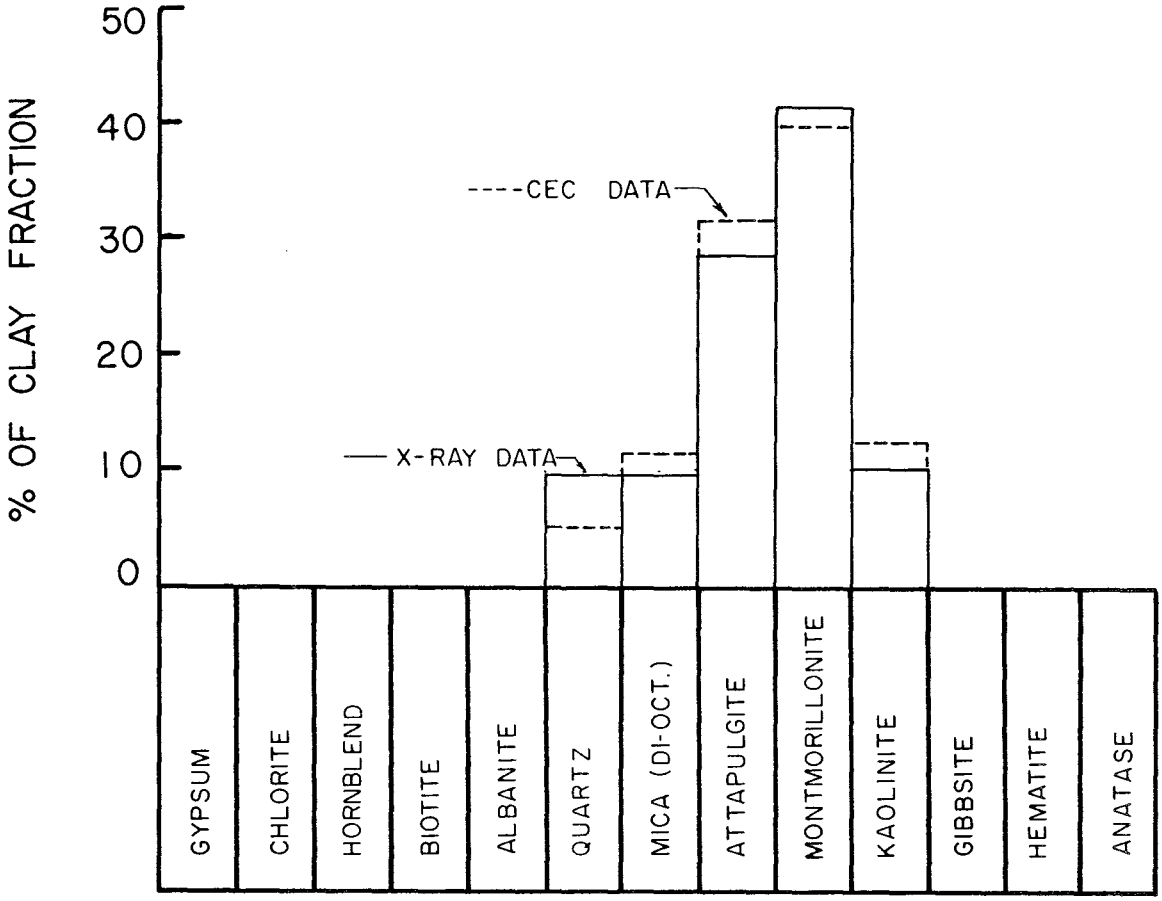

FIG. 30 - MINERAL ESTIMATES PLOTTED ON JACKSON'S WEATHERING SCHEME

4. Plot estimated percentages of minerals on the weathering scheme to verify a normal distribution.

The percentages for material 4 from x-ray diffraction data are shown in Table 9. These percentages are only slightly different from those calculated from the cation exchange capacity data. These differences are within experimental error and within tolerances for the analysis to be done in this study. From a study of these data it is felt that the x-ray diffraction data alone will yield values substantially accurate enough to allow the percentages to be indicative of the material. Since the materials in this study are composed of essentially the same minerals, errors should be minimized and the relative percentages should be accurate.

The remaining materials were prepared similarly to material 4. Both potassium and magnesium saturated samples were prepared in the event it became necessary to determine the presence of minerals such as chlorite or vermiculite which require the heating process. The diffraction patterns for these samples indicated that the separation of the sizes was more complete than that attained for the first separation of material 4. As an example, quartz did not appear in the <0.2μm fraction and montmorillonite did not appear in the 2-0.2μm fraction as much as it did in material 4. For this reason the percentages estimated from these diffraction patterns should be at least as good as or better than those obtained for material 4.

Material 5.-- The x-ray diffraction pattern for material 5 is shown in Fig. 31. The clay minerals noted in the figure are montmorillonite, attapulgite, mica, kaolinite and quartz. There is no quartz in the <0.2μm fraction and essentially no montmorillonite in the 2-0.2μm fraction. The percentages calculated for each mineral are listed in Table 10 and plotted on the weathering sequence in Fig. 32. The plot of the percentages looks very similar to that obtained for material 4 as should be expected.

Material 6B.-- The x-ray diffraction pattern for material 6B

TABLE 9. MINERAL ESTIMATES FOR MATERIAL 4 FROM X-RAY DIFFRACTION

Mineral	Intensity	Percentage	Size Fraction μm	Corrected % (Total Clay Size)
Montmorillonite	42 50	14 69	2-0.2 <0.2	38.8
Mica	6.9 12.7	33.5 8	2-0.2 <0.2	20.0
Attapulgite	5.6 10.2	27.5 7.0	2-0.2 <0.2	20.7
Kaolinite	3.2 1.8	15.0 5.0	2-0.2 <0.2	10.5
Quartz	10.0 8.0	10.0 10.0	2-0.2 <0.2	10.0

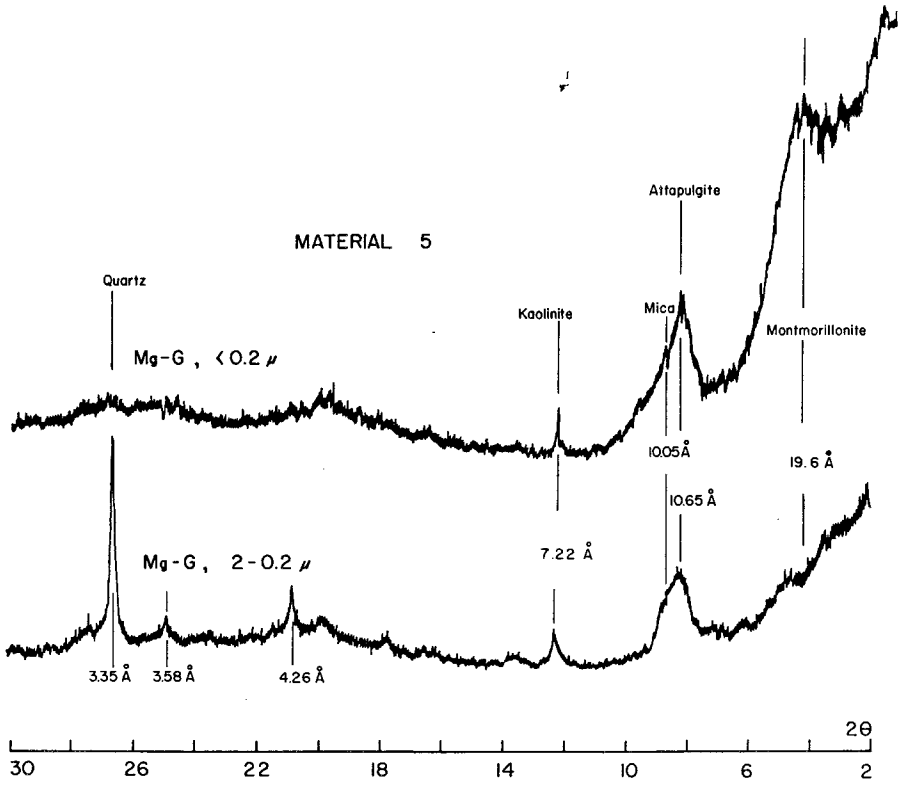

FIG. 31 - X-RAY DIFFRACTION PATTERNS, MATERIAL 5

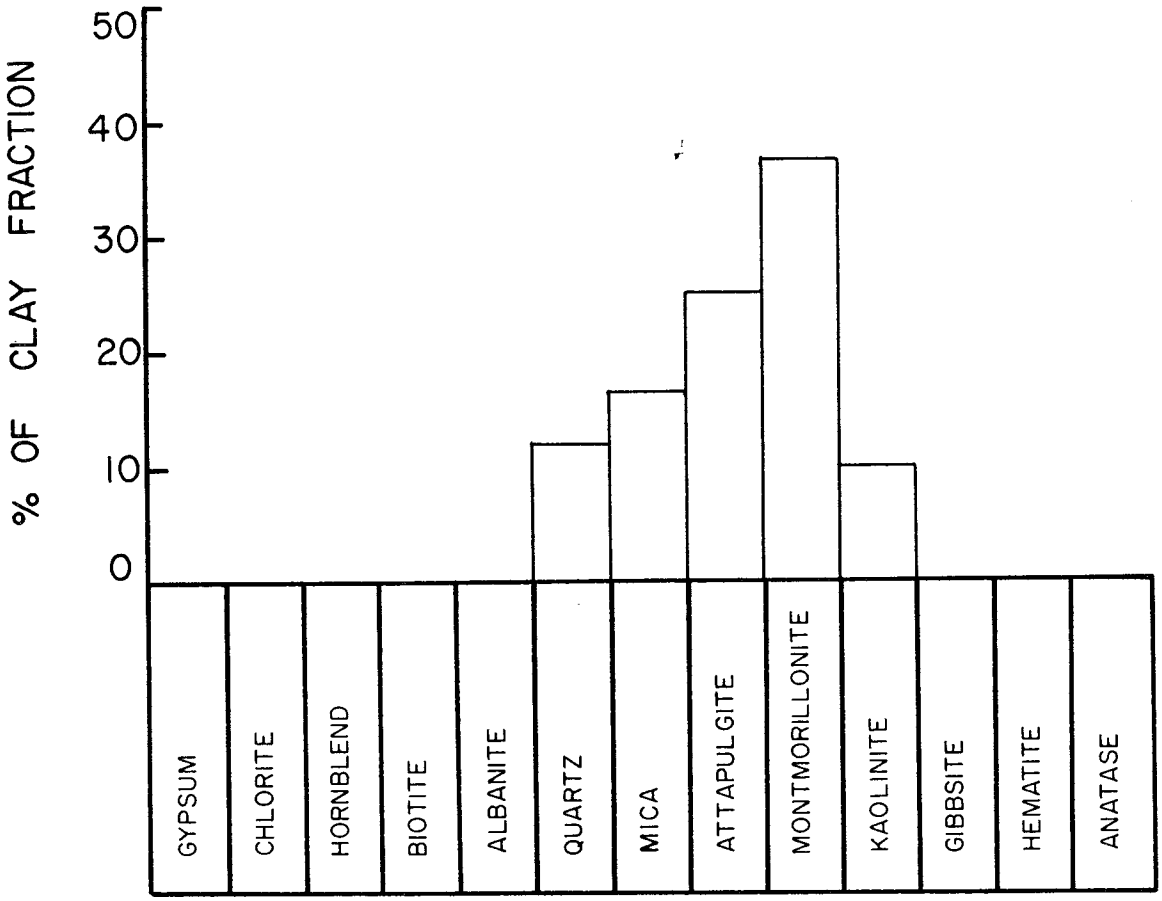

FIG. 32 - MINERAL ESTIMATES FROM X-RAY ANALYSIS PLOTTED ON JACKSON'S WEATHERING SCHEME, MATERIAL 5

is shown in Fig. 33. The clay minerals present include montmorillonite, mica, kaolinite and quartz with a small amount of attapulgite. The peaks for this material were somewhat broad and not as well defined as some of the other samples and for this reason the potassium slide was x-rayed. The quality is comparable to that of the slides for material 4 and the accuracy of the percentages should be comparable. The percentages are given in Table 11.

Material 6B.-- The x-ray diffraction patterns for material 6B are shown in Fig. 34. The minerals present include montmorillonite, attapulgite, quartz and kaolinite. There is a definite absence of mica in this material. The calculated percentages are given in Table 12. The <0.2μm fraction can be seen to be composed entirely of montmorillonite and attapulgite. This would indicate this material to be more active than the others, but perhaps not in a thermal manner. The diffraction peaks were quite strong and well defined. The several intermediate peaks between attapulgite and montmorillonite in the <0.2μm fraction represent sodium montmorillonite not fully expanded (18) as the peaks do not match values for minerals giving peaks in this area. This was verified with heat treatment which collapsed the montmorillonite to 10 Å.

Material 6FS.-- The x-ray diffraction pattern for material 6FS is shown in Fig. 35. The minerals present include montmorillonite, mica, kaolinite and quartz. The percentages of each are listed in Table 13. These values are the most questionable values of those obtained. The reason for this can be seen by examining the x-ray diffraction pattern for the <0.2μm fraction. The peaks for mica and montmorillonite are broad and weak. This could be due to a misalignment of the x-ray diffractometer; but this is not likely as calibration was checked halfway through testing and found to be in order. The reason for the pattern becomes apparent when the manner in which this material was obtained is investigated. This material was obtained from crushing material that was blasted from competent rock formations. Crushing action

TABLE 10. PERCENTAGES FOR MATERIAL 5

Mineral	Percentage
Montmorillonite	35.5
Attapulgite	25.9
Mica	15.8
Kaolinite	11.0
Quartz	11.8

TABLE 11. PERCENTAGES FOR MATERIAL 6B

Mineral	Percentage
Montmorillonite	41.8
Attapulgite	13.7
Mica	7.0
Kaolinite	7.9
Quartz	29.6

TABLE 12. PERCENTAGES FOR MATERIAL 6JD

Mineral	Percentage
Montmorillonite	38.9
Attapulgite	45.3
Quartz	12.9
Kaolinite	2.9

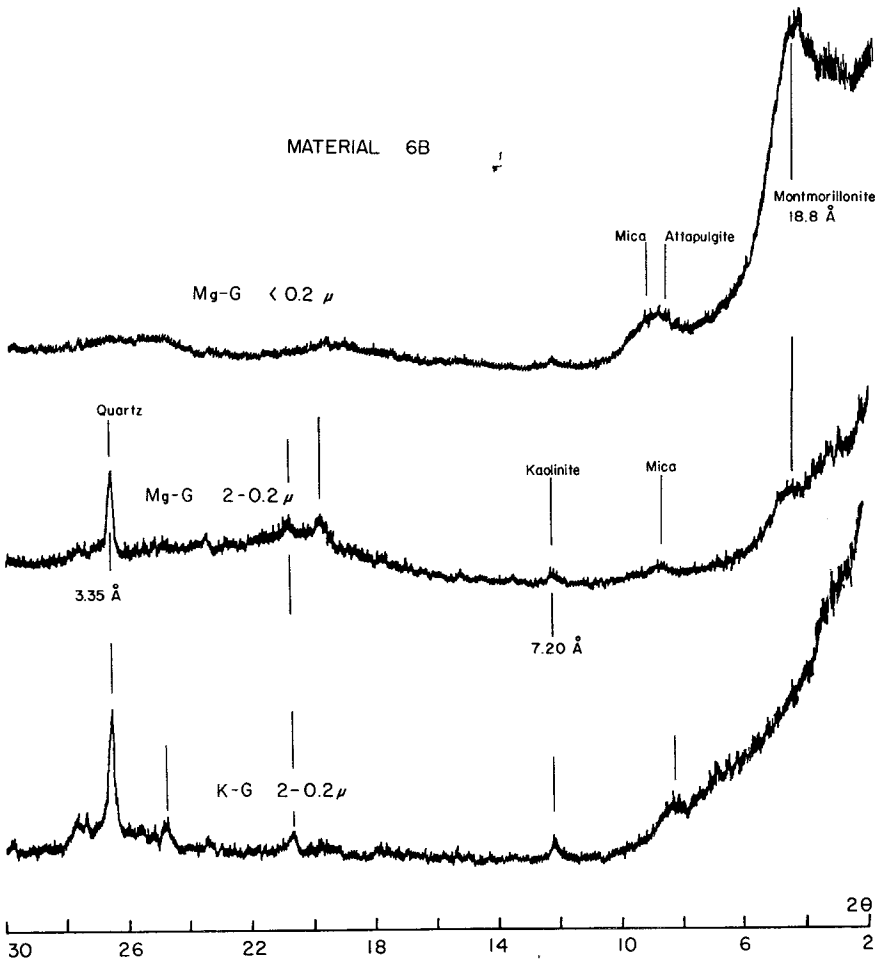

FIG. 33 - X-RAY DIFFRACTION PATTERNS, MATERIAL 6B

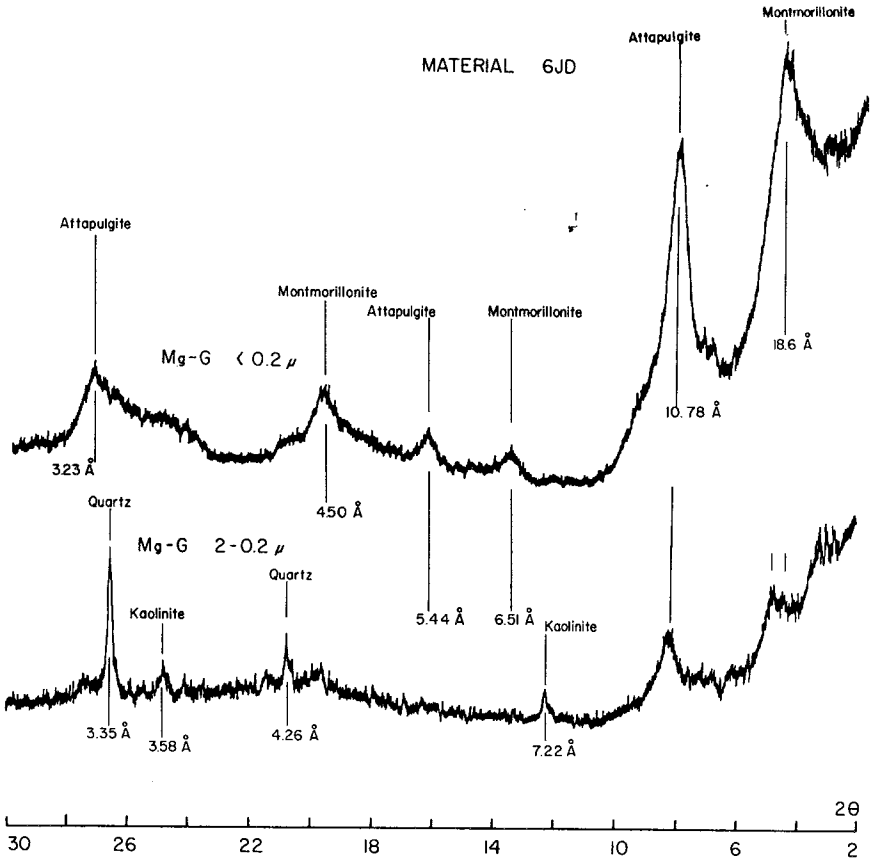

FIG. 34 - X-RAY DIFFRACTION PATTERNS, MATERIAL 6JD

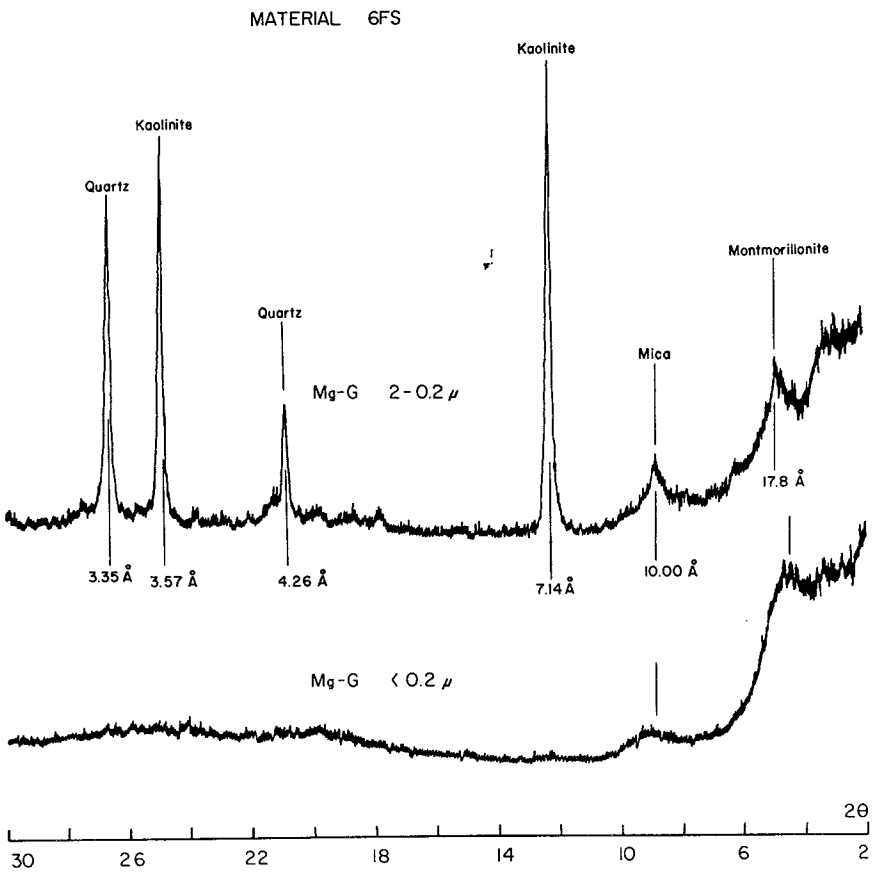

FIG. 35 - X-RAY DIFFRACTION PATTERNS, MATERIAL 6FS

will destroy any crystalline structure present after a certain period of grinding (18). It is felt that excessive crushing action has produced this amorphous material with no crystalline structure which concentrated in the <0.2μm fraction size. A cation exchange capacity determination would be necessary to substantiate this assumption. For the analysis presented here the corrected percentages as calculated for Table 13 will be used. These values assume the material to be 25 percent amorphous.

Material 7SA.-- The x-ray diffraction patterns are given in Fig. 36. The minerals present include montmorillonite, mica, kaolinite and quartz. The percentages calculated from the x-ray diffraction patterns are given in Table 14.

Material 6BAR.-- The x-ray diffraction patterns for material 6BAR are given in Fig. 37. The minerals present include montmorillonite, attapulgite, kaolinite and quartz. The potassium saturated slide was run to check the magnesium saturated sample when difficulty was encountered in running the magnesium slide. The percentages are given in Table 15.

Predictive Relationships

Equilibrium Suction

As mentioned, the moisture in the sample appeared to be most influential in determining sample behavior. The suction, which is greatly influenced by the moisture, gives a much more comprehensive picture of how the moisture is utilized in the sample. Suction is influenced by the grain size, pore structure and the type of clay minerals present. Any change in suction must be accompanied by a change in one of the above variables. Suction is readily measured in-situ and in the laboratory, as stated, and as such provides a common quantity to relate observed behavior with a measurable value.

Typically suction has been predicted in terms of moisture content (45). Such regression equations took the form of:

$$h = a + b \log_{10} w \qquad (2\text{-}3)$$

TABLE 13. PERCENTAGES FOR MATERIAL 6FS

Mineral	Percentage	Corrected Percentage
Montmorillonite	68.7	51.5
Mica	17.3	12.9
Kaolinite	11.2	8.4
Quartz	2.8	2.2

TABLE 14. PERCENTAGES FOR MATERIAL 7SA

Mineral	Percentage
Montmorillonite	58.0
Mica	18.2
Kaolinite	6.2
Quartz	16.2

TABLE 15. PERCENTAGES FOR MATERIAL 6BAR

Mineral	Percentage
Montmorillonite	39.8
Attapulgite	33.0
Kaolinite	13.3
Quartz	13.9

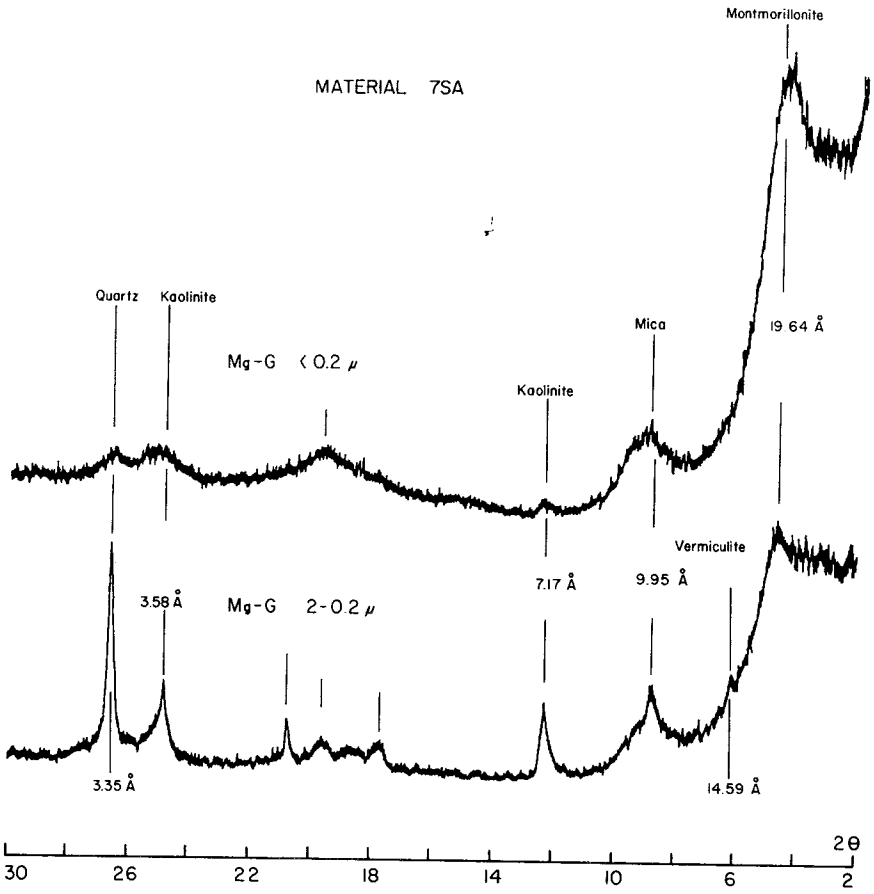

FIG. 36 - X-RAY DIFFRACTION PATTERNS, MATERIAL 7SA

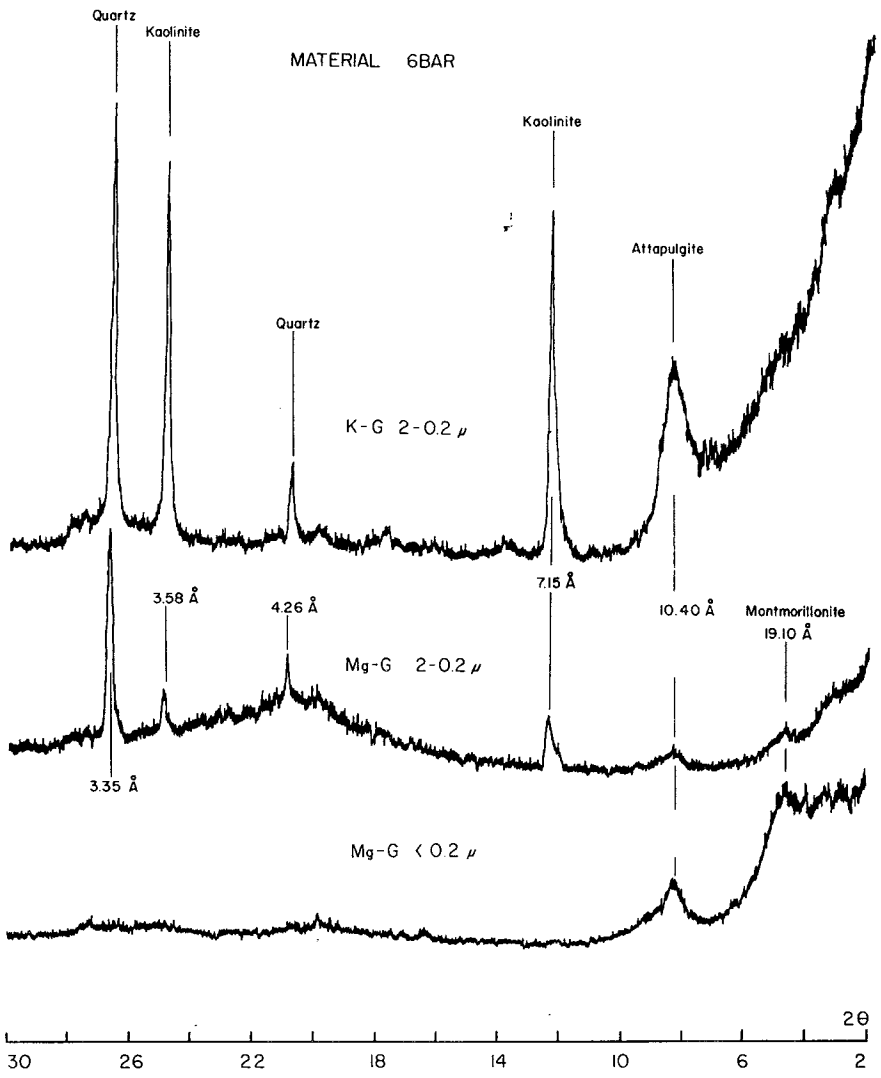

FIG. 37 - X-RAY DIFFRACTION PATTERNS, MATERIAL 6BAR

where

h = suction, in psi, (x 6.9= KN/M^2),

a, b = regression constants, and

w = gravimetric moisture content.

This type of regression equation typically gave a coefficient of determination, R^2, of 0.92. A better approximation was obtained using the following equation:

$$\log h = a + b \log w \qquad (2\text{-}4)$$

where

h = suction, in psi, (x6.9 = KN/M^2)

a, b = regression constants, and

w = gravimetric moisture content.

This equation typically gave correlation coefficients, R^2, of 0.95 and above, for a representative number of samples included in the regression. The equations developed for the base course materials are given in Table 16.

Influence of Percent Clay

The general form of the relation given in equation (2-4) contains two regression constants, a and b, that vary with the material. These constants do show some influence of the compaction effort but a consistent relationship could not be found. This emphasizes the already stated fact that compaction effort has only a minimal effect on the equilibrium suction. The major differences may be accounted for in the different positioning of the psychrometers in the Harvard miniature samples. With this thought the coefficients were regressed against material properties; and a relationship with the percent clay produced the best fit equations. The final equations developed were of the form:

$$a = 2.1995 + 0.3428 \text{ (\% Clay)}, R^2 = 0.97 \qquad (2\text{-}5)$$

$$b = 1.148 + 0.2437 \text{ (\% Clay)}, R^2 = 0.89 \qquad (2\text{-}6)$$

This relationship produced an equation with an R^2 value of 0.76 when comparing the predicted suction to the measured suction.

Freeze-thaw-- Utilizing equilibrium suction as the measured

TABLE 16. REGRESSION EQUATIONS TO PREDICT AS-COMPACTED SUCTION (h) AS A FUNCTION OF GRAVIMETRIC MOISTURE (W)

Material No.	Equation (Modified AASHTO)	R^2
4	log h = 5.596 - 3.638 log W	0.95
5	log h = 4.761 - 3.066 log W	0.96
6B	log h = 6.132 - 4.402 log W	0.93
6JD	log h = 3.561 - 2.130 log W	0.98
6FS	log h = 2.574 - 1.560 log W	0.99
7SA	log h = 4.545 - 3.389 log W	0.93
Material No.	Equation (Harvard Miniature)	R^2
4	log h = 5.089 - 3.103 log W	0.91
5	log h = 5.024 - 3.276 log W	0.97
6B	log h = 4.207 - 2.317 log W	0.92
6JD	log h = 3.637 - 1.881 log W	0.94
6FS	log h = 5.425 - 4.721 log W	0.99
7SA	log h = 7.512 - 6.227 log W	0.96
6BAR	log h = 3.674 - 2.012 log W	

quantity to predict thermal behavior this activity becomes quite predictable. When the freeze coefficient is plotted as a function of the as-compacted suction, Fig. 38 is the result. The shape of the curve is typical for all the materials tested. There is a maximum negative freeze coefficient which falls off to a lesser value for drier samples. The relative position of the optimum moisture point on the two compaction curves was quite conclusive in relation to the point of maximum freeze contraction. The lack of influence of suction on the compaction curves is evident in that the compaction effort could not be used to predict which set of samples would have the largest freeze coefficient. This relationship with the structure provides further insight into the role that is played by moisture interaction with particle structure.

The positions of optimum moisture content are indicated on Fig. 38 for two materials. For the larger compactive effort, modified AASHTO, the optimum position was typically very near the point of maximum thermal activity and often on the dry side (higher suction). For the lower compaction effort, 95 percent of modified, the position of the optimum was shifted away from the area of maximum thermal activity, often into the area of freeze expansion. The suction at the point of maximum thermal activity is important when considered in light of the data collected from the field psychrometer installations mentioned earlier, namely, that a typical base course ends up quite a bit dry of optimum moisture. Thus, for the heavier compactive effort this drying will tend to have little effect on the thermal activity and may tend to decrease it as the sample is moved to the dry side of the maximum coefficient. For the lower compactive effort this drying will change the thermal activity causing it to assume a value very near the maximum. For this reason it becomes apparent that for most base courses in west Texas, thermal activity will be a contraction upon freezing and will probably be near the maximum value for that material.

Suction can also predict the residual strain coefficient, B_1, as is shown in Fig. 38. The data shown in this figure are typical of the data obtained for all materials. For the majority of materials

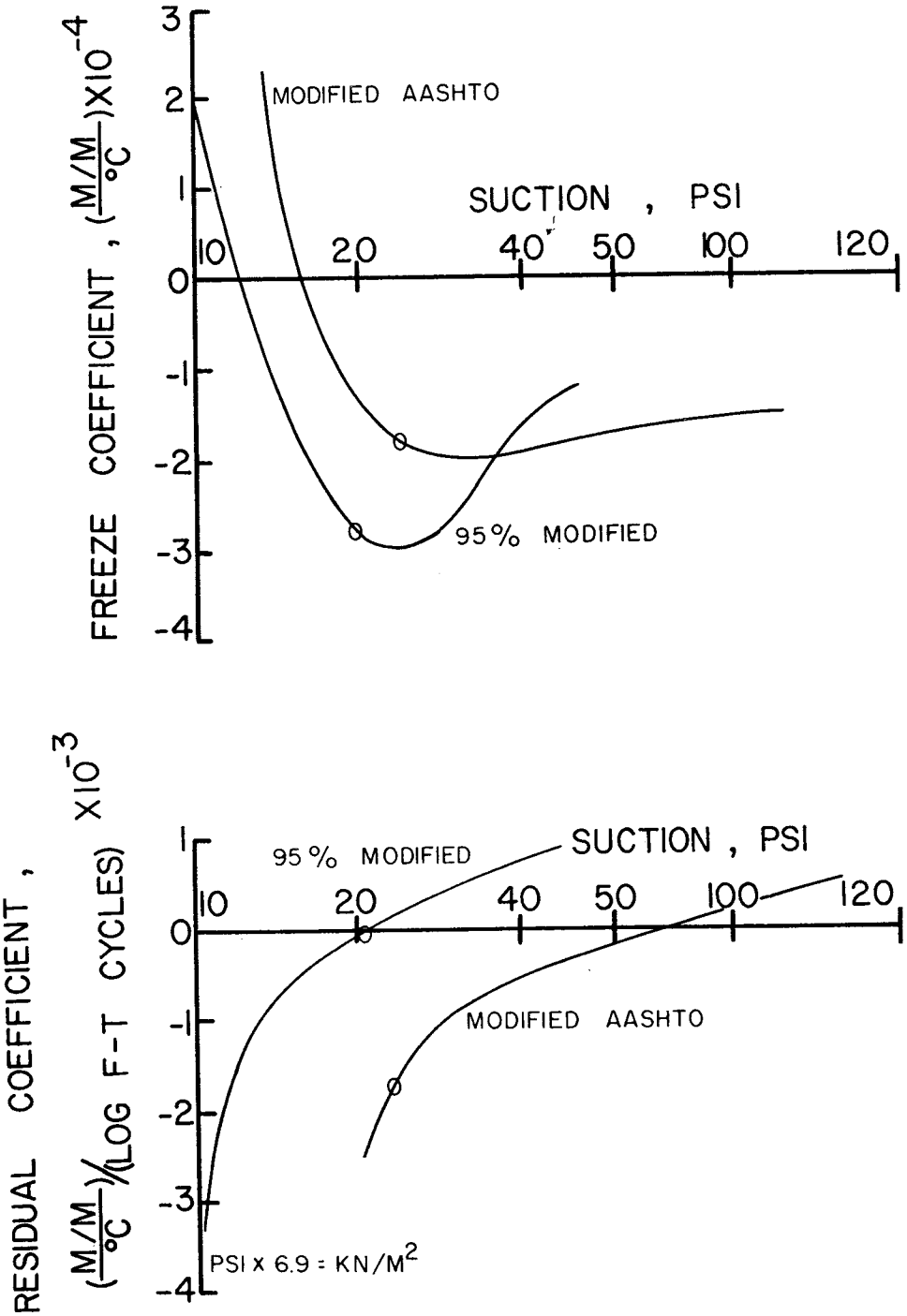

FIG. 38 - FREEZE-THAW DATA SHOWING FREEZE AND RESIDUAL COEFFICIENTS AS A FUNCTION OF SUCTION WITH POSITIONS OF OPTIMUM MOISTURE CONTENT SHOWN BY "O"

increased compaction produces less residual contraction for a given suction; and, in general, a difference in the compaction effort does produce a different behavior in the residual strain.

The effect of suction on the residual strain is the opposite of its relationship with the freeze strain. As the sample becomes drier, the residual strain becomes less and eventually it becomes an expansion. The freeze coefficient, however, becomes greater as the sample becomes drier, Thus, suction inhibits residual strain while enhancing the freeze behavior, up to a point.

The data collected demonstrate that thermal activity can be predicted by knowing the equilibrium suction of the material. Suction, in addition to providing the relationships just discussed, also provides insight into the physical process, the mechanism, of the freeze-thaw activity of the material. Assuming the clay mineralogy and the moisture content do not change during a freeze-thaw cycle, only the changes in grain size, pore structure and distribution of ions are able to account for the noted variations in volume and suction during the freeze-thaw cycling.

The as-compacted suction can be utilized to predict a range of thermal activity although the maximum freeze coefficient for any one material connot be inferred directly from the suction level. The influence of compaction effort, combined with practices which produce the dry base courses, will influence the thermal activity that develops. The next section details the determination of the material properties which allow a maximum value of freeze coefficient to be predicted. The suction relations established in this section provide the capability to predict suction and infer the relative level of freeze-thaw activity. As the grain size for the materials tested are nearly identical, the main variable between materials will be the clay mineralogy.

Relation of Clay Mineralogy to Thermal Activity.--The question which must be considered is how to relate the measured

suctions to the maximum thermal activity. As noted previously, the suction quantities are indicative of the clay mineralogy, the size of the particles and their arrangement (pore structure). The only clay mineral property readily available which could be quantified and related logically to the thermal activity was the specific surface area of the clay minerals.

The laboratory determination of the specific surface area of clay minerals is extremely inconsistent and highly dependent on the technique used. One technique that has found wide acceptance is the Brunauer, Emmett, and Teller method (BET) (8). Typical values determined by this method are given in Table 17. These values will be used in the calculation of the specific surface area of each material's clay fraction. They represent laboratory test data and as such are very different from the theoretical values which have been calculated from the dimensions of the crystalline structure. The major difference between theory and measurement arises with montmorillonite for which theoretical values of specific surface area typically run 800 meters^2/gram. The much lower value in Table 17 indicates that the major part of the potential surface of the mineral could not be reached by the penetrating liquid or gas used in the laboratory test. Since the total surface cannot be readily reached in the laboratory, it may be inferred that the surface of the montmorillonite will not be fully utilized by the moisture in compacted samples. For this reason it is felt that the laboratory determined values for the specific surface area would be more indicative of the moisture particle interaction as it occurs in the actual sample. The specific surface area for the quartz was taken as 29 M^2/gm to represent the larger size that will be present in the clay size fractions.

The values of the specific surface area for the clay fraction in each material were calculated based on the amount of each mineral present. The values thus calculated are presented in Table 18. The specific surface area of the clay fraction demonstrated a consistent relationship with the freeze coefficient.

TABLE 17. TYPICAL VALUES OF SPECIFIC SURFACE AREA (8)

Mineral	Specific Surface Area M^2/ gm
Attapulgite	140
Mica (Illite)	113
Kaolinite	22
Montmorillonite	82

TABLE 18. SPECIFIC SURFACE AREAS OF THE CLAY FRACTION FOR THE BASE COURSE MATERIALS

Material	Specific Surface Area M^2/gm
4	92.5
5	86.2
6B	79.2
6JD	97.2
6FS	59.5
6BAR	83.1
7SA	79.4

These data are shown in Fig. 39 and Fig. 40 with the corresponding values of the freeze coefficient.

These relationships indicate that the amount of -#200 material and likewise the amount of clay present, within the limits examined for the materials in this study, will not affect the freeze-thaw behavior of the base course. The type of clay minerals combined with the amount of each mineral present will affect the thermal activity in a consistent manner allowing the maximum freeze coefficient to be predicted through a study of the clay mineralogy.

There was such a narrow range in percent fines (-#200) in all the base courses studied (a high of 10% to a low of 9%) that a credible statement cannot be made concerning the influence of this variable. Greater thermal activity, however, would be expected of base courses with a higher percentage of fines.

The residual coefficient also showed a similar relationship with the specific surface area as shown in Fig. 41. These data clearly indicate that the type of clay minerals present have a direct bearing on the freeze-thaw behavior of the material. This is important when it is remembered that the base course materials being examined contain between 1 and 9 percent clay, which is a minimal amount.

The regression equations for the relationships pictured are as follows:

Modified AASHTO, Freeze Coefficient

$$FC_{max} = -(2.8104 - 0.6776\ LOG(SSA))^{-20.7} \qquad (2\text{-}7)$$

$$R^2 = 0.98$$

$$FC_{opt} = -(-0.6031 + 0.4298\ LOG(SSA))^{-5.38+2.58x10^{-4}} \qquad (2\text{-}8)$$

$$R^2 = 0.97$$

Harvard Miniature, Freeze Coefficient

$$FC_{max} = -(5551.1 - 2714.5\ LOG(SSA))^{-1.493} \qquad (2\text{-}9)$$

$$R^2 = 0.91$$

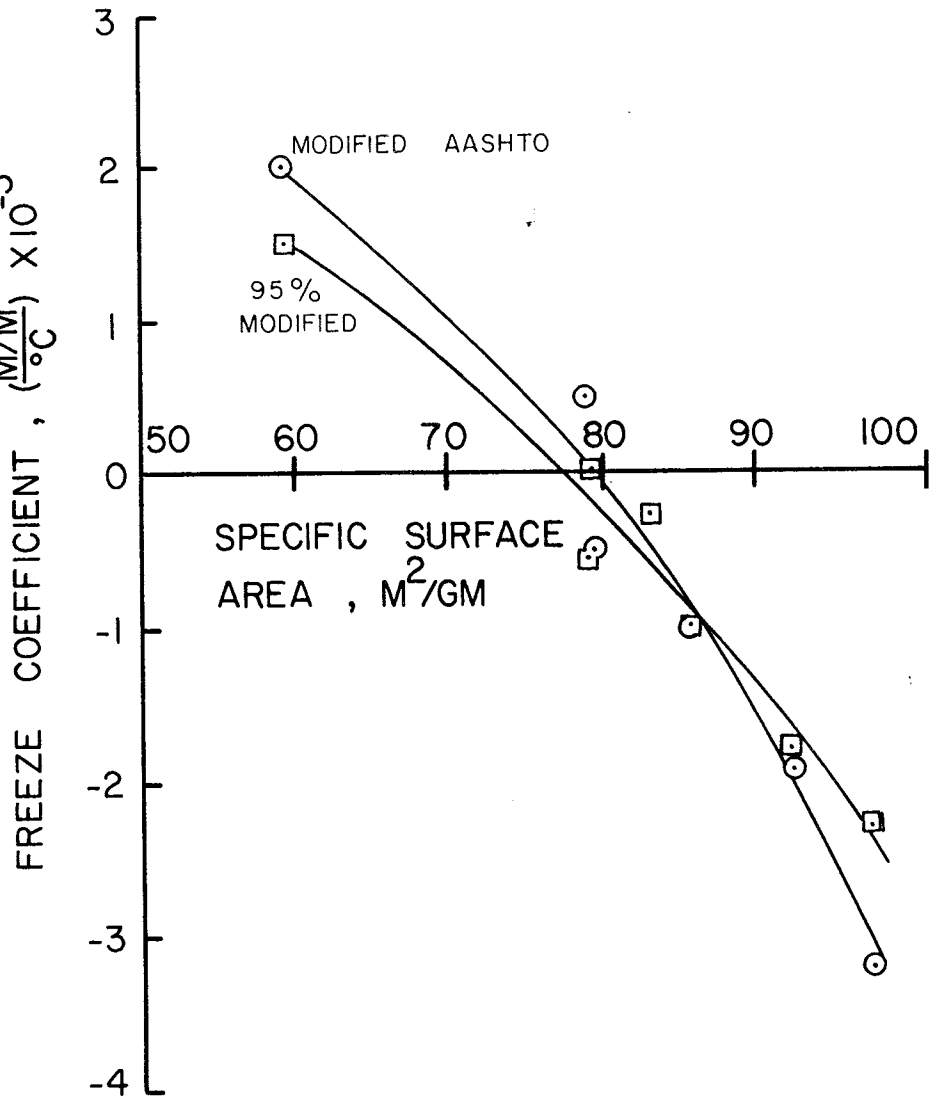

FIG. 39 - FREEZE COEFFICIENT AT OPTIMUM MOISTURE CONTENT AS A FUNCTION OF SPECIFIC SURFACE AREA

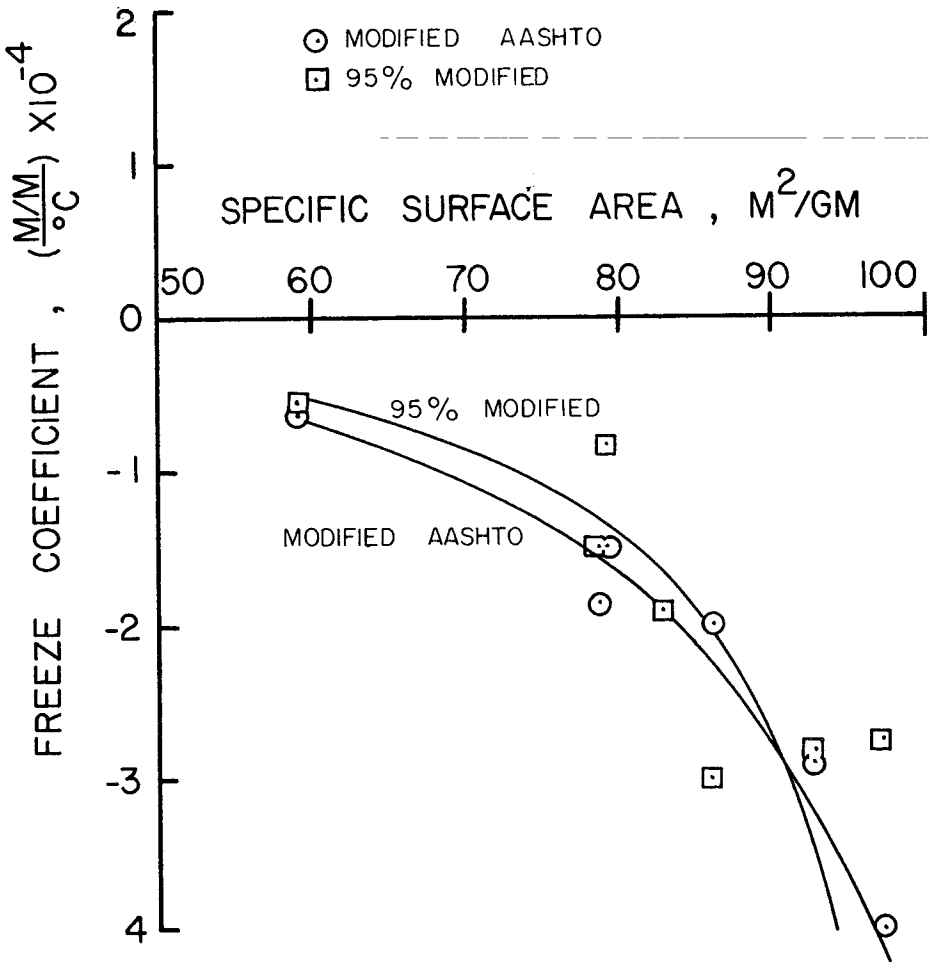

FIG. 40 - MAXIMUM FREEZE COEFFICIENT AS A FUNCTION OF SPECIFIC SURFACE AREA

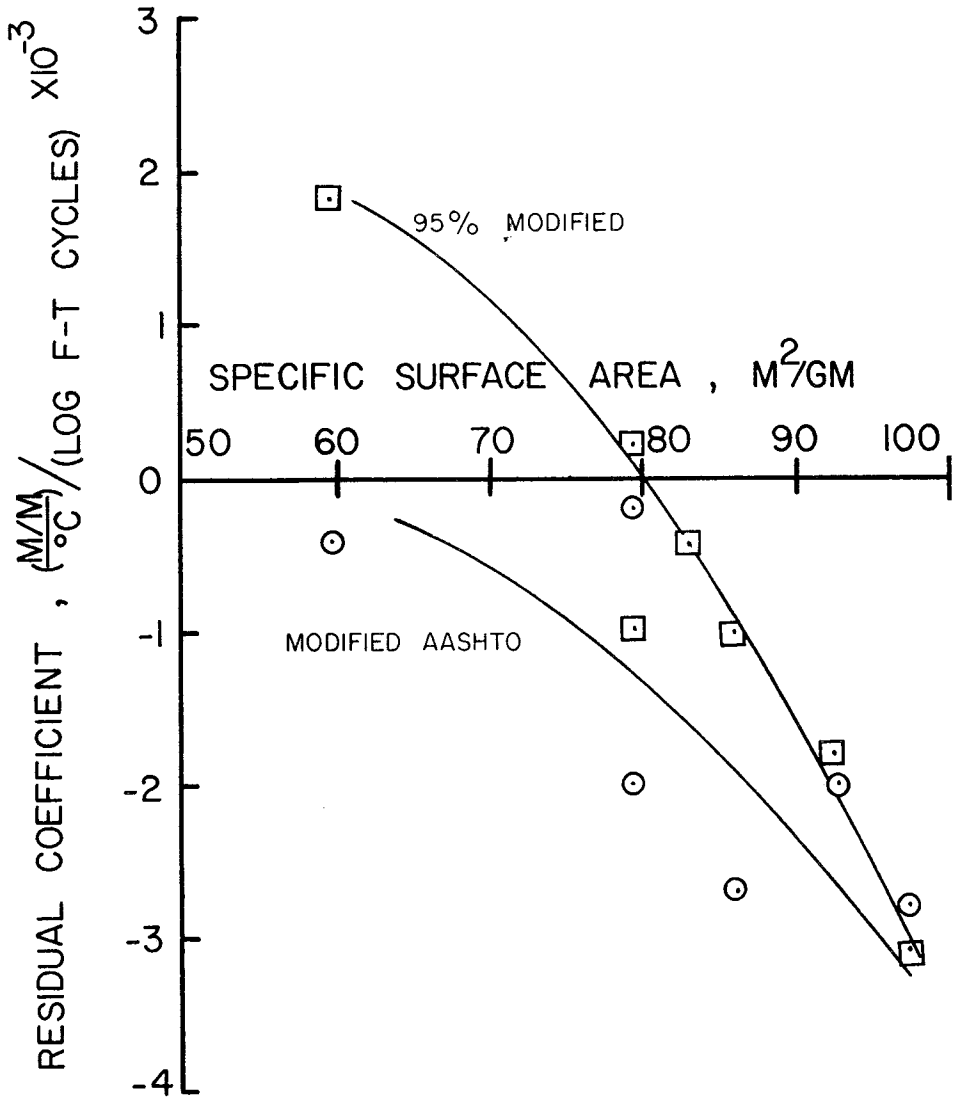

FIG. 41 - RESIDUAL COEFFICIENT AT OPTIMUM MOISTURE CONTENT AS A FUNCTION OF SPECIFIC SURFACE AREA

$$FC_{opt} = -(0.4098 + 0.2748\ LOG(SSA))^{-3.862}+2.03x10^{-4}$$
$$R^2 = 0.98$$

Residual Coefficient

$$RC_{ma} = (-9.4518x10^{-5} + 5.148x10^{-5}\ LOG(SSA))^{0.6893}$$
$$R^2 = 0.58$$

$$RC_{hm} = (-0.2234 + 0.1274\ LOG(SSA))^{2.1567}+1.83x10^{-4}$$
$$R^2 = 0.95$$

Summary

The effect of the environment on the thermal susceptibility (freeze contraction) of the base course material studied here can be inferred. In west Texas the environment will produce high suction in the subgrade and base course as previously shown. This higher suction level will produce conditions that will produce maximum freeze coefficients or freeze coefficients on the dry side of maximum. These coefficients would be of the order of magnitude of those pictured in Fig. 40 (p. 83).

In the eastern portion of the state a lower suction is predicted for the same material. This lower suction could be near optimum moisture content or even wet of optimum. This would initiate freeze coefficients similar to those shown in Fig. 39 (p. 82), whose values are less than those for the drier area of the state. Thus, freeze contraction will be very active in west Texas but not in east Texas.

As was shown previously the residual behavior was influenced, by suction, in an opposite manner to the freeze contraction. Hence, the residual behavior would be more influential in east Texas where the suction would be lower than in west Texas. Figure 41 (p. 84) shows that materials in east Texas would mainly produce contraction with each freeze-thaw cycle; which may also serve to cause transverse cracking. The relationship with specific surface area is generally the same as for freeze behavior.

This chapter clearly shows the importance of the clay minerals and the environment on thermal susceptibility and alludes to

the fact that the environment influences more than just thermal susceptibility and may control the behavior of pavements in a general sense.

PARTICLE REORIENTATION MECHANISM

In the preceding chapters it was shown that the material commonly used as a base course material in west Texas underwent volume change upon freezing. It was further demonstrated that the state of moisture in the soil, viz., soil moisture suction, controlled the sense of this volume change; and for in situ materials this volume change is a contraction. The predictive relationships further show the importance of the clay mineralogy in influencing the magnitude of the contraction. The data indicate the outward appearance but do not explain the physical process behind the contraction. This chapter will examine the data collected, and discuss visual evidence in the formulation of a new theory concerning clay particle structure and reorientation.

Mathematical Model of Freeze-Thaw Behavior

Mathematical models which fit data offer a graphic method to analyze the behavior measured in the laboratory on a small number of samples. This allows the behavior to be predicted over a much wider range of variables. For the data presented here, the Lennard-Jones potential which depicts inter-molecular forces, relates directly to the freeze coefficient-suction data. The Lennard-Jones potential is shown in Fig. 42. The basics of this potential, developed in the study of equilibrium statistical mechanics (26) are the repulsion potential and the Van der Waal's forces of attraction. These two potentials are shown separately in Fig. 42. The equation for the Lennard-Jones potential is

$$\phi(r) = \varepsilon_o\{(\frac{r_o}{r})^{12} - 2(\frac{r_o}{r})^6\} \qquad (3\text{-}1)$$

The force, acting along centers of the molecules then, is

$$\frac{d\phi(r)}{dr} = \frac{12\varepsilon_o}{r_o}\{(\frac{r_o}{r})^{13} - (\frac{r_o}{r})^7\} \qquad (3\text{-}2)$$

and the forces vanish when the spacings is r_o. The relation with

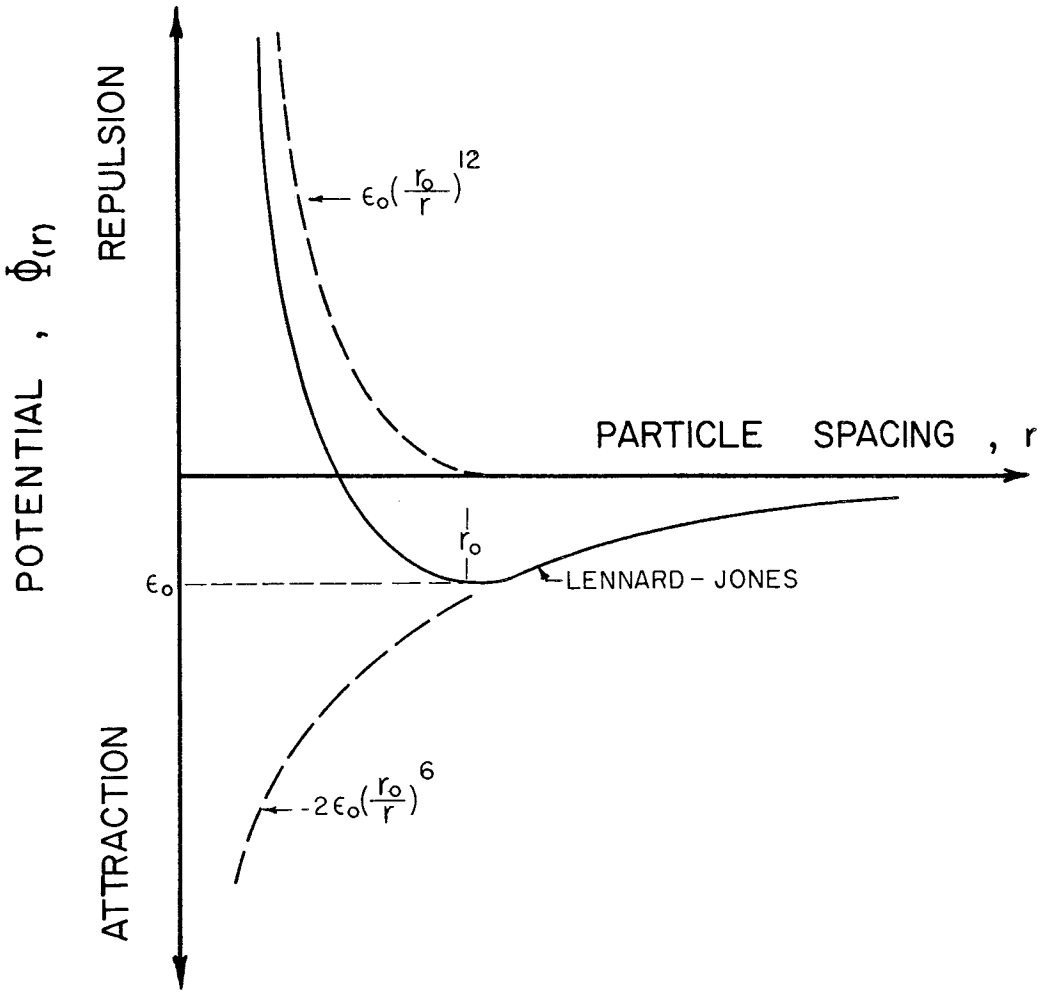

FIG. 42 - LENNARD-JONES POTENTIAL

the freeze data collected becomes apparent only upon studying the clay particles. Figure 43 illustrates the typical clay particle. The clay surface contains negative charges along the face due to substitutions in the mineral's crystalline structure. The edges of the mineral will have a net positive charge. Thus, a preferred orientation of a clay in a pure water system would be an edge to face, flocculated, structure as shown in Fig. 44.

In an actual clay-water system however, cations will be present in varying amounts. These cations are held on the clay surface by the negative charge. They are attracted to the clay surface by a force that varies exponentially away from the particle. (18). This attraction sets up what is commonly termed a diffuse double layer, as shown in Fig. 45.

The effect of these cations is to produce a flocculated structure through repulsion forces rather than attractive forces. The positively charged cations will be concentrated along the faces creating a more positively charged area. Thus, the repulsive forces will orient the clay particles in a preferred orientation, viz., a flocculated structure, much more readily than that formed by the attractive forces, which would be smaller.

The repulsive forces have been related to cation concentration as shown in Fig. 46 (6, 30). For a given repulsive force, an increase in cation concentration will produce a smaller particle spacing, up to some limit. Thus, the shape of the repulsive portion of the Lennard-Jones potential will be highly influenced by the cation concentration. Varied ion concentrations may result from varied solubility of the different salts in the base course materials.

In the Lennard-Jones potential model, intermolecular Van der Waal's force fields are responsible for the attraction potential. Babcock and Overstreet (2) show that "adsorptive force field effects" assumed due to Van der Waal's force fields will be of primary importance in soil systems at sufficiently low moisture contents; and as previously shown, the base course material is typically far below the saturation point. These forces will vary with the size

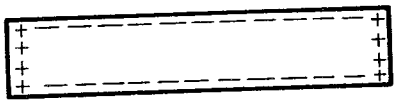

FIG. 43 - TYPICAL CLAY PARTICLE

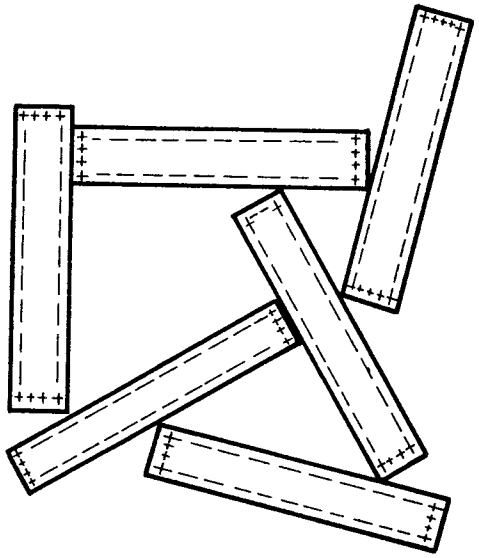

FIG. 44 - FLOCCULATED CLAY STRUCTURE

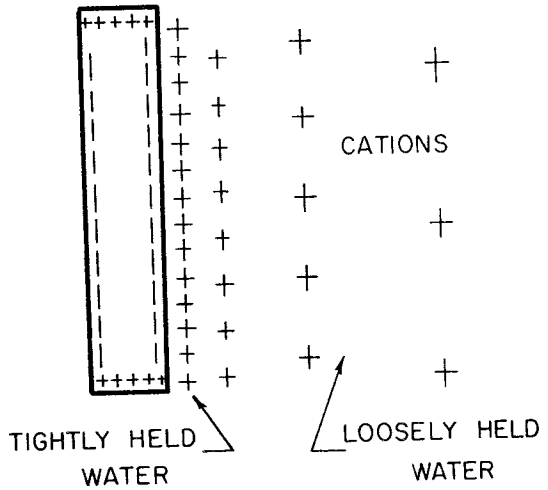

FIG. 45 - ILLUSTRATION OF DIFFUSE DOUBLE LAYER

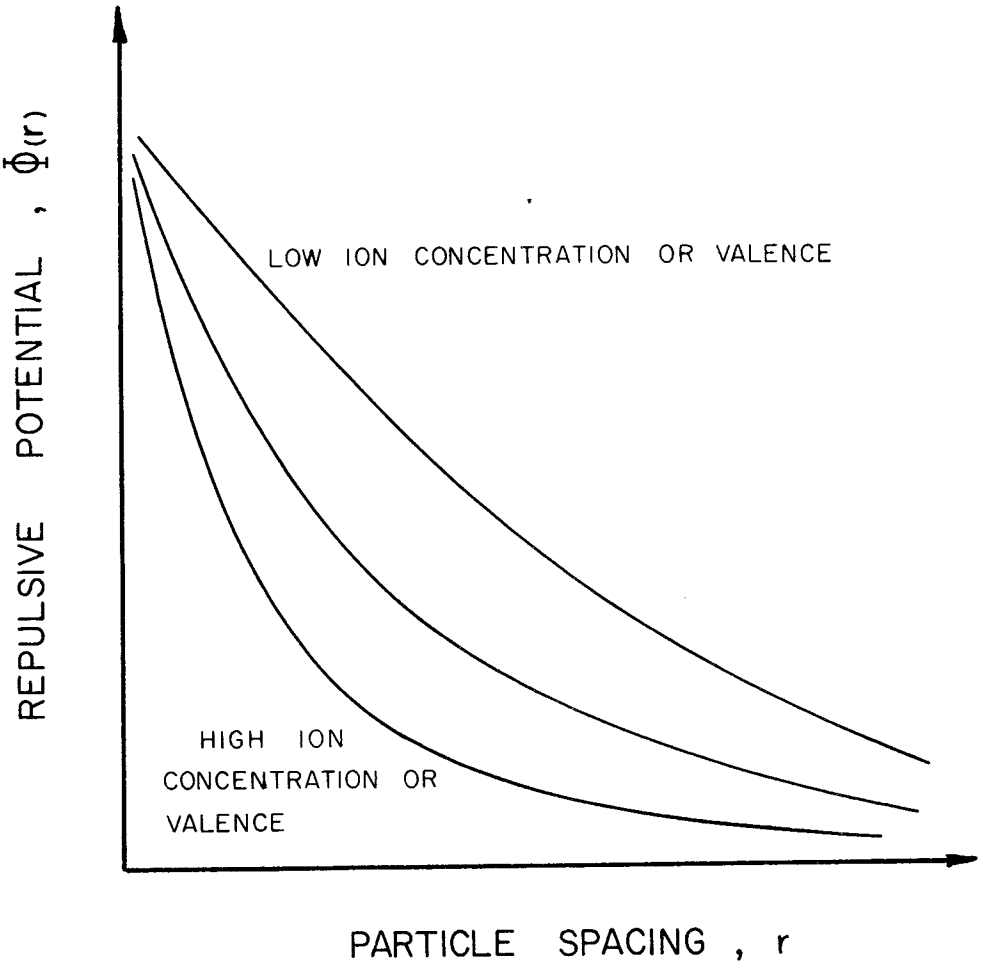

FIG. 46 - INFLUENCE OF ION CONCENTRATION ON CLAY PARTICLE REPULSION POTENTIAL

of the clay minerals (specific surface area) and the interaction of the water molecules with their surface. No data exist relating these forces to a physical property of the clay-water system. However, given the importance of clay mineral size in this "adsorptive force field" a relationship with specific surface area might exist and it might appear similar to the relationship proposed in Fig. 47.

The foregoing discussion hypothesizes that the components of a Lennard-Jones type model may be related to unique properties of the clay fraction. To see if these relationships are valid the ordinate and abscissa quantities must be related to their respective quantities on the freeze coefficient curve, viz., freeze contraction and suction.

Suction-Particle Spacing

As previously mentioned, suction is influenced primarily by particle size and structure in a given sample at a given moisture content. This arises from two considerations: the first being the amount of surface area exposed to the free water and the second being the radius of curvature of the meniscus formed at the particle contacts.

Each clay particle will adsorb moisture on its surface in varying amounts. This moisture is tightly held and possesses a structure somewhat similar to ice (23). As the distance from the clay particle surface increases, the water becomes less structured until it becomes essentially free water. If the particle structure is relatively open, or flocculated, the available water will spread itself relatively thinly over all the particles. This may leave little or no free moisture in the sample, producing a high suction. If the particle structure is relatively closed, or dispersed, the particles will be pulled closer together due to charge imbalances between the clay surface and the ion concentration in the surrounding water. This particle arrangement produces effectively larger particles and lower surface areas which results in lower suctions as there is a larger amount of free water available. This relationship is

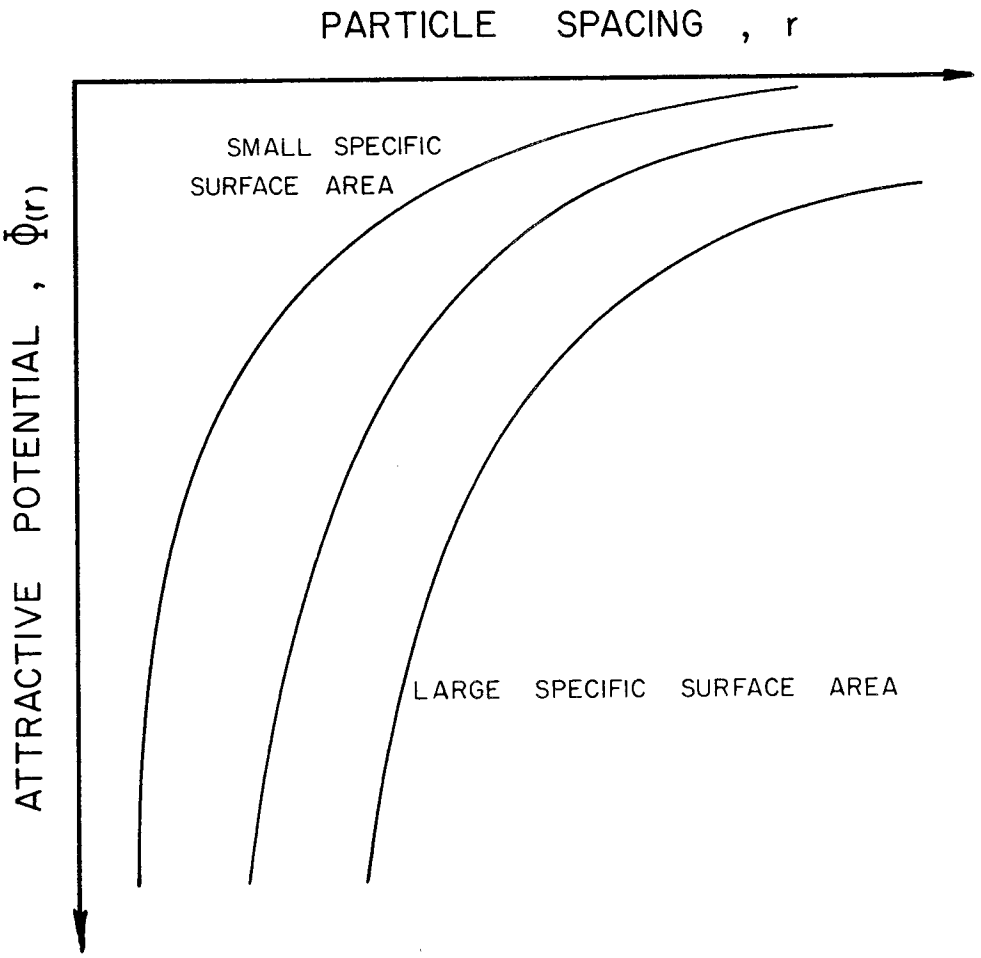

FIG. 47 - PROPOSED RELATIONSHIP BETWEEN SPECIFIC SURFACE AREA AND CLAY PARTICLE ATTRACTION POTENTIAL

depicted schematically in Fig. 48.

Consider a perfectly flocculated particle structure in which the clay particles are aligned edge to face at right angles to each other. This structure would have the highest possible suction of any structure for a given moisture content. The particles would also be at their maximum spacing in this structure. This average center to center distance could be normalized to give the value of unity for the largest spacing.

Considering a perfectly dispersed structure at the same moisture content, the volume will be smaller and the particles will have a face to face orientation. The particles are such that they will have their minimum center to center spacing. Additional water will be utilized solely as free water and will increase the particle center to center spacing.

Structure variations are also produced by compaction (30,38 , 13). The compaction of a wet sample produces a dispersed structure and a low suction; while compaction of a dry sample produces a flocculated sample and a high suction. Suction, acting as a negative pore pressure, produces the structure under the effects of compaction and not the other way around, viz. the structure does not produce the suction; although a relationship between the two is possible either way. Figure 49 is the relationship between moisture content and suction for the base course material used in this study. This curve also gives a relative indication of the structure. The moist end will be dispersed and the dry end will be flocculated. The equation for this relationship was given in Chapter II, equation (2-4) which is:

$$\log h = \log(a) + b \log W \qquad (2\text{-}4)$$

or

$$h = a(W)^{b}$$

The slope is then given by

$$\text{Slope} = b \cdot a \cdot W^{(b-1)} \qquad (3\text{-}3)$$

There are two distinct straight line portions to the curves. One is the low moisture region, the other is at the high moisture content

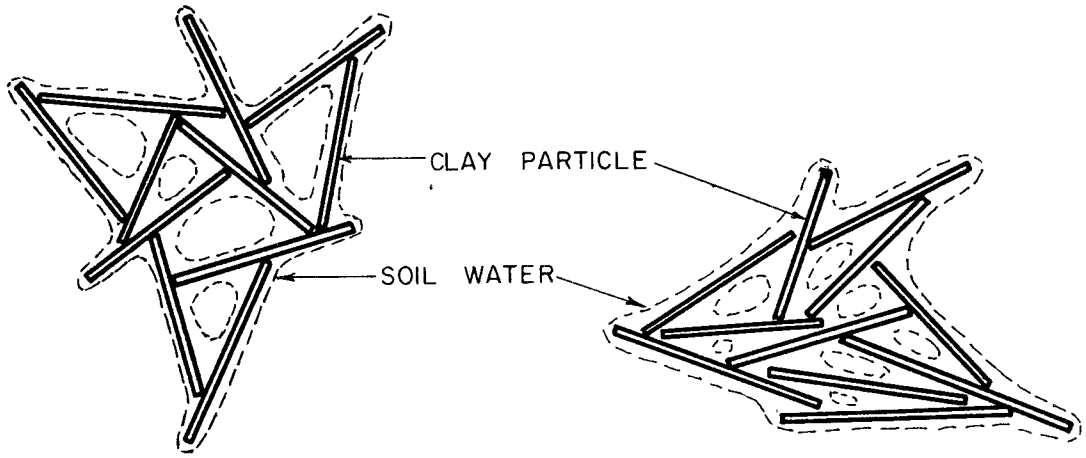

FIG.48 - INFLUENCE OF STRUCTURE ON FREE WATER

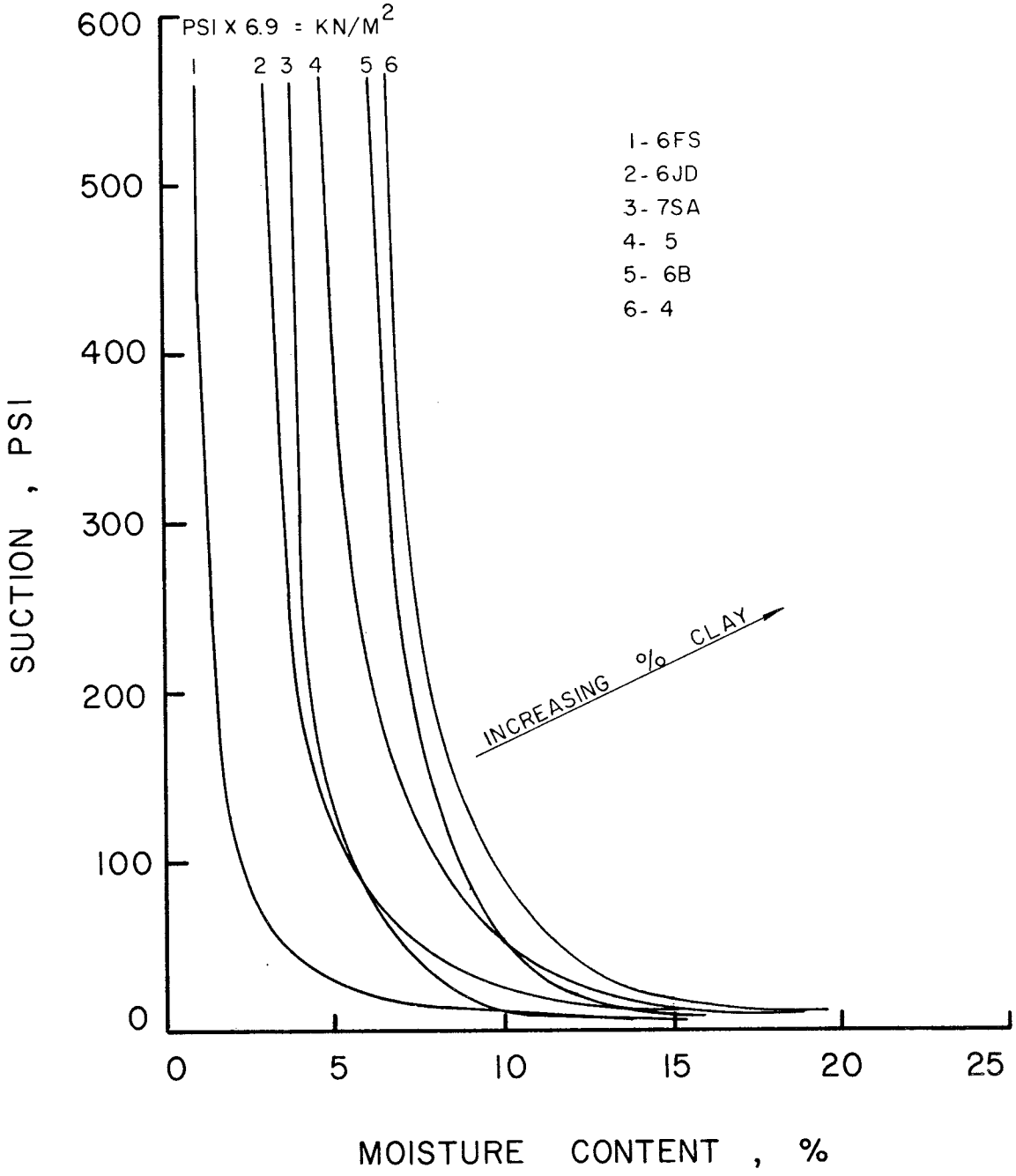

FIG. 49 - SUCTION AS A FUNCTION OF MOISTURE CONTENT FOR THE BASE COURSE SAMPLES

end of the curve. It is postulated that at the extremes of these curves the structures will be relatively constant, and the suction variations will be due primarily to moisture changes. The curved portion of the curve will represent the change in structure in addition to moisture change. This curve could be thought of then as representing a change in the center to center particle spacing. This change would be from a maximum at the linear portion with the highest slope (OR=1.0) to a minimum at the linear portion with the lowest slope (OR=0.0), where OR is the orientation ratio . Letting the orientation of the particles, hence their separation, be designated by θ (the angle between the particles) the spacing between the particles will vary as the sine of the angle θ. Intermediate values of θ were determined by linear interpolation using the moisture content of the asymptotic points on the linear portions of the curves. Table 19 shows the orientation ratio (OR) at which the maximum freeze contraction occurred. The similarity indicates that the maximum freeze contraction occurs at the same particle orientation or structure. This would be expected since the materials are being acted upon by the same external influence. This is not to imply that all the particles are oriented at an average angle of 50 degrees at maximum contraction, but only that similar orientations, regardless of magnitude, are likely. Thus, if the freeze coefficient curve were plotted against the orientation ratio, the curve in Fig.50 would result. This figure is essentially the same as the "Lennard-Jones" type model.

Potential-Freeze coefficient

In the Lennard-Jones potential function, the ordinate represents the potential energy existing between two molecules at varying distances from each other. In the freeze coefficient curve the ordinate represents an expansion or contraction of the structure under a uniform decrease in temperature (energy change). This volume change represents the resultant activity of a force imbalance in the sample. In this instance the force is not related simply to the particle spacing, but to a complex arrangement of moisture and particle spacing. This arrangement is expressed as the soil moisture suction, which has been assumed, in an oversimplification, to be related to particle spacing or orientation

TABLE 19. - ORIENTATION RATIOS FOR THE BASE COURSE MATERIALS

MATERIAL	ORIENTATION RATIO (OR)
4	0.79
5	0.75
6B	0.81
6JD	0.74
7SA	0.75
6FS	0.80

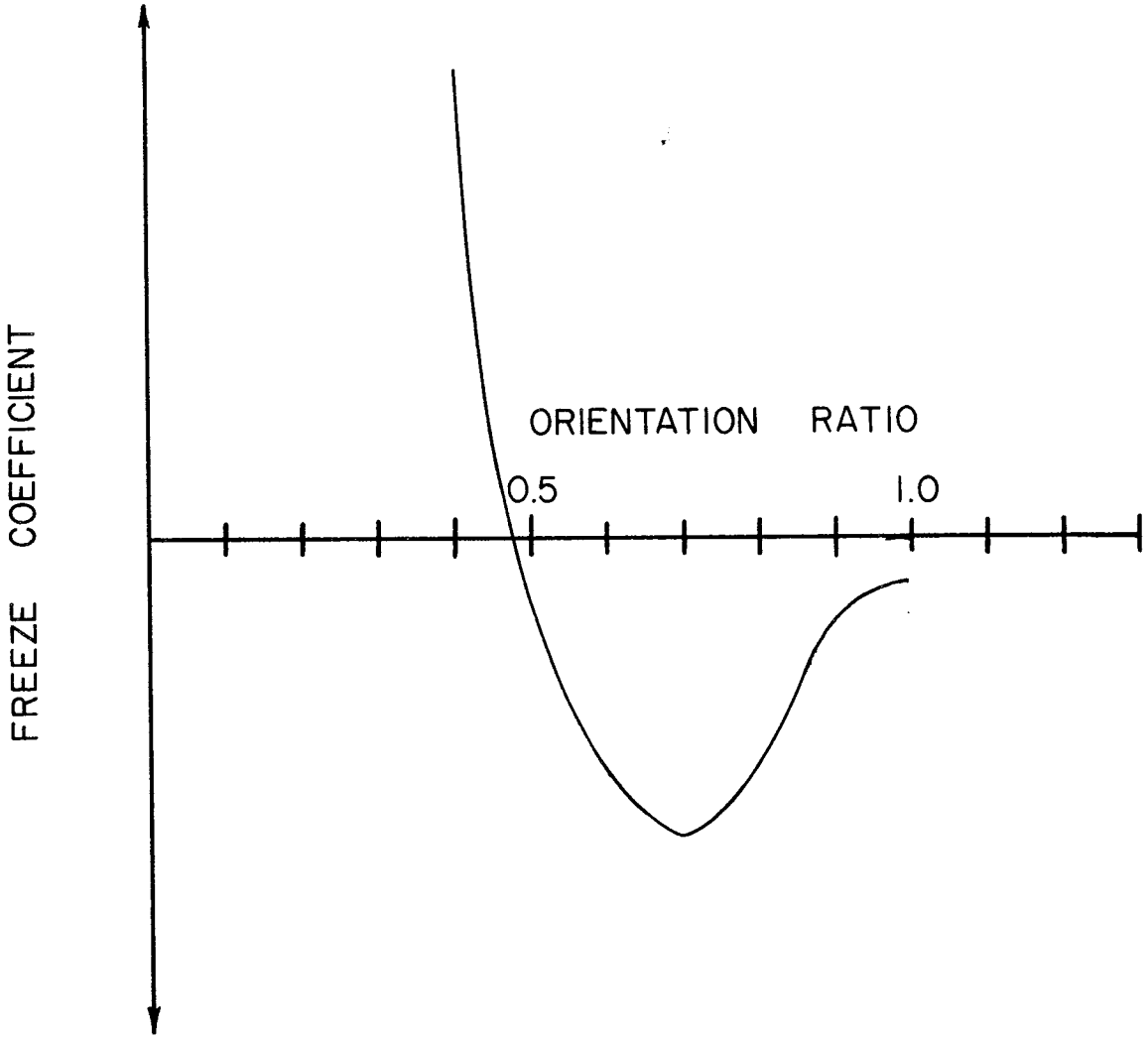

FIG. 50 - FREEZE COEFFICIENT VERSUS ORIENTATION RATIO

alone. The freeze coefficient is representative of the work done by a fixed change in energy status of the sample as a whole. This coefficient is the result of a physical activity within the soil system caused by forces acting between the particles. As such it may be thought of as the resultant movement of the particles if they were allowed to reorient themselves and were not restrained, as would be done if the forces acting were being measured. Thus, the movement would be proportional to the force, and have the same sign. Put another way, molecules have work done on them to separate them a fixed distance. Different molecules need differing amounts of work to move them the same distance. Analogously, under the same amount of work, there will be unequal particle movements. This gives differing forces associated with movement. The freeze coefficient data represents measured movements, which can be compared directly to forces.

In a rather facile method the freeze coefficient curve has been shown to be analogous to the Lennard-Jones potential. If the relationships are valid, the freeze coefficient curve data should indicate the quantities mentioned earlier,viz., the specific surface area and the ion concentration in the soil moisture as depicted in Fig. 46 (p.91) and Fig. 47 (p.93).

Freeze Coefficient Regression Results

The freeze coefficient curve data were regressed to determine the exponents in the "Lennard-Jones" type model proposed for the freeze-thaw behavior. These are listed in Table 20. The resulting curves from these coefficients are shown in Fig. 51 through Fig. 56 for the Modified AASHTO samples. The relationship of these coefficients with the mineral properties, specific surface area and ion concentration, which is illustrated in Fig. 57 and Fig. 58, clearly demonstrates the proposed relationships with freeze activity. The exponent B relates to the specific surface area and the exponent A relates to the ion concentration of the material.

The specific surface area was determined previously. The ion concentration has been illustrated by the resistivity of the samples. Resistivity can be inversely related to the ion concentration in a

TABLE 20. - THE "LENNARD-JONES" COEFFICIENTS, A AND B

MATERIAL	SPECIFIC SURFACE AREA B	ION CONCENTRATION A
4	6.8	18
5	5.0	12
6B	4.0	30
6JD	8.0	14
7SA	3.5	15
6FS	3.0	60

granular material. If a fluid has a very high resistance to the flow of current, this indicates a lack of ions to conduct the electrons. If there is little or no resistance to the flow of current, this indicates a large amount of ions present to conduct the electrons. Thus, if one material is more soluble than another, there will be more ions dissolved in the pore fluids; thereby being made available to the clay particles. This more soluble material would have the lower resistance to current flow.

The base course materials utilized in this study were mixed to a constant moisture content and compacted equally to a thickness of one centimeter. Aluminum foil electrodes were placed on either side of the soil sample and the resistivity across the one centimeter sample was measured. With similar clay materials being present, differences in the resistivity should reflect the differences in the ion concentration in the pore fluids.

These coefficients, as determined, are material property indicators and are independent of the compaction method. This is shown in Fig. 59 through Fig. 63, which illustrate the samples

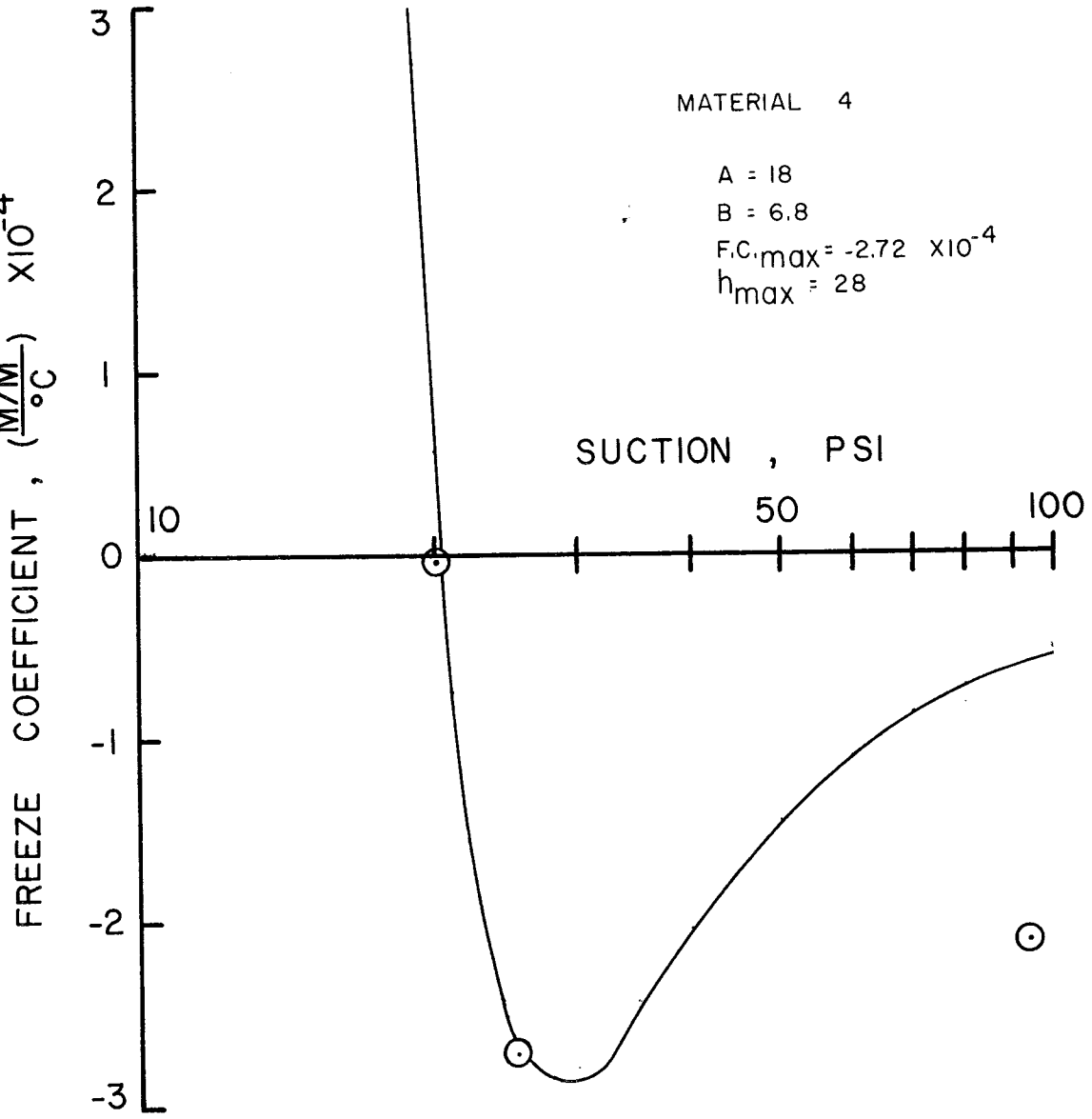

FIG. 51 - FREEZE COEFFICIENT-SUCTION CURVE FOR MATERIAL 4

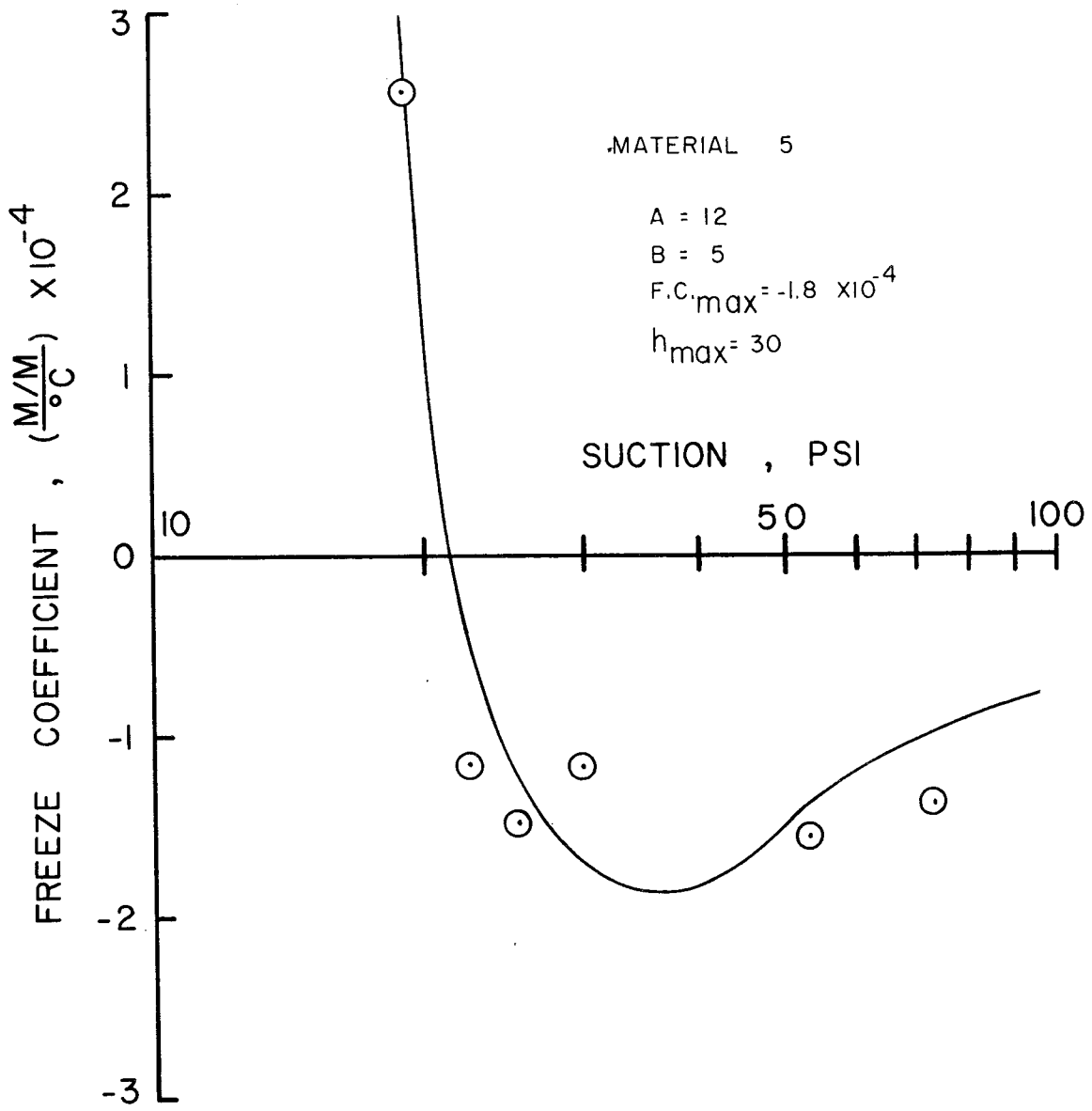

FIG. 52 - FREEZE COEFFICIENT-SUCTION CURVE FOR MATERIAL 5

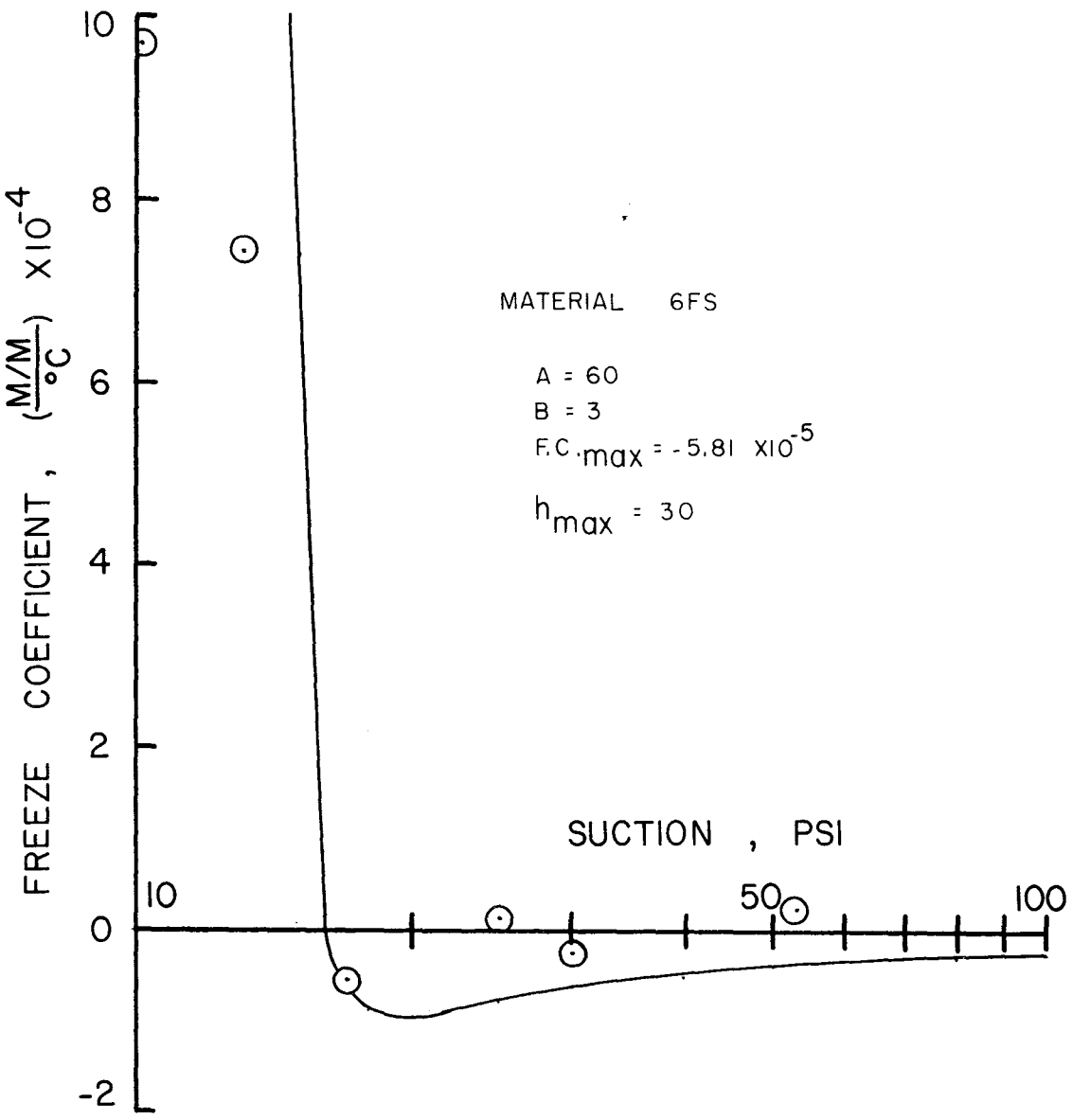

FIG. 53 - FREEZE COEFFICIENT-SUCTION CURVE FOR MATERIAL 6FS

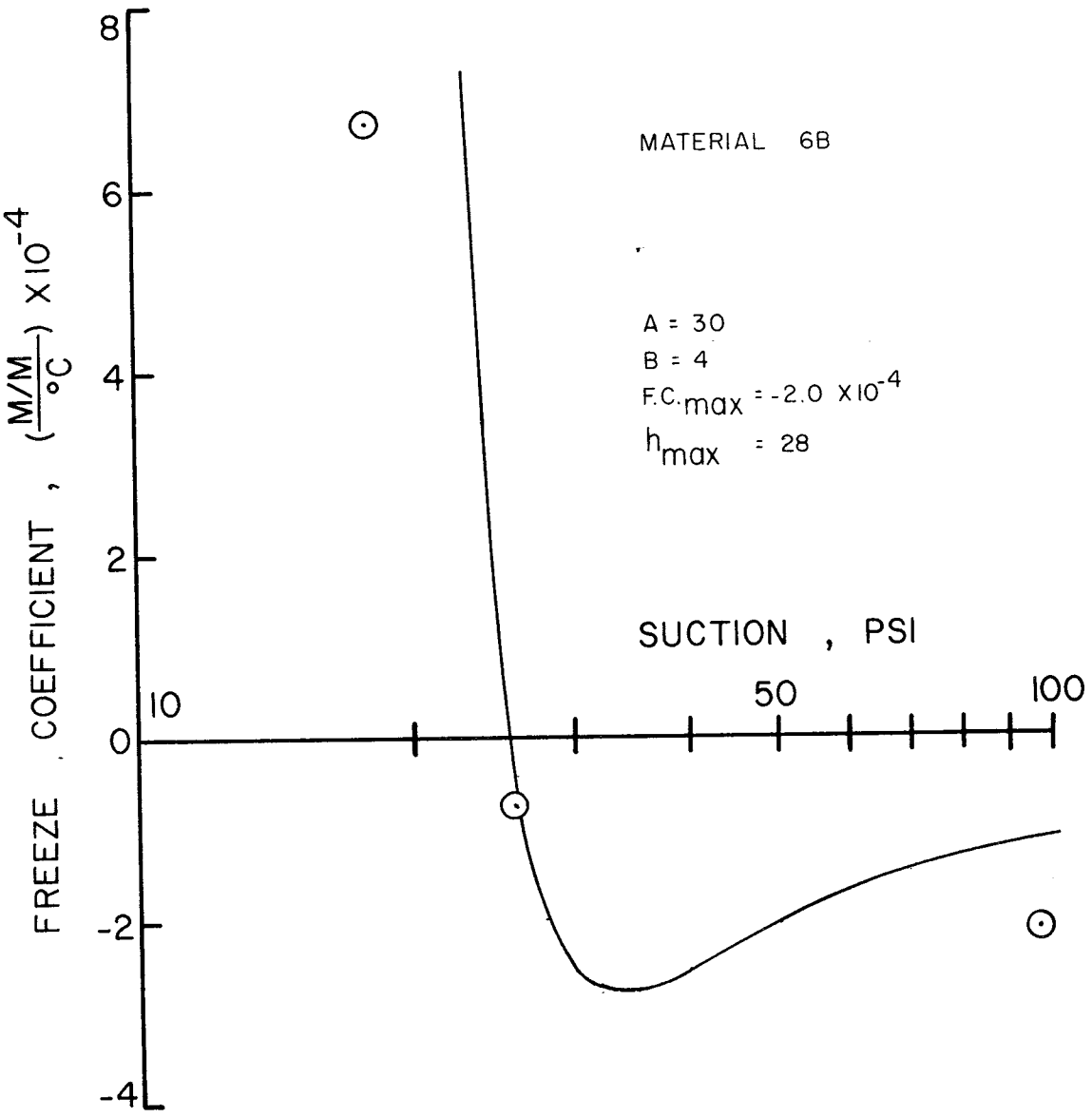

FIG. 54 - FREEZE COEFFICIENT - SUCTION CURVE FOR MATERIAL 6B

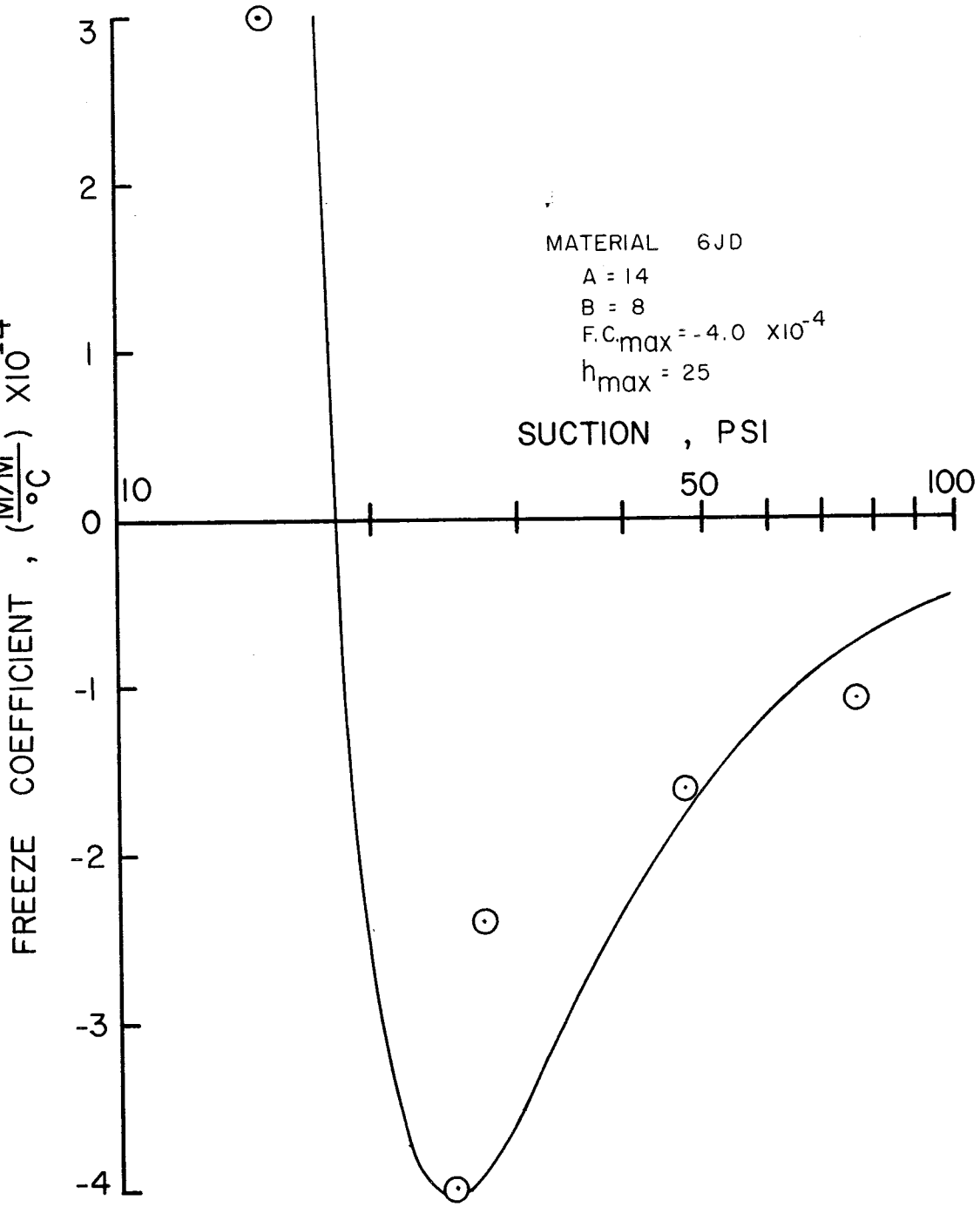

FIG. 55 - FREEZE COEFFICIENT - SUCTION CURVE FOR MATERIAL 6JD

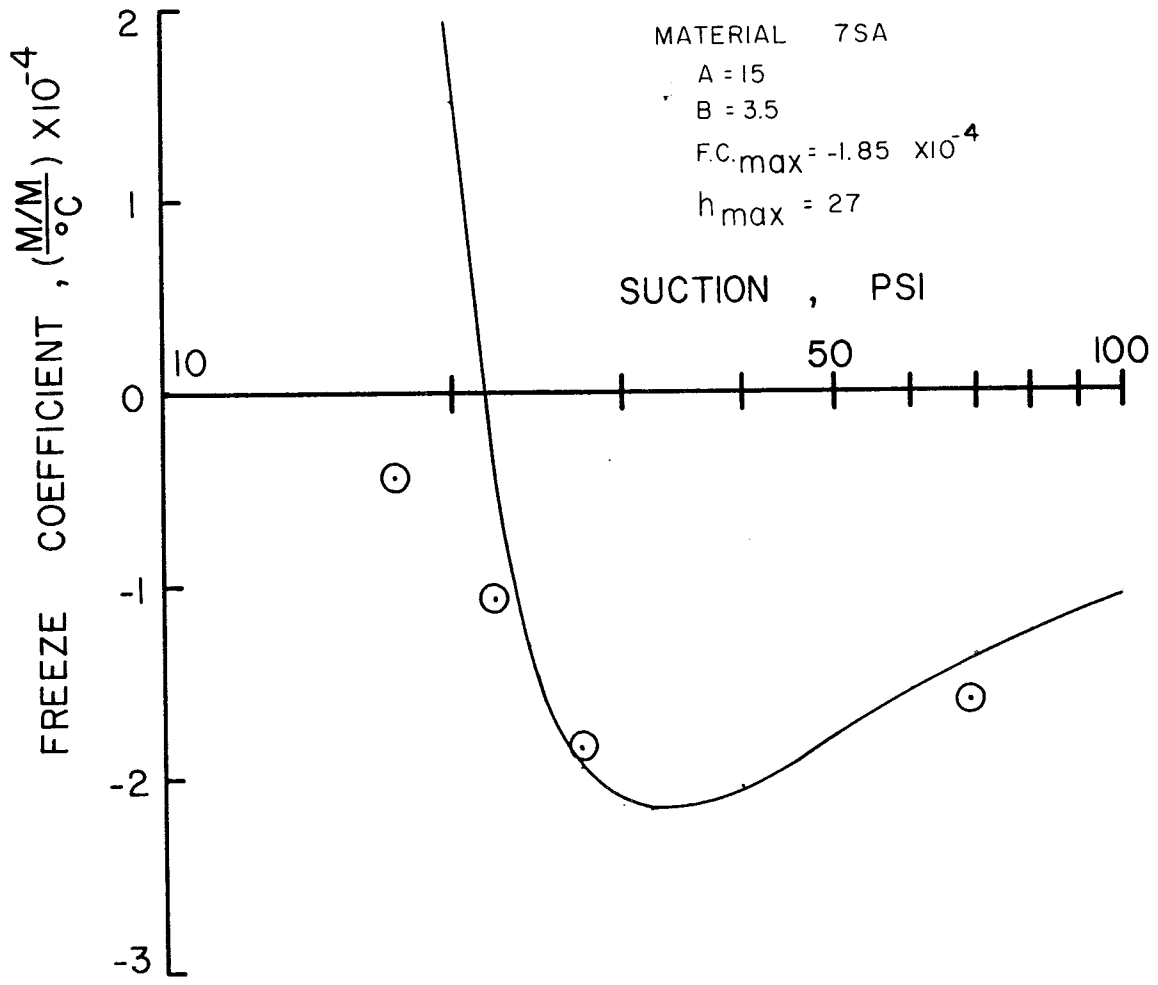

FIG. 56 - FREEZE COEFFICIENT - SUCTION CURVE FOR MATERIAL 7SA

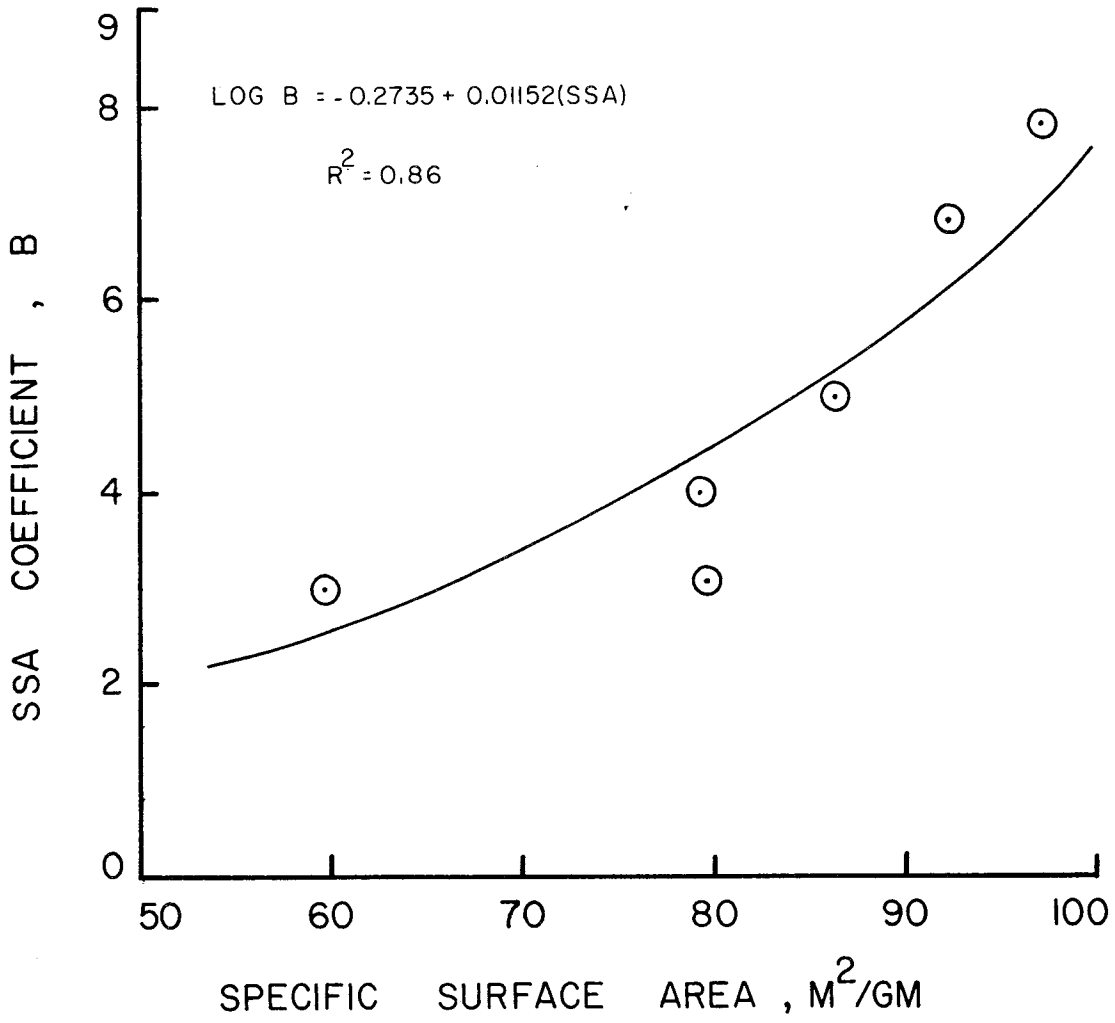

FIG. 57 - LENNARD-JONES B COEFFICIENT AS A FUNCTION OF SPECIFIC SURFACE AREA

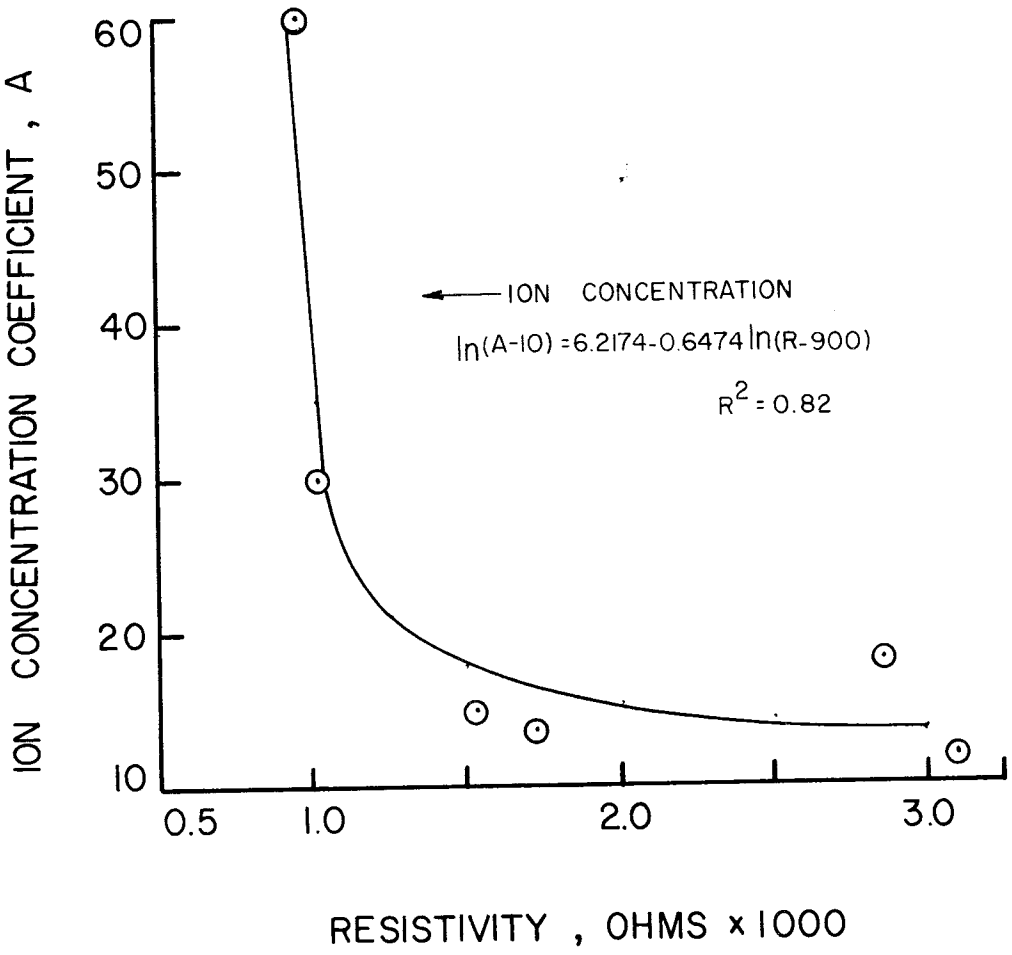

FIG. 58 - LENNARD-JONES A COEFFICIENT AS A FUNCTION OF RESISTIVITY (ION CONCENTRATION)

compacted with the spring loaded compactor to 95 percent of Modified AASHTO with the Lennard-Jones potential plotted through the freeze coefficient data. The exponents determined from the Modified AASHTO samples produced very acceptable data fits with the exception of material 7SA which required higher exponents. The relationships developed clearly indicate the material property relationships for the freeze activity.

The necessary relationships required to predict the freeze coefficient may all be calculated from easily determined material properties. These are as follows:

1) Maximum freeze coefficient from Specific Surface Area by equation (2-7),
2) Suction from the moisture content and percent clay by equations (2-4), (2-5) and (2-6),
3) Suction at the maximum freeze coefficient:

$$h_{max} = 15.705 + 1.4205(\% \text{ Clay}) \qquad R^2 = 0.96 \qquad (3\text{-}3)$$

4) A from the ionic concentration:

$$\ln(A\text{-}10) = 6.2174 - 0.6474 \ln(R\text{-}900) \qquad R^2 = 0.82 \qquad (3\text{-}4)$$

5) B from the Specific Surface Area:

$$\log_{10} B = -0.2735 + 0.01152 \text{ (SSA)} \qquad R^2 = 0.86 \qquad (3\text{-}5)$$

It is apparent that the physical and chemical mineralogical properties are the important quantities in determining the thermal behavior of the base course material.

Residual Coefficients

The residual behavior of the base course is of major importance primarily in extremely wet circumstances as stated previously. The residual behavior is of only secondary importance and is not listed here with the predictive relationships as it does not provide insight into the particle reorientation theory.

Implications of Mathematical Models

The relationship of the "Lennard-Jones" type model with the freeze coefficient curve indicates that the measured movement is directly attributable to the clay minerals. The mechanism behind

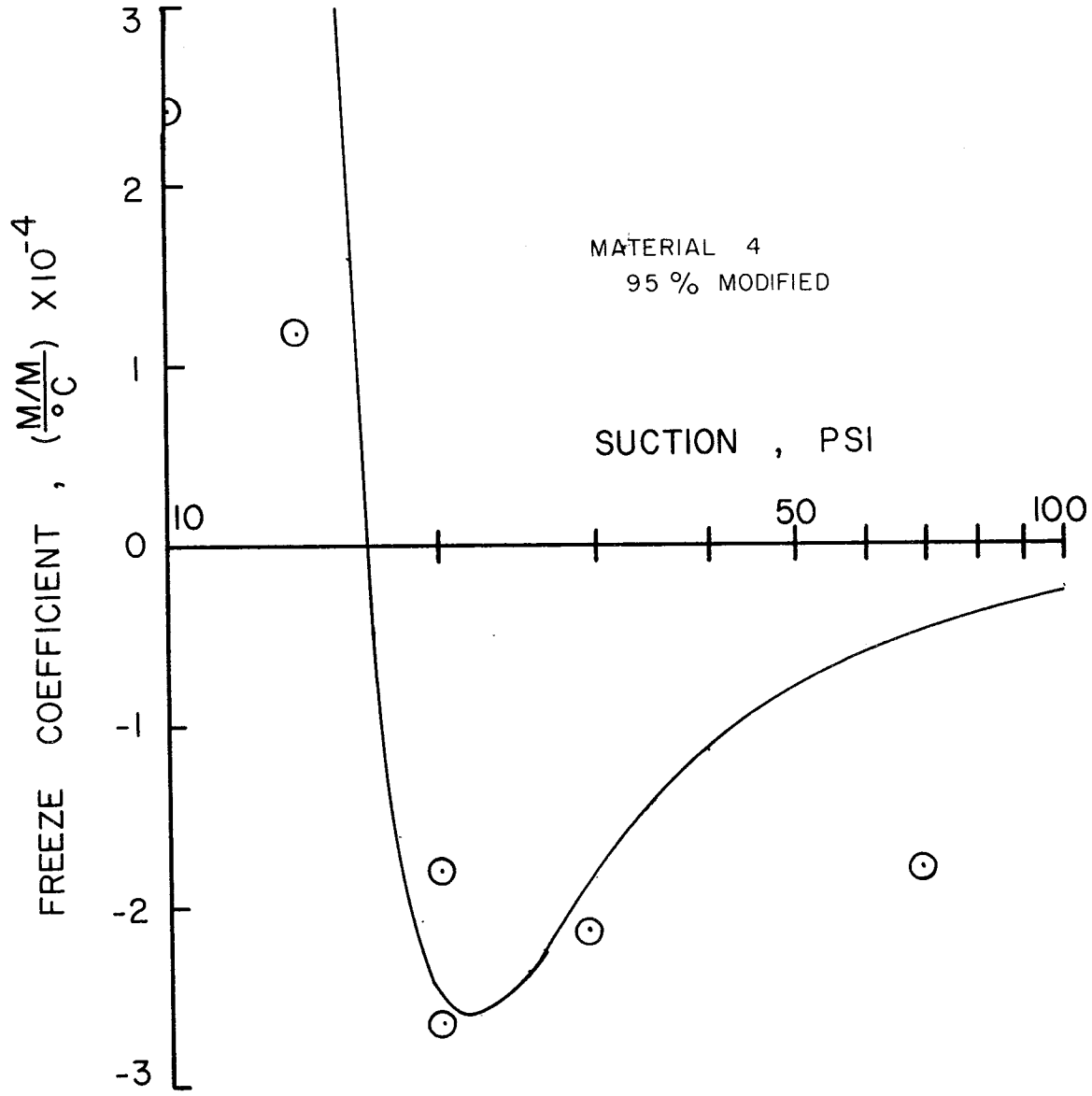

FIG. 59 - FREEZE COEFFICIENT-SUCTION CURVE, 95% MODIFIED, MATERIAL 4

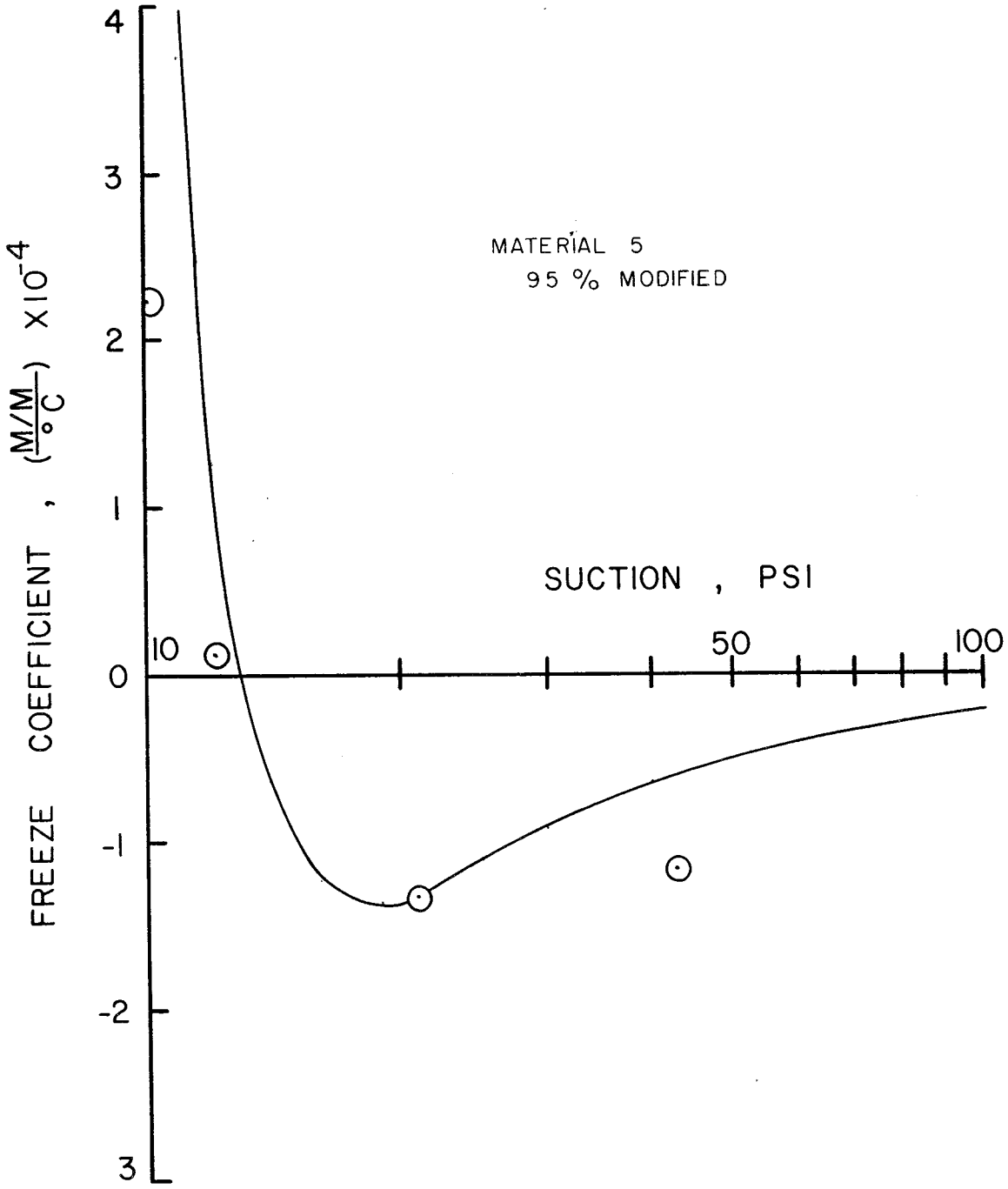

FIG. 60 - FREEZE COEFFICIENT-SUCTION CURVE, 95% MODIFIED, MATERIAL 5

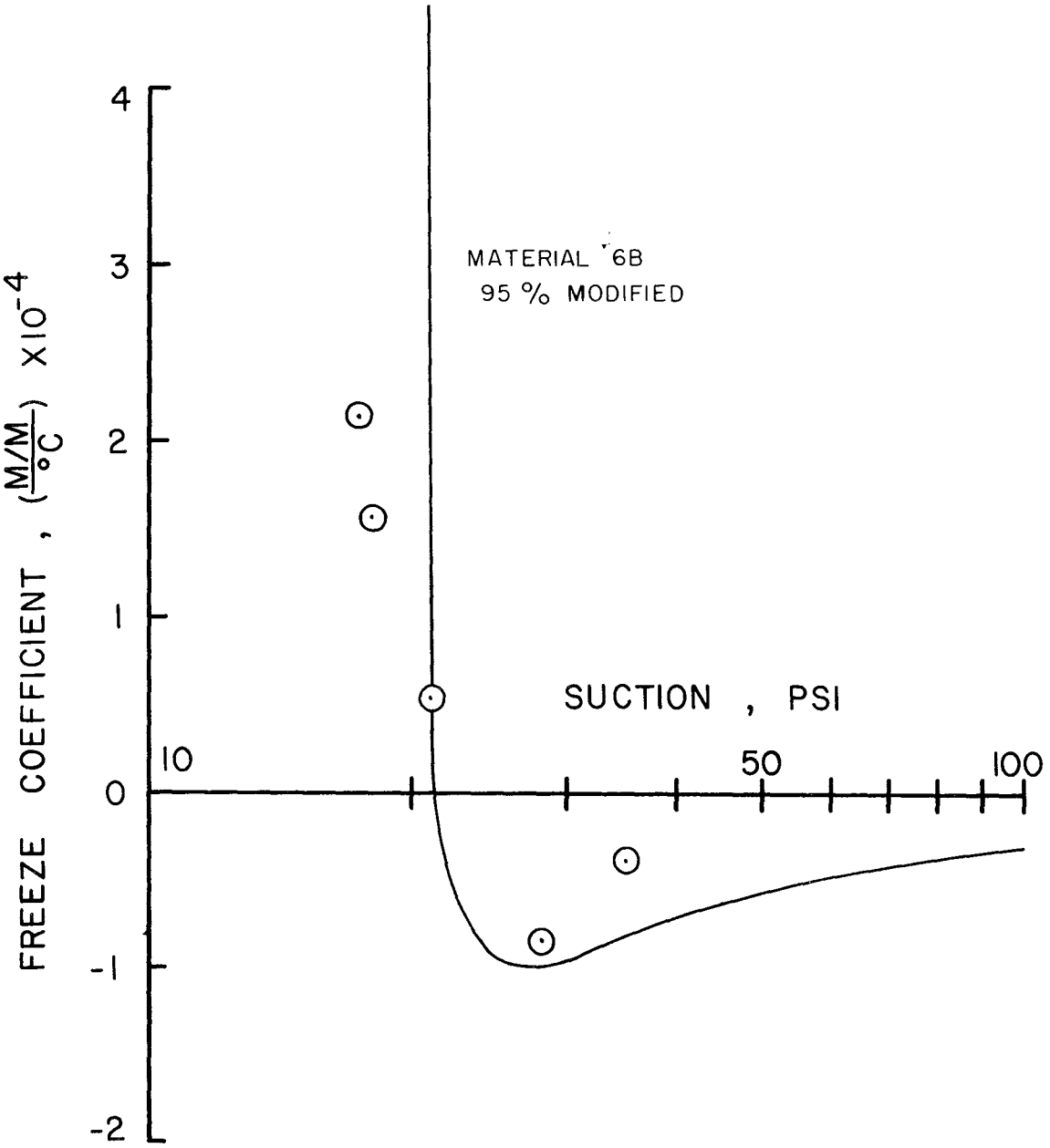

FIG. 61 - FREEZE COEFFICIENT-SUCTION CURVE,95% MODIFIED, MATERIAL 6B

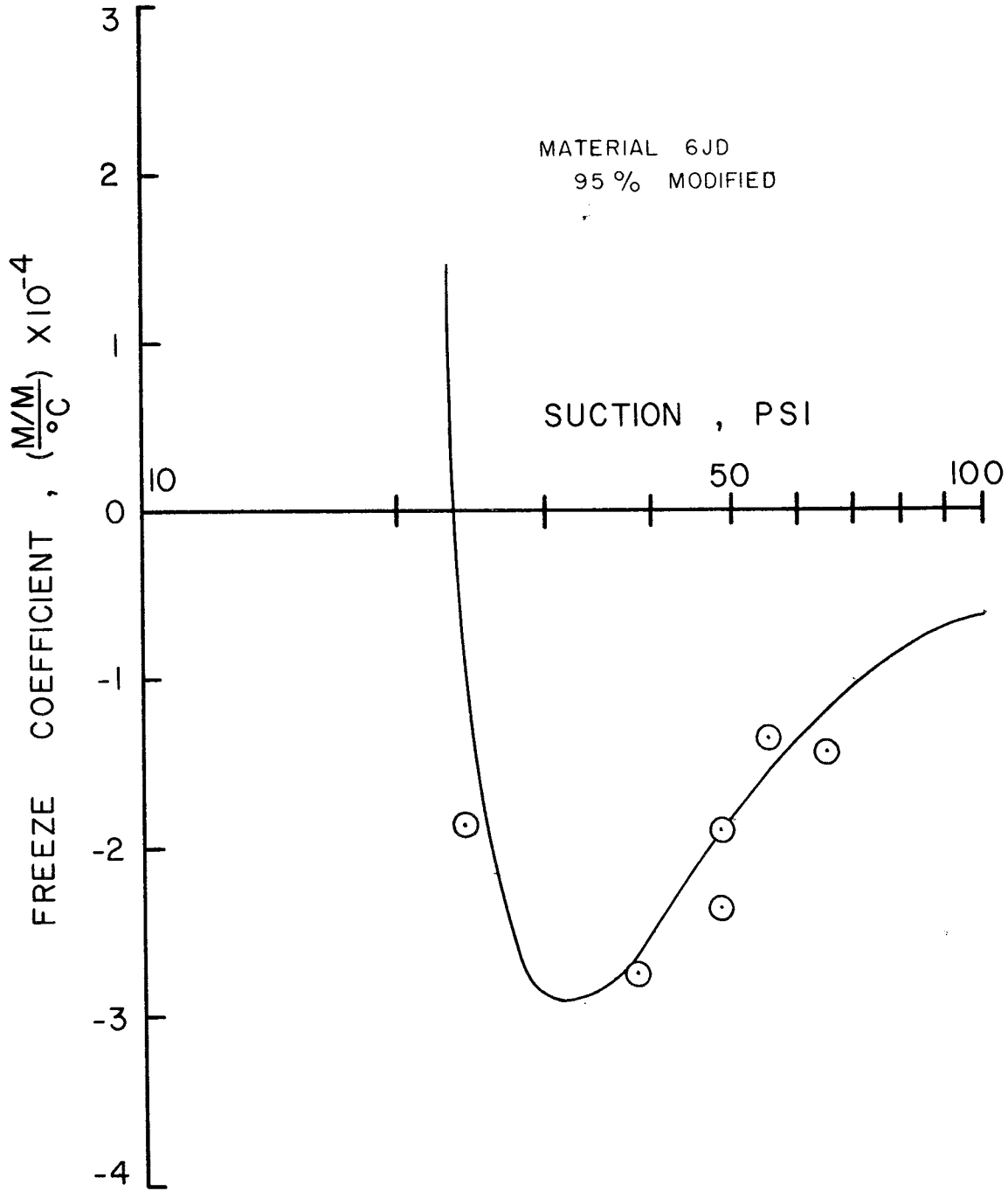

FIG. 62 - FREEZE COEFFICIENT-SUCTION CURVE,95% MODIFIED, MATERIAL 6JD

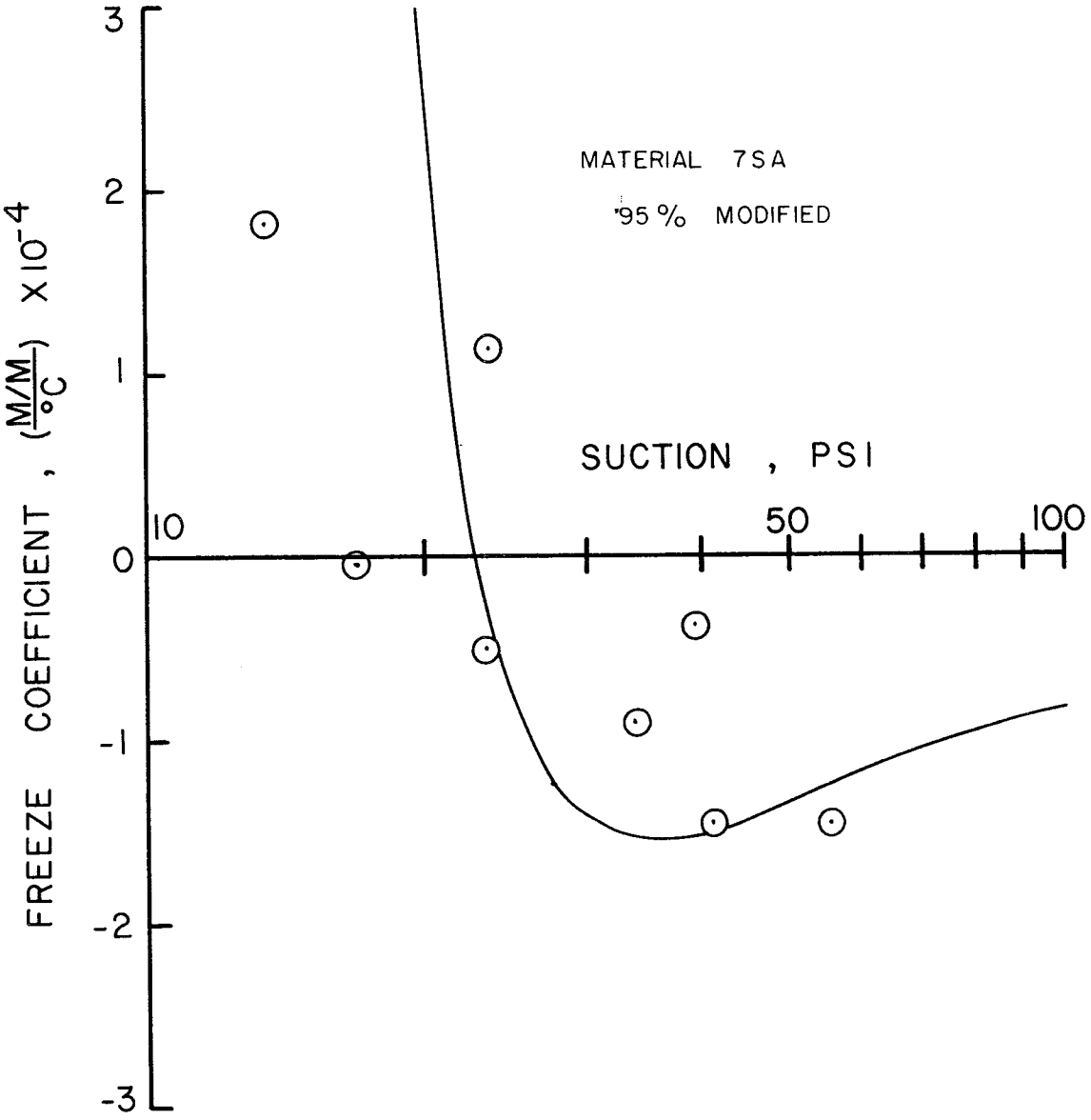

FIG. 63 - FREEZE COEFFICIENT-SUCTION CURVE,95% MODIFIED, MATERIAL 7SA

the volume change then should logically lie in the clay minerals and their interaction with the moisture in the material. The freezing process involves an expansion of the moisture that freezes; therefore, the contraction will come from the clay particles and appears to involve some form of a particle reorientation.

Proposed Mechanism for Freeze-Thaw Activity

There are three areas of freeze activity that can be interpreted from Fig.17 (p.34) and the physical data presented earlier. These areas are:

1. Sample with maximum freeze coefficient.
2. A sample very dry of optimum moisture content with a flocculated structure.
3. A sample very wet of optimum moisture with a dispersed structure.

It has been shown previously that in a soil material all the moisture will not freeze. It was further shown that the moisture in the samples could be estimated by recording the suction. The interpretation of the suction data during freezing and the deformation during freezing and thawing provide the following descriptions of possible mechanisms.

Dry Sample - A dry sample will have a flocculated structure. A perfectly flocculated structure would have the particles at right angles and the only deformation would be bending or elongation and the freeze coefficient would be near zero. The residual behavior for the driest samples typically shows a very small contraction with an expansion possible, possibly as a rebound phenomonen. This sample is of little concern in engineering problems as construction is seldom done with material this dry.

Wet Sample - A completely wet sample will have a dispersed structure. In a dispersed structure as the water freezes the free water in the voids will expand. The increase in suction caused by the freezing will draw a certain amount of water out from around the dispersed clay particles causing a volume decrease.

The expansion and contraction may be balanced giving an overall freeze coefficient of zero. In a wetter sample the expansion of the water would dominate and the freeze coefficient would be positive, expansion .

Sample with Maximum FC - The sample with the maximum freeze coefficient occupies a unique position on the compaction curve and the freeze coefficient curve. For the modified AASHTO samples the maximum freeze coefficient consistently occurred on the dry side of the optimum moisture content position. For the Harvard miniature samples the maximum freeze coefficient consistently occurred on the wet side of the optimum moisture content position. This would at first appear to be a contradiction; however, an understanding of the methods of compaction explains the difference. The Harvard miniature method of compaction is a kneading method of compaction. This method of compaction produces a more flocculated structure than the impact method (30). Thus, a wetter sample compacted by the kneading method would have the same particle structure as the drier sample compacted by the impact method. From this interpretation it is logical to assume that both samples would have the same particle structure while having different moisture contents.

When this sample is frozen several things happen. As the material freezes, the suction increases due to the loss of free water as it becomes ice; however, the adsorbed water and the water held in extremely fine pores will not freeze. As the temperature becomes even lower, still more water freezes and the menisci of the remaining water becomes smaller, serving to increase the suction in the material even more. This action serves to produce greater and greater tensile forces in the menisci. These forces tend to pull the particles surrounded by the adsorbed

water into closer contact, decreasing the available surface area and making more free water available for freezing. These actions continue to the point where lowering the temperature further cannot freeze additional adsorbed water or water held in the extremely fine pore spaces. This tends to explain the behavior noted in Hamilton's study where the soil exhibited nearly all the thermal activity in the temperature range of $32^{o}F$ ($0^{o}C$) to $20^{o}F$ ($-6.7^{o}C$). This suggests that at a temperature of $20^{o}F$ ($-6.7^{o}C$) all the soil moisture is frozen that will freeze.

This freezing action leaves the clay particles pulled together with little more than their film of adsorbed water surrounding them. As this water layer is highly ordered, as previously discussed, the particle arrangement in this frozen state would be such that the parallel faces of the clay minerals would have been pulled into alignment. This configuration is likely, even though the preferred particle attraction is edge to face, since the surface tension forces (suction) increase on freezing and the particle attraction forces may even decrease (32).

As a material thaws, the ice in the smaller voids will thaw first and the larger voids will thaw last. This will result in a general redistribution of water away from the finer particles due to the energy gradient and temperature gradient. Once the material is thawed, the clay minerals will attempt to assume the position they had originally with the preferred edge to face relationship. Although more free water has been made available it has been made available mainly to the larger particles leaving the clay minerals in a more dispersed form held together by the adsorbed water film. The tensile forces exerted by this water film will not allow the particles to separate completely, thus causing the non-recoverable strain noted.

The proposed particle reorientation and permanent volume change will produce a more open or honeycombed soil structure. This structure would account for the observed loss in load carrying strength (5) and viscoelastic properties (39) as well as the noted decrease in suction following freeze-thaw. This decrease

in the suction to a value below that of the original, as-compacted suction, is caused by the increase in free water resulting from the decrease in effective surface area as the clay particles rearranged themselves into tighter groups. This rearrangement of particles continues for each freeze-thaw cycle until an optimum state is attained where the clay particles do not undergo any further rearrangement. This is indicated in the study that measured the effect of freeze-thaw cycles on the viscoelastic characteristics of a clay material. Their results indicate that after nine freeze-thaw cycles there is negligible change in the viscoelastic properties.

The proposed mechanism for the observed volume changes during freeze-thaw cycling is based solely on a clay particle reorientation effected primarily by the soil moisture. This theory is supported by the indirect physical data already discussed and was developed primarily from these data. Direct physical evidence is necessary, however, to support this unique damage theory. This evidence was collected through the use of the scanning electron microscope.

Scanning Electron Microscope Investigation

Methods and Materials

Samples selected for the scanning electron microscope investigation were compacted at the same moisture content, dry of optimum moisture content, by the kneading action of the Harvard miniature compactor; which produces a flocculated structure, tending accentuate the maximum freeze contraction. Half of the sample set were subjected to a series of six freeze-thaw cycles. Upon completion of the final thaw cycle both sets of samples were unsealed and allowed to slowly air dry in a covered dessicator. Upon completion of the slow air drying the samples were fractured to obtain microscope size specimens, approximately one cm. cubes. Surfaces normal and parallel to the direction of compaction were then cleared of damaged particles by the repeated application of

adhesive tape. These specimens were then stored in a vacuum dessicator over a dessicant. This procedure was utilized by Barden and Sides (4) and by Compton (13) with good results for scanning electron microscopy investigation of clay rich samples. All specimens were examined in the secondary electron mode of the scanning electron microscope.

Physical Properties

Since this is an optical investigation of the clay particles the physical properties should be discussed to obtain familiarity with the general topological features. The major minerals are attapulgite, montmorillonite, kaolinite and mica.

Attapulgite

This clay mineral, often termed palygorskite, is a fibrous mineral typically 50-100 Å in diameter and many microns in length as given by Grim (18). The fibers have channel-like interstices which run the length of the fiber. The interstices hold water molecules, termed zeolitic water, which is held tighter than free water, and as such this mineral has a large influence on the suction which would develop. The structure of this mineral gives it an open surface and the specific surface area of 130 M^2/gm given by Brunauer et al., (8) emphasizes the open nature of this mineral and the potential for moisture movement.

Montmorillonite

The structure of this mineral is vastly different from that of attapulgite. Montmorillonite is extremely fined sized, commonly in the range of 0.8μm and smaller in diameter and is extremely thin. Montmorillonite typically forms a fine film since the small particles cling together. The small size (and flat shape) of montmorillonite particles gives them a large specific surface area. Theoretical values typically are 800 M^2/gm. But this small size also serves to reduce the effective surface area since a penetrating liquid or vapor will take a longer time to penetrate the more compact particles. This is evidenced in the

data reported by the BET method, which lists a value of approximately 80 M^2/gm for montmorillonite. This mineral is very active under the effects of moisture loss or addition, experiencing appreciable volume change. It is not unlikely that this mineral may exhibit this volume change when moisture is removed or added by the freeze-thaw activity examined in this study.

Kaolinite

The remaining clay mineral present in the material investigated is kaolinite. This mineral is present mainly in the coarse clay fraction 2.0 to 0.2μm, as is evident in the x-ray diffraction pattern for material 6BAR. This mineral is typically hexagonal in its more crystalline form and relatively thin compared to its diameter. The sharpness of the x-ray diffraction peak illustrates the kaolinite mineral and shows it to be somewhat crystalline. This mineral is relatively inactive and does not appear to play a major role in the proposed mechanism.

Mica

This mineral was present in several materials tested although it is absent from material 6BAR, examined by the electron microscope investigation. It is commonly found in mixtures with expansible minerals such as montmorillonite and vermiculite and are particularly abundant in the coarse clays and fine silts. In clays the mica are typically small irregular flakes with roughly hexagonal outlines. The flakes may be as thin as 30 Å and 1μm in diameter. Mica was not noted as being present in the material to be examined, however since x-ray diffraction cannot sense mica at concentrations below 5 to ten percent, some may be present (14).

Results

Control Sample.-- The control samples which were not subjected to any freeze-thaw cycling show that the two clay minerals of interest, montmorillonite and attapulgite, act together and separately to form a mesh which surrounds the silt sized particles. Figure 64-1 through Fig 64-4 demonstrate the presence of the montmorillonite film enmeshing the larger particles as indicated

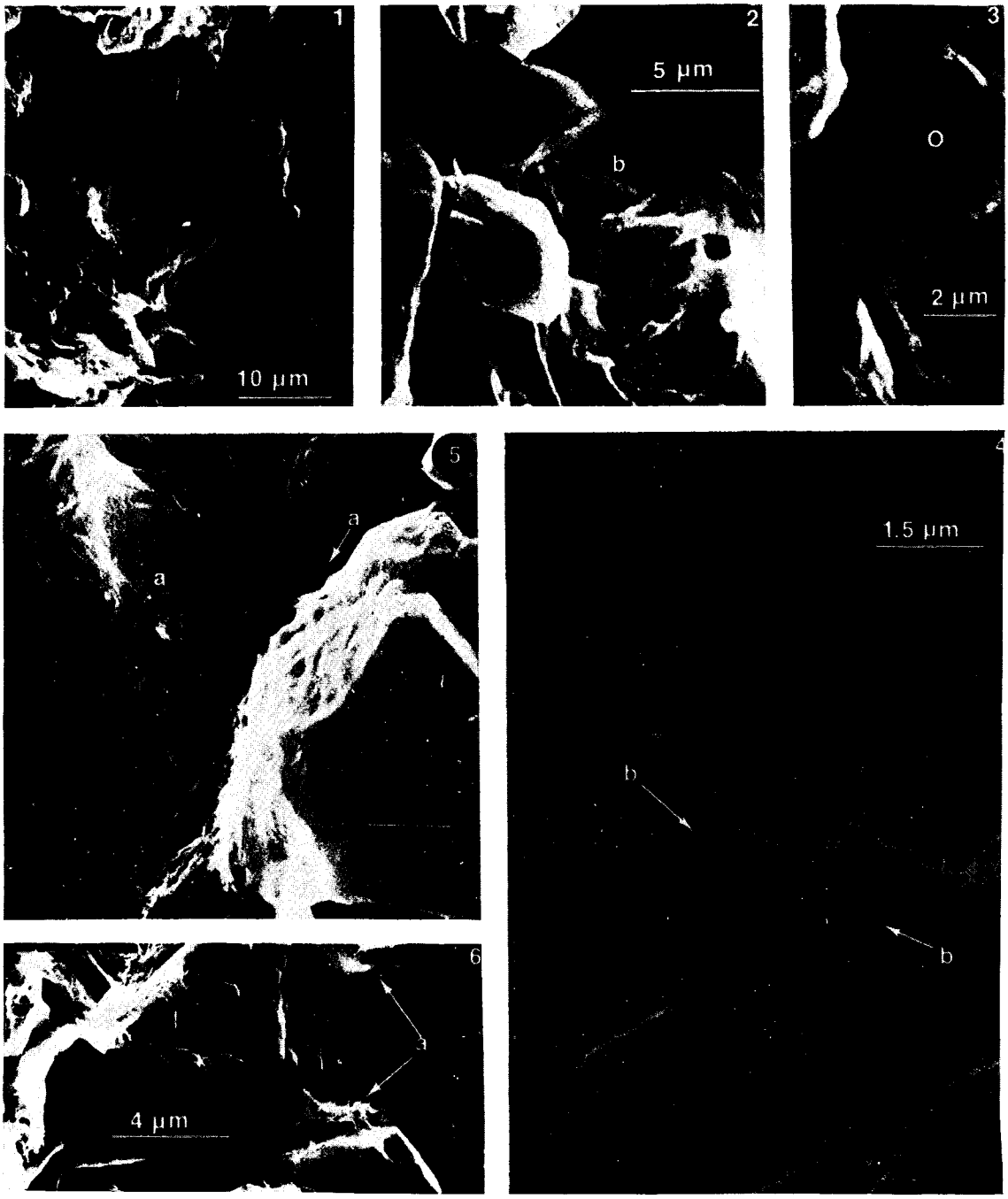

FIG. 64 - ELECTRON MICROGRAPHS OF BASE COURSE SAMPLE WITHOUT FREEZE-THAW HISTORY

by the arrows. Figure 64-3 shows a shell of essentially montmorillonite, indicated by the "0" left when the silt particle was in all probability forcibly removed during the surface preparation. Figure 64-2 is a magnified portion of Fig 64-1 to show the montmorillonite film spread between the particles as indicated by the "b".

Figure 64-5 and Fig. 64-6 demonstrate the unique capability of attapulgite to enmesh the silt sized particles. The fibrous mineral is readily seen to completely cover the silt sized particle as indicated by the "a" in Fig. 64-5. This mineral's covering ability is much more readily apparent than montmorillonite, due mainly to its structure. Figure 64-6 clearly shows the mineral attapulgite covering the particles in a random manner and running between them.

Cycled Samples.-- The samples which underwent freeze-thaw cycling show a major difference in that there is no longer a continuous mesh of the fibers between particles. The fibers appear to have been pulled toward the larger particles forming more or less individual particles covered with attapulgite fibers. The original film-like nature is evident as indicated by the arrows. This structure does not dominate as it did in the control samples, however. The cycled samples are shown in Fig. 65.

The effect of freeze-thaw cycling on the montmorillonite was not nearly as easy to discern as it was for the attapulgite because of the greatly different structure. The presence of montmorillonite was noted in the control samples mainly as a film between particles, thus, it was easily recognized as being a coating on a particle. After freeze-thaw cycling there was no evidence of a montmorillonite film between particles except where attapulgite fibers retained an indication of their original film-like form as indicated in Fig. 65-3 by the "a". The only indication of the presence of montmorillonite came from the edges of the montmorillonite film where it was torn and folded in on itself. This is illustrated in Fig. 65-3 by the "b". The film had broken and been pulled in on itself. This topological feature

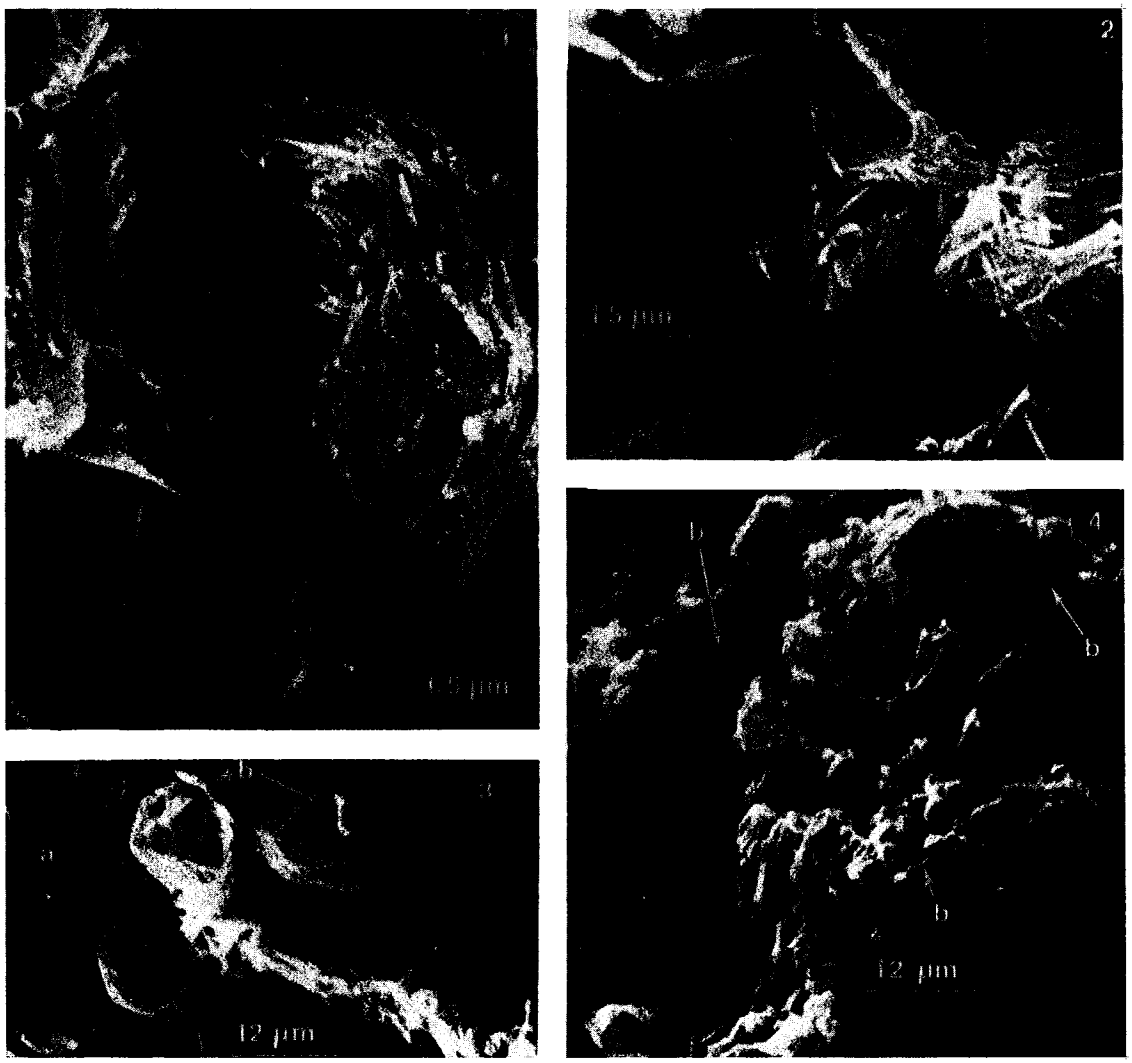

FIG. 65 - ELECTRON MICROGRAPHS OF BASE COURSE SAMPLE AFTER SERIES OF SIX FREEZE-THAW CYCLES

is evident in Fig. 65-3 and Fig. 65-4 as indicated by the arrows. This feature is not as readily apparent as is the reorientation of the attapulgite and does not present as dramatic a picture. When compared with the control sample, however, the difference is quite apparent.

Interpretation of Electron Microscope Study

Clay minerals have been shown to undergo large dimensional changes under the addition and subtraction of moisture by Low, Ravina and White (33), and Morrison (36), particularly montmorillonite. This dimensional change occurs with the addition or subtraction of the interlayer or adsorbed water. This mechanism may be expected to occur to a lesser extent in the other clay minerals as they lose their adsorbed water. This mechanism would explain the freeze-contraction observed by Hamilton (21) in clay rich samples where there is extensive contact between primarily clay minerals.

The base course material examined in this study contain 1.6 to 9.0 percent clay by weight. The particle sizes range from 3/8 inch (9.53 mm) to the clay sized particles, 2μm. The clay rich samples studied previously contained particles which were all smaller than silt size, 74μm. For the base course material presented here, there could be no extensive clay particle contact to account for the large amount of freeze contraction recorded if old theories of particle orientation are accepted. The new mechanism is based on the types of clay minerals present, the moisture change due to freezing and a new particle interaction, proposed to account for the noted volume change.

The commonly held concept of the clay mineral's role in an aggregate material is that the clay minerals arrange themselves in a manner determined by the moisture present as was mentioned earlier. These clay minerals then serve mainly to fill the voids between the larger aggregates with no continuity being ascribed to the clay minerals. The theory put forth is that the clay minerals have a degree of continuity in the flocculated state through a combination of particle forces and suction, or tension in the

adsorbed moisture. The electron micrographs support this theory in that they clearly show the clay minerals forming a coating or skin over the silt sized particles. This structure has been suggested previously by Wood (52) although no particle interaction was suggested.

The large dimensional change in the low clay content base course materials does not seem to be accountable to a change in dimensions of a clay structure which merely occupies the voids between the larger particles. If continuity of a clay skin is assumed, however, the clay particles will work in concert to pull the larger silt sized particles together. This will produce a larger volume change than that which would be expected for a dimensional change in the clay minerals alone.

The two major clay minerals, attapulgite and montmorillonite, may be necessary for this mechanism to develop fully. The materials with more attapulgite generally showed larger freeze contraction. A bonding between the two particles through surface charges is not likely. The physical structure exhibited in the electron micrographs of a meshwork of attapulgite fibers with a film-like covering of montmorillonite suggests that a moisture bonding of the two minerals may be occurring. Sodium montmorillonite has a very high potential for water uptake, although at a very slow rate. Attapulgite is the next most active mineral present as regards water sorption, followed by calcium montmorillonite. This is shown in Fig. 66 which was initially published by White and Pichler (51). The interpretation of these data is that montmorillonite and attapulgite will exert essentially equal potentials for moisture attraction. Given the intimate mineral contact shown in the electron micrographs, this moisture-attraction bonding may be sufficient to cause the two minerals to act in concert, thus, more effectively using the relatively large volume change potential of the montmorillonite.

Summary

This chapter detailed the formulation and validation of a particle reorientation theory and of a particle structure previously

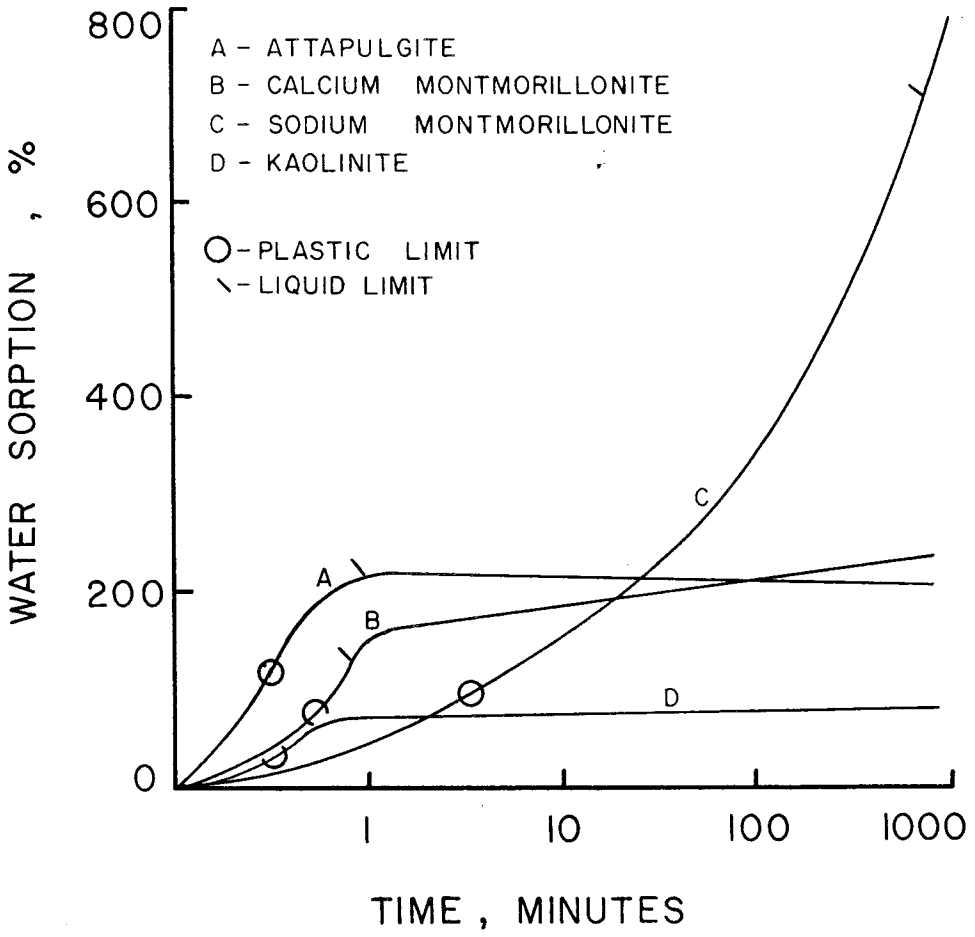

FIG. 66 - RATE OF WATER SORPTION FOR VARIOUS CLAY MINERALS (51)

proposed but never investigated. The combination of the physical data and the visual examination provided data suitable for proposing and validating the mechanism. The development and applicability of the "Lennard-Jones" type model to the freeze coefficient data validates the structure and energy influence on the reorientation and volume change. The regression analysis performed on the freeze coefficient data, specific surface area and the ion concentration (solubility), as measured by the resistivity, clearly shows the importance of the clay mineralogy in influencing the freeze behavior. The observed influence of the ion concentration as it relates to moisture-particle interaction and the freeze-thaw activity has implications in the effectiveness of stabilization procedures which will be addressed in a later section.

PREDICTING FREQUENCY OF CRACKING

The previous three chapters detail the material property description of thermal susceptibility of the base course and provide insight into an interpretation of the form of damage this mechanism could cause. To be useful to the pavement design engineer the mechanism must be capable of being expressed in such a manner that the material properties can be used to predict damage under the influence of the environment. This mathematical expression allows the variation of the material properties to be studied as they affect the amount of damage produced. In the case of thermal susceptibility, the damage appears primarily as transverse cracking at the pavement surface. This crack is most likely to initiate in the base course, and it will then propagate through the asphalt concrete due to thermal cycling as was shown by Chang (11). The development of a design procedure should follow these steps:

1) Predict crack spacing as a function of material and environmental parameters.
2) Predict propagation with time.
3) Study material properties to provide a suitable means of controlling the damage.

This procedure would permit the engineer to assess all the factors that affect the life of the pavement and to produce a rational design that incorporates a systems approach to provide an economical pavement. Steps 1) and 2) will be presented in this section, and 3) will be presented in the following section.

The effectiveness of the design is then measured by the amount of damage that appears. In any systems approach a certain amount of damage is acceptable and is often provided for in the design. In this instance, a set maximum crack spacing may be the most important feature. This arises from the contraction of the pavement when cracked. The longer the intact pavement, the larger will be the crack opening since the deformation of the

opening may be approximated by

$$L_c = \alpha \Delta T L \tag{4-1}$$

where α = coefficient of thermal activity, strain/^oC,

ΔT = temperature drop below freezing, ^oC

L = existing crack spacing, and

L_c = crack opening.

The wider the crack opening, the more easily moisture intrusion can occur; and the more rapid the deterioration due to subsequent traffic loading will be.

Thus, a maximum crack spacing may be specified to avoid large crack openings; but a minimum acceptable crack spacing must also be considered to avoid excessive maintenance. The purpose of this chapter is to provide a model which a design engineer could use in deciding which crack spacing to design for. It is apparent that being able to predict crack spacing is the major requirement.

Predicting Crack Spacing

As a restrained material contracts there will be a stress buildup in the material. When this stress reaches the tensile strength the material will crack. In a pavement with existing cracks in the base course this stress buildup will occur at the center of the intact material. The first step in predicting crack spacing would be to predict the stress that occurs in the base course material, since this is the most active layer.

Stress Predictions

The finite element procedure allows the boundary conditions necessary to model a cracked pavement to be included very easily. The pavement configuration being examined here consists of a base course with pre-existing cracks placed between the asphaltic concrete and the subgrade. As the base course contracts with each freeze cycle a tensile stress will build up to a maximum at the center of the crack spacing as shown in

Fig. 67. The value of the stress at the crack will not be zero due to the restraint of the asphaltic concrete, but will be a percentage of the maximum value, typically 60 to 70 percent. When this maximum stress exceeds the tensile strength the base course will crack, producing a crack spacing of one half of the initial crack spacing (the crack spacing existing prior to the temperature drop, L). The variables necessary to calculate the stress resulting from the thermal contraction are as follows:

1) Young's Modulus for the asphaltic concrete, E_A, base course, E_B, and the subgrade, E_S,
2) Freeze coefficient, α, of the base course,
3) The initial crack spacing present before the temperature drop, L,
4) The value of the temperature drop below freezing at the top of the base course, ΔT,
5) Boundary conditions were used as follows:
   a) A crack with no resistance to horizontal movement was placed at each end of the base course.
   b) The asphaltic concrete and subgrade were restrained from horizontal movement, modeling an intact material.
   c) A thermal loading was distributed on the face of the crack along the depth of the base course. This loading, ($E \alpha \Delta T$) times the nodal spacing, produced tensile stresses in the base course.

The maximum stresses that were calculated for the initial crack spacings, L, were regressed against the input values to obtain a mathematical model which is as follows:

$$\sigma_{TENSILE} = (5.616\text{x}10^{-3})(E)(\alpha)^{0.7886}(\Delta T)^{1.4506}(-1.868+ 22.8998\ LOGL)^{0.68596} \quad (4\text{-}2)$$

where the parameters are as previously defined. Solving this equation for length, L, and letting σ_T be the tensile strength, the following equation results:

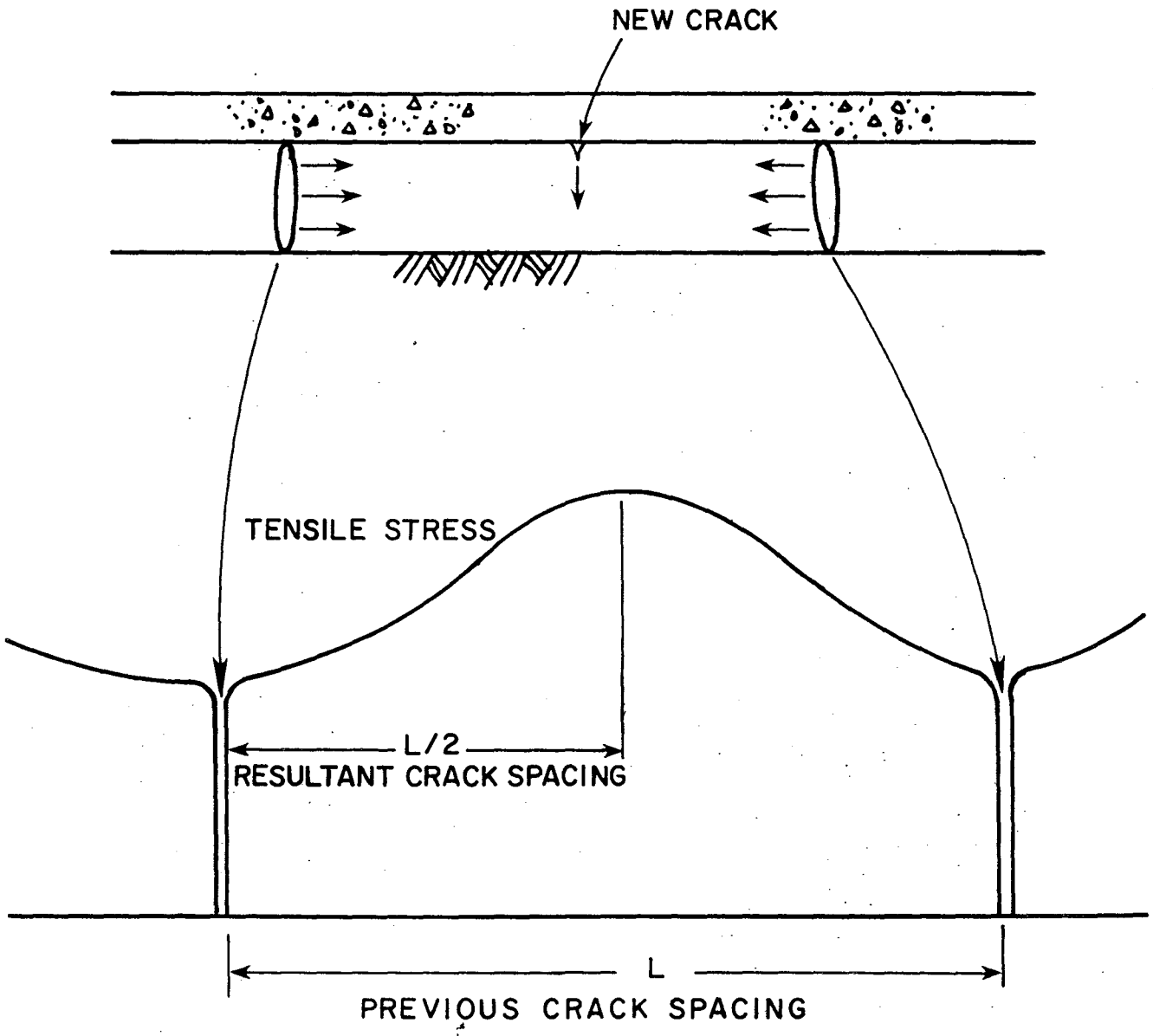

FIG. 67- Distribution Of Thermal Tensile Stresses In Base Course Between Two Cracks.

$$\text{LOG } L = \frac{4.508\text{x}10^{-12} \ (\sigma_T)^{1.4578} \ (E)}{(\Delta T)^{2.1149} \ (\alpha)^{1.1496}} + 8.151 \text{ x } 10^{-2} \qquad (4\text{-}3)$$

Because L is the crack spacing before the low temperature is reached, L/2 will be the final crack spacing.

Figure 68 and Fig. 69 are plots of equation (4-3) for two levels of thermal activity (-2.0 and $-4.0\text{x}10^{-4}$ M/M/^{o}C) and one Young's Modulus (250,000 psi) in the base course. These figures show the initial crack spacing present in the base course that will crack, for a given tensile strength, when a certain value of ΔT is reached. The crack spacing produced by this ΔT is then L/2.

Initial Crack. - The initial crack spacing is infinity for a very small ΔT value. In reality this cannot occur, and the initial crack length is more likely caused by material property variations than the magnitude of the temperature drop. The curves become asymptotic around a crack spacing of 200 ft (61 M). For ease of analysis the first crack spacing will be assumed to be a multiple of the minimum initial spacing, and in the range of 200 ft.

Cracking must occur at one-half intervals of the maximum spacing since this is where the maximum tensile stress will occur. This divides the crack spacing curve into distinct intervals which require a definite temperature drop below freezing, ΔT, to produce a new crack spacing. This is demonstrated in Fig. 70 where the crack spacings have been delineated. Once the initial crack has occurred, the next crack spacing will not occur until a subsequent freeze-thaw cycle drops the temperature into the next crack spacing interval. A crack may initiate and propagate under repeated cycles of this stress. The rate will not be nearly as rapid, however, as when there is a crack present and the base course can fully deform at the crack opening. This will be discussed more fully in the following section that discusses the rate of crack propagation.

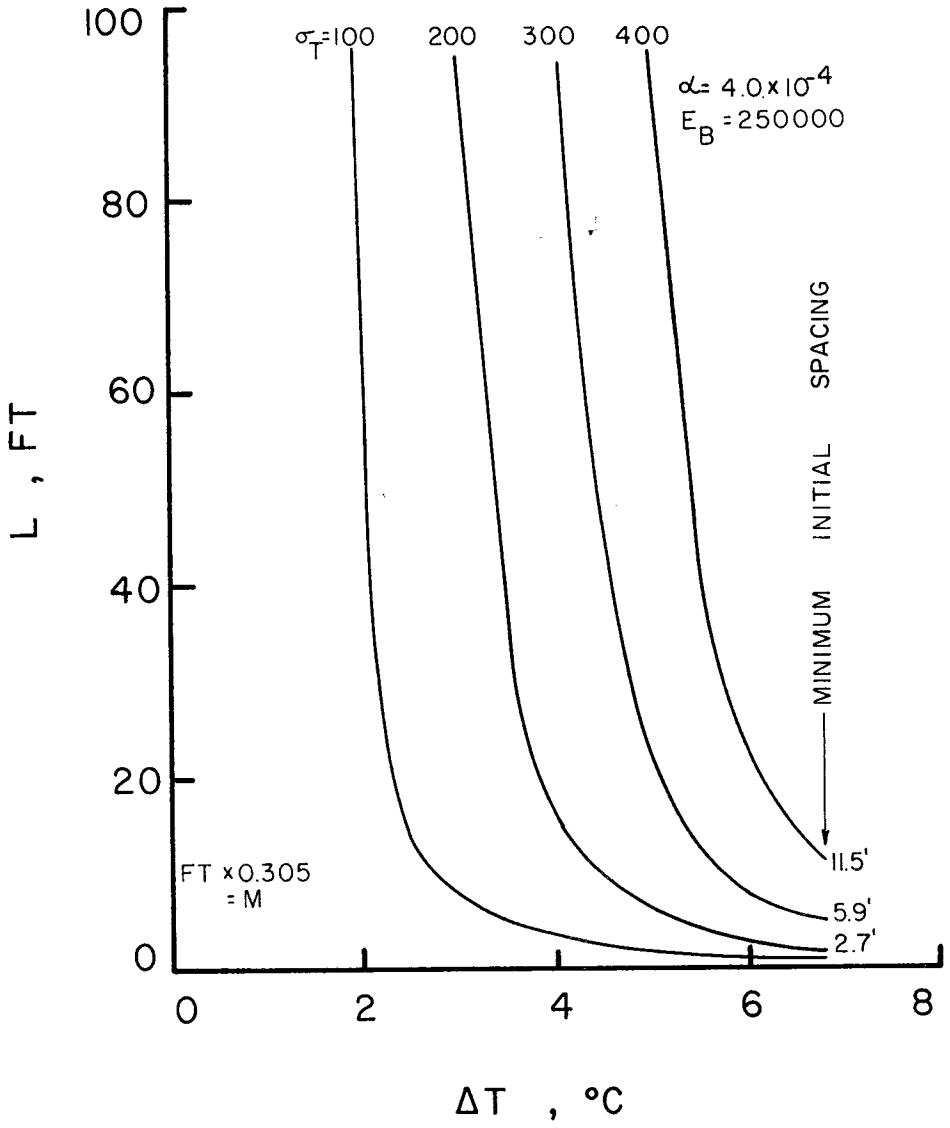

FIG. 68 - INITIAL CRACK SPACING AS A FUNCTION OF TEMPERATURE DROP FOR VARIOUS TENSLIE STRENGTHS, α= -4.0 x 10^{-4}

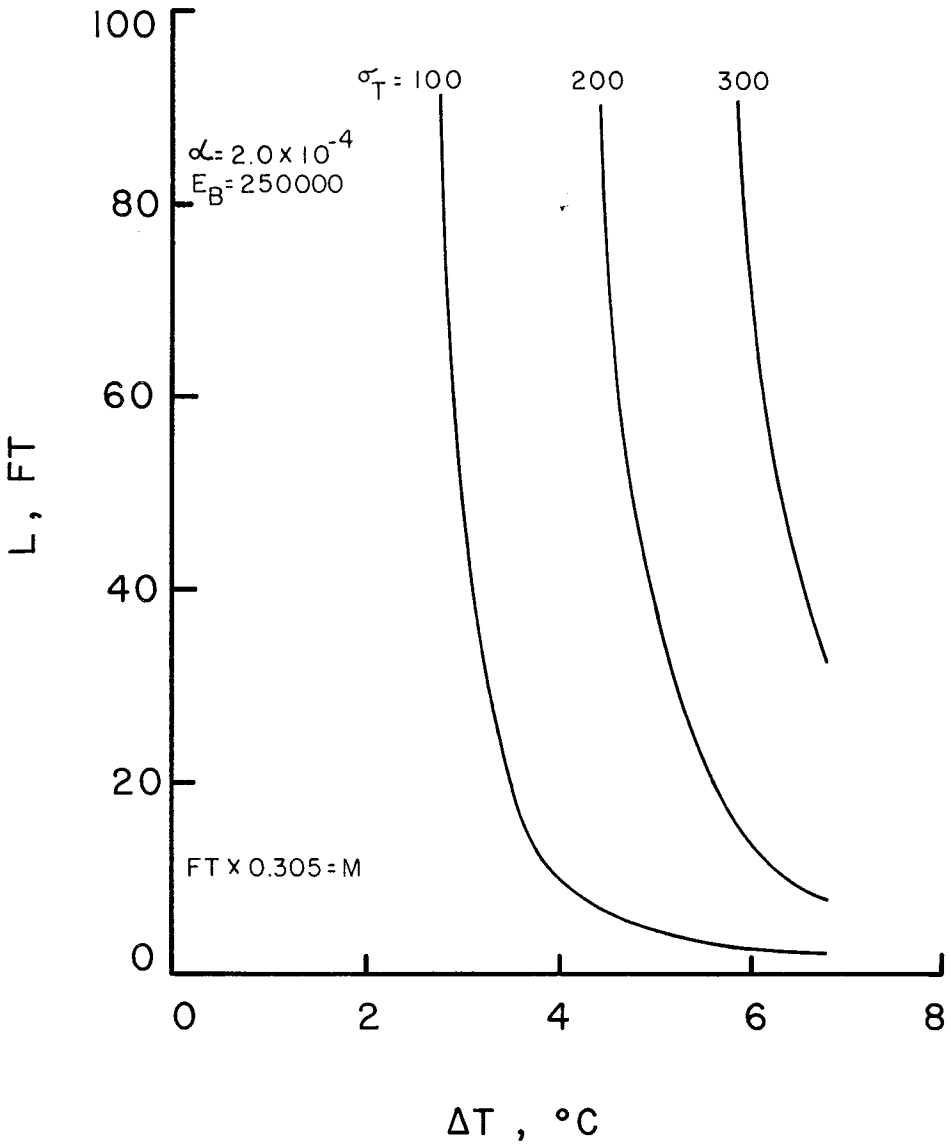

FIG. 69 - INITIAL CRACK SPACING AS A FUNCTION OF TEMPERATURE DROP FOR VARIOUS TENSILE STRENGTHS, $\alpha = -2.0 \times 10^{-4}$

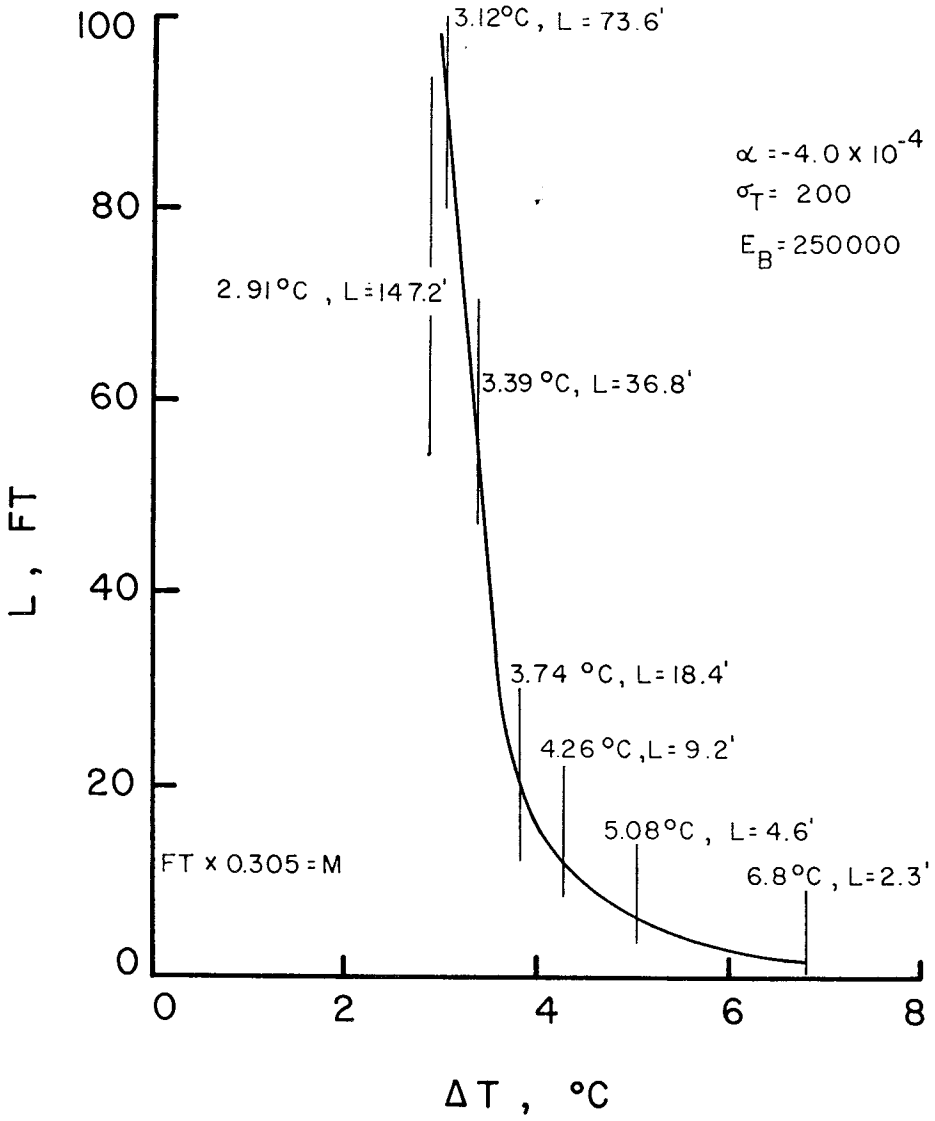

FIG. 70 - INITIAL CRACK SPACING AS A FUNCTION OF TEMPERATURE DROP WITH TEMPERATURE REGIONS INDICATED AS A MULTIPLE OF THE MINIMUM VALUE OF INITIAL CRACK SPACING

Predicting Crack Propagation Rates

The procedure developed by Chang (11) will be utilized to calculate the rate of crack propagation for a given base course material and a typical asphalt. In a design process many more material properties would need to be studied. The procedure presented here will demonstrate the procedure which a full analysis would follow.

The equation governing crack growth was first presented by Paris (40) and is as follows:

$$N_f = \int_{C_o}^{C_f} \frac{dc}{A_n(\Delta K)^n} \qquad (4\text{-}4)$$

where C is the crack length,

N_f is the number of cycles to failure,

A_n is a fracture property,

n is a viscoelastic property = 2(1 + 1/m),

m is the slope of the logarithmic creep compliance curve, and

ΔK is the change in stress intensity factor caused by a cycle.

When the material properties, A_n and n, are known, the critical variable influencing the rate of crack propagation is the stress intensity factor. The larger the stress intensity factor the faster the propagation. Presently, numerical methods are the easiest method to obtain stress intensity factors. The finite element method is the simplest numerical technique available, and also one of the more accurate (10).

Finite Element Calculations

The finite element program utilized here (11) uses a hybrid super-element developed by Tong et al. (48), to calculate the stress intensity factor for a cracked pavement. In this analysis of the base course, the stress intensity factor at the tip of a crack is influenced by the opening deformation and the length of the crack into the surface layer. It is not possible to calculate the deformation of the crack in the base course by equation (4-1) since the base course will be restrained by

bonding with the asphalt and subgrade. This deformation was, however, produced by a tensile stress. This tensile stress can be predicted from equation (4-2) which was developed with the previously mentioned boundary conditions. This stress can be used analogously to the deformation in stress intensity factor calculations.

The second variable that will influence the stress intensity factor is the length the crack has propagated into the asphaltic concrete layer. As the crack tip advances away from the thermally active base course the stress intensity factor will change. This relationship between crack length, C, and stress intensity factor, K, is necessary to permit the numerical integration of equation (4-4).

Figure 71 shows the pavement configuration and the parameters chosen for use in the stress intensity factor calculations. The stresses are applied only in the base course. The crack propagates through the asphaltic concrete layer with the viscoelastic and fracture properties shown. These properties are typical for actual pavements in use in Texas (10).

The results of the calculations for the stress intensity factor are shown in Fig. 72. This figure shows the variation in the stress intensity factor with increasing crack length for the stress levels investigated. The results are as expected, with the stress intensity factor being greater when the crack tip is near the stress applied by the contracting base course and decreasing as the crack tip advances away from the applied stress.

Chang predicted crack propagation resulting principally from thermal stresses in the asphaltic concrete layer (10). In Fig. 73 a curve for the stress intensity factor as a function of crack length taken from this work is shown. The Young's Modulus and thickness were chosen to be the same. This curve is opposite to that calculated for thermal activity of the base course. This arises from the fact that the temperature is lower

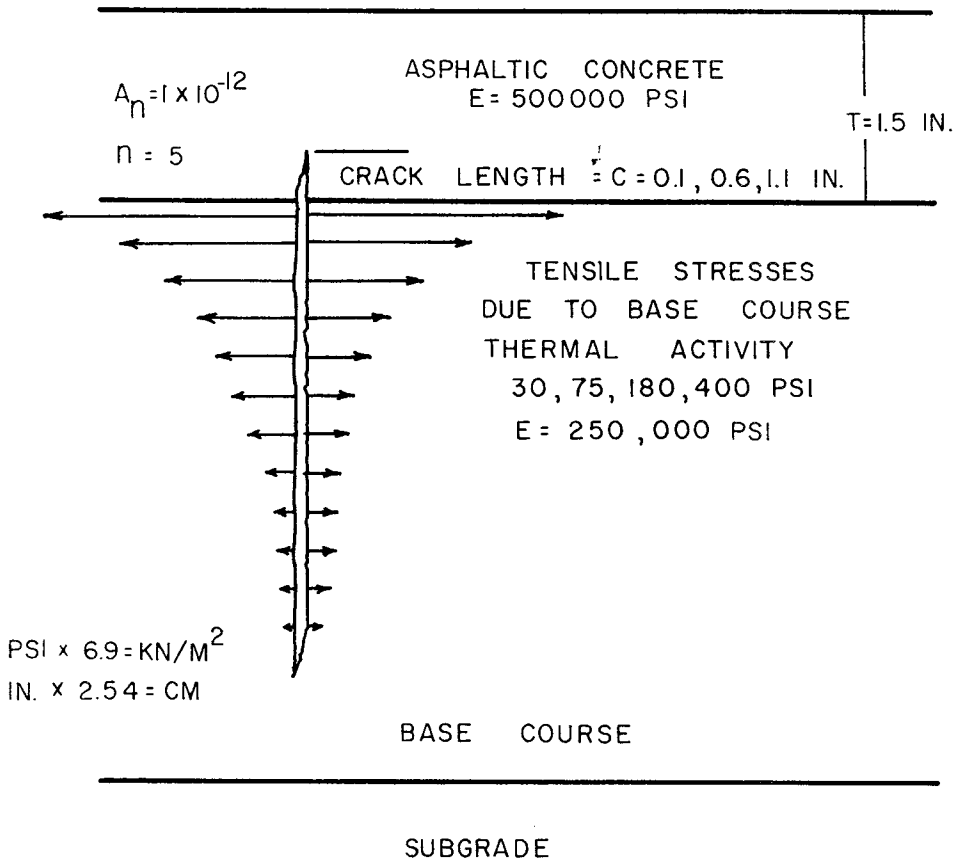

FIG. 71 - PAVEMENT CONFIGURATION WITH MATERIAL PROPERTIES SHOWN

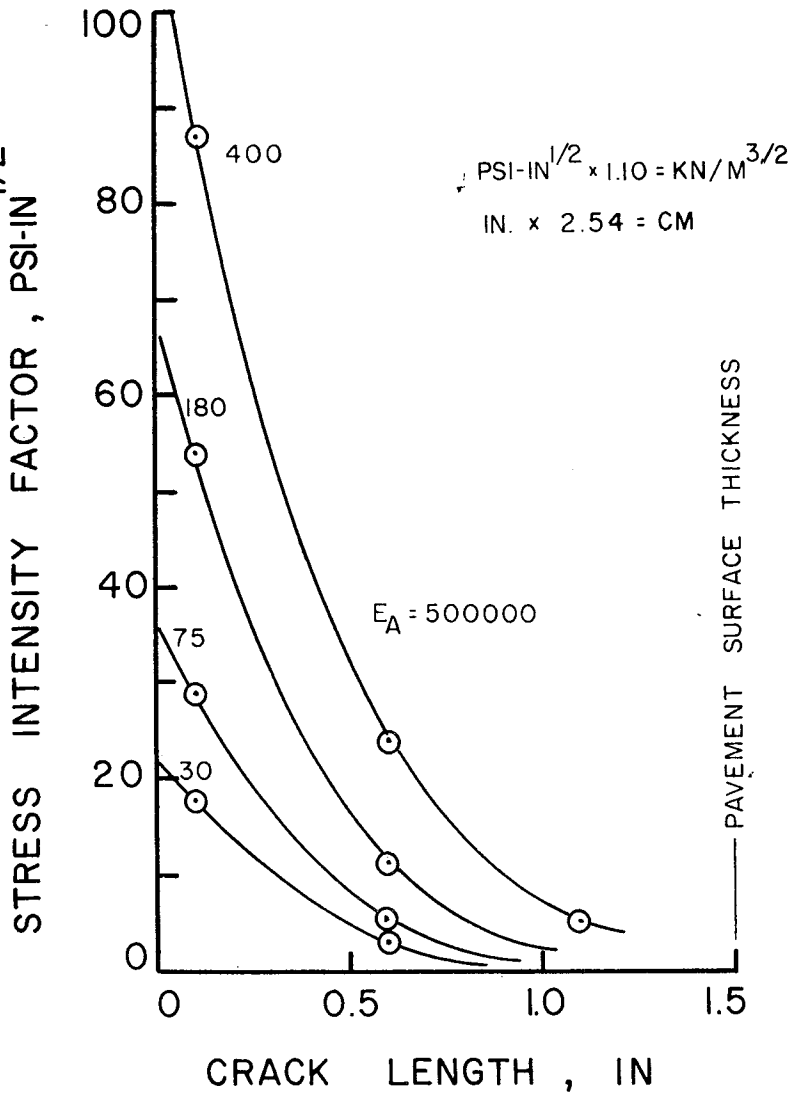

FIG. 72 - STRESS INTENSITY FACTOR AS A FUNCTION OF CRACK LENGTH FOR VARIOUS TENSILE STRESSES

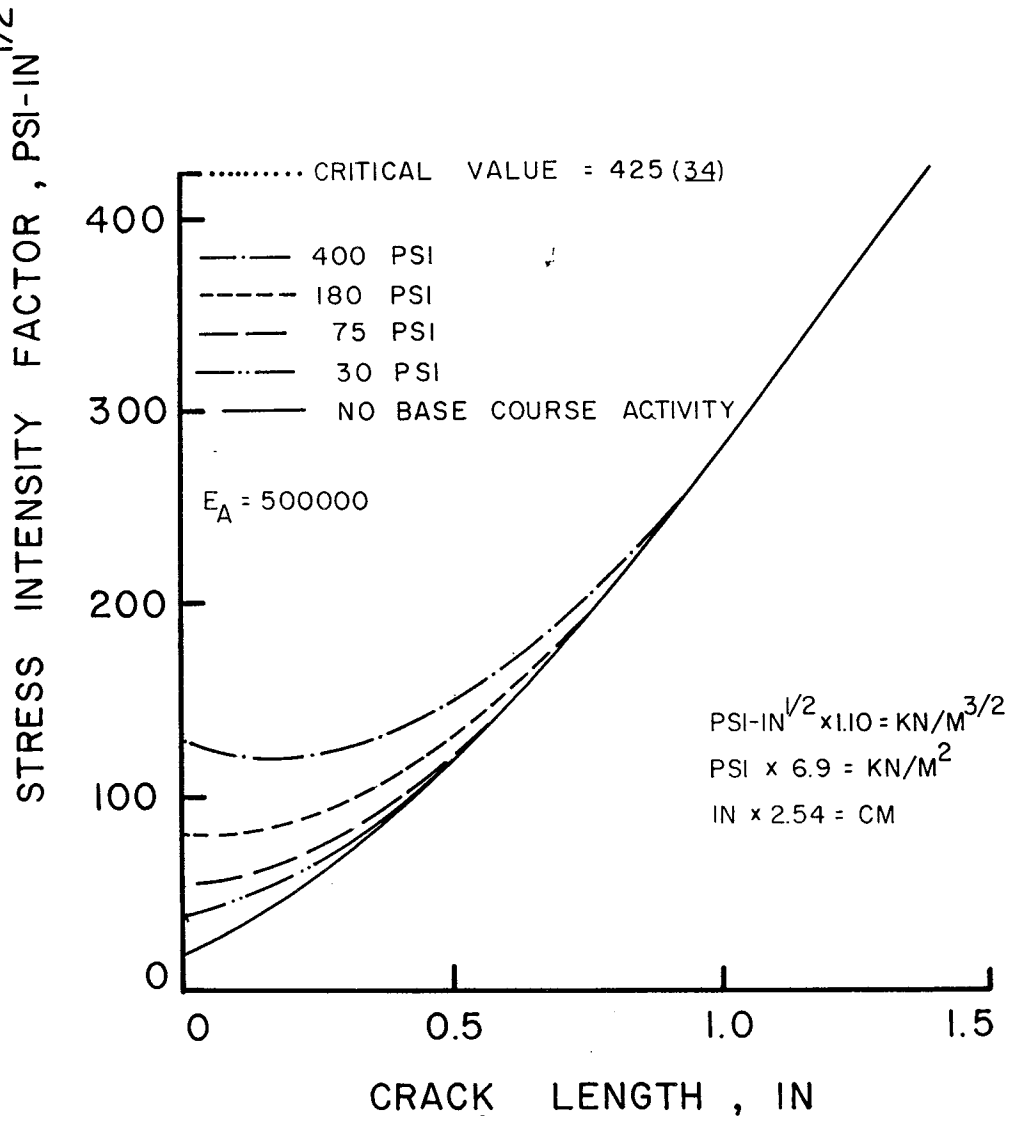

FIG. 73 - STRESS INTENSITY FACTOR FOR THE COMBINED ACTION OF THERMAL ACTIVITY IN THE BASE COURSE AND THE ASPHALTIC CONCRETE.

on the surface of the asphalt than at the bottom. With crack propagation commencing at the bottom of the asphalt layer the crack tip would propagate from a low stress area into a higher stress area. Thus the stress intensity factor would begin low and increase as the crack tip propagated.

Figure 73(p. 141) also shows the effect of superposing the stress intensity factors for the thermal activity of the asphalt layer with those of the thermal activity of the base course. This superposition provides a substantially larger stress intensity factor for the smaller crack lengths. As the number of cycles to failure is inversely proportional to the stress intensity factor, this larger stress intensity factor for the initial portion of the curve should greatly decrease the number of cycles required to propagate the crack through the asphaltic concrete.

For the material properties of the asphaltic concrete investigated here the reduction in the number of cycles to failure is very large. For a Young's modulus in the asphaltic concrete of 500,000 psi (x6.9 = KN/M^2) the number of cycles to failure for thermal cycling in the asphalt alone is 500 cycles. For a stress of 30 psi (x6.9 = KN/M^2) in the base course, the number of cycles drops to 129. For the large stress of 400 psi (x6.9 = KN/M^2) the number of cycles drops even further to 9 cycles. Figure 74 shows the decrease in service life with increasing stress level as would be expected. The stresses which develop in the base course will be a function of the actual drop in temperature below freezing. This quantity, ΔT, will be a random variable with a distribution in magnitude. The effect of each cycle is cumulative for each level of crack spacing, however, which suggests that a Miner's law approach would allow the random occurrence of stresses to be logically utilized to predict failure.

Miner's Law Approach - This approach follows the basic tenet that a material will fail when the damage from each

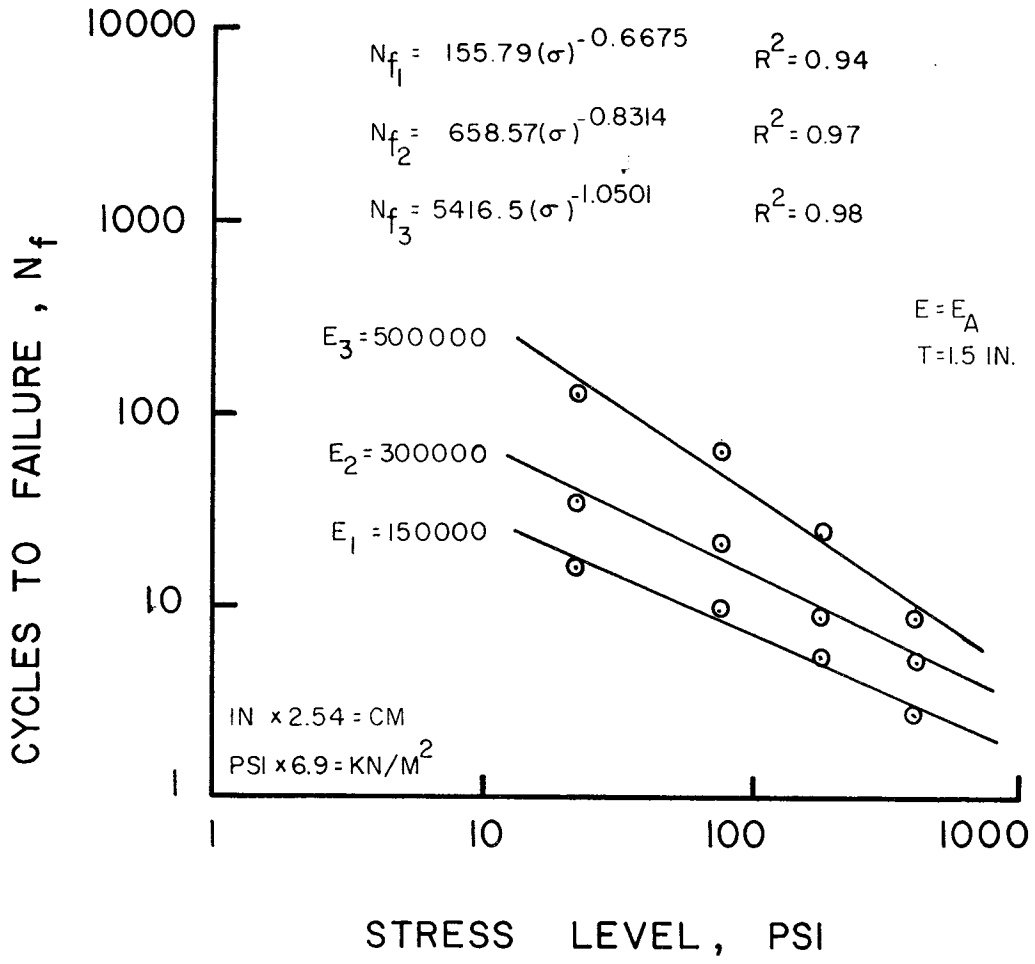

FIG. 74 - SERVICE LIFE AS A FUNCTION OF TENSILE STRESS IN BASE COURSE

individual cycle sums up to a total damage quantity which causes failure. In this study the damage caused by a low stress cycle will be normalized to be a percentage of the damage which causes failure in the highest stress cycle. The equation for N_f as a function of base course stress and elastic modulus of the surface course is:

$$N_f = 10^m 6^n$$

where

$$m = 1.5176 + 4.1427 \times 10^{-6} E \qquad (4\text{-}5)$$

$$n = -0.5035 - 1.0935 \times 10^{-6} E$$

The stress shown in this equation is the maximum stress at the center of the base course between the two cracks with spacing L. When this stress causes the base course to crack, the opening deformation will be the driving force in initiating and propagating a crack in the asphaltic concrete. When the temperature which produced this crack occurs again, the crack will experience the same deformation. This deformation implies that in the analysis presented here the damage from this cycle could be predicted from the stress level given by equation (4-2), even though this stress does not occur at the crack.

If the next temperature drop, ΔT, is sufficient to cause a new crack to form, the tensile stress would once again be at the tensile strength. The deformation, however, would be less than the deformation that resulted for the same stress level in the longer crack spacing. Subsequent crack spacings would produce even smaller deformations at their cracks necessitating the use of smaller and smaller stresses to model the decreasing deformation that will occur. This will be discussed in the section that delineates the computer model.

Predicting Environmental Parameters

Stress calculations at the top of the base course are the only calculations necessary to predict the rate of crack appearance with time, at the surface of the asphalt pavement.

The only environmental parameter necessary to obtain this stress is the temperature drop below freezing, ΔT.

The best available method to obtain the temperature profile in a layered system is the heat transfer model developed by Dempsey and Thompson (15). The equation developed by Barber (3) and modified by Shahin and McCullough (46) to calculate the temperature variation within the asphalt layer represents a reasonable selection as second choice when the temperature distribution in the asphalt layer is all that is needed. This equation utilizes daily temperatures, wind velocity and solar radiation as climatic inputs. The pavement thermal properties are the absorptivity, thermal conductivity and mix density.

The temperature equation developed by Barber and modified by Shahin is as follows:

$$T = T_M + T_V\left(\frac{H\, e^{-XC}}{((H+C)^2 + C^2)^{1/2}}\right) \text{Sin}(S_i) \qquad (4\text{-}6)$$

where

$S_1 = 6.81768(.0576t - .075xC - .288)$ for t = 7 am to 2 pm,
$S_2 = 14.7534(.02057t - .075xC - .288)$ for t = 3 pm to 7 pm,
$S_3 = -6.94274(.02057t - .12xC - .288)$ for t = 8 pm to 6 am,
$T_V = .5\, T_R + 3R$ for Sin $(S_i) \geq 0$,
$T_M = T_A + R$ for Sin $(S_i) \geq 0$,
$T_V = .5\, T_R$ for Sin $(S_i) < 0$,
$T_M = T_A + .5R$ for Sin $(S_i) < 0$,
H = (Surface Coefficient)/conductivity,
X = Depth below surface, and
$C = (0.131/\text{diffusivity})^{0.5}$.

These relationships were programmed to calculate the hourly temperature at three positions within the asphalt layer for daily climatic input; including the temperature at the top of the base course. The climatic data were stored on computer tapes for periods of record of 40 years or longer for a representative number of cities in Texas. The input thermal properties are given in Table 21 (15).

Table 21. PAVEMENT PROPERTIES (15)

Absorptivity	0.95
Thermal Conductivity	0.80 BTU/hr
Specific Heat	0.22
Density	146 pcf
Thickness	1.5 in

The temperature calculations were incorporated into a computer program that calculated the stress for each freeze cycle that penetrated into the base course. This stress either produced a crack, if large enough, or accumulated damage that propagated existing cracks.

Predicting Crack Appearance

The development to this point has provided three studies which predict crack spacing in the base course, rates of crack propagation through the pavement and predictive relationships for the base course thermal susceptibility mechanism. The integration of the computer studies and the prediction scheme for temperatures at the top of the base course will allow the appearance of the cracks at the surface of the asphalt to be predicted with time. A computer model was developed to do the necessary calculations and is shown in Appendix D with the necessary input data cards.

The computer model first uses equation 4-3 to calculate the minimum spacing that can occur with the given base course material properties and the maximum temperature drop in which thermal activity is considered to occur in the base course (20°F or -6.7°C). The multiple crack spacings are then calculated. These crack spacings are then used in equation (4-3) to solve for the corresponding temperatures necessary to produce these crack spacings.

Equation 4-6 is used with actual climate data to calculate temperatures at the top, middle, and bottom of the surface course, the latter also being the temperature at the top of the base course. The surface course temperatures are used to calculate an average temperature and rate of change of temperature which, in turn, are used in the viscoelastic theory presented in Research Report 18-3 to predict the "effective elastic" modulus of the surface course. It is this "effective elastic" modulus which is used in the crack propagation calculations.

The minimum base course temperature is calculated for each day and is compared with the calculated temperature levels to indicate the level of crack spacing that develops in the base course.

The crack propagation rate in the surface course is calculated based on the stress level that builds up in the base course at the current level of crack spacing (Eq. 4-2) and the "effective elastic" modulus of the surface course. The damage caused by each daily stress cycle is calculated from the relationships developed in Fig. 74 (p. 143) and in Equation 4-5. The damage is accumulated for each crack; and when the damage level exceeds that required to propagate a crack to the surface, the pavement is then considered to have that crack spacing in the surface course. When this crack has propagated through the asphaltic concrete the boundary conditions involved in the finite element stress drop the restraint at the crack, and lower the stress in the base course somewhat. However, with the freeze coefficient, α, for the base course being on the order of ten times greater than that of the asphaltic concrete there will still be appreciable resistance to the contraction; and tensile stresses on the order of those calculated by equation (4-2) will develop. These stresses could be expected to develop for crack spacings down to the spacing size investigated in in this analysis. Crack spacings below five feet, although predicted, will occur with longitudinal cracking which will further invalidate the assumptions.

As the crack spacings decrease, the opening deformation decreases as mentioned earlier. Since the stress in the base course is used as a measure of the opening deformation of each crack in the base course, the stress must decrease also. This is handled in the computer model by decreasing the stress in proportion to the number of cracks that have developed in the base course between the two cracks which formed at the largest possible spacing.

The major assumption in the construction of this computer model lies in the use of equation (4-2) to predict a stress level for the cracks in the base course as well as in the center of these cracks. The explanation presented thus far assumes that each and every crack will continue to deform to some extent under the effects of a freeze cycle and a stress will develop for that crack spacing just as it did the first time that crack was formed. With subsequent cracks, the deformation and stress must be lowered.

In order to calculate the "effective modulus" of the asphalt surface course the computer program requires as input two viscoelastic curves; one is the creep compliance and the other is the time-temperature shift curve. Examples of these are shown in Figs. 75 and 77 for asphalt concrete and sulfur asphalt.

Creep compliance is a record of the time response of a material to an applied stress that is held constant. The compliance D(t), is the ratio of the strain, $\varepsilon(t)$ in the material to the constant stress, σ

$$D(t) = \frac{\varepsilon(t)}{\sigma} \qquad (4 - 7)$$

Figure 75 shows how the strain increases with time for both asphalt and sulfur asphalt. Although it is not exactly true, the compliance may be taken as the reciprocal of the elastic (or relaxation) modulus of the material, $\varepsilon(t)$. In fact, the relation between the compliance and the relaxation modulus at any time, t, is

$$E(t)\ D(t) = \frac{\sin n\pi}{n\pi} \qquad (4 - 8)$$

where n = the slope of the log creep compliance vs log time curve. For values of n between 0.0 and 0.25 the ratio of $\frac{\sin n\pi}{n\pi}$ is very nearly one. This means that for $0.0 \leq n \leq 0.25$,

$$E\ (t) \simeq \frac{1}{D(t)} \qquad (4 - 9)$$

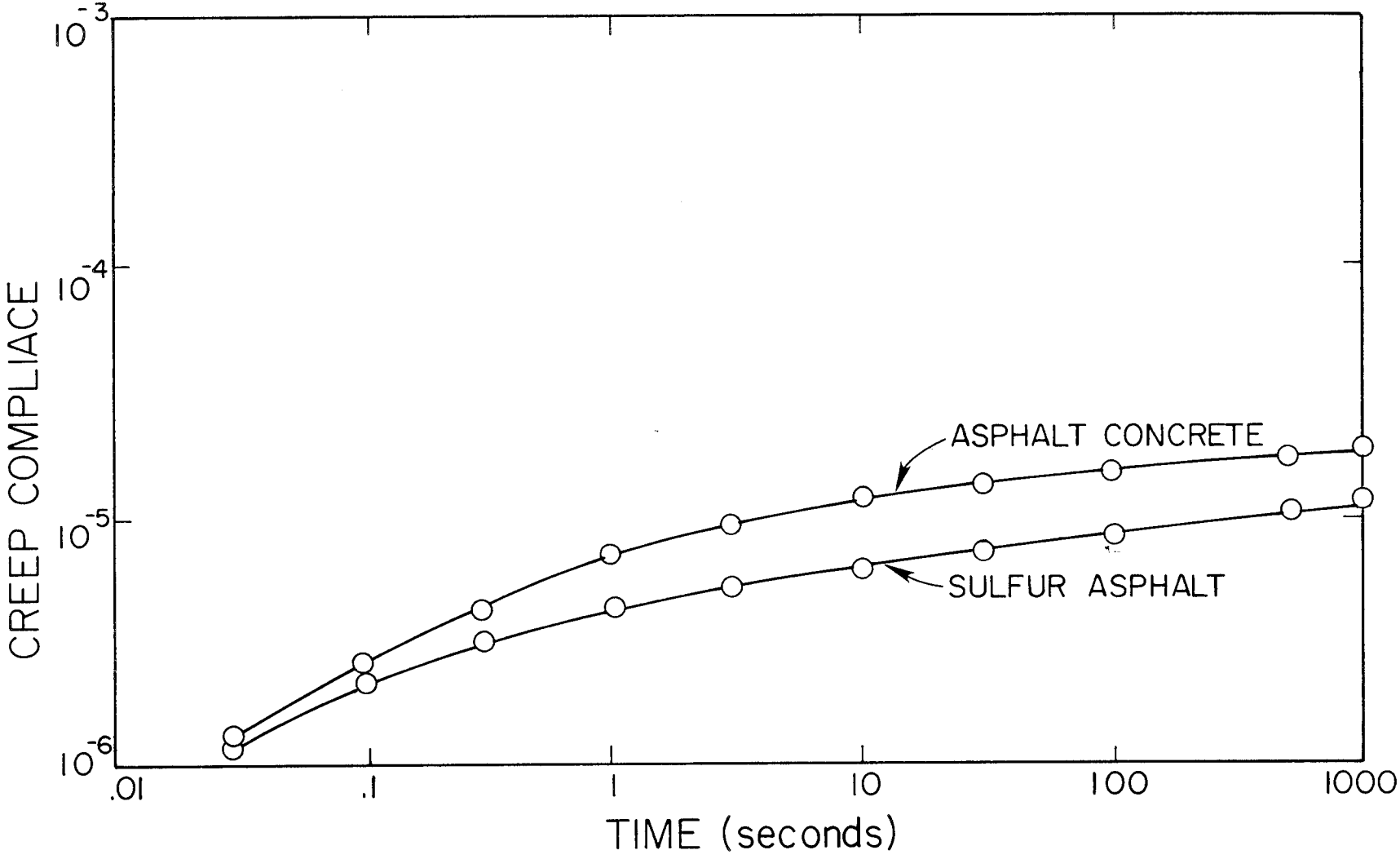

FIG. 75 — Creep Compliance Of Asphalt Concrete And Sulfur Asphalt.

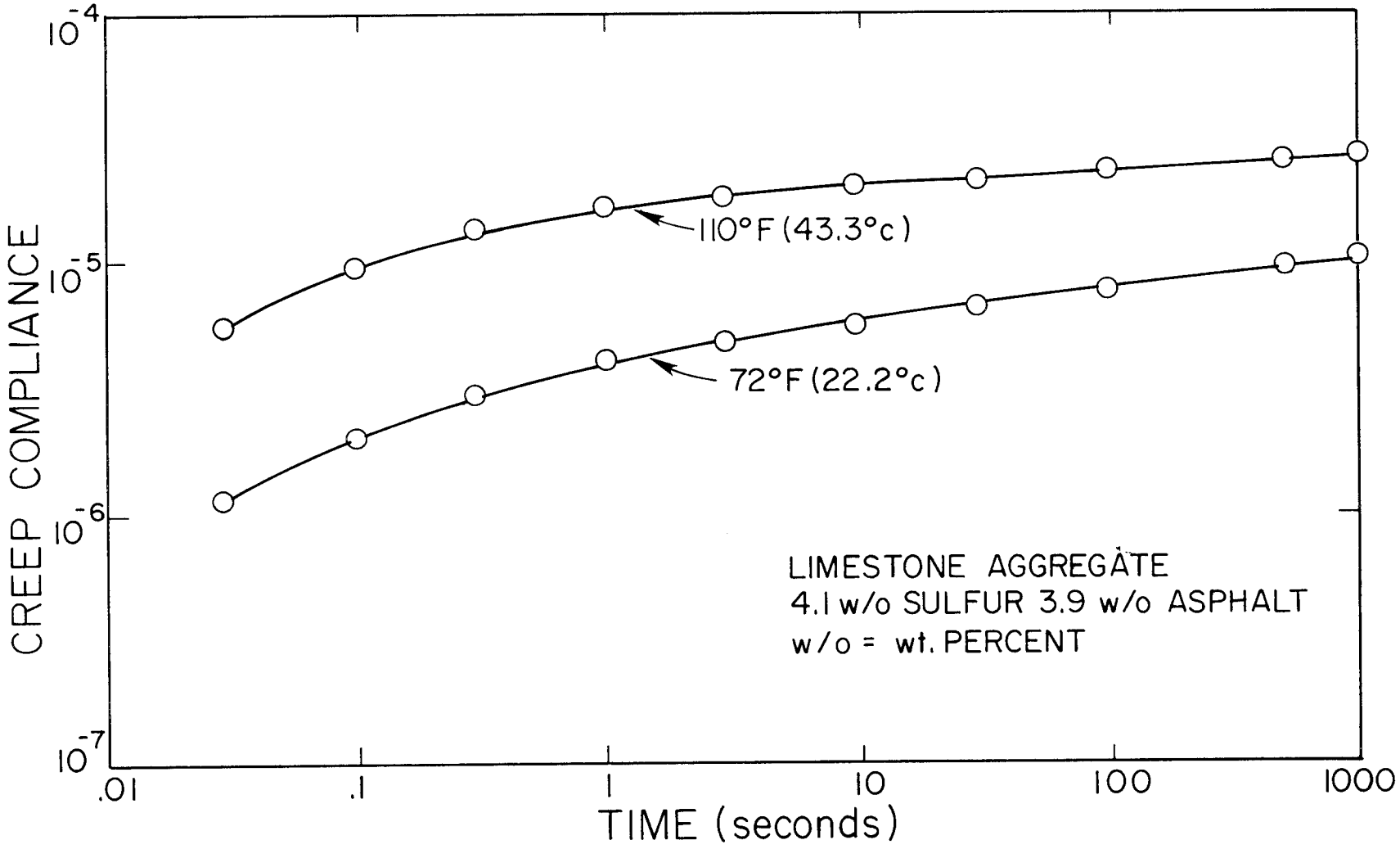

Fig. 76 - Variation Of Creep Compliance With Temperature.

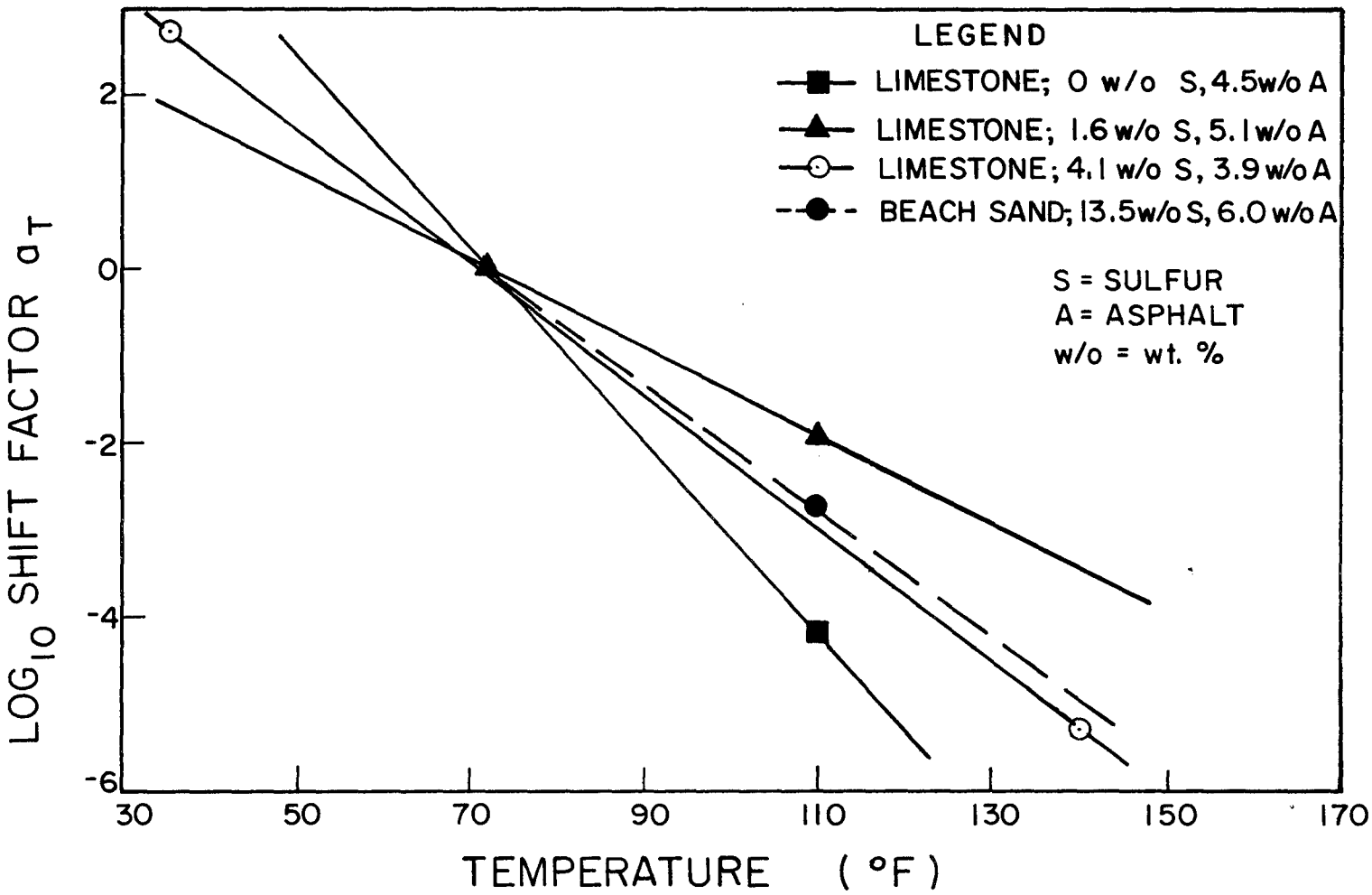

FIG.77 - Shift Factor As A Function Of Temperature For Sulfur Asphalt Mixtures.

The creep compliance depends upon the temperature at which the test is conducted. More strain is expected at higher temperatures than at lower temperatures. Typical curves for asphalt concrete are shown in Fig. 76. For some materials it is possible to translate the curves along the time axis. The ratio of the times at which the same value of creep compliance is measured is the time - temperature shift factor, a_T

$$a_T = \frac{t}{t_{To}} \qquad (4 - 10)$$

A graph of a_T versus temperature is shown in Fig. 77 for both asphalt concrete and sulfur asphalt.

The equation for creep compliance included in the computer program is the power law form:

$$D(t) = D_o + D_1 t^n \qquad (4 - 11)$$

where D_o = A constant which is nearly the glassy compliance.

D_1 = The intercept of the compliance curve where log time = 0

n = The slope of the log compliance versus log time curve

The equation which represents the time - temperature shift factor is also a power law form:

$$a_T = \left(\frac{T - T_A}{To - T_A}\right)^{\beta} \qquad (4 - 12)$$

where T = a given temperature

T_o = the temperature at which the master creep compliance curve was measured

T_A = a temperature constant that is usually near the glass transition temperature of a material.

Typical creep compliance and time-temperature shift properties of asphaltic pavement materials are given in Table 22.

Several example runs of the computer program were made to compare the cracking behavior of asphalt concrete and sulfur asphalt paving materials in Abilene and Amarillo, two of the many stations in Texas for which U. S. Weather Bureau data are available. All Pavements are assumed to be constructed on July 1, 1950 with a surface course thickness of 1.5 inches.

A wide variety of base course activity is possible and several of these variables are considered in these example problems. The range of base course properties used in these problems is given in Table 23.

Fig. 78 shows the effect of decreasing the compliance, (increasing the stiffness) of the asphalt mix. The base course used in this set of problems had both the high tensile strength and high thermal coefficient. This graph shows that the stiffer mixes will last longer. The stiffest mix was broken into 40 cracks per station in the severe winter of 1957-58. As will be shown presently, pavement cracking behavior will improve considerably if the base course has less extreme thermal properties.

In Fig. 79, a more severe climate, that of Amarillo, is investigated. An asphalt compliance, D_1, of $10^{-6.4}$ in.^{2}/lb. is used in all problems. The longest lasting pavement rested on the base course with the lowest tensile strength and lowest thermal coefficient. The two pavements which lasted the shortest period of time both rested on pavements with a high tensile strength. This shows the importance of reducing the base course tensile strength to as low a value as can be tolerated. Only small improvement can be expected by reducing the thermal coefficient by a factor of only two.

Table 22. Typical Properties of Asphaltic Pavement Materials

	Asphalt Concrete	Sulfur Asphalt
Do, in^2/lb	$10^{-7.0}$	$10^{-7.0}$
D_1, in^2/lb	$10^{-6.4}$	$10^{-5.77}$
n	0.50	0.25
To, ^oF	40	72
T_A, ^oF	-	-161
β	15.5	43

Table 23. Typical Base Course Properties

Property	Symbol	High	Low
Frozen Elastic Modulus, psi	E	150,000	30,000
Tensile Strength, psi	σ_T	250	100
Thermal Coefficient, $\times 10^{-4}$ in/in/^{o}F	α	3.5	1.5

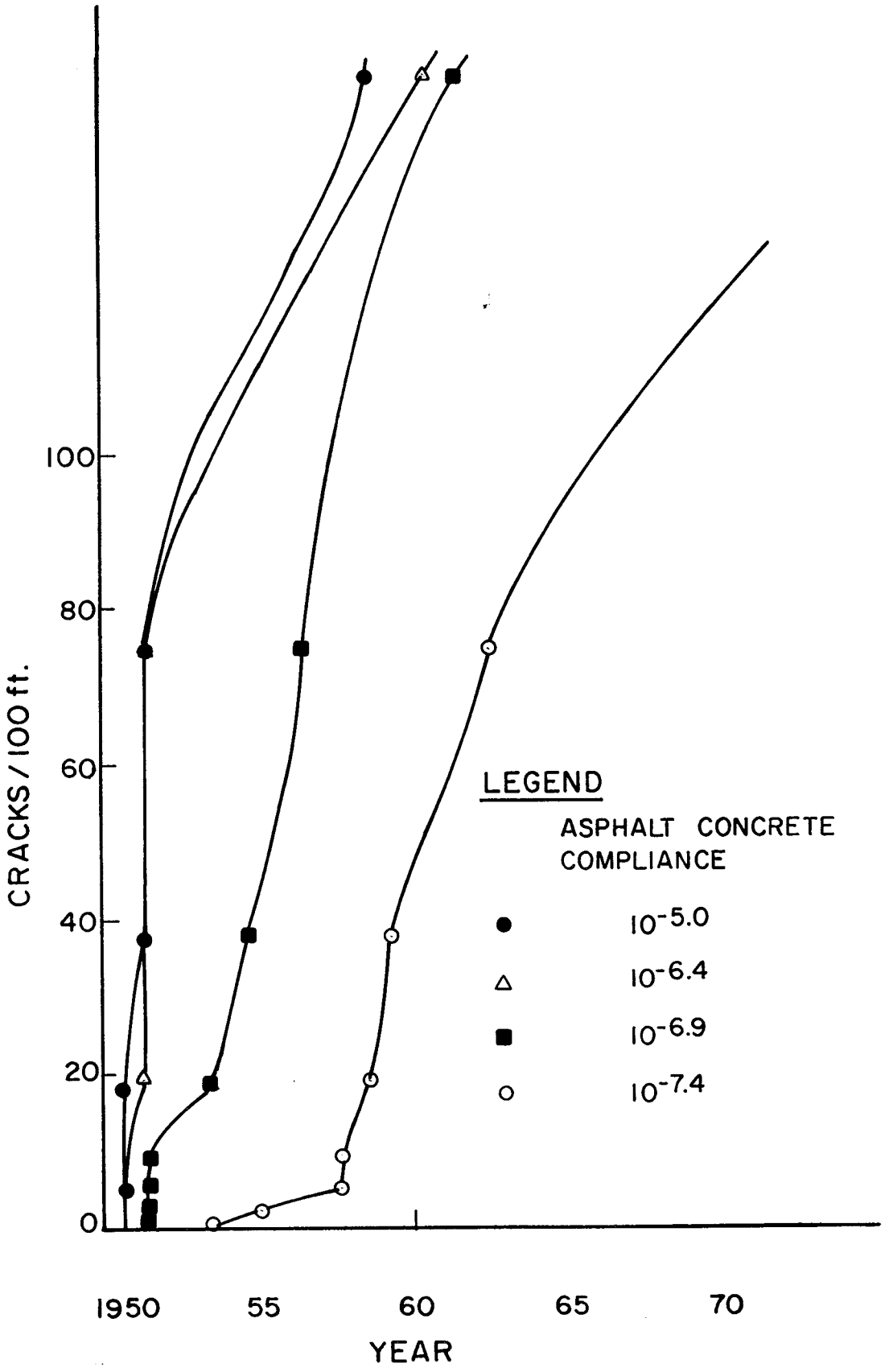

FIG. 78 PREDICTED THERMAL CRACKING OF ASPHALT CONCRETE IN ABILENE, TEXAS.

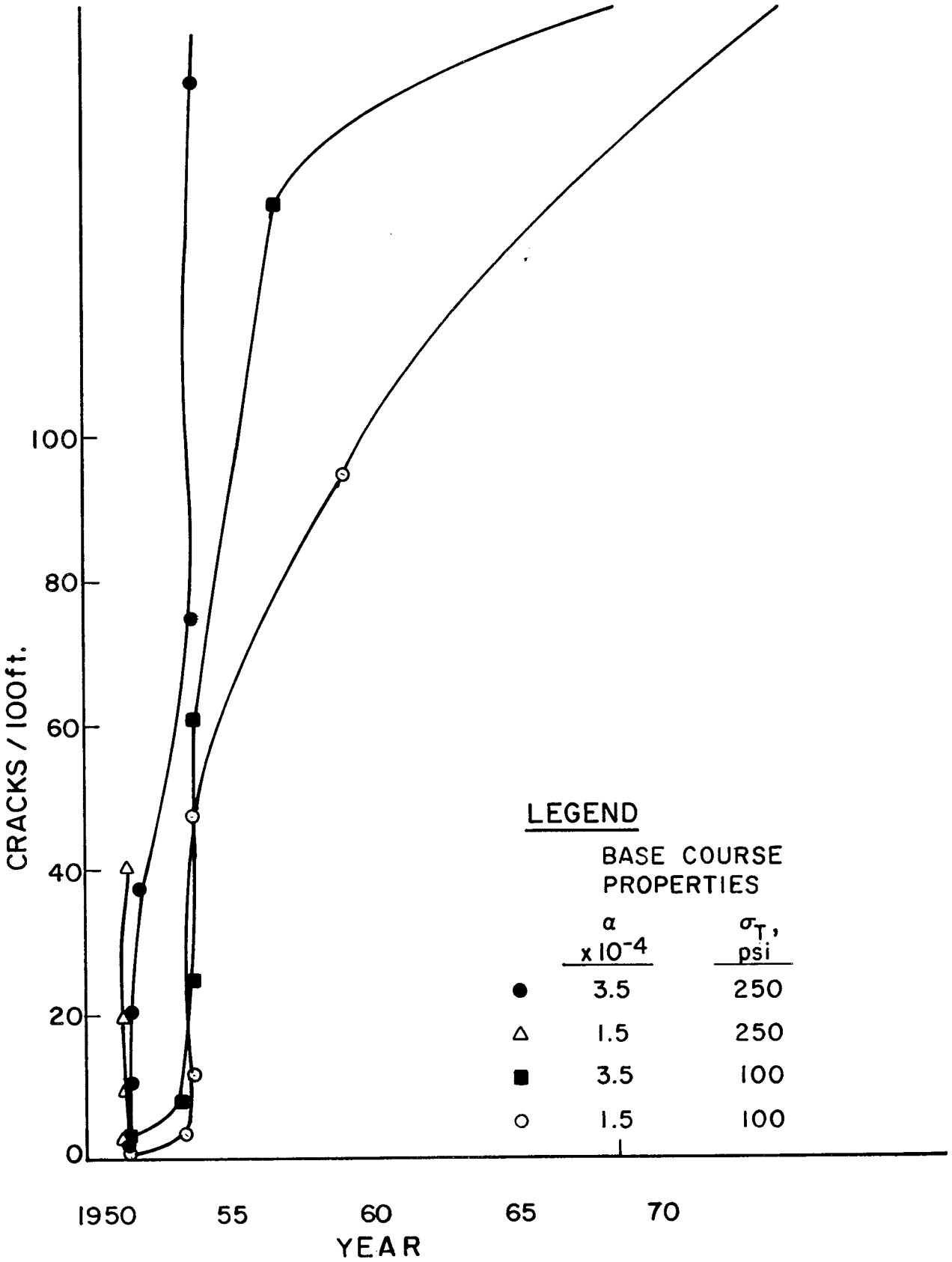

FIG 79. PREDICTED THERMAL CRACKING OF ASPHALT CONCRETE IN AMARILLO, TEXAS.

Figure 80 shows the behavior of sulfur asphalt pavement in the same Abilene climate as in Fig. 78. A variety of compliance and base course properties are considered here. Even with the low base course properties, the ordinary sulfur asphalt pavement would have cracked during the winter of 1957-58. A thicker pavement probably would not have cracked. However, a stiffer mix with a D_1 of $10^{-7.0}$ would not have cracked for 20 years even though it rested on the base course with the worst properties.

A similar result is predicted for Amarillo in Fig. 81, where the same stiffer sulfur asphalt mix remained uncracked for 20 years while resting on the base course with the lowest thermal coefficient and tensile strength. The less stiff mix cracks at different rates depending upon the properties of the base course on which it rests.

By way of comparing asphalt concrete and sulfur asphalt directly, Fig. 82 shows the two ordinary mixes resting on the least active base course in Abilene. Although the asphalt concrete would break up into 40 cracks per station by 1960, the sulfur asphalt mix will suffer the same amount of distress in 1967.

In concluding this set of example problems, it is apparent that the best way to design a crack resistant pavement would be to:

1. Reduce the tensile strength of the base course
2. Increase the stiffness of the mix
3. Possibly increase the thickness of the pavement.
4. Reduce the thermal coefficient of the base course.

The curves in Figs. 78-82 are for a 1.5 inch (3.8cm) thick pavement with the properties previously stated. Different relations would be

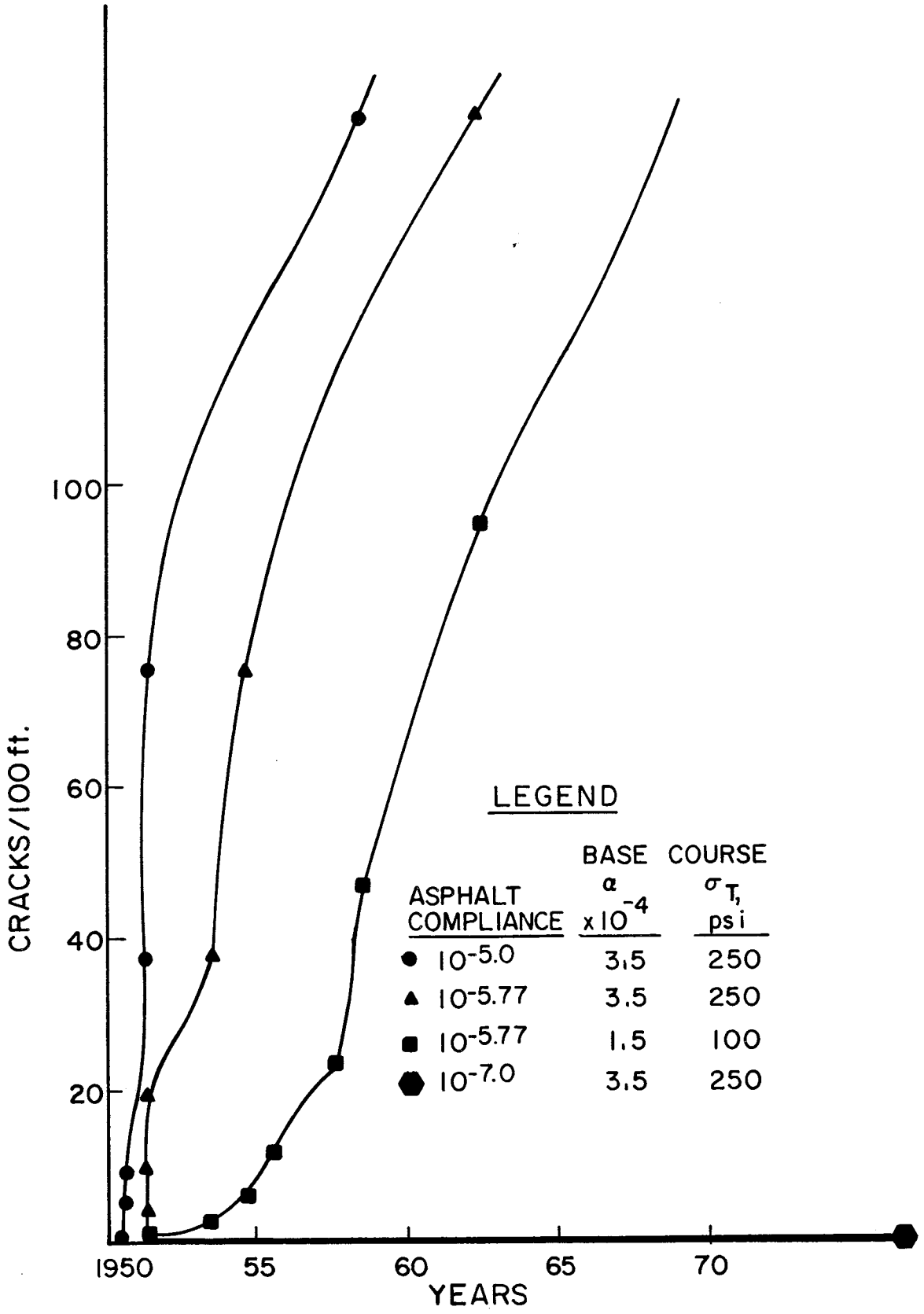

FIG. 80 PREDICTED THERMAL CRACKING OF SULFUR ASPHALT IN ABILENE, TEXAS.

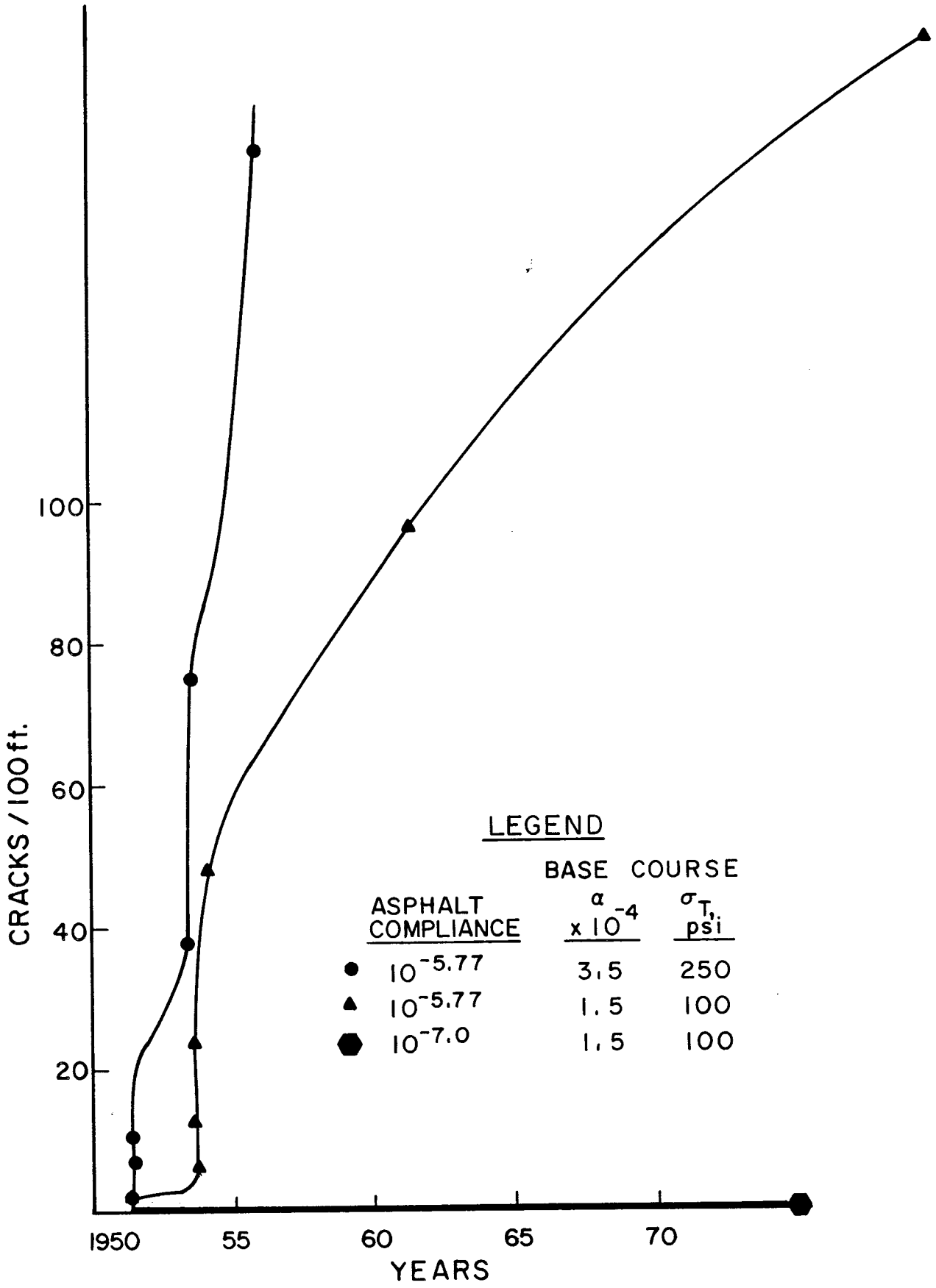

FIG. 81 PREDICTED THERMAL CRACKING OF SULFUR ASPHALT IN AMARILLO, TEXAS.

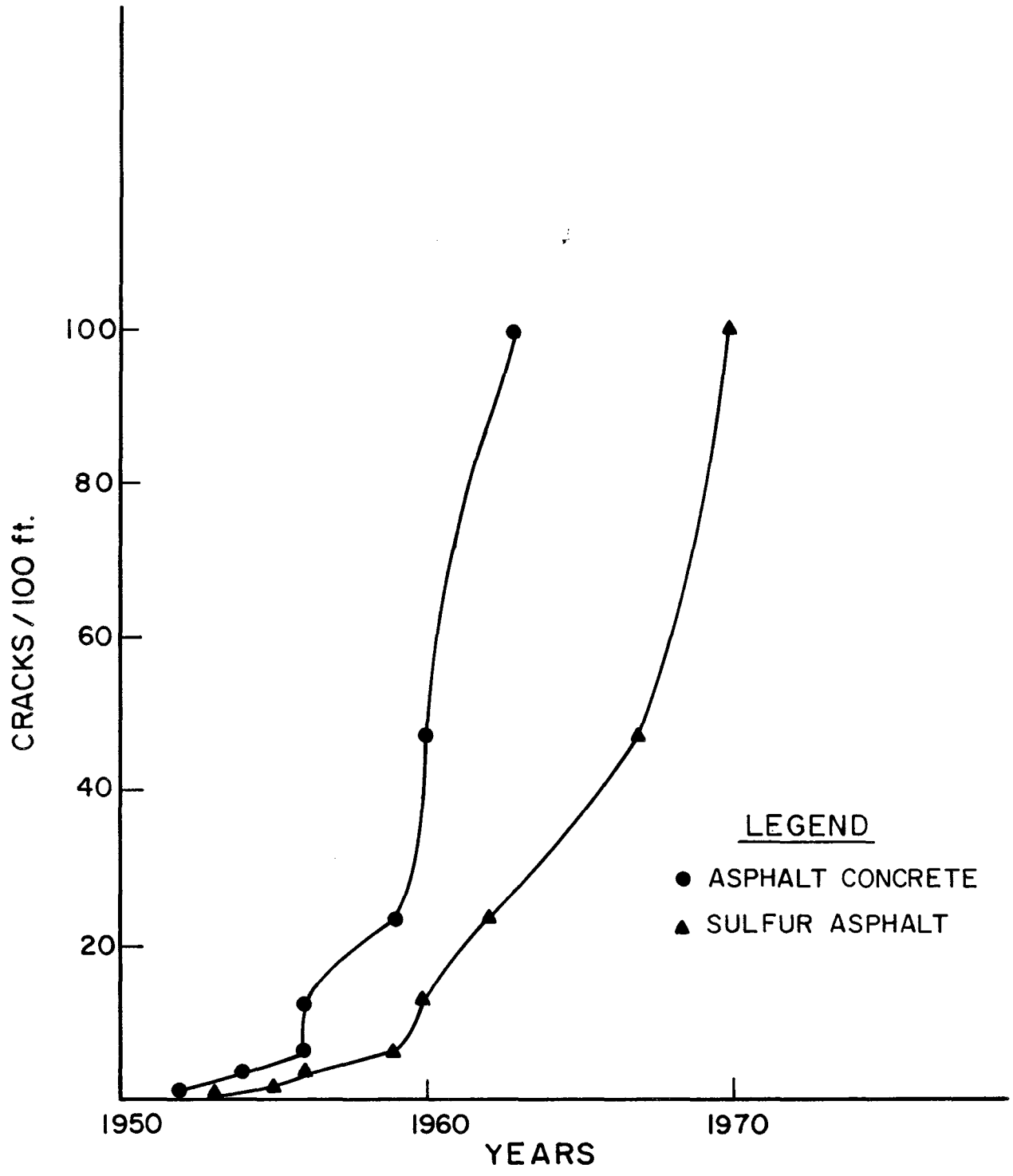

FIG. 82 PREDICTED THERMAL CRACKING IN ABILENE, TEXAS.

obtained if the properties and physical characteristics of the pavement were changed. The tensile strength, fracture toughness and viscoelastic properties would alter the fracture mechanics approach and produce a different number of cycles to failure under the same environmental conditions as acted on the original pavement. A physical change such as reinforcing would alter the stress intensity calculations. The effect of varying the material properties on the predicted crack appearance, will be discussed in the next section.

The shape of the predicted curves for Amarillo and Abilene are not unlike the data obtained from Canadian test pavements and the predictions made by Shahin and McCullough (46). These data and predictions are shown in Fig. 83. The data were collected from test sections constructed using a variety of asphalts. The prediction scheme incorporates thermal fatigue with low temperature cracking of the asphalt surface course in predicting crack appearance with time. A proper knowledge of the material properties as they exist in the pavement would show how accurate the prediction scheme developed in this research is in predicting the damage from base course thermal susceptibility in the west Texas area and throughout the Great Plains States which have a similar environment.

The data indicate how the same pavement in Abilene will take longer to crack than in Amarillo. This difference is due solely to the difference of the environment in the two areas and its influence on the activation of the thermal susceptibility mechanism in the base course.

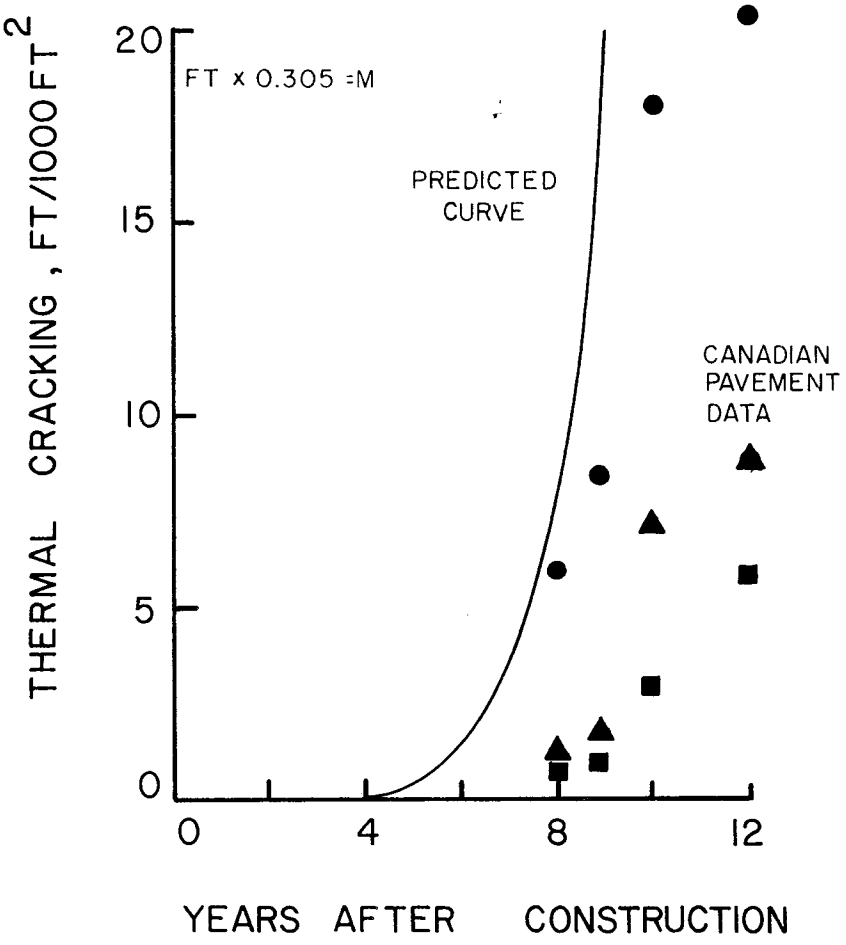

FIG. 83 - CRACK FREQUENCY PREDICTIONS FROM SHAHIN AND MCCULLOUGH'S PREDICTIVE SCHEME (46)

CONTROLLING TRANSVERSE CRACKING

The predictive model developed in the preceding chapter illustrates the applicability of a design procedure based solely on the material property relationships. The model allows the effect of different material properties to be studied in a direct manner, and the effect on the pavement performance to be predicted. The predictive curves in Figs. 78 through 82 illustrate how variations in material properties affect the crack spacing. This chapter discusses methods of varying the material properties and the resulting effect on the predicted crack spacing-time curves.

Asphaltic Concrete

Modulus

The modulus of the asphaltic concrete is a very important factor in determining the rate of crack propagation. A lower modulus will produce a higher stress intensity factor and provide for more rapid crack propagation. Chang (11) has presented data on the effect of modulus on rate of crack propagation. The analysis utilized in this study takes into account the viscoelastic nature of the asphalt which requires the modulus to be different for different rates of temperature drop and different minimum temperatures. The viscoelastic analysis allows the modulus to be predicted from the calculated temperatures and permits the effect of viscoelastic modulus values to be accounted for in a Miner's law approach to damage prediction.

In this analysis, the modulus of the asphalt concrete does not affect the crack spacing that develops since this model initiates the crack in the base course. Further, the base course is assumed to have little or no thermal activity below $20^{o}F$ ($-6.7^{o}C$). Thus, for a severe freeze, this model would not predict excessive damage to the pavement system. For extremely low temperatures, which do occur occasionally in the west

Texas area, a crack could be expected to form in the asphaltic concrete in a manner similar to those found in the colder regions. Christison (12) was very successful in predicting the appearance of cracks in test pavements in Canada using viscoelastic analysis. The predictive schemes for studying cracking in extremely cold regions without the application of fracture mechanics may be attributed to the behavior of the asphalt. At these extremely low temperatures the asphalt will be very brittle, as it will be very near or below the glassy temperature. In this state the asphalt would crack and produce a crack through the thickness of the asphaltic concrete. Thus, fracture mechanics is not needed. With the proper viscoelastic analysis, as previously mentioned, the low temperature effects will be accounted for in the effective modulus of the asphaltic concrete. This would allow for the rare occurrence of cracking initiating in the asphaltic concrete.

Although not directly studied in this research since the prediction schemes developed were for a 1.5 inch (3.81 cm) thick pavement surface, the effects of thickness are evident. A thicker asphalt layer would act like an insulating layer and not allow the low temperatures to reach the base course. This would cut down on the freeze-thaw activity of the base course and lower the propagation rate of any cracks that might exist.

Base Course

Tensile Strength

The material properties of the base course are all interrelated as shown by equation (4-2), (p. 131) in the last chapter. Lower tensile strength (frozen state) produces much smaller crack spacings as shown in

Fig. 68 (p. 134). These are produced much sooner than cracks in a high strength base course. However, since the cracking is at a much smaller spacing, the stresses that develop will be much lower and the rate of crack propagation through the surface course will be slower. This was illustrated in Figs. 79, 80, and 81. On the other hand, a high strength base course will crack through the surface course, have larger cracks, and a greater total amount of visible cracking. As shown in the numerical studies, a small tensile strength gives the greatest insurance against thermal cracking. One convenient way to lower the tensile strength of caliche base courses is to reduce the fines and add sand. As would be expected, river run gravel has a very low tensile strength and usually performs very well in the west Texas climate.

Modulus

The modulus of the base course entered in equations (4-2) and (4-3), which show that a higher modulus will produce a higher stress. This stress will vary with the crack spacing, and will produce a faster rate of propagation than with lower modulus base courses.

Freeze Coefficient

The effect of the base course freeze coefficient, α, on crack appearance is very critical and is the prime cause of the environmental damage studied in this research. The theoretical relationships established previously indicate that by varying the ion concentration and the specific surface area, the freeze coefficient could be decreased thus effecting a thermal stabilization. This stabilization is accomplished with additives, several of which are quite common.

Stabilization of the Freeze Coefficient

The use of additives in the stabilization of the thermal activity is the most common method of stabilization in use today. As the mechanism of thermal susceptibility does not change behavior as the strength changes, additives were considered only if they would produce a change in the mechanism as presented earlier. This excluded the use of asphalts and cement which primarily increase strength. These additives are well documented and should be considered in the design process when investigating the influence of strength.

Commercilly available, economic additives to accomplish the two methods of stabilization are lime and salts. Lime provides ion exchange as the primary stabilization process. The pozzolanic reaction serves as a specific surface area reducer through particle cementation. The salt additive would provide ions to the pore water and increase the osmotic potential in the suction. Thus, it would be possible to observe the effects of two distinct types of stabilization and form conclusions regarding the effectiveness of the methods used. Potassium chloride (KCl) was chosen as the salt to study the influence of a different ion than the calcium ion provided by the lime. Considerations of the stabilization results led to the use of gypsum ($CaSO_4 7H_2O$) as a stabilizing additive. The results are discussed in the subsequent sections.

Sample Preparation

A given percentage of each additive was dissolved in the mixing water and thoroughly mixed in a given quantity of material. (6BAR was used initially, and 6BAR #2 was obtained from a nearby pit for the $CaSO_4$ study). The mixed material was then stored overnight in a moisture room in a sealed container. The material was compacted the following day using the Harvard miniature spring loaded compactor (95% of modified

AASHTO) and a thermocouple psychrometer was sealed in each sample to record the equilibrium suction. When the equilibrium suction value was attained (typically 2-3 weeks) the psychrometers were removed and the samples were subjected to a repetitive series of six freeze-thaw cycles as was done for all previous samples.

Lime

The results of lime addition show that low percentages were quite effective in altering the freeze activity. Since the low percentages did not vary the suction appreciably, the stabilization may be attributed mainly to the cation exchange. Figure 84 illustrates the freeze behavior variation with the suction for each of the percentages of additive in material 6BAR. The highest percentage of lime begins to show an increase in the suction due to an increase in the ion concentration, hydration and possibly the pozzolanic reaction. these effects may be seen more readily in Fig. 85 and Fig. 86 which show the freeze coefficient for comparable samples taken from the moistune-density curves. These appears to be an optimum percentage of lime, above which the behavior worsens again. For the samples dry of optimum, which are expected to occur in the field, the freeze contraction returns as more lime is added. This may be explained by considering that cementation is brought about by large percentages of lime are based on the amount of clay present the amounts of additive are between 6 and 21 percent which shows that there is actually a large excess of lime available to react with the clay minerals. This cementation will primarily serve to accentuate the moisture-related contraction phenomena (19).

Salt

Potassium chloride was chosen primarily to avoid the effect already

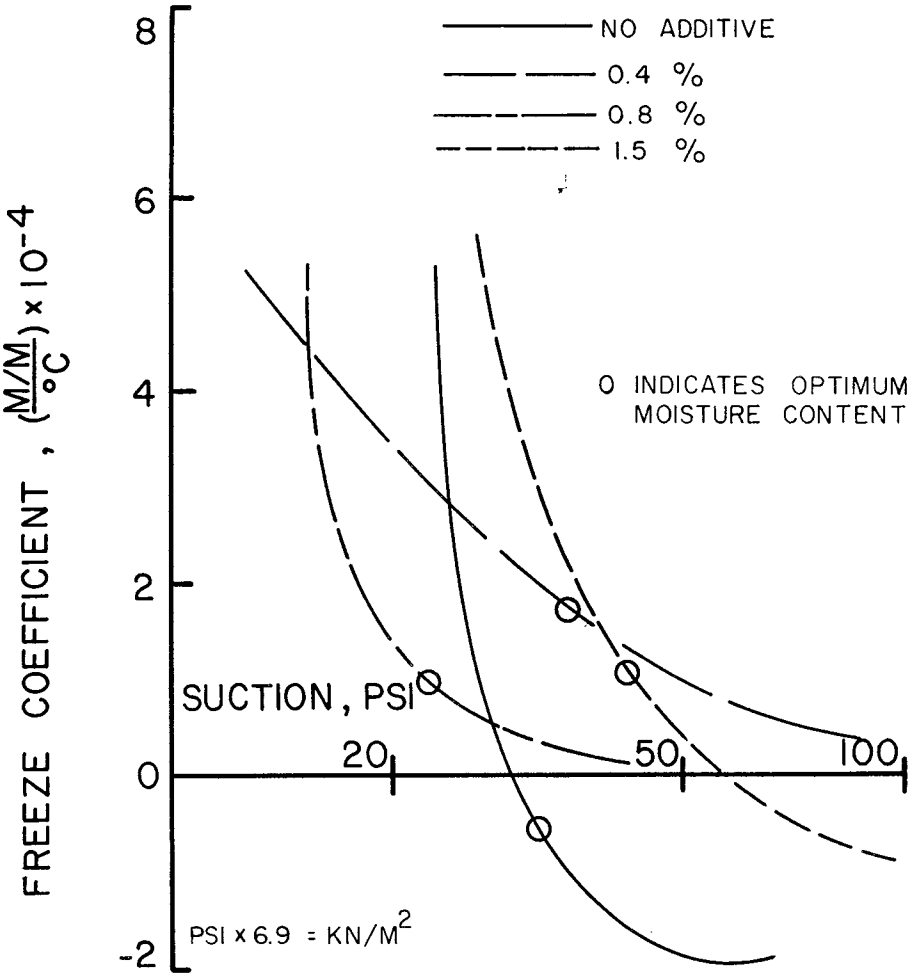

FIG. 84 - CHANGE IN FREEZE COEFFICIENT-SUCTION CURVE WITH ADDITION OF LIME, MATERIAL 6BAR

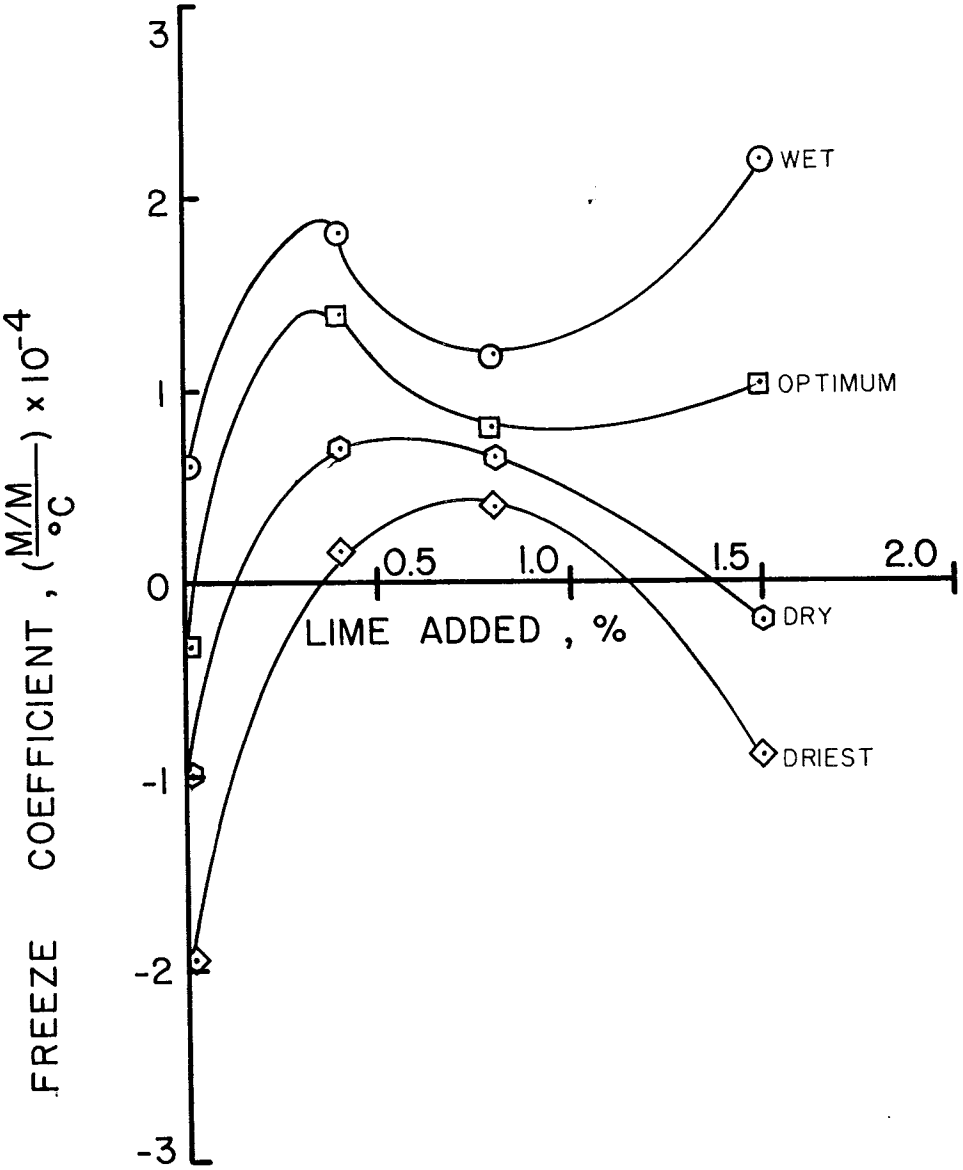

FIG. 85 - CHANGE IN FREEZE COEFFICIENT WITH ADDITION OF LIME FOR SAMPLES AT EQUIVALENT MOISTURE CONTENTS, MATERIAL 6BAR

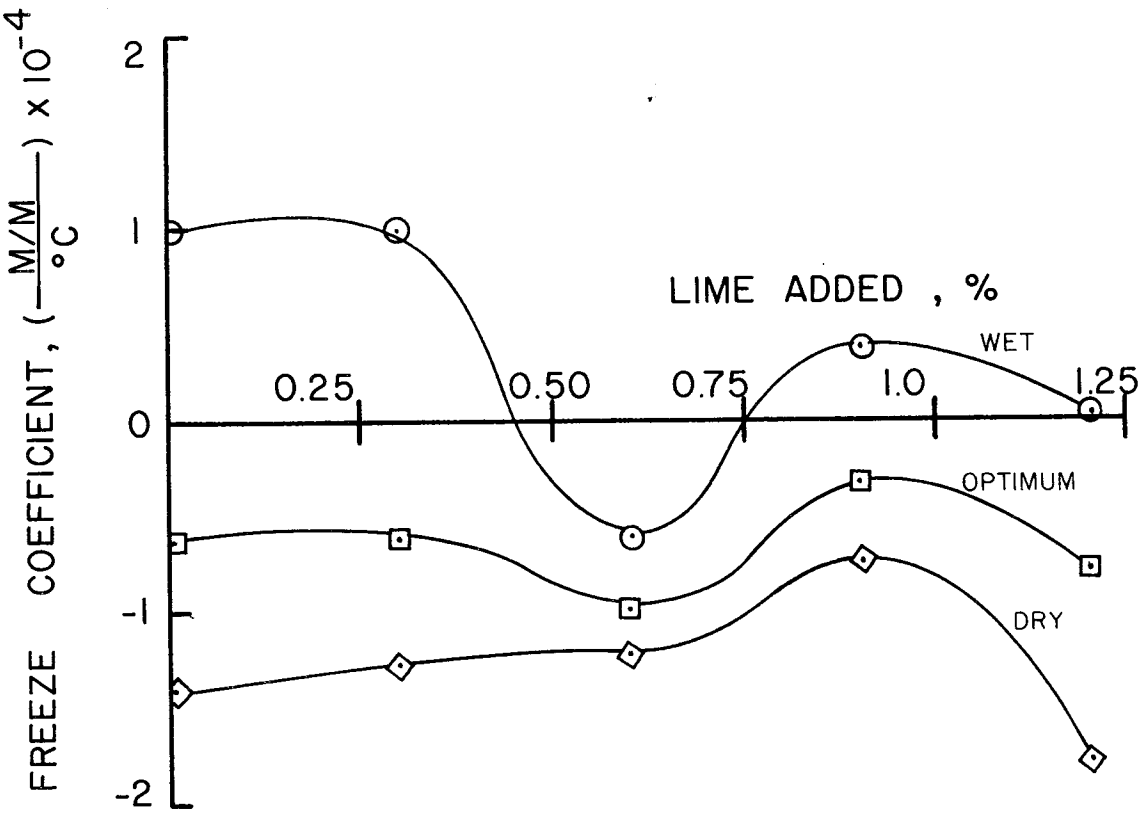

FIG. 86 - CHANGE IN FREEZE COEFFICIENT WITH ADDITION OF LIME FOR SAMPLES AT EQUIVALENT MOISTURE CONTENTS, MATERIAL 6BAR#2

shown through the calcium ion exchange of the lime. The potassium ion has a much smaller radius of hydration than other ions and is monovalent (18), thus, the potassium ion should not distrub the adsorbed water structure as much as the larger ions. There is further evidence that potassium does not readily hydrate, making the ions effectively even smaller.

The effect of increased salt concentration on the freeze coefficient and suction is shown in Fig. 87 for material 6BAR. Increased salt concentration clearly altered the freeze behavior, changing the freeze coefficient from contraction to expansion and increasing the suction. There was also considerable change in the position of optimum moisture. Figure 88 and Fig. 89 show the freeze coefficient for comparable sample positions on the moisture-density curve.

Interpretation

The stabilization with the salt is different from that obtained with the lime stabilization, although the percentages are similar, around 0.5 percent or less. The basic mechanism behind the stabilization remains essentially the same for both additives. Both methods of stabilization flocculate the structure and involve cation exchange. The presence of an excessive amount of cations on the clay surface bonds the clay mineral particles tighter together and produces a thinner layer of adsorbed water. This action provides more free water while at the same time immobilizing clay mineral moisture activity to some extent. This, in turn, accentuates the expansive nature of the free moisture when it freezes, which then dominates the freeze behavior.

The salt is a much more effective flocculant than is the lime; and the more flocculated structure produces adsorbed water layers that are thinner than those produced by lime. This provides even more free

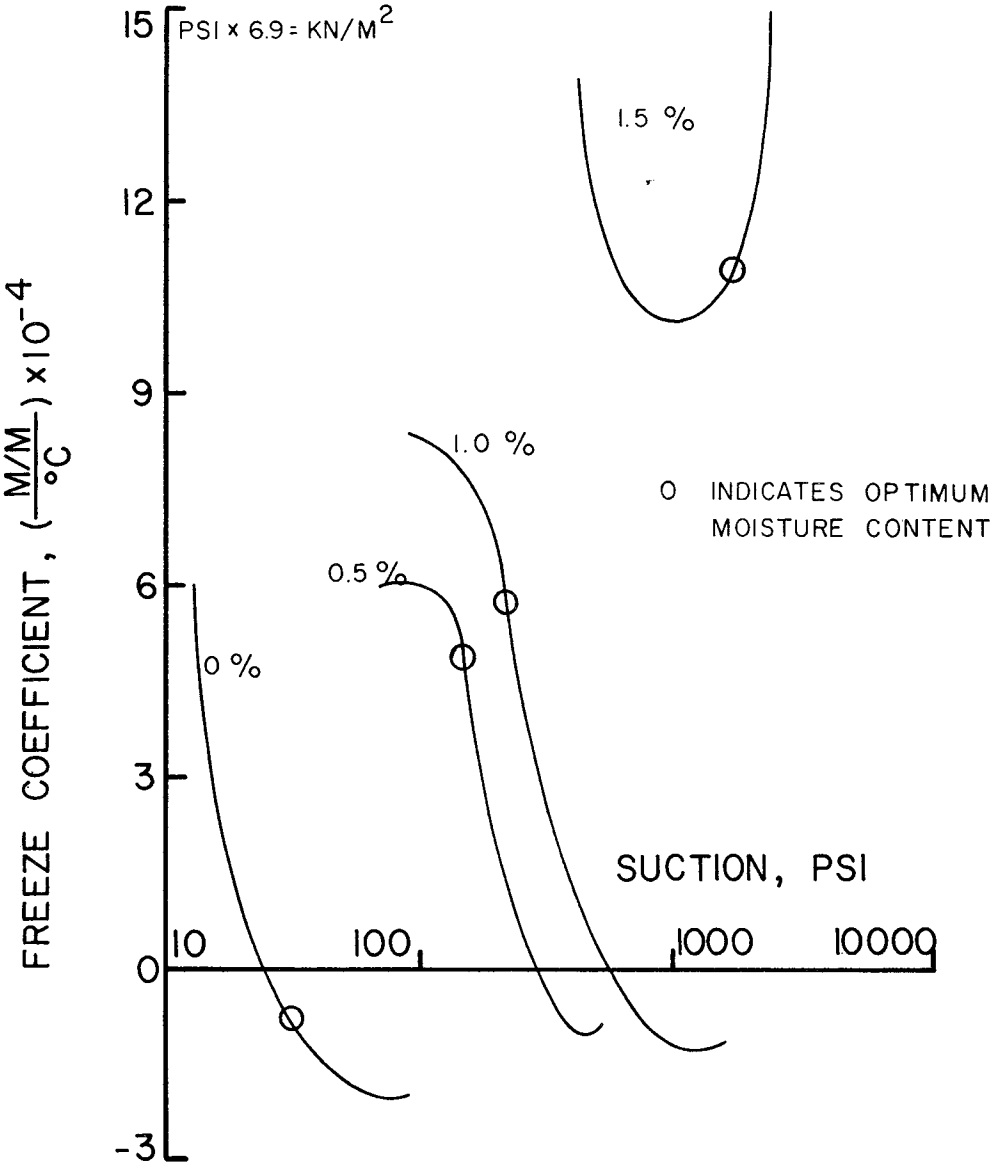

FIG. 87 - CHANGE IN FREEZE COEFFICIENT-SUCTION CURVE WITH ADDITION OF SALT, KCl, MATERIAL 6BAR

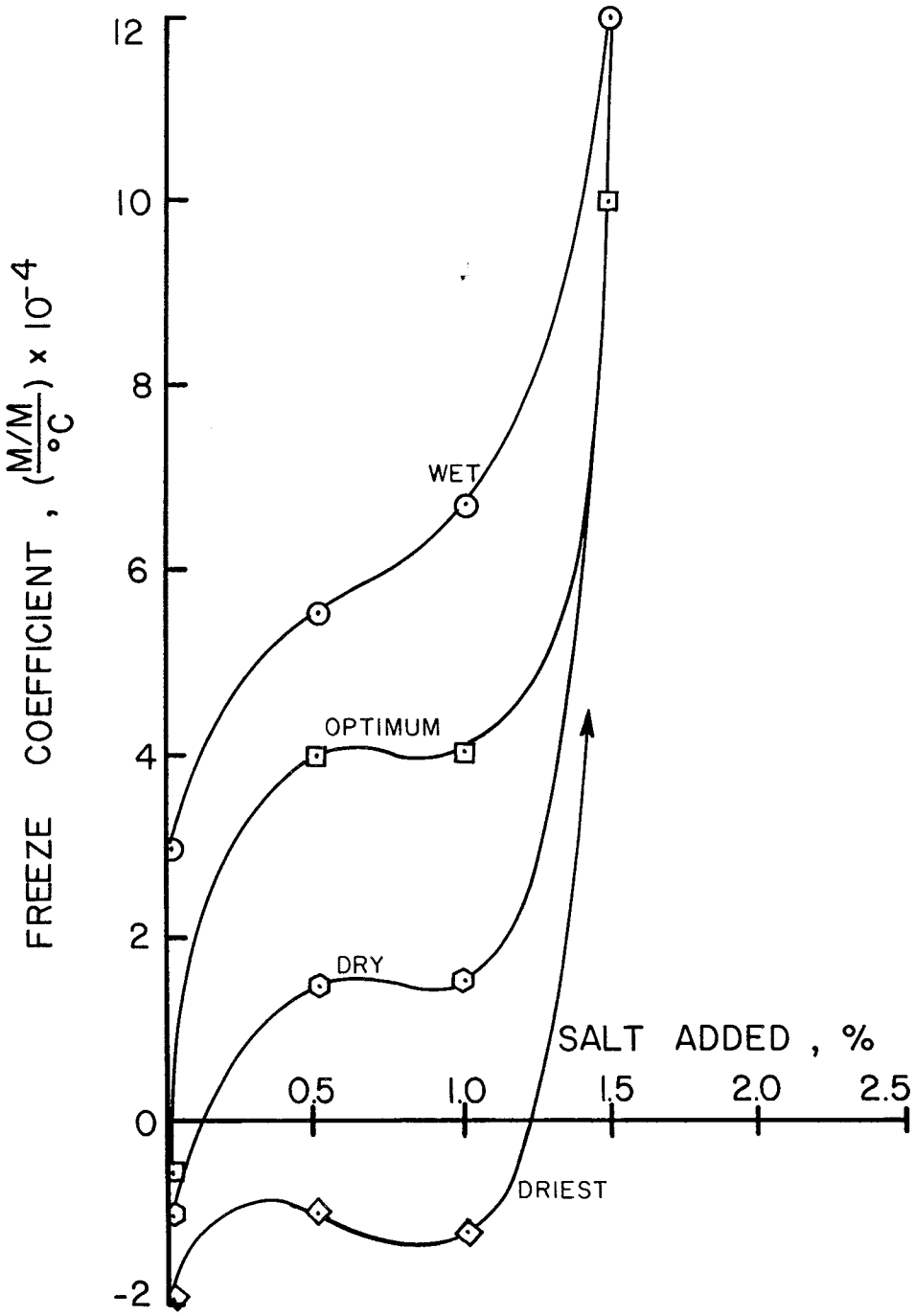

FIG. 88 - CHANGE IN FREEZE COEFFICIENT WITH ADDITION OF KCl FOR SAMPLES AT EQUIVALENT MOISTURE CONTENTS, MATERIAL 6BAR

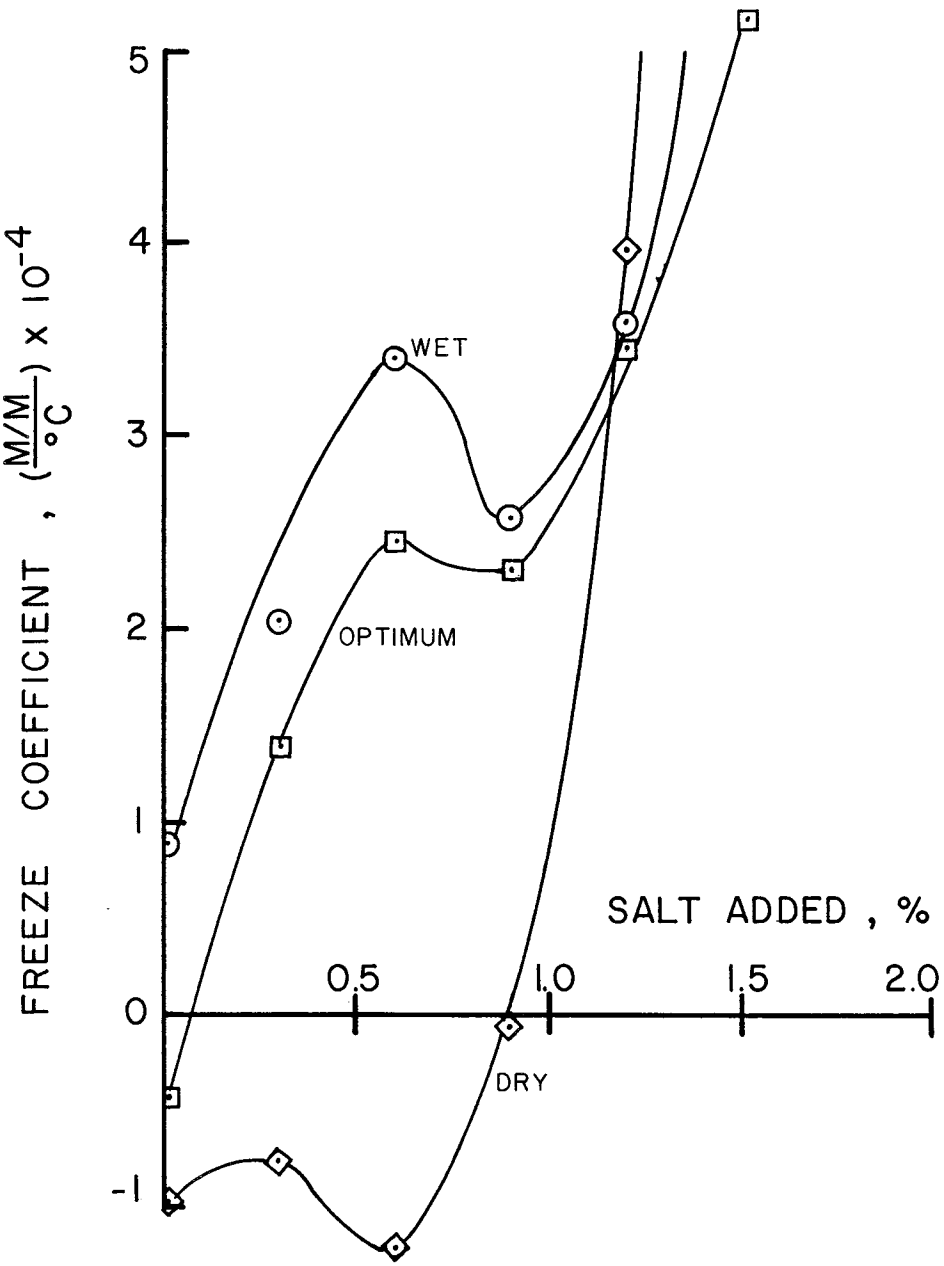

FIG. 89 - CHANGE IN FREEZE COEFFICIENT WITH ADDITION OF KCl FOR SAMPLES AT EQUIVALENT MOISTURE CONTENTS, MATERIAL 6BAR#2

water and adds more restraint to the clay minerals, accentuating the expansion of the free water even more. This is evidenced in the extreme expansion exhibited by the salt treated samples. Also important is the lack of cementation such as was caused by lime, which serves to counteract the expansion.

The result for both materials are similar. Material 6BAR #2 which has approximately half the amount of clay as in material 6BAR did show the same trend in stabilization. The difference in the effectiveness of the lime stabilization could result primarily from the lower clay content not providing sufficient clay for the pozzolanic reaction and ion exchange to develop fully.

The results do show two distinct types of variation, however, with increased salt causing increased expansion due to increased ion concentration and increased lime causing increased contraction, due to decreased specific surface area.

Calcium Sulfate

Calcium sulfate provides the components of lime and salt and would appear to possess the probability of being able to produce stabilization over a larger range of additive. Additionally, calcium sulfate, when hydrated, occurs in abundance in west Texas as gypsum. Thus, this additive would be very ecenemical to obtain.

The results of the calcium sulfate tests are given in Fig. 90. The results indicate explicitly that stabilization over all moisture contents occurs between 0.5 and 1.0 percent additive. The curves begin to diverge at 1.0 percent similarly to the lime stabilization, indicating that cementation may be the dominant stabilizing mechanism. The overall effectiveness of gypsum stabilization is much more pronounced

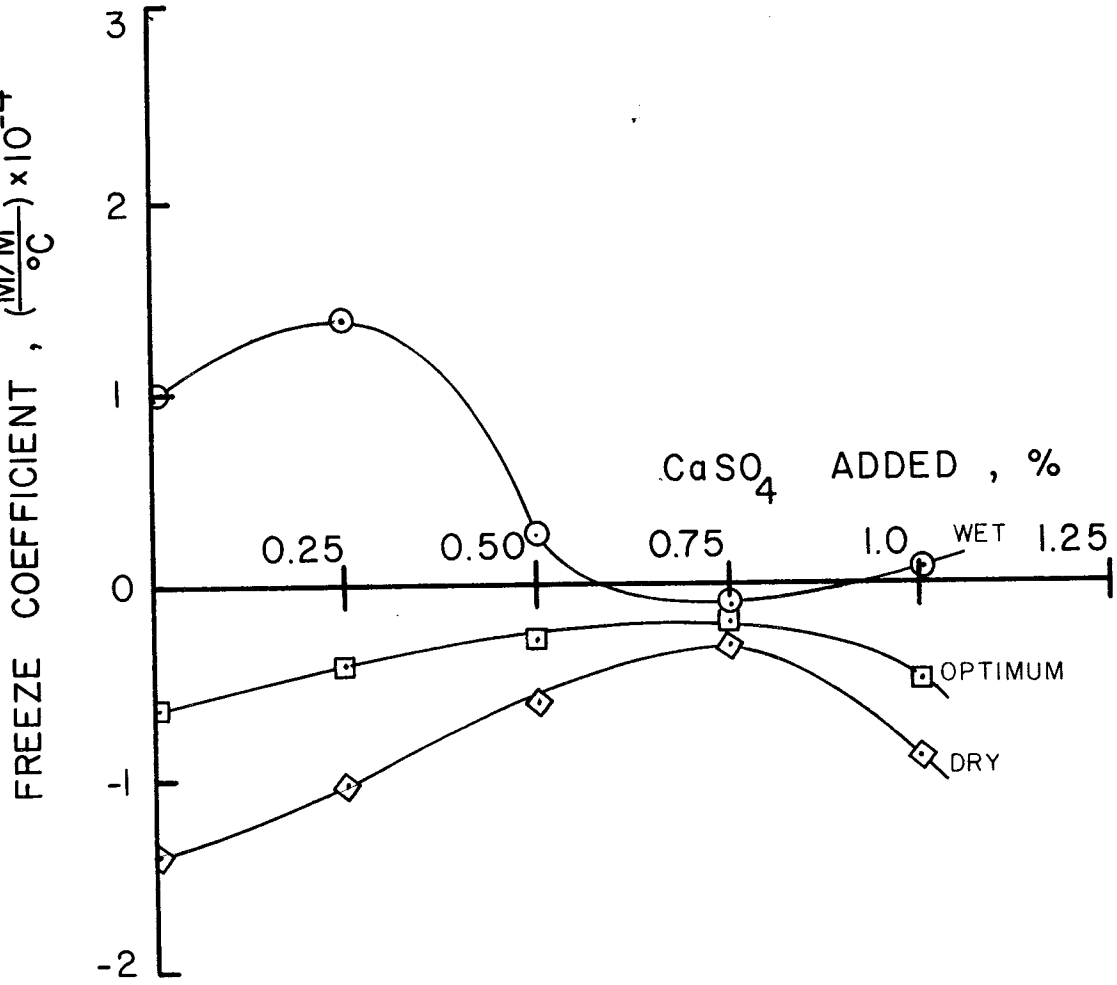

FIG. 90 - CHANGE IN FREEZE COEFFICIENT WITH ADDITION OF $CaSO_4$ FOR SAMPLES AT EQUIVALENT MOISTURE CONTENTS, MATERIAL 6BAR#2

than for the other additives which indicates that even for such a very small working range the behavior may be much more stable and less susceptible to small concentration changes.

This study of stabilization of the freeze coefficients illustrates that it can be done, but great care must be exercised in mixing the additives with the base course to insure uniform concentrations. This may not be possible economically; but it does provide consideration in the design process to allow reduction of the freeze coefficient to a value that will produce minimum damage.

CONCLUSIONS

This study of environmental deterioration of pavement in west Texas has provided new information concerning a damage mechanism that has never before been considered in pavement design. The mechanism has logical material property relationships and compares extremely well with the behavior that might be expected from a theoretical derivation concerning intermolecular or particle forces. The data obtained from laboratory tests and field installations indicate that the mechanism could be expected to be most active in west Texas and possibly throughout the Southwestern United States since the general environment and the base course materials necessary for this mechanism are similar throughout this area. The mechanism is shown to be capable of producing the transverse cracks common to west Texas. A design procedure was developed and sample calculations predicting crack frequency with time for a particular pavement were shown.

The major conclusions from this study may be restated as follows:

1) Thermal susceptibility of the base course is a valid deterioration mechanism. Additionally, the volumetric contraction, activated by freezing and thawing, is quite prevalent in base course materials from west Texas.
2) Soil moisture suction, a measure of the energy state of the moisture, is a parameter that directly relates the influence of the environment to the engineering behavior of the soil. The relationship with the mechanism of thermal susceptibility accentuates the need to fully characterize a material by testing it in the environment in which it will be used. The environment in west Texas is such that the mechanism of thermal susceptibility is enhanced.
3) Although the clay contents of the base course were relatively low, and were within specifications, the clay mineralogy of

the base course was very influential on the mechanism. The percent clay determined the level of suction which developed for a given moisture content. The specific surface area determined the maximum amount of contraction that developed in a given material. The strength of these relationships was such that they could be used to predict the thermal activity of the base course material.

4) A theoretical interpretation of the freeze coefficient-suction curves illustrated the effect of specific surface area and ion concentration on interparticle forces and how these are indicated by the freeze coefficient-suction curves.
5) The volume change of the freeze contraction is attributed to a particle reorientation under the drying effects of freezing water in the pores. This reorientation is supported by the physical data and a scanning electron microscope study of base course samples with and without freeze-thaw cycling.
6) The mechanism of thermal susceptibility will produce a crack in the base course and subsequent temperature cycles will propagate this crack through the asphalt and produce more cracks in the base course. Using the viscoelastic fracture mechanics approach with proper temperature calculations, the rate of crack appearance at the surface of the asphaltic concrete with the passage of time is possible.
7) The computer model developed will allow the environmental damage caused by a thermal susceptible base course to be analyzed in a "stress and distress system" type of analysis. This scheme will allow material properties to be studied and included in the design decision.
8) Stabilization of this mechanism using additives is possible within a very narrow range of additive concentration. This narrow range may make stabilization impractical for lime and salts such as KCl since a slight excess produces drastic changes in the thermal behavior. Calcium sulfate, or gypsum, may provide a more stable material over a slightly

greater variation in concentration. Stabilization by itself may not be the answer, and all aspects of the design material properties would need to be investigated. An example of this is the effect produced by increased surface modulus, which increases the service life of the pavement, assuming the other variables of the surface remain constant. This shows that additives such as sulphur, which increases the modulus of the asphaltic concrete, may prove to be beneficial to the performance of the pavements subjected to thermal susceptibility.

10) Although not addressed directly, the problem of longitudinal cracking may be inferred. When the crack spacing becomes nearly the same as the width of the roadway, the contraction in both the transverse and longitudinal directions will be of the same magnitude. In this situation, cracking in both directions may be expected to occur. Thus, once the cracking has reached a certian level, the deterioration of the pavement would proceed at an accelerated rate, over that predicted by this study; which has concentrated primarily on transverse cracking.

11) The calculations for crack spacing and appearance point up the need to fully study the properties of the base course in the frozen state. Little information is available today concerning the frozen tensile strength and modulus values. It is the frozen properties that most severely affect the crack spacing and rate of propagation in the asphaltic concrete.

The final result of this study is the ability to predict environmental damage in the form of transverse cracks. This prediction is in terms of the measurable material properties that are validly related to the conditions that will be found in an actual pavement. The severity of thermal susceptibility in the base course is demonstrated by the large decrease in the cycles to failure as compared to thermal activity of the asphaltic concrete alone. The analysis performed to obtain the stress intensity factors was conducted for a pavement 1.5 inch (3.8 cm) thick. To expand the concept developed in this study, it would be necessary to include a more complete description of the behavior of the

surface layer.

The steps necessary to accomplish the inclusion of the proper factors to produce a truly general environmental deterioration model may be delineated as follows:

1) A new analysis to predict the stress intensity factors in the surface layer, as a function of crack length, pavement thickness, modulus values, and stress levels would be needed. This anaysis would provide a series of curves similar to those shown in Fig. 73 (p. 141).
2) The stress predictions at a crack in the base course should be replaced by the actual deformation predicted for the crack by the finite element procedure. This would eliminate the need to use a reduced stress at the crack to model the behavior, as was done in this model.

The accuracy of this prediction model, with the assumptions made, and given the proper material properties, is pointed out quite vividly in Fig. 76 (p. 150) which shows the predictions for Abilene. A driving force behind the search for a valid environmental deterioration mechanism has always centered on the question concerning the severe pavement breakup in 1957 and 1958 that occurred in Abilene. The data shown in Fig. 82 for asphalt concrete resting on a base course with less active thermal properties show a crack spacing change from nearly 34 feet (10.4 m.) in early 1956 to 8 feet (2.4 m.) in late 1958. This drastic increase in the amount of cracking indicates the effect that thermal contraction of the base course had on the Abilene pavement breakup. Undoubtedly, heavy truck traffic occurring at the same time that the pavement was under heavy tensile stress tended to

accelerate the rate of crack propagation. The effect of traffic on the stress intensity factor is additive but is not considered in the computer program presented in this report.

At the same time that the asphalt pavement went from a crack spacing of 34 feet (10.4 m.) to 8 feet (2.4 m.), the sulfur asphalt pavement resting on the same base course cracked from a 67-foot (20.4 m.) spacing down to a 34-foot (10.4 m.) spacing, indicating the possible superiority of sulfur asphalt in reducing thermal cracking in west Texas.

The sensitivity of a pavement to climatic influences is heavily dependent upon material properties of the asphalt and the base course. The most vivid contrast of pavement cracking due to variations in material properties is shown in Fig. 80 where one compliant pavement lasted only two years until its crack spacing was 2.7 feet (0.8 m.) and another pavement had no thermal cracks reported in 20 years. The major differences in material properties in these curves was in the tensile strength of the base course and the stiffness (or compliance) of the asphalt mix. This graph emphasizes the fact that pavement cracking in west Texas is greatly dependent on the material properties of the base course and the surface course and that cracking can be reduced by properly choosing and controlling those properties. It appears that the most effective means of reducing cracking is to reduce the tensile strength of the base course. The second most effective means is to increase the stiffness or tensile strength of the surface course.

APPENDIX A

REFERENCES

1. Aitchison, G.D., Editor, Moisture Equilibria and Moisture Changes in Soils Beneath Covered Areas, A symposium in Print, Butterworths, 1965.

2. Babcock, R.L., and Overstreet, R., "The Extra-Thermodynamics of Soil Moisture," Soil Science, Vol. 80, p. 455, 1957.

3. Barber, E.S., "Calculations of Maximum Pavement Temperatures from Weather Reports," Highway Research Board, Research Bulletin 168, 1957.

4. Barden, L., and Sides, G.R., "The Influence of Structure on the Collapse of Compacted Clay," Second International Conference on Expansive Clay Soils, Texas A&M University, 1969.

5. Bergan, A.T., and Monismith, C.L., "A Characterization of Subgrade Soils in Cold Regions for Pavement Design Purposes," Highway Research Board Record No. 431, 1973.

6. Bolt, G.H., "Physical Chemical Analysis of Compressibility of Pure Clay," Geotechnique, Vol. 6, p. 86, 1956.

7. Bradley, W.F., "The Structural Scheme of Attapulgite," American Mineralogist, 25: 405-413, 1940.

8. Brunauer, S., Emmett, P.H., Teller, E., "Adsorption of Gases in Multimolecular Layers," Journal of the American Chemical Society, 60, 309-319, 1938.

9. Carothers, H.P., "Freeze Damage in Flexible Pavements," Highway Design Division, Texas Highway Department, 1948.

10. Chang, H.S., Lytton, R.L., and Carpenter, S.H., "Numerical Analysis of Thermal Crack Propagation in Pavement Overlays," Proceedings, Second International Conference on Numerical Methods in Geomechanics, June 1976.

11. Chang, H.S., "Prediction of Thermal Reflection Cracking in West Texas," Master's Thesis, Texas A&M University, 1975.

12. Christison, J.T., "The Response of Asphaltic Concrete Pavements to Low Temperatures," Ph.D. Thesis, University of Alberta, pp. 59-60, 1972.

13. Compton, P.V., "A Study of the Swelling Behavior of An Expansive Clay as Influenced by the Clay Microstructure, Soil Suction, and External Loading," Technical Report No. AFWL-TR-70-26 Air Force Weapons Laboratory, 1970.

14. Dixon, J.B., Class Notes, Soil Mineralogy, Texas A&M University.

15. Dempsey, B.J., and Thompson, M.R., "A Heat Transfer Model for Evaluating Frost Action and Temperature Related Effects in Multi-layered Pavement Systems," Highway Research Record No. 342, 1970.

16. Edlefson, N.W., and Anderson, A.B.C., "Thermodynamics of Soil Moisture," Hilgardia, Vol. 15, No. 31, p. 298, 1943.

17. Edris, E.V., "Dynamic Properties of Subgrade Soils, Including Environmental Effects," Master's Thesis, Texas A&M University, 1976.

18. Grim, R.E., Clay Mineralogy, McGraw Hill, 1968.

19. George, K.P., "Mechanism of Shrinkage Cracking in Soil-Cement Base," Highway Research Record No. 442, 1973.

20. Hajek, J.J., and Haas, R.C.G., "Predicting Low-Temperature Cracking Frequency of Asphalt Concrete Pavements," Research Record 407, Highway Research Board, Washington, D.C., 1972.

21. Hamilton, A.B., "Freezing Shrinkage in Compacted Clays," Canadian Geotechnical Journal, 111:1, 1-17, 1966.

22. Haas, R.C.G., Chairman, ad-hoc Committee on Low-Temperature Behavior of Flexible Pavements, "Low-Temperature Pavement Cracking in Canada, The Problem and Its Treatment," Proceedings, Canadian Good Roads Association, 1970.

23. Hendricks, S.B., and Jefferson, M.E., "Structure of Kaolin and Talc-Pyrophyllite Hydrates and Their Bearing on Water Sorption in Clays," American Mineralogist, 23:863-875, 1938.

24. Jackson, M.L., Willis, A.L., Pennington, R.P., "Standards for Quantitative X-Ray Diffraction Analysis of Soil Clays: I. Abridgement of Component Percentages Based on Weathering Sequence," Proceedings Soil Science Society of America, Vol. 12, pp. 400-406, 1947.

25. Jackson, M.L., et. al., "Weathering Sequence of Clay Size Minerals in Soils and Sediments I.," Journal of Physical and Colloid Chemistry, Vol. 52, pp. 1237-1260, 1948.

26. Jackson, A.E., "Equilibrium Statistical Mechanics," Prentice-Hall, p. 53, 1968.

27. Johnson, A.W., "Frost Action in Roads and Airfields," Highway Research Board, Special Report #1, 1953.

28. Johnson, A.W., and Scellberg, J.R., "Factors That Influence Field Compaction of Soils," Highway Research Board Bulletin No. 272, 1960.

29. Kaplar, C.W., "Phenomenon and Mechanism of Frost Heaving," Highway Research Board, Highway Research Record 304, 1970.

30. Lambe, T.W., "Structure of Compacted Clay," Proceedings, American Society of Civil Engineers, Vol. 84, SM2, p. 1655, 1958.

31. Lambe, T.W., "Soil Testing for Engineers," John Wiley & Sons, 1951.

32. Low, P.F., and Lovell, C.W., "The Factor of Moisture in Frost Action," Highway Research Record No. 225, Highway Research Board, Washington, D.C., 1959.

33. Low, P.F., Ravina, I., and White, J.L., "Changes in b-Dimension of Na-Montmorillonite with Interlayer Swelling," Nature, Vol. 226, London, pp. 445-446, 1970.

34. Majidzadeh, K., Kauffmann, E.M., and Chang, C.W., "Verification of Fracture Mechanics Concepts to Predict Cracking of Flexible Pavements," Report No. FHWA-RD-73-91, 1973.

35. McLeod, N.W., "Influence of Hardness of Asphalt Cement on Low Temperature Transverse Pavement Cracking," Canadian Good Roads Association, Montreal, 1970.

36. Morrison, G.L., "The Structure of the Interlayer Water in Montmorillonite," Ph.D. Dissertation, University of Oklahoma, Norman, Oklahoma, 1974.

37. "Non-Traffic Load Associated Cracking of Asphalt Pavements Symposium," Association of Asphalt Paving Technologists, Vol. 35, 1966.

38. Olsen, R.E., and Scott, J.D., Discussion of "Structure and Strength Characteristics of Compacted Clays," Journal of Soil Mechanics and Foundation Division, ASCE, October, 1959.

39. Pagen, C.A., and Khosla, V.K., "Effect of Freeze-Thaw on Rheological Parameters of a Compacted Clay," Transportation Research Record No. 497, Transportation Research Board, Washington, D.C., 1974.

40. Paris, C.P., and Erdogan, F.J., "A Critical Analysis of Crack Propagation Laws," Journal of Basic Engineering, Transactions, ASME, Series D, Vol. 85, p. 528, 1963.

41. Peck, A.J., "Theory of the Spanner Psychrometer, 1. The Thermocouple," Agricultural Meteorology, Vol. 5, pp. 433-447, 1968.

42. Richards, B.G., Murphy, H.W., Chan, C.Y.L., and Gordon, R., "Preliminary Observations on Soil Moisture and Dry Compaction in Pavement Design on the Darling Downs, Queensland ," Proceedings, Australian Road Research Board, Vol. 5, Part 5, pp. 116-146, 1970.

43. Russam, K., and Coleman, J.D., "The Effect of Climatic Factors on Subgrade Moisture Conditions," Geotechnique, Vol. II, pp. 1-22, 1961.

44. Russell, T., "Depth of Evaporation in the United States," Monthly Weather Review, Vol. 16, pp. 235-239, 1888.

45. Shackel, B., "Changes in Soil SUction in a Sand-Clay Subjected to Repeated Triaxial Loading," Highway Research Board, Highway Research Record No. 429, pp. 29-39, 1973.

46. Shahin, M.Y., and McCullough, B.F., "Prediction of Low-Temperature and Thermal Fatigue Cracking in Flexible Pavements," Research Report No. 123-14, Center for Highway Research, Austin, Texas, August, 1972.

47. Texas Agricultural Experiment Station, General Soils Map of Texas, published in cooperation with the Soil Conservation Service, 1973.

48. Tong, P., Pian, T.H.H., and Lasry, S.J.,"A hybrid-Element Approach to Crack Problems in Plane Elasticity," International Journal for Numerical Methods in Engineering, Vol. 7, p. 297, 1973.

49. Thornthwaite, C.W., "An Approach Toward a Rational Classification of Climate," The Geophysical Review, Vol. 38, No. 1, pp. 55-94, 1948.

50. Transeau, E.N., "Forest Centers of Eastern America," American Naturalist, Vol. 39, pp. 875-889, 1905.

51. White, A.W., and Pichler, E., "Water Sorption Characteristics of Clay Minerals," Illinois State Geological Survey, Circular #266, 1959.

52. Wood, F.W., "Salt Stabilization Research," Highway Research Record No. 294, Highway Research Board, Washington, D.C., pp. 42-45, 1969.

APPENDIX B

MOISTURE SUCTION MEASUREMENTS

There are various methods available to measure the soil moisture suction. The method used in this study combines the highest repeatability and accuracy for both field and laboratory testing. This method utilizes the thermocouple psychrometer as was shown in Fig. 13(p. 22). This device consists of a very fine thermocouple tip which is a welded bead of two dissimilar metals, copper and constantan. A junction of this type produces an emf (electro-motive force) on the order of several microvolts which is proportional to the temperature of the junction. By reading the induced emf the temperature of the junction may be inferred. The junction is protected by a ceramic tip which is porous to moisture in its vapor form only. This protects the junction from contaminants in the soil and moisture.

The moisture in the soil is utilized differently depending on the type of soil and the structure. As moisture is added to, or taken away from the soil, work must be done as compared to a common datum usually taken as a pool of pure water at the same elevation, which is typically given a value of zero. Thus, as the soil is dried out, or moisture removed, energy is expended. This gives the remaining moisture energy a negative value; and as more moisture is removed the soil moisture suction, which is a measure of this energy level, increases in magnitude. Thus, suction is a negative quantity as was shown in the Kelvin equation (1-4)(p.17).

As mentioned in the text, the soil moisture suction is related to the relative humidity of the soil. The thermocouple psychrometer determines this quantity in the following manner:

1. A zero reading is taken of the sample by recording the emf of the thermocouple. This is the dry bulb reading.

2. A current is passed through the thermocouple to produce cooling of the junction tip. This cooling produces a condensation of moisture on the tip when the temperature of the tip falls below the dew point temperature.
3. When the cooling current is switched off, the tip will stabilize at the dew point temperature prior to the evaporation of the moisture. This emf is recorded and is the wet bulb temperature.
4. The difference in the wet bulb and dry bulb temperature is proportional to the relative humidity which is in turn proportional to the soil moisture suction.

To avoid the mathematics involved what is done is to calibrate the thermocouple psychrometers in salt solution of a known osmotic suction. There are two components of suction in a soil. These are:

1. Osmotic or solute,
2. Matrix or capillary.

Total suction is equal to the sum of the osmotic and matrix suction. Since psychrometers measure only total suction they cannot differentiate between the two components and the reading will be the same for similar total suction values, independent of the magnitude of the separate components.

Suction values for solution concentrations are shown in Table B1. These solutions were used to construct the calibration curve shown in Fig. B1. This curve shows the linearity of the psychrometric technique over 40 bars (x100.= KN/M^2). With individual calibration the thermocouple psychrometers are accurate to within 5 percent of the actual reading.

A more advanced measuring technique is termed the dew point method. In this method, the thermocouple junction tip is maintained at the dew point temperature by an electronically regulated flow of cooling current. The measurements are obtained as follows:

TABLE B1

RELATIVE ACTIVITIES (Aw) AND WATER POTENTIALS
OF KCl SOLUTIONS AT 25°C

Molality* (m)	Aw	ℓnAw	Ψ_2 Bars (x100.=KN/M^2)	Ψ_2 Psi
.1	0.996668	-0.0033375	-4.59	-66.57
.3	.99025	-.0097978	-13.48	-195.51
.5	.98394	-.016190	-22.28	-323.15
.7	.97763	-.022624	-31.13	-451.51
1.0	.96818	-.032337	-44.49	-645.28
1.2	.9619	-.038845	-53.45	-775.24
1.4	.9556	-.045416	-62.49	-906.35
1.6	.9492	-.052136	-71.74	-1040.52

*Molality = Number of molecular weights/1.0 liter of H_2O at 25°C

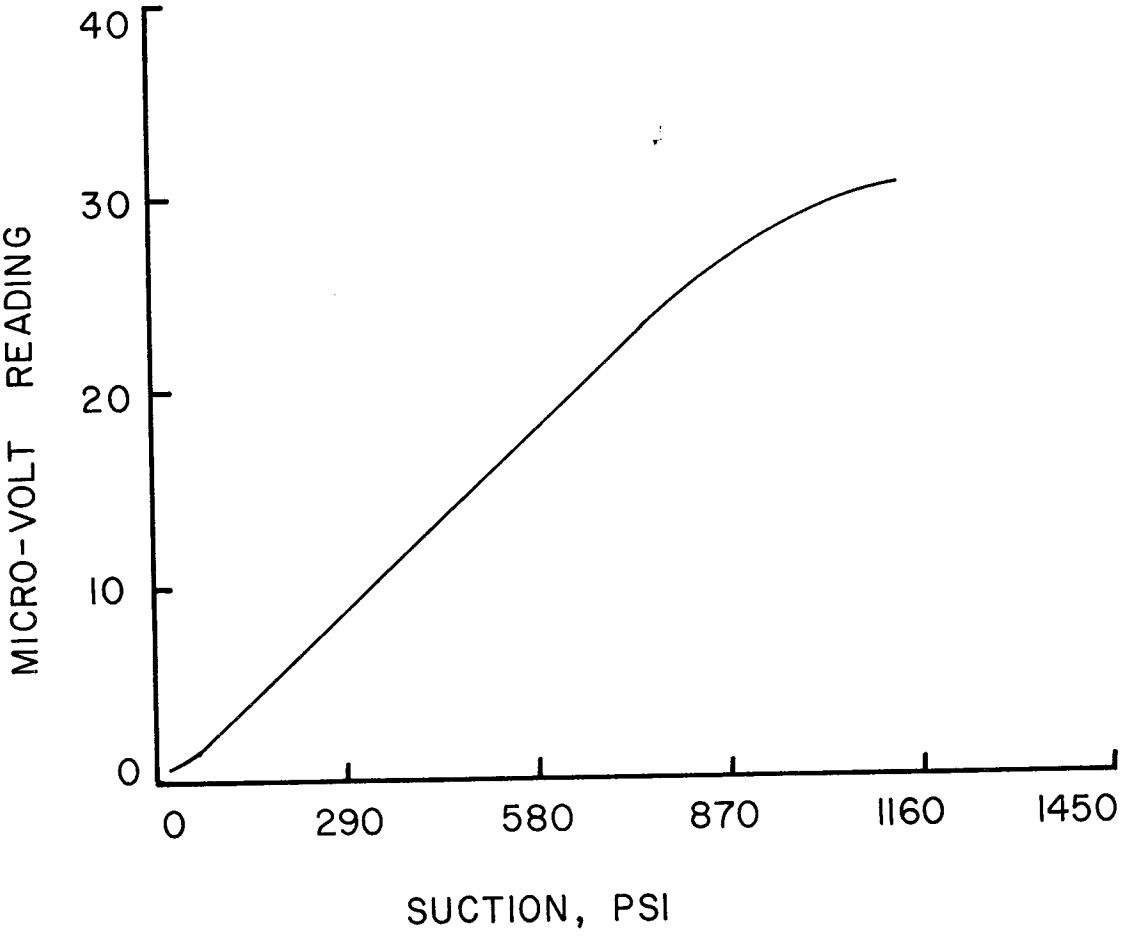

FIG. B1 - TYPICAL CALIBRATION CURVE FOR A PSYCHROMETER

1. A cooling coefficient, which is a function of the tip geometry determined when the psychrometer is constructed is set on the measurement box. This setting is adjusted to account for temperature calibration.
2. The microvoltmeter is zeroed and a cooling current passed through the tip to condense a bead of water.
3. The function switch is rotated to dew point. The cooling current then is maintained at a level such that heat is removed from the tip at the same rate it flows in from the surroundings. This process continues until the temperature of the tip is at the dew point where evaporation ceases. The device maintains the tip at the dew point temperature.

The current necessary to maintain the dew point temperature is proportional to the relative humidity. This method of operation produces a larger range of linear operation than the psychrometric technique and yields more reproducible results.

Both methods are highly susceptible to temperature change during measurements and to temperature gradients. The dew point technique allows temperature correction to be made electronically during the measurement while the psychrometric technique requires several correction calculations after the uncorrected measurement is taken. For these reasons the dew point technique was utilized extensively in this study.

APPENDIX C

CLAY FRACTIONATION AND DISPERSION PROCEDURES

General Information

Samples (<2 mm) will be washed with pH 5 buffer, H_2O_2 treated, Fe removed and fractionated into 2 mm-50 µm, 50-20 µm, 20-5 µm, 5-2 µm 2-0.2 <m, and <0.2 µm. Samples of greater than 5 µm diameter material will be stored dry in vials in file cases provided. Fractions 5 µm diameter will be stored in suspension at a pH between 5 and 7 free of salts. All samples will be clearly labeled with profile number, soil name (or number keyed to the name), depth, size fraction, date and initials of student with a pen or secure gummed label.

Removal of Divalent Cations and Binding Materials

1a. Destruction of carbonates and removal of exchangeable divalent cations. Weigh each sample (size dependent on texture) of 2 mm air dry soil to give 20 gm. per 250 ml. labeled centrifuge tube (10 gm. for clays and clay loams). A moist material may be used and allowance for moisture content must be made.

1b. In every case, moisture loss at 105-110°C is determined on a representative sample. A sample of about 5 g is weighed to the nearest mg in a tared 50 ml beaker, dried overnight at 105 to 110°C, cooled 20 min. in a desiccator and reweighed. This determination will permit calculation of particle size data at the conclusions of the fractionation.

2. Add 10 ml. of pH 5 N NaOAc buffer per gram of soil and bring soil into suspension by stirring with a policeman. Heat the sample in a near-boiling water bath for 10 minutes, set it on the bench and observe immediately for bubbles indicative of the presence of carbonates. A few bubbles may arise from HOAc and a

continuous flow of bubbles indicates carbonates. If carbonates are present, return the sample to the water bath and heat for 20 minutes longer.

3. Wash the sample by mixing with a policeman and centrifuging at about 2000 r.p.m. for 5 minutes or longer as necessary to make the supernatant clear. Repeat the heating in fresh buffer solutions as needed to destroy carbonates. If carbonates were completely dissolved or none were present police down the sides of the container and wash two additional times with pH 5 N NaOAc. Extra acid addition is required for efficient processing of highly calcareous samples.
4. Removal of organic matter and H_2O_2. First add 10 ml. of pH 5.0 N NaOAc and then slowly add 10 ml. of 30% H_2O_2 to the sample, which is in the form of a centrifuge cake. Cover the sample with a watchglass and allow it to stand overnight without heating. Surface soils may froth over and therefore, should be observed until foaming ceases. If it is not convenient to leave the sample overnight, proceed directly to the heating step but the probability of frothing over is greater. Add another 10 ml. of 30% H_2O_2 and place the bottle in a water bath controlled at about 100°C. Keep the container covered with a tightly fitting cover glass during H_2O_2 treatment when the sample is not being stirred. Watch the sample and stir vigorously or cool in a water bath as necessary to prevent frothing over. CAUTION: Avoid contact of 30% H_2O_2 with the skin or eyes. Never stopper a container containing even a small amount of H_2O_2.
5. When the reaction has subsided remove the sample from the water bath, police down the sides of the bottle with a minimum of water, centrifuge and discard the clear supernatant. If the sample contained a large amount of organic matter and is still dark or has an

organic "scum" on top, add 10 ml. of pH 5 N NaOAc and 10 ml. of 30% H_2O_2 and mix thoroughly as before. When the reaction subsides, place the sample in the water bath and observe until the reaction reaches its peak and subsides. Centrifuge and decant the clear supernatant.

6. Repeat step 5 above until the black or dark brown color is destroyed or until no further reduction of dark color is detected. NOTE: About 2 ml. of 30% H_2O_2 per gram of surface soil may be adequate.
7. The sample is then diluted to about 200 ml. with pH 5 N NaOAc and washed two times with the pH 5 solution.
8. The sample is then washed two times with absolute methanol or a mixture of 25% water and 75% acetone. Keep the volume to 2/3 of tube capacity as deflocculation may occur. NOTE: Flocculate as necessary by mixing 1 g. NaCl or 5 ml. saturated NaCl solution with the sample and warming in a hot water bath.
9. Free Fe Removal. (optional step) About 20 gm. of sample (10 gm. for red clays and clay loams) per tube is treated for iron removal at 80°C in a water bath. 80 ml. of 0.3 M Na citrate solution and 10 ml. of 1 M $NaHCO_3$ solution are added to a sample and mixed. The mixture is heated in the water bath for 5 to 10 minutes to bring the solution to 80°C.
10. Add 2 gm. of sodium dithionite powder with a spoon. Stir vigorously for a minute to mix the reagent thoroughly with the sample and prevent frothing over. A red sample should turn grey immediately. Mixing is continued at intervals of 2 or 3 minutes throughout the 15 minute treatment.
11. Centrifuge and decant the clear supernatant into a 1 l. volumetric flask.

12. The treatment (steps 9 and 10) is repeated two times. Use NaCl as needed to flocculate clay as described above. The decantate after each treatment is combined into the 1 l. volumteric flask and saved for analysis.
13. After the three treatments wash the sample 3 times with Na citrate and combine the washings in the same 1 l. volumetric flask. NOTE: Do not leave the sample in the citrate for a long period of time. The three treatments to remove iron oxides should be done consecutively, preferably without delay, to avoid oxidation of Fe. If it is necessary to stop during iron removal or citrate washing, leave the sample tightly stoppered as a centrifuge cake after decantation of the citrate solution.
14. Determine the Fe extracted by a KSCN or atomic absorption method.
15. Mix the sample in 100 ml. of pH 10.0 Na_2CO_3 solution for 5 minutes with a "milk-shake" type blendor.

Separation of Sand at the 50 µm lower Limit with a 300 Mesh Sieve

1. The well-mixed sample is allowed to stand for about 20 sec. to allow all sand to settle.
2. The supernatant is decanted onto a 50 µm sieve resting on a large funnel which drains into a 600 ml. beaker. A jet of pH 10.0 Na_2CO_3 is used to aid the passage of the solution through the sieve where necessary.
3. The sample remaining in the tube is mixed with another 100 ml. of pH 10.0 solution and is decanted onto one side of the sieve. This step is repeated until most of the sample has been transferred to the sieve. Using a fine jet wash bottle, wash the remaining particles of soil down to the bottom side of the tube held in a horizontal position, then wash all of the particles onto the sieve.

4. Wash the particles on the sieve by tilting it to one side and playing a stream of pH 10.0 solution back and forth across the sample until all of the particles have accumulated at the lower side of the sieve. Tilt the sieve in the opposite direction and repeat the process until the solution passing through is clear.
5. Wash the material on the sieve with acetone dispensed from a wash bottle to remove most of the water.
6. Dry the sample a few minutes until visibly dry on glazed paper on a 100°C plate or in the oven. Place the top and bottom on the sieve and shake it for about 5 minutes until no more particles pass through the sieve. Transfer the material from the bottom of the sieve into the beaker which contains the silt and clay.
7. Transfer all the sand particles from the sieve to a tared Al. dish and dry them for an hour in the oven at 110°C. Cool them in a desiccator and weigh them on the analytical balance.

Preliminary Separation of Silt and Clay

1. Pour the silt and clay suspension into a 250 ml. centrifuge tube. Fill the tube to the line 10 cm. above the inside bottom and centrifuge for 5 minutes at 2000 r.p.m. Pour the supernatant suspension into a 3 l. flask labeled <2 μm.
2. Repeat step C.1 until all of the suspension has been centrifuged. Do not mix the material in the bottom of the tube prior to these centrifugations.
3. Add pH 10.0 Na_2CO_3 solution to fill it to the 10 cm. mark. Mix the sample thoroughly with a policeman or by shaking. Centrifuge for 5 min. at 1500 r.p.m.
4. Fill the tube one-half full with pH 10.0 Na_2CO_3 and mix the sample 5 min. with the electric stirrer.

5. Add pH 10.0 Na_2CO_3 solution to the 10 cm. mark, mix the sample, and centrifuge the prescribed time and speed to make the 2 μm separation at 25°C. Decant the supernatant suspension into the flask labeled <2 μm.
6. Repeat step C.5 until the supernatant is almost clear. About 6 washings are commonly required.

Separation of Silt Fractions

1. The fine silt 5-2 μm is now removed by filling to the 10 cm. mark with pH 10.0 Na_2CO_3 solution, mixing the sample, and centrifuging the prescribed time for 5 μm separation and for 25°C suspension. Decant the supernatant into a beaker marked 5-2 μm.
2. Repeat the previous step until the supernatant solution is nearly clear. Allow the suspension in the beaker marked 5-2 μm to settle 3.5 hours per 5 cm. of suspension depth and decant the supernatant into the container marked <2 μm if it is not completely clear. If it is clear discard it.
3. Wash the 5-2 μm fraction two times with distilled water and store it in a solution of 50:50 ethanol and water. Obtain the 5-2 μm fraction weight as for the 2-0.2 μm fraction. (E.2).
4. The silt remaining in the tubes is transferred to a 500 ml. tallform beaker for separation at 20 μm by sedimentation. The silt is sedimented in pH 10.0 Na_2CO_3 solution for 2 min. 5 sec. per 5 cm. sedimentation depth. The supernatant is decanted into a beaker labeled 20-5 μm.
5. Step D.4 is repeated until the supernatant becomes almost clear. Then 2 more washings are made with distilled water to remove the sodium carbonate and the sample in the beaker is dried at 110°C, weighed and stored in a vial labeled 50-20 μm.

6. The 20-5 μm fraction is transferred to 250 ml. centrifuge tubes with distilled water, centrifuged for 5 minutes at 2000 r.p.m. and the clear supernatant is discarded. The sample is consolidated into one 250 ml. centrifuge tube, washed with distilled water two times and dried. The sample is transferred to a tared 100 ml. beaker with a minimum of water, dried overnight at 110°C, weighed, and transferred to a vial labeled 20-5 μm.

Fractionation of the Clay

1. The suspension of <2 μm material is transferred to 250 ml. centrifuge tubes if there is less than 2.4 l. volume. Where more than 2.4 l. volume is involved a preliminary supercentrifuge separation is desirable to reduce volume before fractionation of the clay at 0.2 μm. Where the volume is less than 2.4 l. the suspension is centrifuged for about 30 minutes at 2400 r.p.m. to fractionate at 0.2 μm depending on the average suspension temperature, centrifuge tube and centrifuge trunnion cup employed. The average of the suspension temperatures before and after centrifugation is employed. The supernatant is decanted into a 2 or 3 l. flask labeled <0.2 μm.
2. Fractionation at 0.2 μm as described in E.1 is repeated after combining the sample into one tube with pH 10.0 Na_2CO_3 solution as transferring solution. Removal of the 0.2 μm material is continued by repeated centrifuge washings with pH 10.0 Na_2CO_3 solution as described in E.1 until the supernatant is almost clear following centrifugation. The 2-0.2 μm clay in the centrifuge cake is washed two times with distilled water and the supernatant is combined with the 0.2 μm suspension. The 2-0.2 μm material is transferred to a volumetric 200 ml. flask with distilled water and made to volume so that the

final mixture is 50:50 ethanol and water. Mix the sample thoroughly and immediately pipette a 20 ml. aliquot into a tared 50 ml. beaker or weighing bottle to determine the amount of the fraction. The aliquot is dried on the 100°C plate and finally two hours in the oven at 110°C before final weighing.

3. Where the clay is fractionated only at 0.2 μm the clay in the beaker labeled 0.2 μm is flocculated by dropwise addition of 1N HCl until the clay flocculates or until pH 4.5 is reached. Do not permit the acidity to exceed pH 4.5. Heat the sample on the hot plate to accelerate flocculation. Allow the sample to stand overnight and siphon or decant off the clear supernatant. Wash the sample chloride free with methanol or ethanol. Transfer the <0.2 μm clay to a 200 ml. volumetric flask with water and ethanol to make the final volume exactly 200 ml. in a 50:50 mixture ethanol and water. Mix the sample thoroughly and immediately pipette a 20 ml. aliquot into a tared 50 ml. beaker or weighing bottle. Dry the aliquot and weigh as for the 2-0.2 μm sample (E.2).

Preparation of Clay by Magnesium Saturation for CEC, XRD, and DTA

350 mg sample of clay is transferred to a glass 50 ml. centrifuge tube.

1. Wash the sample once with pH 5 N NaOAc buffer.
2. Treat the centrifuge cake in 1 ml of pH 5.0 NaOAc with 2 ml H_2O_2. Heat in beaker of boiling water until reaction subsides. Avoid frothing over of sample. Wash sample 3 times with pH 5.0 NaOAc. Discard supernatant.
3. Wash sample 3 times with pH 7 MgOAc.
4. Wash sample 2 times with N $MgCl_2$.
5. Wash sample free of salts by using:
   a. Two washings or more with 70% alcohol and water mixture.

b. Wash with alcohol until free of chloride by $AgNO_3$ test. Do not add $AgNO_3$ to sample. Make the test in a 50 ml. beaker. Remove aliquot for x-ray analysis (1/7 of total sample).

6. Make a final wash of sample remaining in the tube with acetone and centrifuge a minimum to get rid of the supernatant. Allow the loose centrifuge cake to air-dry at room temperature.
7. Lightly grind 100 mg DTA sample with mortar and pestle to pass 70 mesh screen and transfer to weighing bottles provided. Label the bottle with your initials, sample name, and particle size.
8. Equilibrate the sample over saturated $Mg(NO_3)_2 \cdot 6\ H_2O$ solution in a vacuum desiccator for 4 days or longer. (about 56% RH).
9. Use the greatest possible precautions to keep a uniform procedure for loading and packing the sample in the sample holder.
10. The remaining 200 mg sample in the centrifuge tube will be used for CEC determination according to the procedure provided.

Saturation of Clays and Silts for X-ray Analysis

K and Mg saturation are done on duplicate 50 mg samples for x-ray analysis. Saturate with each cation separately.

1. Steps 1 through 5 are the same as above except the K salts are used for K saturation and the H_2O_2 treatment may be omitted.
2. Add glycerol to the sample as 10% solution in water as follows: 5-2μ 0.1 ml, 2-0.2μ 0.2 ml, <0.2μ 0.3 ml of the 10% solution. The sample should appear moist after water has evaporated.
3. Add sufficient water to make the sample volume to about 1 ml or more for montmorillonitic fine clays.
4. Mix thoroughly and decant the sample onto a labeled slide placed on a level surface.

5. Cover samples with a raised glass on large stoppers to prevent contamination or disturbance while they are drying. Sample should dry to a smooth uniform film.

Cation Exchange Determination

Objective: To determine the cation exchange capacity of two clay samples in duplicate by saturating the clay with Ca^{++}, determining the interstitial salt solution, and replacing the exchangeable Ca^{++} (plus the interstitial solution) with Mg^{++}.

About 100 mg of clay is required for each determination and the exact weight must be determined. Half the 200 mg sample (use a spatula) from the combined DTA and XRD saturation procedure and place each 100 mg sample in a separate tared 50 ml glass centrifuge tube. Dry the sample overnight or until constant weight at 100°C, cool it 20 minutes in a desiccator and weigh the sample in the tube quickly to enable calculating clay weight to the nearest 0.1 mg by difference.

Ca^{++} Saturation and Ca^{++}/Mg^{++} Exchange:

1. The Mg^{++} saturated clay is first dispersed by trituration with a rubber policeman in a few drops of pH 4.0 N NaOAc.
2. The samples are washed three times with 7.0 N NaOAc (20 ml per wash) and the clear supernatant is discarded. This step (2) adjusts the sample pH to 7.0.
3. The sample is then washed two times with N $CaCl_2$ (10 ml/wash).
4. The sample is then washed three times with 0.01 N $CaCl_2$ to complete saturation of the cation exchange sites with Ca^{++} (10 ml/wash). The sample is washed last with 0.01 N salt to permit weighing interstitial solution to determine its volume.
5. Wipe each tube clean and weigh the clay and interstitial solution in the tube. Calculate the solution volume by difference assuming a solution density of one g per ml.
6. The Ca-clay plus interstitial solution is washed five

times with N $MgCl_2$ and the clear supernatant is saved in 100 ml volumetric flask (10 ml/wash for 100 mg clay) for atomic absorption analysis and CaEC calculation.

7. The CaEC will aid in quantitative clay mineral estimation.
8. Formula for calculating CaEC:

$$\frac{\text{CaECmeq}}{100\text{g}} = \frac{[(\text{Ca } \mu\text{g/ml} \times 100 \text{ ml})_r - (\text{Ca } \mu\text{g})_i](10^{-3}\text{mg}/\mu\text{g})\ (10^5\text{mg})}{(\text{s mg})\qquad (20.0 \text{ mg/meq})\qquad (100)}$$

$( )_r$ = Ca^{++} replaced from sample

$( )_i$ = Interstitial Ca^{++} determined by multiplying volume determined gravimetrically (Step 5) times the concentration determined

s = sample weight.

APPENDIX D

COMPUTER MODEL TO PREDICT PAVEMENT THERMAL FATIGUE

The computer model presented in this Appendix uses actual climatic data to calculate temperatures and thermal stresses and the consequent cracking that occurs in the base course and asphalt concrete surface course. The input climatic data includes daily maximum and minimum air temperatures and wind speeds read from U. S. Weather Bureau magnetic tapes. Solar radiation data for the site of interest are also read in. A variety of material properties are also input, including thermal conductivity and viscoelastic properties of the asphalt concrete and strength and elastic properties of the base course.

A general flow chart of the program is included later in this Appendix. As indicated there, the program has three major parts as follows:

1. Input and calculation of expected crack spacings and the temperature drops required to cause the crack spacings.
2. Temperature calculations and calculations of viscoelastic moduli and stresses in the surface course.
3. Calculation of additional stresses due to contraction of base course, computation of damage done and accumulation of damage at each crack spacing.

As can be seen in the sample output in this Appendix, calculations of longitudinal crack spacing are also made in the program, but the results are probably inaccurate due to the fact that the stress conditions which

cause transverse cracking are not the same as those which act across the width of the pavement.

This Appendix includes a listing of the program, a flow chart, an input format, and a sample of the program output.

```
      C   COMPUTER PROGRAM TO PREDICT CRACK GROWTH AND TO PRINT
0001        IMPLICIT REAL*8 (A-H, O-Z)                                        00000020
0002        DIMENSION XX(3),TE(3,24),TI(3,24),XCRKL(5),DELTCL(5)              00000025
0003        DIMENSION TMAX(31),TMIN(31),AL(372),N(12), LKEY(31),              00000030
           &NDAY(31),KEY(31),AFAIL(31),XCRACK(31),DELTC(15),TITLE(10)         00000035
0004        DIMENSION DAY(31) ,V(31)                                          00000040
0005        DIMENSION TC(11), TH(11)                                          00000045
0006        DIMENSION HC(3)
0007        DATA HC/'COOLING ','HEATING ','ISOTHERM'/
0008        DIMENSION AFAILL(31)
0009        DIMENSION ITMX(3),ITMN(3),IV(3)
0010         COMMON /IN/ CN,CM,ALPHA,TM,TR,TA,F1,F2,F1,EE                     00000050
0011        INTEGER DAY                                                       00000055
0012        IKOUNT=1
      C*****  SET NTRACE = 1 TO TURN DEBUGGING OUTPUT ON  ****
0013        NTRACE=0
0014        NPAGE=100
      C  DATA THE DAYS IN THE MONTH                                           00000060
0015        N(1)=31                                                           00000065
0016        N(2)=28                                                           00000070
0017        N(3)=31                                                           00000075
0018        N(4)=30                                                           00000080
0019        N(5)=31                                                           00000085
0020        N(6)=30                                                           00000090
0021        N(7)=31                                                           00000095
0022         N(8)=31                                                          00000100
0023         N(9)=30                                                          00000105
0024        N(10)=31                                                          00000110
0025         N(11)=30                                                         00000115
0026        N(12)=31                                                          00000120
      C                                                                       00000125
0027        XYZTIM=14.0                                                       00000130
0028        XYZTEM=80.0                                                       00000135
0029        DO 241 I=1,31                                                     00000140
0030        XCRACK(I)=0.0                                                     00000145
0031        NDAY(I)=0                                                         00000150
0032        KEY(I)=0                                                          00000155
0033        AFAIL(I) = 0.0                                                    00000160
0034        AFAILL(I)=0.0D0
0035        LKEY(I) = 0                                                       00000165
0036      241 CONTINUE                                                        00000170
      C   READ THE SOLAR RADIATION CONSTANTS HERE                            00000175
0037        READ(5,115) SR1,SRM                                               00000180
0038      115 FORMAT(2F10.0)                                                  00000185
      C   SR1 IS THE JULY VALUE OF DAILY AVERAGE SOLAR RADIATION              00000190
      C   SRM IS THE YEARLY DAILY AVERAGE OF SOLAR RADIATION                  00000195
      C                                                                       00000200
0039        READ(5,100) LYEAR,X,W,S,AK,B                                      00000205
0040      100 FORMAT(I5,5F10.0)                                               00000210
      C   LYEAR IS THE LAST UEAR TO BE ANALYZED                               00000215
      C   W IS THE DENSITY OF THE SASPHALT                                    00000220
      C   S IS THE SPECIFIC HEAT                                              00000225
      C   AK IF THE THERMAL CONDUCTIVITY                                      00000230
      C   B IS THE ABSORPTIIVITY                                              00000235
      C                                                                       00000240
0041        READ(5,3) IYEAR,ISTAT                                             00000245
0042      3 FORMAT(I5,I6)                                                     00000250
      C   IYEAR IS THE FIRST YEAR TO BE ANALYZED                              00000255
```

```
C    ISTAT IS THE STATION BEING ANALYZED                                    00000260
0043       READ(5,998)EU,SIGMAT,ALPHAB,THCKB,E,XLWDTH,XKIC,THCKA
0044     998 FORMAT(8F10.0)                                                  00000270
C        ALPHAB IS THE FREEZE COEFFICIENT OF THE BASE COURSE                00000275
C        EU  IS THE UNFROZEN ELASTIC MODULUS
C        E  IS THE ELASTIC MODULUS WHEN FROZEN
C     SIGMAT IS THE TENSILE STRESS IN THE FROZEN BASE C OURSE               00000285
0045     102 READ(1,101,END=251 ) NSTAT,NYEAR                               00000290
0046     101 FORMAT(4X,I6,I3)
0047         BACKSPACE 1                                                    00000305
0048         IF(NSTAT.EQ.ISTAT.AND.NYEAR.EQ.IYEAR)GO TO 105
0049         READ(1,106)                                                    00000310
0050     106 FORMAT(30(/),11(31(/)))
0051         GO TO 102                                                      00000320
0052     105 CONTINUE                                                       00000325
C    TAPE IS POSITONED AT PROPER STATION AND YEAR                           00000365
0053         READ(1,710)                                                    00000370
0054     710 FORMAT(30(/),5(31(/)))
C    THIS POSITIONS THW ANALYZIS TO BEGIN JULY 1 OF THE YEAR                00000380
C    CALCULATE THE CRACK SPACINGS                                           00000385
                                                                            00000390
0055         WRITE(6,28) NYEAR, NSTAT
0056      28 FORMAT(////, 2X, 'BEGINNING YEAR IS 1', I3 // 2X, 'STATION IS',  00000395
          1        2X,I6)                                                   00000396
0057         XCRACK(1)=(10.**(((4.508E-12)*(SIGMAT**1.4578)*E)/             00000400
            &((6.8**2.1149)*(ALPHAB**1.1496))+8.151E-02))*0.5               00000405
0058         XCRACK(2)=2.0*XCRACK(1)                                        00000410
0059         XCRACK(3)=2.0*XCRACK(2)                                        00000415
0060         XCRACK(4)=2.0*XCRACK(3)                                        00000420
0061         XCRACK(5)=2.0*XCRACK(4)                                        00000425
0062         XCRACK(6)=2.0*XCRACK(5)                                        00000430
0063         XCRACK(7)=2.0*XCRACK(6)                                        00000435
0064         XCRACK(8)=2.0*XCRACK(7)                                        00000440
0065         XCRACK(9)=2.0*XCRACK(8)                                        00000445
0066         IF(XCRACK(1).LT.1.21)XCRACK(1)=1.21
0067         IF(XCRACK(2).LT.1.21)XCRACK(2)=1.21
C CALCULATE THE CRITICAL STRESS INTENSITY FACTORS HERE                      00000450
C                                                                           00000455
0068         WRITE(6,702) THCKB,EU,E,SIGMAT,ALPHAB,XKIC,X
0069     702 FORMAT(1H1,25X,'MATERIAL PROPERTIES',//,5X,'BASE COURSE',       00000465
            &/,8X,'THICKNESS',T30,F5.2,' INCHES',//,8X,'ELASTIC MODULUS',   00000470
            2T30,E9.4,' PSI UNFROZEN',/,8X,T30,E9.4,' PSI FROZEN',//,5X,'   00000475
            3TENSILE STRENGTH',2X,E9.4,' PSI',' FROZEN',//,8X,'FREEZE COEFFICIE00000480
            4NT',3X,F9.4,' STRAIN PER DEGREE CENTIGRADE',//,8X,'CRITICAL STRESS00000485
            5 INTENSITY FACTOR',5X,F8.3,////,5X,' ASPHALT CONCRETE',' THICKNESS'00000490
            6,F5.2,'INCHES')                                                00000495
C  READ THE VISCOELASTIC DATA IN HERE.                                      00000500
C                                                                           00000505
0070         READ(5,11) IX,UNU                                              00000510
0071      11 FORMAT(I5,5X,F10.0)                                            00000515
C    IX=0,PLANE STRESS                                                      00000520
C    IX=1,PLANE STRAIN                                                      00000525
C    UNU=POISSON'S RATIO                                                    00000530
0072         READ(5,12) TITLE                                               00000535
0073      12 FORMAT(10A8)                                                   00000540
C  IF INDEX = 1, READ IN POWERS OF RELAXATION MODULI, D1 AND DF,
C  WHERE E1 = 10 ** D1 AND EE = 10 ** DF.
C
C  IF INDEX IS 0 READ IN POWERS OF COMPLIANCES, D1 AND DF, WHERE
```

```
C  E1 = APPROX. 10 ** (=D1) AND EE = 10 ** (=DF).
0074        READ(5,13) INDEX,D1,DF                                          00000545
0075     13 FORMAT(I5,5X,2F10.0  )                                          00000550
0076        WRITE(6,566)INDEX,D1,DF
0077    566 FORMAT('0','INDEX = ',I2,' D1 = ',G13.4,' DF = ',G13.4)
0078        READ(5,14) CN,CM,ALPHA,TM,TR,TA,E1,E2                           00000555
0079     14 FORMAT(8F10.0)                                                  00000560
0080        WRITE(6,567)TA
0081    567 FORMAT('0REFERENCE TEMPERATURE FOR AT CURVE: ',F5.1)
0082        DF=10.D0**DF                                                    00000565
0083        D1=10.D0**D1                                                    00000570
0084        WRITE(6,15) TITLE                                               00000575
0085     15 FORMAT('1',10X,'* * * ',10A8,' * * * ')                         00000580
0086        IF(INDEX.EQ.1) GO TO 16                                         00000585
0087        PI=3.1415926                                                    00000590
0088        PIN=PI*CN                                                       00000595
0089        E1=1.D0/D1*(DSIN(PIN)/PIN)                                      00000600
0090        IF(DF.EQ.1.0) GO TO 17                                          00000605
0091        EF=1.D0/DF                                                      00000610
0092        GO TO 18                                                        00000615
0093     17 EE=D1                                                           00000620
0094        GO TO 18                                                        00000625
0095     16 E1=D1                                                           00000630
0096        EE=DF                                                           00000635
0097     18 CONTINUE                                                        00000640
0098        WRITE(6,19) TM                                                  00000645
0099     19 FORMAT('0',5X,'REFERENCE TEMP. FOR MASTER CURVE.',T48,G13.4)    00000650
0100        WRITE(6,24) TR                                                  00000655
0101     24 FORMAT('0',5X,'REFERENCE TEMP. FOR ZERO STRESS STATE',T48,G13.4/) 00000660
0102        WRITE(6,25) ALPHA                                               00000665
0103     25 FORMAT('0',5X,'COEFF. OF THERMAL EXPANSION',T48,G13.4,//)       00000670
0104        WRITE(6,26) E1,EE,CN,CM                                         00000675
0105     26 FORMAT('0',5X,'*** E1 = ',G13.4,2X,'*** EE = ',G13.4,/,5X,      00000680
          1       '*** CN = ',G13.4,2X,'CM= ',G13.4,/)                      00000685
0106        WRITE(6,27)                                                     00000690
0107     27 FORMAT('0',2X,'CURVE FOR EFFECTIVE MODULUS RATIO')              00000695
0108        CALL CURVE(TH,TC)                                               00000700
C    CALCULATE THE TEMPERATURE RANGES THAT PRODUCE CRACKS                   00000705
0109        DO 200 I=1,8                                                    00000710
0110         M1=10-I                                                        00000715
0111        DELTC(I)=(4.508D-12*SIGMAT**1.4578D0*E/(ALPHAB**1.1496D0*(DLOG10
           &(2.D0*XCRACK(M1))-8.151D-2)))**(1.D0/2.1149D0)
0112    200 CONTINUE                                                        00000735
0113        DELTC(9)=6.8
0114        WRITE(6,703)                                                    00000740
0115    703 FORMAT(1H1,20X,'CALCULATED CRACK SPACINGS',//, 5X,              00000745
           &'TRANSVERSE CRACK SPACING IN BASE COURSE')                      00000750
0116        WRITE(6,704)(XCRACK(10-IKB),DELTC(IKB),IKB=1,9)
0117    704 FORMAT(//,5X,F8.3,2X,'FEET WILL BE PRODUCED BY A TEMPERATURE OF', 00000760
           &2X,'=',F6.3,1X,'CENTIGRADE')
C    CALCULATE LONGITUCILAL CRACKING OCCURRENCE                             00000770
0118        DO 2000 IB=1,4                                                  00000775
0119        XCRKL(IB)=XLWDTH/(2.**(IB-1))
0120        DELTCL(IB)=(4.508D-12*SIGMAT**1.4578D0*E/(ALPHAB**1.1496D0*(DLOG10
           &(2*XCRKL(IB))-8.151D-2)))**(1.D0/2.1149D0)
0121   2000 CONTINUE                                                        00000790
0122        WRITE(6,705)                                                    00000810
0123    705 FORMAT(//,5X,'LONGITUDINAL CRACK SPACING WILL OCCUR AT THE MID POI00000815
```

```
                &NT OF THE CROSS SECTION',/,20X,'OF THE PAVEMENT THAT WAS PAVED IN 00000820
                & ONE  OPERATION,'/,20X,'CONSTRUCTION JOINTS ARE CRACKS.')          00000825
0124              WRITE(6,706)(XCRKL(IJB),DELTCL(IJB),IJB=1,4)                      00000830
0125          706 FORMAT(//,5X,F8.3,2X,'FEET WILL BE PRODUCED BY A TEMPERATURE OF', 00000835
                &2X,'=',F6.3,1X,'CENTIGRADE')
              C   CALCULATE THE DAILY SOLAR RADIATION VALUES                       00000845
              C                                                                    00000850
                                                                                   00000855
0126              DO 109 IJK=1,360                                                 00000860
0127              F=IJK/57.2958                                                    00000865
0128              AL(IJK) = SRM + (SR1-SRM) * DCOS( F )/0.966                      00000870
0129          109 CONTINUE                                                         00000875
0130              DO 108 IJK=361,366                                               00000880
0131              AL(IJK)=AL(360)                                                  00000885
0132          108 CONTINUE                                                         00000890
0133          138 CONTINUE                                                         00000895
              C   BEGIN A YEARS CALCULATIONS                                       00000900
0134              DO 1 LJ=1,12
0135              DO 3333 I=1,31
0136              READ(1,999)NTAPE,NSTAT,NYEAR,DAY(I),ITMX,ITMN,IV
0137          999 FORMAT(I4,I6,I3,I4,2X,2(3A1),53X,3A1,19X)
              C
              C*****  CONV IS AN ASSEMBLY LANGUAGE SUBROUTINE THAT CONVERTS THE
              C*****  ZONED DECIMAL TAPE FIELDS TO INTEGERS FOR FORTRAN        ******
              C
0138              CALL CONV(ITMX,ITMX2)
0139              TMAX(I)=ITMX2
0140              CALL CONV(ITMN,ITMN2)
0141              TMIN(I)=ITMN2
0142              CALL CONV(IV,IV2)
0143              V(I)=IV2
0144          3333 CONTINUE
0145              LL=LJ+6
0146              IF(LL.GT.12)LL=LL-12
0147              JYR=N(LL)
                                                                                   00000925
              C       CONDUCT LEAP YEAR CHECK HERE                                 00000930
0148              X1=(980.-NYEAR)/4.                                               00000935
0149              M=(980-NYEAR)/4                                                  00000940
0150              IF((M-X).EQ.0.) N(2)=29                                          00000945
0151              IF((M-X1).EQ.0.) MAXDAY=366                                      00000950
0152              IF((M-X1).LT.0.) MAXDAY=365                                      00000955
0153              DO 2 NI=1,JYR
0154              IF(NTRACE.EQ.1)
                 XWRITE(6,557)LJ,NI,DAY(NI),TMAX(NI),TMIN(NI),V(NI)
0155          557 FORMAT('0&&&&& RECORD ',I2,'/',I2,' : DATE = ',I4,' TMAX = ',
                1   F6.1,' TMIN = ',F6.1,' V = ',F6.1)
0156              TAVG=0.5*(TMIN(NI)+TMAX(NI))
0157              TRANG=TMAX(NI)-TMIN(NI)
                                                                                   00000970
0158              AH=1.3+0.62*(V(NI)/24.)**0.75                                    00000975
0159              H=AH/AK                                                          00000980
0160              AC=AK/(S*W)                                                      00000985
0161              C=(0.131/AC)**0.5                                                00000990
0162              R=0.67*B*3.69*AL(IKOUNT)/(24.*AH)                                00000995
              C  SET UP TO CALCULATE TEMPERATURE AT TOP,MIDDLE AND BOTTOM OF AC.   00001000
0163              DO 10 ITHCK=1,3                                                  00001005
0164              XX(ITHCK)=X/ITHCK                                                00001010
0165              IF(ITHCK.EQ.3)XX(3)=0.0                                          00001015
              C  X(1)=BOTTOM TEMPERATURE                                           00001020
              C  X(2)= MIDDLE TEMPERATURE
```

```
                C  X(3)= TOP TEMPERATURE.                                                00001025
                C   CALCULATE THE TEMPERATURES FOR A COMPLETE DAY                       00001030
                                                                                         00001035
0166                   Z2=(-XX(ITHCK))*C/12.0                                            00001040
0167                   Z3 = DEXP(Z2) * H/(( H+C)**2. + C**2.) ** 0.5                     00001045
0168                   DO 10 J=2,25                                                      00001050
0169                   TIM=J                                                             00001055
0170                   IF(J.GT.9) GO TO 31                                               00001060
0171                   Z4=6.8176*(.0576*TIM+0.144*Z2-0.288)                              00001065
0172                   GO TO 35                                                          00001070
0173                31 IF(J.GT.14) GO TO 32                                              00001075
0174                   Z4=-14.7534*(0.02057*TIM+0.075*Z2-0.288)                          00001080
0175                   GO TO 35                                                          00001085
0176                32 Z4=-6.94274*(0.02057*TIM+0.12*Z2-0.288)                           00001090
0177                35 Z5 = DSIN(Z4)                                                     00001095
0178                   IF(Z5) 21,22,22
0179                21 TM=TAVG+0.5*R
0180                   TV=.5*TRANG                                                       00001110
0181                   GO TO 23
0182                22 TV=.5*TRANG+3.*R
0183                   TM=TAVG+R                                                         00001125
0184                23 TEMP=TM+TV*Z3*Z5                                                  00001130
0185                   IF(J.GT.19) TIM=TIM-24                                            00001135
0186                   ITM = TIM + 5                                                     00001140
0187                   TE(ITHCK,ITM)=TEMP                                                00001145
0188                   TI(ITHCK,ITM)=ITM                                                 00001150
0189                10 CONTINUE
0190                   IF(NTRACE.EQ.1)
                      XWRITE(6,562)
0191               562 FORMAT('0***** TEMPERATURES IN EACH THICKNESS  *****'/)
0192                   IF(NTRACE.EQ.1)
                      XWRITE(6,561)((TE(I,J),J=1,24),I=1,3)
0193               561 FORMAT(' ',24F5.1)
0194                   IF(NTRACE.EQ.1)
                      XWRITE(6,563)
0195               563 FORMAT('0*****  TIMES FOR THICKNESS TEMPERATURES  *****'/)
0196                   IF(NTRACE.EQ.1)
                      XWRITE(6,564)((TI(I,J),J=1,24),I=1,3)
0197               564 FORMAT(' ',24F5.1/)                                               00001155
                C   ONE DAYS CALCULATIONS COMPLETE                                     00001160
0198                20 IKOUNT=IKOUNT+1                                                  00001165
0199                   IF(IKOUNT.EQ.MAXDAY+184) IKOUNT=1                                 00001170
0200                   DO 110 L1=1,3                                                     00001175
0201                   DO 110 L=2,23                                                     00001180
0202                   IF(TE(L1,L).LE.TE(L1,L-1).AND.TE(L1,L).LE.TE(L1,L+1)) GO TO 112   00001185
0203                   GO TO 118                                                         00001190
0204               112 CONTINUE                                                          00001195
                C    YOU GET HERE WITH MINIMUM TEMPERATURES
0205                   IF(L1.EQ.1)TEMP1=TE(1,L)
0206                   IF(L1.EQ.2)TEMP2=TE(2,L)
0207                   IF(L1.EQ.3)TEMP3=TE(3,L)                                          00001215
                C  TIME FOR MINIMUM TEMPERATURE
0208                   IF(L1.EQ.1)TIM1=TI(1,L)
0209                   IF(L1.EQ.2)TIM2=TI(2,L)
0210                   IF(L1.EQ.3)TIM3=TI(3,L)                                           00001235
                C  NOW YOU NEED TO FIND THE MAXIMUM TEMPERATURE                         00001240
0211               118 CONTINUE                                                          00001245
0212                   IF(TE(L1,L).GE.TE(L1,L-1).AND.TE(L1,L).GE.TE(L1,L+1)) GO TO 113   00001250
0213                   GO TO 110
```

```
0214          113 CONTINUE                                                          00001255
0215              IF(L1.EQ.1)TEMP4=TE(L1,L)
0216              IF(L1.EQ.2)TEMP5=TE(L1,L)
0217              IF(L1.EQ.3)TEMP6=TE(L1,L)
0218              IF(L1.EQ.1)TEMP7=TE(L1,L+1)
0219              IF(L1.EQ.2)TEMP8=TE(L1,L+1)
0220              IF(L1.EQ.3)TEMP9=TE(L1,L+1)
                C     TIME FOR MAXIMUM TEMPERATURE
0221              IF(L1.EQ.1)TIM4=TI(L1,L)
0222              IF(L1.EQ.2)TIM5=TI(L1,L)
0223              IF(L1.EQ.3)TIM6=TI(L1,L)
0224          110 CONTINUE                                                          00001310
0225              IF(NTRACE.EQ.1)
                 XWRITE(6,559)TIM1,TIM2,TIM3
0226          559 FORMAT(' ** TIM1 = ',F6.2,' ** TIM2 = ',F6.2,' ** TIM3 = ',F6.2)
0227              IF(NTRACE.EQ.1)
                 XWRITE(6,560)TIM4,TIM5,TIM6
0228          560 FORMAT(' ** TIM4 = ',F6.2,' ** TIM5 = ',F6.2,' ** TIM6 = ',F6.2)
                C  IF THE MAXIMUM TEMP IS ABOVE 75 F, FIND THE TIME AT WHICH 75 OCCURS  00001315
                C  DEL IS THE TEMPERATURE DROP PER HOUR                               00001335
0229              DEL1=(TEMP4-TEMP1)/(-TIM4+TIM1)
0230              DEL2=(TEMP5-TEMP2)/(-TIM5+TIM2)
0231              DEL3=(TEMP6-TEMP3)/(-TIM6+TIM3)
0232              IF(NTRACE.EQ.1)
                 XWRITE(6,558)DEL1,DEL2,DEL3
0233          558 FORMAT(' ** DEL1 = ',F6.2,' ** DEL2 = ',F6.2,' ** DEL3 = ',F6.2)
0234              IF(TEMP4.GT.TR) TIM4=TIM4+(TEMP4-TR)/DEL1                         00001340
0235              IF(TEMP5.GT.TR) TIM5=TIM5+(TEMP5-TR)/DEL2                         00001345
0236              IF(TEMP6.GT.TR) TIM6=TIM6+(TEMP6-TR)/DEL3                         00001350
                C  NOW WE HAVE TIME AND TEMPERATURE DATA NEEDED                       00001355
                C  CALCULATE THE AVERAGE VALUES IF THEY WILL BE USED.                 00001360
                C      IF(KEYAVG.EQ.1) GO TO 114                                      00001365
                C 114 CONTINUE                                                        00001370
                C  KEYAVG=1.. USE AVERAGE VALUES                                      00001375
0237              TMEN=(1./3.)*(TEMP1+TEMP2+TEMP3)                                  00001380
0238              TMEX=(1./3.)*(TEMP4+TEMP5+TEMP6)                                  00001385
0239              IF(TMEX.GT.TR) TMEX=TR                                            00001390
0240              TIMMIN=(TIM1+TIM2+TIM3)/3.0                                       00001395
0241              TIMMAX=(TIM4+TIM5+TIM6)/3.                                        00001400
0242              PERIOD=24.0-XYZTIM+TIMMIN                                         00001405
0243              XYZTIM=TIMMAX                                                     00001410
                C  VISCOELASTIC MODULUS AND STRESS CALCULATIONS BEGIN HERE            00001415
0244              DELT=TMEN-TR                                                      00001425
0245              XYZTEM=TMEX                                                       00001430
                C  TMIN IS THE MINIMUM TEMPERATURE                                    00001435
0246              IF(NTRACE.EQ.1)
                 XWRITE(6,556)PERIOD,TMEN,TMEX,TIMMIN,TIMMAX
0247          556 FORMAT(' ** PERIOD = ',F6.1,' ** TMEN = ',F6.1,' ** TMEX = ',
                1   F6.2,' ** TIMMIN = ',F6.1,' ** TIMMAX = ',F6.1)
0248              IF(NTRACE.EQ.1)
                 XWRITE(6,554)
0249          554 FORMAT('0',4X,'PROCESS',5X,'TEMP.',2X,'(AT)',2X,'NORMALIZED',4X,
                1   'MODULUS',5X,'SECANT',6X,'EFFECTIVE',4X,'STRAIN',6X,'STRESS',
                2   6X,'TIME',8X,              /,' ',22X,'LOG.',1X,'TEMP. CHANGE',
                3   4X,'RATIO',6X,'MODULUS',5X,'MODULUS')
0250          1000 CONTINUE                                                         00001445
0251              DT=DELT
0252              TIME=PERIOD*3600.
```

```
0253              TTN=TIME**(-CN)
0254              T=TR+DT                                                    00001480
0255              AT=((TM-TA)/(T-TA))**CM
0256              ATN=AT**CN                                                 00001495
0257              DTN=DT/(TR-TA)                                             00001500
0258              DTR=DABS(DTN*10.0)                                         00001505
0259              NN=IDINT(DTR)                                              00001510
0260              DIF=DTR-NN                                                 00001515
0261              NG = NN + 1                                                00001520
0262              IF(NG.GT.11)STOP 1
0263              IF(DELT) 90,29,30                                          00001525
0264           90 RATIO = (TC(NG+1) - TC(NG)) * DIF + TC(NG)                 00001530
0265              J=1                                                        00001535
0266              GO TO 120                                                  00001540
0267           29 RATIO=1.D0                                                 00001545
0268              J=3                                                        00001550
0269              GO TO 120                                                  00001555
0270           30 RATIO = (TH(NG+1) - TH(NG)) * DIF + TH(NG)                 00001560
0271              J=2                                                        00001565
0272          120 CONTINUE                                                   00001570
0273              ESS=ATN*E1*TTN/(1.D0-CN)                                   00001575
0274              EEF=EE+RATIO*(ESS-EE)                                      00001580
0275              STRAIN=ALPHA*DT                                            00001585
0276              GI=DFLOAT(IX)/(1.0-UNU)                                    00001590
0277              IF(IX.EQ.0) GI=1.0                                         00001595
0278              STRESS=GI*STRAIN*EEF
                C    THE PRINT STATEMENTS FOR THE STRESS AND MODULI VALUES HAVE BEEN LEFT00001600
0279              IF(NTRACE.EQ.1)
                   XWRITE(6,555)I,HC(J),T,AT1,DTN,RATIO,ESS,EEF,STRAIN,STRESS,HOUR
0280           555 FORMAT('0',I3,A8,3F8.2,2X,F12.2,2X,4G12.4,F8.2,2(1X,G11.4))
0281          1001 CONTINUE
0282              Q=EEF                                                      00001610
0283              IF(TEMP1.GE.32.0) GO TO 111                                00001615
0284              DELT=(32.0-TEMP1)*5./9.
0285               IF(DELT.GT.6.8) DELT=6.8                                  00001625
                C    THIS IS DELTA TEMP.                                    00001630
                C    CALCULATE THE CRACK REGION                             00001635
0286              IF(DELT.LT.DELTC(1)) NCRACK=0                              00001640
0287              IF(DELT.GE.DELTC(1).AND.DELT.LT.DELTC(2)) NCRACK =1        00001645
0288              IF(DELT.GE.DELTC(2).AND.DELT.LT.DELTC(3)) NCRACK =2        00001650
0289              IF(DELT.GE.DELTC(3).AND.DELT.LT.DELTC(4)) NCRACK =3        00001655
0290              IF(DELT.GE.DELTC(4).AND.DELT.LT.DELTC(5)) NCRACK =4        00001660
0291              IF(DELT.GE.DELTC(5).AND.DELT.LT.DELTC(6)) NCRACK =5        00001665
0292              IF(DELT.GE.DELTC(6).AND.DELT.LT.DELTC(7)) NCRACK =6        00001670
0293              IF(DELT.GE.DELTC(7).AND.DELT.LT.DELTC(8)) NCRACK =7        00001675
0294              IF(DELT.GT.6.75) NCRACK=8                                  00001680
0295              IF(NCRACK.EQ.0) GO TO 712                                  00001685
0296              XDIV=NCRACK*1.000                                          00001690
                C    CALCULATE THE STRESS LEVEL IN TH BASE                  00001695
0297              SIGMA=(5.616D-03)*E*(ALPHAB**.7886)*(DELT**1.4506)*        00001700
                 &(-1.868+22.8998*DLOG10(XCRACK(9-NCRACK)))**.68596          00001705
0298              IF(NCRACK.LE.2) SIGMA=SIGMA/XDIV                           00001710
0299              IF(NCRACK.GT.2) SIGMA=0.75*SIGMA/XDIV                      00001715
                C    THIS PRORATES THE STRESS, EMPHASISING THE FACT THAT THE 00001720
                C    DEFORMATION IS THE CONTROLLING FACTOR IN               00001725
                C    PROPAGATING THE CRACK                                  00001730
                C    THE PROCEDURE IS TO NOTE THAT THE SAME STRESS WILL     00001735
                C       PRODUCE SMALLER DEFORMATIONS FOR SMALLER CRACK      00001740
```

```
                C   SPACINGS THAN THE ORIGINAL VALUES                                    00001745
                                                                                        00001750
0300                  GO TO 714                                                         00001755
0301              712 CONTINUE                                                          00001760
0302              713 SIGMA=1.00                                                        00001765
0303              714 CONTINUE                                                          00001770
                C   CALCULATE THE DAMAGE THIS STRESS CYCLE WILL DO                    00001775
0304                  L1=NCRACK+1                                                       00001780
                C   DAMAGE EQUATION                                                   00001785
                C   THIS SECTION CALCULATES THE CRACK DAMAGE PERCENTAGES              00001790
                C   REGRESSION EQUATION FOR CRACK DAMAGE FOR EACH STRESS IN THE BASE COU00001795
0305                  XNF=1.0/((10.0**(1.5176+4.4127D-06*(Q)))*SIGMA**(-0.5035-1.0935D-000001800
                     &6*(Q)))                                                           00001805
0306                  DO 230 L2=1,L1                                                    00001810
0307                  IOUT=10-L2                                                        00001815
0308                  AFAIL(L2)=AFAIL(L2)+XNF                                           00001820
0309                  IF(KEY(L2)) 229,229,230                                           00001825
0310              229 IF(AFAIL(L2).GT. 1.0 )  PRINT 701,XCRACK(IOUT),                   00001830
                     &DAY(NI),NYEAR
0311              701 FORMAT('0*****  AN EXISTING TRANSVERSE CRACK SPACING OF ',F8.2,
                    1' FEET HAS CRACKED AT MID SPACING ON ',I5,'/1',I3,' *****'/)
0312                  IF(AFAIL(L2).GT.1.)NPAGE=NPAGE+3
0313                  IF(AFAIL(L2).GT. 1.0 )  KEY(L2)=1                                 00001835
0314              230 CONTINUE                                                          00001855
0315                  DELTL=DELT                                                        00001860
0316                  IF(DELTL.LT.DELTCL(1)) LCRACK=0                                   00001865
0317                  IF(DELTL.GE.DELTCL(1).AND.DELTL.LT.DELTCL(2))LCRACK=1             00001870
0318                  IF(DELTL.GE.DELTCL(2).AND.DELTL.LT.DELTCL(3))LCRACK=2             00001875
0319                  IF(DELTL.GE.DELTCL(3).AND.DELTL.LT.DELTCL(4))LCRACK=3             00001880
0320                  IF(DELTL.GT.6.79) LCRACK=4                                        00001885
0321                  IF(LCRACK.EQ.0) GO TO 2020                                        00001890
0322                  XLDIV=LCRACK*1.0                                                  00001895
0323                  SIGMAL=(5.616D-03)*E*(ALPHAB**0.7886)*DELTL**1.4506 *             00001900
                     &(-1.868+22.8998*DLOG10(XCRKL(5-LCRACK)))**.68596                  00001905
0324                  IF(LCRACK.LE.2) SIGMAL=SIGMAL/XLDIV                               00001910
0325                  IF(LCRACK.GT.2) SIGMAL=0.75*SIGMAL/XLDIV                          00001915
0326                  GO TO 2021                                                        00001920
0327              2020  SIGMAL=1.0                                                    00001925
0328              2021 CONTINUE                                                         00001930
0329                  LL1=LCRACK+1                                                      00001935
0330                  XLNF=1.0/((10.0**(1.5176+4.4127D-06*(Q)))*SIGMAL**                00001940
                     &(-0.5035-1.0932D-06*(Q)))                                         00001945
0331                  DO 2023 LL2=1,LL1                                                 00001950
0332                  AFAILL(LL2)=AFAILL(LL2)+XLNF
0333                  IF(LKEY(LL2))2029,2029,2023                                       00001965
0334              2029 IF(AFAILL(LL2).GT.1.0) PRINT 7010,XCRKL(LL2),DAY(NI),NYEAR
0335              7010 FORMAT('0***** AN EXISTING LONGITUDINAL CRACK SPACING OF ',
                    1F8.3,' HAS CRACKED AT MID-SPAN ON ',I5,'/1',I3,' *****'/)
0336                  IF(AFAILL(LL2).GT.1.)NPAGE=NPAGE+3
0337                  IF(AFAILL(LL2).GT.1.0) LKEY(LL2)=1
0338              2023 CONTINUE                                                         00001995
0339                  IF(NPAGE.LT.55)GO TO 5555
0340                  WRITE(6,568)
0341               568 FORMAT('1',9X,13('*'),' TRANSVERSE CRACKING ',29('*'),5X,
                    1'** LONGITUDINAL CRACKING **')
0342                  WRITE(6,569)(XCRACK(10-I),I=1,9),(XCRKL(I),I=1,4)
0343               569 FORMAT(' ',2X,'DATE',3X,F5.1,'FT',8(1X,F4.1,'FT'),4X,
                    1       4(1X,F4.1,'FT')/)
0344                  NPAGE=0
```

```
0345          5555 CONTINUE
0346               NMON=DAY(NI)/100
0347               NDAYY=DAY(NI)-100*NMON
0348               NYR=NYEAR-900
0349               WRITE(6,570)NMON,NDAYY,NYR,(AFAIL(I),I=1,9),(AFAILL(I),I=1,4)
0350           570 FORMAT(' ',2(I2,'/'),I2,1X,9(1X,F6.4),4X,4(1X,F6.4))
0351               NPAGE=NPAGE+1                                                  00002000
0352           111 CONTINUE                                                       00002005
0353             2 CONTINUE                                                       00002010
0354             1 CONTINUE                                                       00002015
0355               IF(NYEAR.EQ.LYEAR) GO TO 250                                   00002020
0356               GO TO 138                                                      00002025
0357           250 CONTINUE                                                       00002030
0358           235 CONTINUE                                                       00002035
0359           251 CONTINUE                                                       00002040
0360               REWIND 1                                                       00002045
0361               STOP                                                           00002050
0362               END
```

```
0001                  SUBROUTINE CURVE(TH,TC)                                   00002055
0002                  IMPLICIT REAL*8(A-H,O-Z)                                  00002060
0003                  DIMENSION TH(11),TC(11)                                   00002065
0004                  COMMON /IN/ CN,CM,ALPHA,TM,TR,TA,F1,F2,E1,EE              00002070
0005                  DIMENSION HC(2)                                           00002075
0006                  DATA HC/'COOLING','HEATING'/                              00002080
0007                  COMMON /GT/GAB1                                           00002085
0008                  DIMENSION F(50)                                           00002090
0009                  COMMON HH(11),ZZ                                          00002095
0010                  COMMON /KK/I                                              00002100
0011               100 CONTINUE                                                 00002105
0012                  INT=40                                                    00002110
0013                  A=CM/(CM+1.0)+CN-2.0                                      00002115
0014                  B=-CN                                                     00002120
0015                  DM=(1.0-CN)/(CM+1.0)**(1.0-CN)                            00002125
0016                  WRITE(6,12)                                               00002130
0017                12 FORMAT('-',13X,'DTN',10X,'CONS',10X,'AREA',10X,'RATIO') 00002135
0018                  GA=DGAMMA(A+1.0)                                          00002140
0019                  GB1=DGAMMA(B+1.0)                                         00002145
0020                  GAB1=GA*GB1/DGAMMA(A+B+2.0)                               00002150
0021                  TH(1)=1.0                                                 00002155
0022                  TC(1)=1.0                                                 00002160
0023                  TC(11)=0.0                                                00002165
0024                  DO 40 INDEX=1,2                                           00002170
0025                  WRITE(6,14)                                               00002175
0026               14 FORMAT(' ')                                               00002180
0027                  HH(1)=1.0                                                 00002185
0028                  AREA=0.0                                                  00002190
0029                  ZZ=0.0                                                    00002195
0030                  DTN=0.0                                                   00002200
0031                  DO 10 I=1,10                                              00002205
0032                  DTN=DTN+0.1                                               00002210
0033                  DTR=DABS(DTN)                                             00002215
0034                  IF(INDEX.EQ.1) GO TO 21                                   00002220
                   C--- HEATING PROCESS                                         00002225
0035                  H=(DTN+1.0)**(CM+1.0)                                     00002230
0036                  HH(I+1)=H                                                 00002235
0037                  HS=(HH(I+1)-HH(I))/(INT-1)                                00002240
0038                  CALL HEAT(A,B,H,INT,F,AREA,HS)                            00002245
0039                  CONS=DM*(1.0+1.0/DTN)**(1.0-CN)                           00002250
0040                  TII=CONS*AREA                                             00002255
0041                  TH(I+1)=TII                                               00002260
0042                  GO TO 25                                                  
                   C--- COOLING PROCESS                                        00002265
0043               21 CONTINUE                                                  00002270
0044                  IF(I.EQ.10) GO TO 10                                      00002275
0045                  RR=-DTR                                                   00002280
0046                  H=(1.0+RR)**(CM+1.0)                                      00002285
0047                  HH(I+1)=H                                                 00002290
0048                  HS=(HH(I)-HH(I+1))/(INT-1)                                00002295
0049                  CALL COOL(A,B,H,AREA)                                     00002300
0050                  CONS=DM*(-1.0-1.0/RR)**(1.0-CN)                           00002305
0051                  TII=CONS*AREA                                             00002310
0052                  TC(I+1)=TII                                               00002315
0053               25 CONTINUE                                                  00002320
0054                  WRITE(6,30) HC(INDEX),DTN,CONS,AREA,TII                   00002325
0055               30 FORMAT('0',2X,A8,4G12.4)                                  00002330
0056               10 CONTINUE                                                  00002335
```

```
0057          40 CONTINUE                                          00002340
0058             RETURN                                            00002345
0059             END                                               00002350
```

```
0001                  SUBROUTINE HEAT(A,B,H,INT,F,AREA,HS)                    00002355
0002                  IMPLICIT REAL*8(A-H,O-Z)                                00002360
0003                  DIMENSION F(INT)                                        00002365
0004                  COMMON HH(11),ZZ                                        00002370
0005                  COMMON /KK/I                                            00002375
0006                  DA=H**(A+1.0)*(-1.0+H)**(B+1.0)/(B+1.0)                 00002380
0007                  DB=-(A+B+2.0)/(B+1.0)                                   00002385
0008                  DO 10 J=1,INT                                           00002390
0009                  XX=HH(I)+HS*(J-1)                                       00002395
0010                10 F(J)=XX**A*(-1.0+XX)**(B+1.0)                          00002400
0011                  CALL INTGRT(INT,F,HS,AR)                                00002405
0012                  ZZ=ZZ+AR                                                00002410
0013                  AREA=DA+ZZ*DB                                           00002415
0014                  RETURN                                                  00002420
0015                  END                                                     00002425
```

```
0001                  SUBROUTINE INTGRT(N,F,H,AREA)                          00002430
0002                  IMPLICIT REAL*8(A-H,O-Z)                               00002435
0003                  DIMENSION F(N)                                         00002440
0004                  AREA=0.0                                               00002445
0005                  S=0.5*H                                                00002450
0006                  DO 10 I=2,N                                            00002455
0007                  AREA=AREA+S*(F(I-1)+F(I))                              00002460
0008                10 CONTINUE                                              00002465
0009                  RETURN                                                 00002470
0010                  END                                                    00002475
```

```
FORTRAN IV G LEVEL  21                COOL                DATE = 78020          00/18/52                PAGE 0001

0001                  SUBROUTINE COOL (A,B,H,AREA)                                                    00002480
0002                  IMPLICIT REAL*8(A-H,O-Z)                                                        00002485
0003                  REAL*4 SH,SA1,SB2,SP                                                            00002490
0004                  REAL*4 SNGL
0005                  COMMON /GT/GAB1                                                                 00002495
0006                  A1=A+1.0                                                                        00002500
0007                  B1=B+1.0                                                                        00002505
0008                  P=0.0                                                                           00002510
0009                  SH=SNGL(H)                                                                      00002515
0010                  SA1 = SNGL(A1)
0011                  SB2=SNGL(B1)                                                                    00002520
0012                  SP=SNGL(P)                                                                      00002525
0013                  CALL MDBETA(SH,SA1,SB2,SP,IER)                                                  00002530
0014                  IF(IER.EQ.0) GO TO 10                                                           00002535
0015                  WRITE(6,20) IER,SP,SH,SA1,SB2                                                   00002540
0016                20 FORMAT('=',50X,'* *ERROR IER',6X,'P',10X,'H',10X,'A',10X,'B',                  00002545
                     &/,'0',58X,I5,4G12.4)                                                           00002550
0017                10 CONTINUE                                                                       00002555
0018                  P=DBLE(SP)                                                                      00002560
0019                  H=DBLE(SH)                                                                      00002565
0020                  A1=DBLE(SA1)                                                                    00002570
0021                  B2=DBLE(SB2)                                                                    00002575
0022                  AREA=GAB1*(1.D0-P)                                                              00002580
0023                  RETURN                                                                          00002585
0024                  END                                                                             00002590
```

WEATHER SERVICE TAPE FAMILIES 3004 AND 3016 CONTAIN SOME DATA IN A FORMAT AWKWARD FOR FORTRAN TO HANDLE. THE MAXIMUM AND MINIMUM TEMPERATURE FIELDS AND THE WIND SPEED FIELD ARE PRESENT IN ZONED DECIMAL FORMAT. THIS MEANS THAT INSTEAD OF A HEXADECIMAL 'F' IN THE FIRST FOUR BITS OF THE RIGHTMOST BYTE OF THE FIELD, THERE MAY BE A HEX 'C' (INDICATING A POSITIVE NUMBER) OR A HEX 'D' (INDICATING A NEGATIVE NUMBER). LEFT AS THEY ARE, THESE CODES WOULD CAUSE FORTRAN'S INPUT ROUTINE TO ISSUE AN 'ILLEGAL DECIMAL CONVERT' ERROR, AND THE RECORD WOULD BE PRINTED OUT WITH ALPHABETIC CHARACTERS IN THESE POSITIONS.

THIS PROBLEM IS HANDLED BY READING IN THE TEMPERATURE AND WIND SPEED FIELDS AS CHARACTER DATA, AND CALLING AN ASSEMBLY LANGUAGE SUBROUTINE TO PASS BACK TO FORTRAN THE SIGNED FULLWORD INTEGER REPRESENTATION OF THE NUMBER. THE SOURCE CODE FOR THIS ASSEMBLER SUBROUTINE IS INCLUDED IN THIS APPENDIX AND SHOULD INSURE OPERATION ON IBM 360/370 OR AMDAHL 470 MACHINES. USERS WITH OTHER MACHINES MUST SUPPLY THEIR OWN SUBROUTINE TO CONVERT THE 3 BYTE ZONED DECIMAL CHARACTER STRING TO A 4 BYTE SIGNED INTEGER.

```
  LOC  OBJECT CODE     ADDR1 ADDR2  STMT   SOURCE STATEMENT                                    ASM 0200 23.42 01/19/78
000000                              3+CONV     CSECT

                                    5+*
                                    6+*        SYMBOLIC REGISTER ASSIGNMENT
                                    7+*

                              00000   9+R0       EQU   0
                              00001  10+R1       EQU   1
                              00002  11+R2       EQU   2
                              00003  12+R3       EQU   3
                              00004  13+R4       EQU   4
                              00005  14+R5       EQU   5
                              00006  15+R6       EQU   6
                              00007  16+R7       EQU   7
                              00008  17+R8       EQU   8
                              00009  18+R9       EQU   9
                              0000A  19+R10      EQU   10
                              0000B  20+R11      EQU   11
                              0000C  21+R12      EQU   12
                              0000D  22+R13      EQU   13
                              0000E  23+R14      EQU   14
                              0000F  24+R15      EQU   15
                              00000  25+         USING CONV,15
000000 47F0 F00A       0000A        26+         B     10(0,15)                  BRANCH AROUND ID        00180000
000004 04                           27+         DC    AL1(4)                    LENGTH OF IDENTIFIER    00220000
000005 C3D6D5E5                     28+         DC    CL4'CONV'                 IDENTIFIER              00300000
000009 00
00000A 90EC D00C       0000C        29+         STM   14,12,12(13)              SAVE REGISTERS          01480000
00000E 18AF                         30+         LR    R10,R15
                              00000  31+         USING CONV,10
                                    32+         DROP  R15
000010 182D                         33+         LR    R2,R13
000012 41D0 A024       00024        34+         LA    R13,SAVE0001
000016 50D2 0008       00008        35+         ST    R13,8(R2)
00001A 502D 0004       00004        36+         ST    R2,4(R13)
00001E 47F0 A06C       0006C        37+         B     SAVE0001+72
000022 0000
000024 0000000000000000             38+SAVE0001 DC    18F'0'
00006C 5821 0000       00000        39          L     2,0(1)              PUT ADD OF INPUT IN R2
000070 5831 0004       00004        40          L     3,4(1)              PUT ADD OF RESULT IN R3
000074 D200 A0A2 2000 000A2 00000   41          MVC   WORK(1),0(2)
00007A D200 A0A3 2004 000A3 00004   42          MVC   WORK+1(1),4(2)
000080 D200 A0A4 2008 000A4 00008   43          MVC   WORK+2(1),8(2)
000086 F272 A0B0 A0A2 00B0 000A2    44          PACK  PACKED,WORK         PACK THE DECIMAL INPUT
00008C 4F50 A0B0       000B0        45          CVB   5,PACKED            CONVERT IT TO BINARY
000090 5053 0000       00000        46          ST    5,0(3)              GIVE RESULT BACK IN A FULLWORD
000094 58D0 A028       00028        47          L     13,SAVE0001+4       RESTORE REG 13
                                    48          RETURN (14,12),RC=0
000098 98EC D00C       0000C        49+         LM    14,12,12(13)                RESTORE THE REGISTERS   00260000
00009C 41F0 0000       00000        50+         LA    15,0(0,0)                   LOAD RETURN CODE        00700000
0000A0 07FE                         51+         BR    14                          RETURN                  00800000
0000A2                              52 WORK     DS    CL3               WORK AREA
0000A8                              53 RES      DS    F
```

```
 LOC  OBJECT CODE     ADDR1 ADDR2  STMT   SOURCE STATEMENT

000080                             54 PACKED   DS     D
                                   55         END
```

PACKED INTERMEDIATE STAGE

INPUT FORMATS

CARD 1

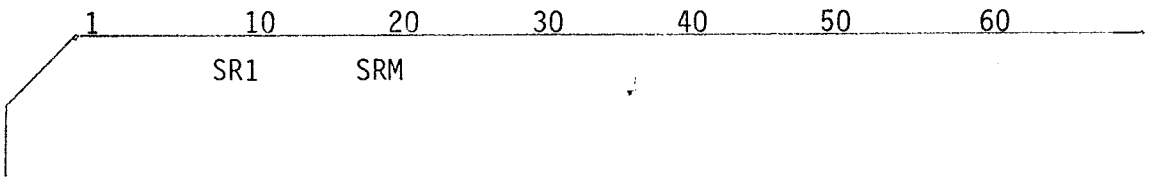

FORMAT (2F10.0)

SR1 is the average solar radiation for July, Langleys per day.

SRM is the yearly average solar radiation, Langleys per day.

CARD 2

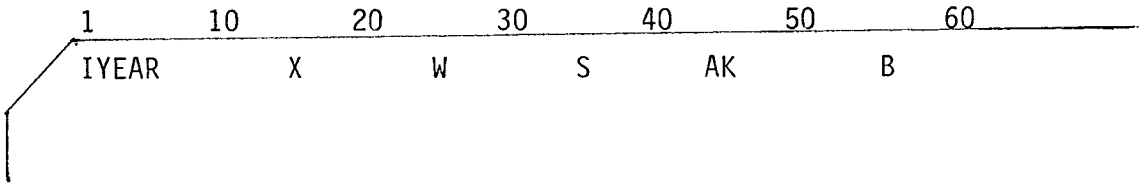

FORMAT (15,5F10.0)

LYEAR is the last year to be analyzed.

X is the thickness of the asphaltic concrete, inches.

W is the density of the asphaltic concrete, PCF

S is the specific heat of the asphaltic concrete.

AK is the thermal conductivity of the asphaltic concrete, $BTU/FT^2/HR$.

B is the absorbtivity of the asphaltic concrete.

CARD 3

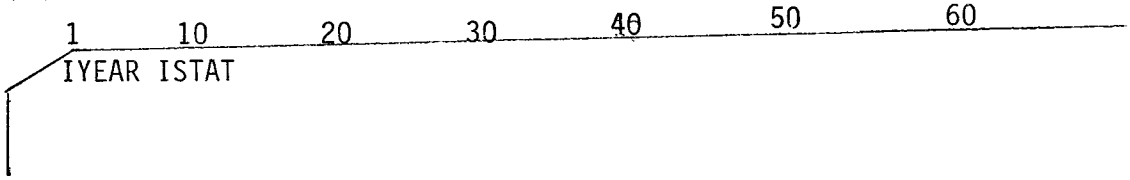

FORMAT (15,16)

IYEAR is the first year to be analyzed

ISTAT is the station to be analyzed

CARD 4

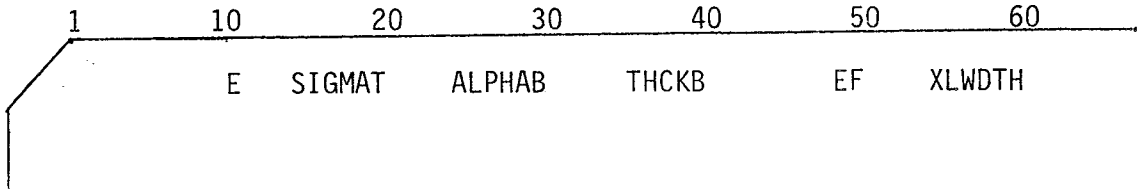

FORMAT (6F10.0)

E is the Youngs modulus of the base course when unfrozen, PSI.

SIGMAT is the frozen tensile of the base course, PSI.

ALPHAB is the freeze coefficient of the base course, M/M/^{o}C.

THCKB is the thickness of the base course.

EF is the frozen Youngs modulus of the base course.

XLWDTH is the longitudinal width of the pavement that is free of construction joints or cracks.

CARD 5

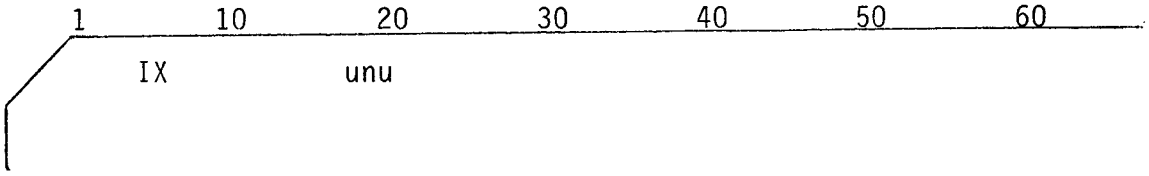

FORMAT (15,5X,F10.0)

IX = 0 for plane stress

IX = 1 for plane strain

UNU is poisson's ratio.

CARD 6

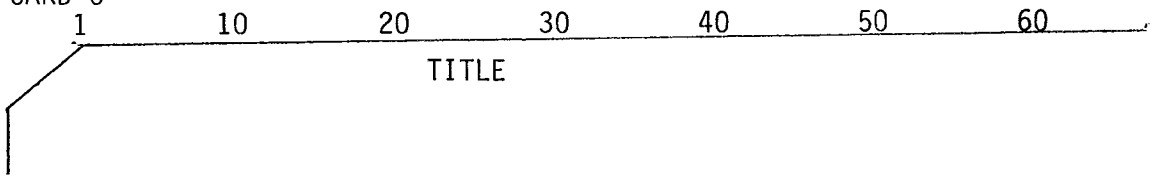

FORMAT (10A8) TITLE

TITLE is a description of the analysis being performed.

CARD 7

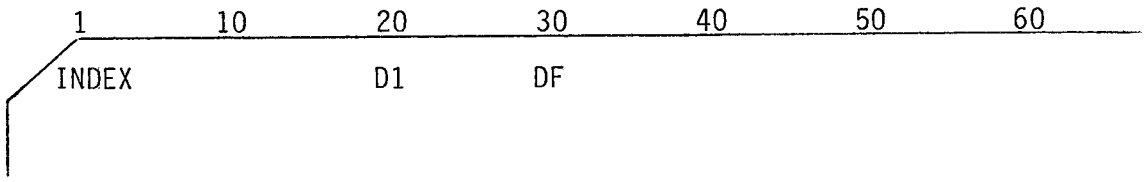

FORMAT (15,5X,2F10.0)

INDEX = 0 is the input data from master creep compliance curve.

INDEX = 1 is the input data from master relapation modulus curve.

D1 is the intercept value for log t=0 of the creep curve.

DF is the initial value of the creep curve.

CARD 8

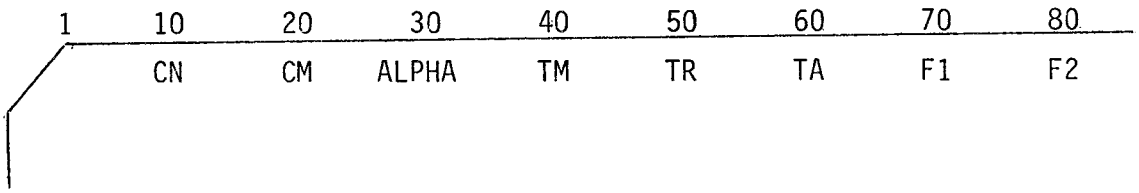

FORMAT (8F10.0)

CN is the slope of the creep compliance curve.

CM is the slope of the power law curve for the shift factor.

ALPHA is the thermal expansion coefficient for the asphalt.

TM is the reference temperature of the master curve.

TR is the temperature of the stress free state.

TA is the power law constant for the shift factor.

F1 is the constant for the WLF shift factor.

F2 is the constant for the WLF shift factor.

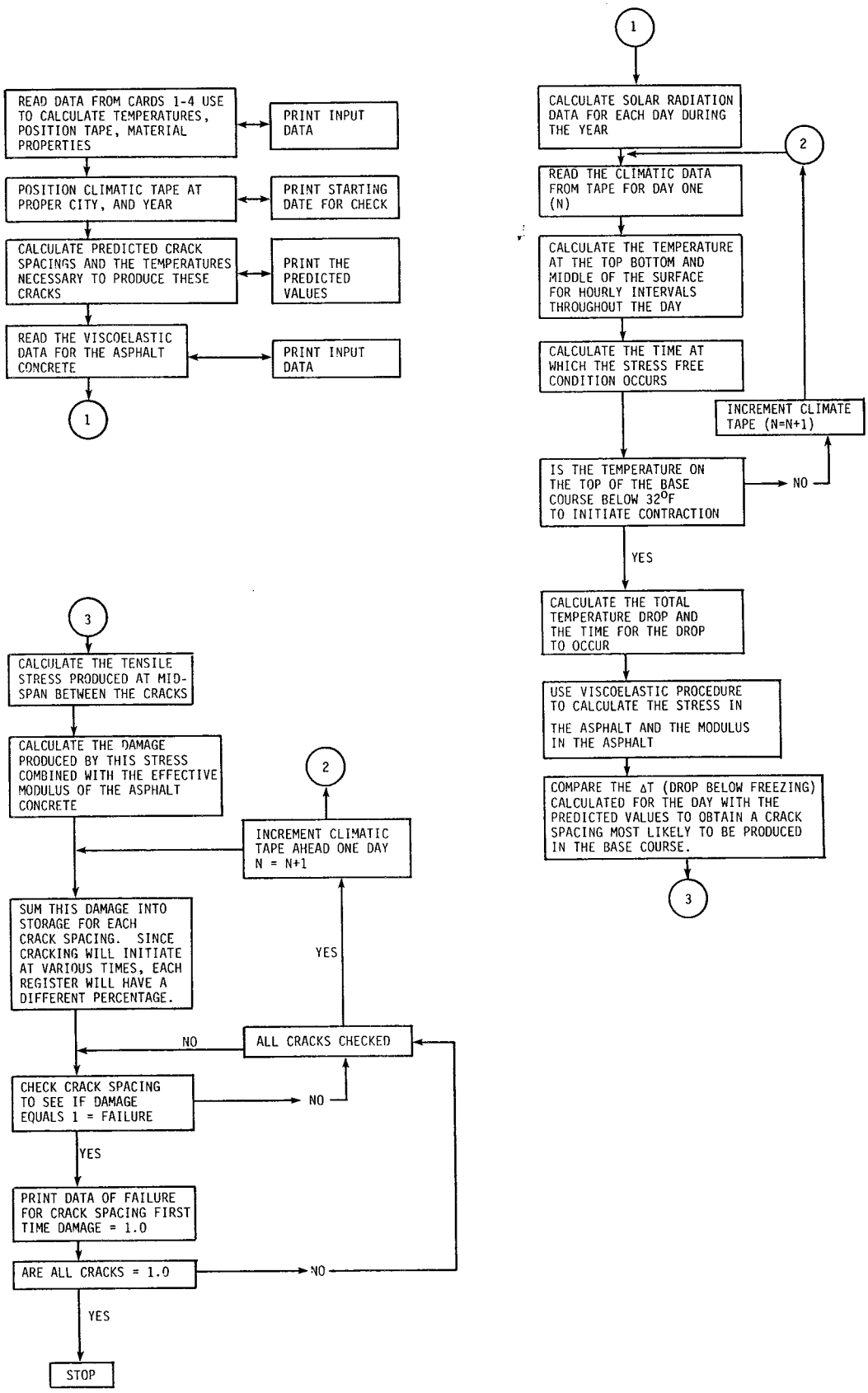
READ DATA FROM CARDS 1-4 USE TO CALCULATE TEMPERATURES, POSITION TAPE, MATERIAL PROPERTIES
PRINT INPUT DATA
POSITION CLIMATIC TAPE AT PROPER CITY, AND YEAR
PRINT STARTING DATE FOR CHECK
CALCULATE PREDICTED CRACK SPACINGS AND THE TEMPERATURES NECESSARY TO PRODUCE THESE CRACKS
PRINT THE PREDICTED VALUES
READ THE VISCOELASTIC DATA FOR THE ASPHALT CONCRETE
PRINT INPUT DATA
1
1
CALCULATE SOLAR RADIATION DATA FOR EACH DAY DURING THE YEAR
2
READ THE CLIMATIC DATA FROM TAPE FOR DAY ONE (N)
CALCULATE THE TEMPERATURE AT THE TOP BOTTOM AND MIDDLE OF THE SURFACE FOR HOURLY INTERVALS THROUGHOUT THE DAY
CALCULATE THE TIME AT WHICH THE STRESS FREE CONDITION OCCURS
INCREMENT CLIMATE TAPE (N=N+1)
IS THE TEMPERATURE ON THE TOP OF THE BASE COURSE BELOW 32°F TO INITIATE CONTRACTION
NO
YES
CALCULATE THE TOTAL TEMPERATURE DROP AND THE TIME FOR THE DROP TO OCCUR
USE VISCOELASTIC PROCEDURE TO CALCULATE THE STRESS IN THE ASPHALT AND THE MODULUS IN THE ASPHALT
COMPARE THE ΔT (DROP BELOW FREEZING) CALCULATED FOR THE DAY WITH THE PREDICTED VALUES TO OBTAIN A CRACK SPACING MOST LIKELY TO BE PRODUCED IN THE BASE COURSE.
3
3
CALCULATE THE TENSILE STRESS PRODUCED AT MID-SPAN BETWEEN THE CRACKS
CALCULATE THE DAMAGE PRODUCED BY THIS STRESS COMBINED WITH THE EFFECTIVE MODULUS OF THE ASPHALT CONCRETE
2
INCREMENT CLIMATIC TAPE AHEAD ONE DAY N = N+1
SUM THIS DAMAGE INTO STORAGE FOR EACH CRACK SPACING. SINCE CRACKING WILL INITIATE AT VARIOUS TIMES, EACH REGISTER WILL HAVE A DIFFERENT PERCENTAGE.
YES
NO
ALL CRACKS CHECKED
CHECK CRACK SPACING TO SEE IF DAMAGE EQUALS 1 = FAILURE
NO
YES
PRINT DATA OF FAILURE FOR CRACK SPACING FIRST TIME DAMAGE = 1.0
ARE ALL CRACKS = 1.0
NO
YES
STOP

MATERIAL PROPERTIES

BASE COURSE
THICKNESS 10.00 INCHES

ELASTIC MODULUS .5000D 05 PSI UNFROZEN
.1500D 06 PSI FROZEN

TENSILE STRENGTH .1000D 03 PSI FROZEN

FREEZE COEFFICIENT .1500D-03 STRAIN PER DEGREE CENTIGRADE

CRITICAL STRESS INTENSITY FACTOR 425.000

ASPHALT CONCRETE THICKNESS 1.50INCHES

INDEX = 0 D1 = -6.900 DF = 1.000

REFERENCE TEMPERATURE FOR AT CURVE: -71.0

* * * FREEZE THAW OF BASE COURSE = ABILENE

REFERENCE TEMP. FOR MASTER CURVE. 40.00

REFERENCE TEMP. FOR ZERO STRESS STATE 75.00

COEFF. OF THERMAL EXPANSION -0.1350D-04

*** E1 = 0.5057D 07 *** EE = 0.1000D 00
*** CN = 0.5000 CM= 15.50

CURVE FOR EFFECTIVE MODULUS RATIO

	DTN	CONS	AREA	RATIO
COOLING	0.1000D 00	0.3693	2.349	0.8673
COOLING	0.2000	0.2462	2.987	0.7352
COOLING	0.3000	0.1880	3.268	0.6145
COOLING	0.4000	0.1508	3.384	0.5101
COOLING	0.5000	0.1231	3.425	0.4216
COOLING	0.6000	0.1005	3.437	0.3454
COOLING	0.7000	0.8058D-01	3.439	0.2771
COOLING	0.8000	0.6155D-01	3.440	0.2117
COOLING	0.9000	0.4103D-01	3.440	0.1411
HEATING	0.1000D 00	0.4082	2.762	1.127
HEATING	0.2000	0.3015	4.089	1.233
HEATING	0.3000	0.2562	5.162	1.323
HEATING	0.4000	0.2303	6.070	1.398
HEATING	0.5000	0.2132	6.854	1.461
HEATING	0.6000	0.2010	7.533	1.514
HEATING	0.7000	0.1918	8.122	1.558
HEATING	0.8000	0.1846	8.626	1.593
HEATING	0.9000	0.1788	9.036	1.616
HEATING	1.000	0.1741	9.334	1.625

CALCULATED CRACK SPACINGS

TRANSVERSE CRACK SPACING IN BASE COURSE

268.619 FEET WILL BE PRODUCED BY A TEMPERATURE OF = 2.187 CENTIGRADE

134.309 FEET WILL BE PRODUCED BY A TEMPERATURE OF = 2.315 CENTIGRADE

67.155 FEET WILL BE PRODUCED BY A TEMPERATURE OF = 2.470 CENTIGRADE

33.577 FEET WILL BE PRODUCED BY A TEMPERATURE OF = 2.663 CENTIGRADE

16.789 FEET WILL BE PRODUCED BY A TEMPERATURE OF = 2.913 CENTIGRADE

8.394 FEET WILL BE PRODUCED BY A TEMPERATURE OF = 3.253 CENTIGRADE

4.197 FEET WILL BE PRODUCED BY A TEMPERATURE OF = 3.758 CENTIGRADE

2.099 FEET WILL BE PRODUCED BY A TEMPERATURE OF = 4.632 CENTIGRADE

1.210 FEET WILL BE PRODUCED BY A TEMPERATURE OF = 6.800 CENTIGRADE

LONGITUDINAL CRACK SPACING WILL OCCUR AT THE MID POINT OF THE CROSS SECTION OF THE PAVEMENT THAT WAS PAVED IN ONE OPERATION, CONSTRUCTION JOINTS ARE CRACKS.

12.000 FEET WILL BE PRODUCED BY A TEMPERATURE OF = 3.063 CENTIGRADE

6.000 FEET WILL BE PRODUCED BY A TEMPERATURE OF = 3.470 CENTIGRADE

3.000 FEET WILL BE PRODUCED BY A TEMPERATURE OF = 4.112 CENTIGRADE

1.500 FEET WILL BE PRODUCED BY A TEMPERATURE OF = 5.373 CENTIGRADE

DATE	********** TRANSVERSE CRACKING ********** 268.6FT	****FT	67.2FT	33.6FT	16.8FT	8.4FT	4.2FT	2.1FT	1.2FT	** LONGITUDINAL CRACKING ** 12.0FT	6.0FT	3.0FT	1.5FT
11/ 4/50	0.0144	0.0	0.0	0.0	0.0	0.0	0.0	0.0	0.0	0.0144	0.0	0.0	0.0
11/10/50	0.0340	0.0	0.0	0.0	0.0	0.0	0.0	0.0	0.0	0.0967	0.0823	0.0823	0.0823
11/11/50	0.0651	0.0312	0.0312	0.0312	0.0312	0.0312	0.0312	0.0	0.0	0.1484	0.1341	0.0823	0.0823
11/24/50	0.0963	0.0624	0.0624	0.0624	0.0624	0.0624	0.0624	0.0312	0.0	0.2224	0.2081	0.1563	0.1563
12/ 5/50	0.1248	0.0908	0.0908	0.0908	0.0908	0.0908	0.0908	0.0597	0.0	0.2917	0.2774	0.2256	0.2256
12/ 6/50	0.1305	0.0965	0.0965	0.0965	0.0965	0.0965	0.0965	0.0654	0.0057	0.3971	0.3827	0.3309	0.3309
12/ 7/50	0.1358	0.1019	0.1019	0.1019	0.1019	0.1019	0.1019	0.0707	0.0110	0.4964	0.4820	0.4303	0.4303
12/ 8/50	0.1916	0.1577	0.1577	0.1577	0.1019	0.1019	0.1019	0.0707	0.0110	0.5125	0.4820	0.4303	0.4303
12/20/50	0.2100	0.1577	0.1577	0.1577	0.1019	0.1019	0.1019	0.0707	0.0110	0.5309	0.4820	0.4303	0.4303
12/26/50	0.2273	0.1577	0.1577	0.1577	0.1019	0.1019	0.1019	0.0707	0.0110	0.5482	0.4820	0.4303	0.4303
12/27/50	0.2492	0.1577	0.1577	0.1577	0.1019	0.1019	0.1019	0.0707	0.0110	0.5701	0.4820	0.4303	0.4303
12/28/50	0.2662	0.1577	0.1577	0.1577	0.1019	0.1019	0.1019	0.0707	0.0110	0.5871	0.4820	0.4303	0.4303
12/30/50	0.2820	0.1577	0.1577	0.1577	0.1019	0.1019	0.1019	0.0707	0.0110	0.6028	0.4820	0.4303	0.4303
1/ 7/51	0.2976	0.1577	0.1577	0.1577	0.1019	0.1019	0.1019	0.0707	0.0110	0.6732	0.5524	0.5006	0.5006
1/ 8/51	0.3258	0.1858	0.1858	0.1858	0.1300	0.1300	0.1300	0.0707	0.0110	0.7204	0.5996	0.5006	0.5006
1/21/51	0.4650	0.3251	0.1858	0.1858	0.1300	0.1300	0.1300	0.0707	0.0110	0.7390	0.5996	0.5006	0.5006
1/28/51	0.7934	0.6535	0.1858	0.1858	0.1300	0.1300	0.1300	0.0707	0.0110	0.7603	0.5996	0.5006	0.5006
1/29/51	0.8005	0.6606	0.1929	0.1929	0.1371	0.1371	0.1371	0.0778	0.0181	0.8787	0.7180	0.6190	0.6190
1/30/51	0.8073	0.6674	0.1997	0.1997	0.1439	0.1439	0.1439	0.0846	0.0249	0.9940	0.8333	0.7343	0.7343
***** AN EXISTING LONGITUDINAL CRACK SPACING OF 12.000 HAS CRACKED AT MID-SPAN ON 131/1951 *****													
1/31/51	0.8144	0.6744	0.2067	0.2067	0.1509	0.1509	0.1509	0.0916	0.0320	1.1120	0.9513	0.8523	0.8523
***** AN EXISTING LONGITUDINAL CRACK SPACING OF 6.000 HAS CRACKED AT MID-SPAN ON 201/1951 *****													
2/ 1/51	0.8204	0.6804	0.2128	0.2128	0.1570	0.1570	0.1570	0.0976	0.0380	1.2203	1.0596	0.9606	0.9606
***** AN EXISTING LONGITUDINAL CRACK SPACING OF 3.000 HAS CRACKED AT MID-SPAN ON 202/1951 *****													
***** AN EXISTING LONGITUDINAL CRACK SPACING OF 1.500 HAS CRACKED AT MID-SPAN ON 202/1951 *****													
2/ 2/51	0.8249	0.6850	0.2173	0.2173	0.1615	0.1615	0.1615	0.1022	0.0425	1.3132	1.1525	1.0535	1.0535
2/13/51	0.8585	0.7186	0.2509	0.2509	0.1951	0.1951	0.1951	0.1358	0.0425	1.3921	1.2314	1.1324	1.1324
2/14/51	0.9052	0.7653	0.2976	0.2976	0.2418	0.2418	0.2418	0.1825	0.0425	1.5003	1.3396	1.2406	1.2406
2/15/51	0.9375	0.7976	0.3299	0.3299	0.2741	0.2741	0.2741	0.2148	0.0425	1.5772	1.4164	1.3175	1.3175
3/13/51	0.9538	0.7976	0.3299	0.3299	0.2741	0.2741	0.2741	0.2148	0.0425	1.5935	1.4164	1.3175	1.3175
11/ 2/51	0.9754	0.7976	0.3299	0.3299	0.2741	0.2741	0.2741	0.2148	0.0425	1.6150	1.4164	1.3175	1.3175
***** AN EXISTING TRANSVERSE CRACK SPACING OF 268.62 FEET HAS CRACKED AT MID SPACING ON 1117/1951 *****													
11/17/51	1.0136	0.8357	0.3681	0.3681	0.3123	0.3123	0.3123	0.2148	0.0425	1.6770	1.4784	1.3175	1.3175
11/18/51	1.0577	0.8798	0.4122	0.4122	0.3564	0.3564	0.3564	0.2148	0.0425	1.7492	1.5506	1.3897	1.3897
12/ 9/51	1.1519	0.9741	0.5064	0.4122	0.3564	0.3564	0.3564	0.2148	0.0425	1.7688	1.5506	1.3897	1.3897
12/10/51	1.1699	0.9741	0.5064	0.4122	0.3564	0.3564	0.3564	0.2148	0.0425	1.7868	1.5506	1.3897	1.3897
12/11/51	1.1856	0.9741	0.5064	0.4122	0.3564	0.3564	0.3564	0.2148	0.0425	1.8025	1.5506	1.3897	1.3897
12/14/51	1.2008	0.9741	0.5064	0.4122	0.3564	0.3564	0.3564	0.2148	0.0425	1.8176	1.5506	1.3897	1.3897
12/15/51	1.2067	0.9800	0.5124	0.4181	0.3623	0.3623	0.3623	0.2207	0.0484	1.9249	1.6579	1.4969	1.4969
12/16/51	1.2234	0.9800	0.5124	0.4181	0.3623	0.3623	0.3623	0.2207	0.0484	1.9417	1.6579	1.4969	1.4969
***** AN EXISTING TRANSVERSE CRACK SPACING OF 134.31 FEET HAS CRACKED AT MID SPACING ON 1220/1951 *****													
12/20/51	1.2466	1.0032	0.5355	0.4412	0.3854	0.3854	0.3854	0.2439	0.0484	2.0004	1.7166	1.5556	1.5556
12/21/51	1.2811	1.0377	0.5700	0.4757	0.4199	0.4199	0.4199	0.2783	0.0484	2.0865	1.8028	1.6418	1.6418

APPENDIX E

NOTATION

A = Lennard-Jones coefficient for ion concentration;
A_n = fracture property of asphalt;
a = moisture suction regression coefficient;
Å = Angstrom;
B = Lennard-Jones coefficient for specific surface area;
B_o = residual strain coefficient;
B_I = residual strain coefficient;
b = moisture-suction regression coefficient;
C = given crack length;
c = instantaneous crack length;
C_f = final crack length;
C_o = original crack length;
DTA = differential thermal analysis;
d = deficit of rainfall;
ΔH = change in sample height caused by freezing;
ΔN = percentage of that cycles damage, related to failure;
ΔT = temperature drop below freezing °C;
E = evaporation;
E_p = potential evapotranspiration;
FC = freeze coefficient of base course, % strain/°C;
G_s = specific gravity;
g = gravitational constant;
H_o = original height of sample;
h = suction, psi;
I_m = Thornthwaite moisture index;
K_I = stress intensity factor, $lb/(in)^{-3/2}$;
L = initial crack spacing, twice the final spacing;
L_c = crack opening distance;
m = slope of compliance curve;
N_f = number of various stress cycles to cause failure;
N_{400} = number of 400 psi stress cycles to cause failure;
n = viscoelastic material property = $2(1+1/m)$;

P = pressure;

p = relative vapor pressure of soil moisture;

p_o = relative vapor pressure of pure water;

R = universal gas constant;

R^2 = coefficient of determination;

S = surplus of rainfall;

s = specific entropy;

SSA = specific surface area, m^2/gm;

T = temperature;

TC = thermal coefficient of base course, % strain/°C;

v = specific volume;

W_l = liquid limit;

W_p = plastic limit;

X = thickness of asphaltic concrete surface;

α = coefficient of thermal activity, % strain/°C;

σ_T = tensile stress;

θ = angle assumed between two clay particles;

2θ = angle relationship for x-ray diffraction test; and

$\phi_{(r)}$ = representation of Lennard-Jones Potential.